



Universitat d'Alacant
Universidad de Alicante

LIKELY EFFECTS OF CLIMATE CHANGE ON WATER RESOURCES AND
VEGETATION GROWTH PERIOD IN THE PROVINCE OF ALICANTE,
SOUTHEASTERN SPAIN

Hassane Moutahir



Tesis Doctorales

www.eltallerdigital.com

UNIVERSIDAD de ALICANTE



Universitat d'Alacant
Universidad de Alicante

DEPARTAMENTO DE ECOLOGÍA

FACULTAD DE CIENCIAS

**LIKELY EFFECTS OF CLIMATE CHANGE ON WATER RESOURCES AND
VEGETATION GROWTH PERIOD IN THE PROVINCE OF ALICANTE,
SOUTHEASTERN SPAIN**

HASSANE MOUTAHIR

Tesis presentada para aspirar al grado de

DOCTOR POR LA UNIVERSIDAD DE ALICANTE

MENCIÓN DE DOCTOR INTERNACIONAL

DOCTORADO EN CONSERVACIÓN Y RESTAURACIÓN DE ECOSISTEMAS

Dirigida por:

Pr. JUAN BELLOT

Catedrático de Ecología

Departamento de Ecología, de la Universidad de Alicante

-Julio 2016-



Universitat d'Alacant
Universidad de Alicante

DÉPARTEMENT D'ÉCOLOGIE
FACULTÉ DES SCIENCES

LIKELY EFFECTS OF CLIMATE CHANGE ON WATER RESOURCES AND
VEGETATION GROWTH PERIOD IN THE PROVINCE OF ALICANTE,
SOUTHEASTERN SPAIN

HASSANE MOUTAHIR



Thèse présentée pour aspirer au degré de
DOCTEUR DE L'UNIVERSITÉ D'ALICANTE
MENTION DU DOCTEUR INTERNATIONAL
DOCTORAT DANS LA CONSERVATION ET LA RESTAURATION DES
ECOSYSTEMES

Dirigée par:

Pr. JUAN BELLOT

Professeur d'écologie

Département d'Écologie, Université d'Alicante

-Juillet 2016-



Universitat d'Alacant
Universidad de Alicante

Pr. Juan BELLOT ABAD Catedrático del Dpto. de Ecología de la Universidad de Alicante

Hace constar:

Que el trabajo descrito en la presente memoria, titulado: “LIKELY EFFECTS OF CLIMATE CHANGE ON WATER RESOURCES AND VEGETATION GROWTH PERIOD IN THE PROVINCE OF ALICANTE, SOUTHEASTERN SPAIN” ha sido realizado bajo su dirección por Hassane MOUTAHIR en el Departamento de Ecología de la Universidad de Alicante, y reúne todos los requisitos necesarios para su aprobación como Tesis Doctoral.

Universitat d'Alacant
Universidad de Alicante
Alicante, 26 de Julio de 2016

Pr. Juan BELLOT ABAD

El doctorando

Hassane MOUTAHIR

معنى الحديث : " لَا تُسْرِفْ فِي الْمَاءِ وَلَوْ كُنْتَ عَلَى نَهْرٍ جَارٍ "

معنى الحديث " إِنْ قَامْتَ عَلَى أَحَدْكُمْ الْقِيَامَةُ، وَفِي يَدِهِ فَسِيلَةٌ فَلْيَعْرِسْهَا "

"No malgastes el agua aunque estés en la orilla de un río"

"Si te alcanza el día del fin del mundo y tienes en tus manos una plántula y puedes plantarla, plantala"

El profeta del islam

"La Tierra no es una herencia de nuestros padres, sino un préstamo de nuestros hijos."

Un proverbio indio



A mi madre

A mis hermanas y hermanos

A mi familia

A todos mis amigos

Y a todas aquellas personas que comparten la información sin complejos!

Universitat d'Alacant
Universidad de Alicante

Agradecimientos

Quiero expresar mi más sincero agradecimiento a todas aquellas personas e instituciones que han contribuido a la realización de esta tesis doctoral y muy especialmente:

A JUAN F. BELLOT ABAD, director de esta Tesis, por su valiosa dirección y su ayuda en todos los sentidos. La ventaja que tuve con Juan es esa libertad que me dio para probar varios caminos hasta llegar a esta versión final de mi tesis. Esa flexibilidad que él mostró a la hora de aceptar cambios en el plan original del trabajo a lo largo de este camino me permitió probar muchas cosas y aprender mucho. También quiero agradecerle la participación en varios proyectos de investigación de los cuales he aprendido muchísimo. Otra cosa muy importante es la oportunidad que me dio para impartir clases en el máster de Gestión y restauración del medio natural y antes me ayudó a organizar un curso de GIS de libre elección. Todo eso sin nombrar las formaciones, congresos y estancias... por todo eso MUCHAS GRACIAS JUAN!

A todos los profesores del Dpto. de Ecología que muchos de ellos se han convertido en buenos amigos. A Andreu Bonet por ser tan buena persona y por ayudarme en lo administrativo en un momento muy difícil. A Susana y Paco por contestar todas mis preguntas y sin olvidar las becas que Susana me dio en momentos de vacas flacas. A Juan Ra, María José, Jordi, Esteban, Jaime (no ha parado en animarme a acabar esto), Joanet y Josep... A toda la gente del Dpto. de Ecología.

A todas las personas de fuera del Dpto. que me ayudaron y mucho: Martin de Luis, Mario Herrera, Roberto Monjo, Miguel García y otros más.

A Barron y Grant por darme la oportunidad de hacer una estancia en una universidad en Estados Unidos donde he disfrutado mucho y he aprendido mucho. Y por las revisiones y sus comentarios para mejorar algunos de los capítulos de esta tesis. Especial agradecimiento a Grant y su pequeña familia que ha sido mi familia durante los tres meses de estancia. Y A mis compañeros de laboratorio allí y especialmente Tanner (y Hailey) y Lauren.

A todos mis amigos y compañeros de la Universidad y de Alicante: Adrian, Ana, Andrea, Angela, Ángeles, Anna, Azucena, Carlos Andarcio, Carles, Cholo, Cristian, David, Diana, Dídac, Elysa, Fran, Germán, Karen, Klemen, Lorena,

Luna, Nuria, Pepe, Rosario, Samantha, Sara, Sofía, Thanos... Con ellos he compartido muy buenos momentos dentro de la universidad y fuera. A Luna, gracias por traer al mundo al Dídac (lo mejor que ha salido del Dpto. de Ecología). A todos aquellos amigos extranjeros, sobre todo los de Brasil, que por su paso por el Dpto. de Ecología dejaron buenos recuerdos.

A todos mis amigos y compañeros árabes de la Universidad y fuera: Mohammed, Issam. Haroun, Idris, Bouchra, Zakaria, Imane, Fatima, Intissar, Abdollah, Soumaya, Israe, SiMohammed, Aziz, Amer, Tijani, Bassima...

A todos mis amigos sin excepción por si se me olvidó algún nombre...

A mi madre por darnos la oportunidad de ir a la escuela en un entorno que no ayudaba mucho a hacerlo, mis hermanas y hermanos, mis sobrinos y toda la familia. Y especialmente a Sidi Salah por su apoyo.

A todas aquellas personas e instituciones que pusieron a nuestra disposición los datos climáticos, satelitales y software para su tratamiento de forma gratuita. Gracias a la comunidad del software libre por esa mentalidad de compartirlo todo con todo el mundo.

A todos gracias!

Universitat d'Alacant
Universidad de Alicante

Esta tesis se ha realizado en el marco de los proyectos: ECOBAL (CGL2011-30531-C02-01) y ALTERACLIM (CGL2015-69773-C2-1-P) financiados por el Ministerio de Economía y Competitividad.

Alicante, el 26 de julio del 2016

ÍNDICE

Listado de Tablas

Listado de Figuras

CAPÍTULO 1. Introducción general	1
CAPÍTULO 2. Análisis de los eventos climáticos extremos en la provincia de Alicante, , sureste de España	25
CAPÍTULO 3. Likely effects of climate change on groundwater availability in a Mediterranean region of Southeastern Spain	41
CAPÍTULO 4. Land surface phenology (LSP) changes in relation to climatic variables in the Mediterranean natural areas, Southeastern Spain: observed and projected changes	73
CAPÍTULO 5. Assessing the crop growing period according to the climate change forecasts for Marina Baixa (SE Spain)	117
CAPÍTULO 6. HydrobalPCR: a model based on an environmental modelling framework to evaluate of the likely effects of climate change on water balance under different vegetation covers	135
CAPÍTULO 7. Resumen de los resultados	179
CAPÍTULO 8. Conclusiones	191
APÉNDICES	197

LISTADO DE FIGURAS

CAPÍTULO: 1

Figura 1.1: a) Anomalía observada en el promedio mundial de temperaturas en superficie, terrestres y oceánicas combinadas, 1850-2012. Las anomalías son relativas a la media del período 1961-1990. b) El cambio anual en la temperatura media global en superficie respecto de 1986-2005. Series temporales simuladas, basadas en modelos múltiples de la quinta fase del Proyecto de comparación de modelos acoplados (CMIP5) de los escenarios RCP2.6 y RCP8.5, entre 1950 y 2100 (Fuente: IPCC, 2013).

Figura 1.2: a) Mapa de los cambio observado en la precipitación entre 1951 y 2010 (Fuente: IPCC, 2014). b) el cambio de la media porcentual de la precipitación media anual en el periodo 2081-2100 respecto de 1986-2005. Mapas de resultados medios de modelos múltiples de la quinta fase del Proyecto de comparación de modelos acoplados (CMIP5) de los escenarios RCP2.6 y RCP8.5 (Fuente: IPCC, 2013)

Figura 1.3: los pisos bioclimáticos en la provincia de Alicante según la clasificación de Rivas-Martínez (1983) y las zonas de transición entre los periodos 1953-1982 y 1983-2012. Los puntos representan las estaciones meteorológicas usadas (Fuente: elaboración propia)

Figura 1.4: Evolución de las temperaturas máximas y mínimas en la provincia de Alicante en el periodo 1953-2012. La línea en negrita es media móvil cada 9 años (Fuente: elaboración propia)

Figura 1.5: Evolución proyectada de: a) la anomalía de la precipitación de 204-2099 respecto de 1953-2012. b) la temperatura media en la provincia de Alicante en el periodo 2040-2099. Media de nueve CMIP5 bajo dos escenarios RCP4.5 (línea azul) y RCP8.5 (línea roja). Zonas coloreadas son el intervalo de variación de las dos variables según los nueve modelos (Fuente: elaboración propia)

CAPÍTULO: 2

Figura 2.1: Mapa del índice PRCPTOT (a) y su tendencia (b)

Figura 2.2: Mapa del índice R95ptot (a) y su tendencia (b)

Figura 2.3: Mapa del índice R99ptot (a) y su tendencia (b)

Figura 2.4: Mapa del índice Rx1day (a) y su tendencia (b)

Figura 2.5: Mapa del índice Rx5day (a) y su tendencia (b)

Figura 2.6: Mapa del índice SDII (a) y su tendencia (b)

Figura 2.7: Mapa del índice R1mm (a) y su tendencia (b)

Figura 2.8: Mapa del índice R10mm (a) y su tendencia (b)

Figura 2.9: Mapa del índice R20mm (a) y su tendencia (b)

Figura 2.10: Mapa del índice CDD (a) y su tendencia (b)

Figura 2.11: Mapa del índice CWD (a) y su tendencia (b)

CAPÍTULO: 3

Figure 3.1: Study area location and used meteorological stations. Section numbers represent the ten clusters.

Figure 3.2: Mean (plain bars) and standard deviation (error bars) of the monthly precipitation for the entire province of Alicante over the period 1953-2012. Black and white bars represent the monthly mean precipitation of the driest and wettest weather stations respectively.

Figure 3.3: Mean annual precipitation (plain bars) and standard deviation (error bars) per cluster over the period 1953-2012

Figure 3.4: (a) Variation profile of the determination coefficient (R^2) from linear regression of monthly observed water level increments number against the number of rainfall events above a given threshold varied between 5 and 60 mm and incremented by 5 mm over the period 2006-2012. (b) the % of the total number of water level increments and of the number of ≥ 20 mm events occurred in each month over the period 2006-2012.

Figure 3.5: (a) Monthly number of HREs in the Cluster 8. (b) The wavelet power spectrum (white areas represent the low values). The region under the cone line is the cone of influence, where zero padding has reduced the variance. Black contour is the 5% significance level, using a white-noise background spectrum. (c) The global wavelet spectrum. The dashed line is the significance for the global wavelet spectrum, assuming the same significance level and background spectrum as in (b)

Figure 3.6: The GWS of clusters 1 to 10 from wavelet analysis applied to HREs time series over the period 1953-2012 (thick line) and sub-periods 1953-1982 (thin line) and 1983-2012 (dashed line). (Upper thick, thin and dashed lines are the 95% significance levels for global power spectrum over the three periods respectively)

Figure 3.7: Mean annual number of HREs (a), Mean annual volume of water produced by HREs (b) and Mean size of events (mm/event) (c) over the period 1953-2012 and the two sub-periods 1953-1982 and 1983-2012. The difference with respect to the first sub-period is *significant at 10%, **significant at 5%, ***significant at 1%.

Figure 3.8: Evolution of the trend direction and of the magnitude of change (event per decade) in the number of HREs over a moving 30-year window over the period 1953-2012. Black dots show the significant trends at 5%.

Figure 3.9: Projection of the expected mean annual number of HREs by the nine CMIP5 models under RCP4.5 (a) and RCP8.5 (b) scenarios for the period (2040-2099). Thick, thin and dashed lines are the observed, RCP4.5 and RCP8.5 mean numbers of HREs for the entire region and the nine models respectively.

Figure 3.10: Projected change in mean values under the nine CMIP5 models and the two RCP scenarios with respect to the observed period of the expected (a) mean annual number of HREs; (b) mean annual volume of water produced by HREs; and (c) the mean size of HREs. The difference with respect to the observed period is *significant at 10%, **significant at 5%, ***significant at 1%.

CAPÍTULO: 4

Figure 4.1: Study area location and elevation map.

Figure 4.2: Temperature and precipitation stations. Stations outside the province of Alicante were used to ovoid the border effect.

Figure 4.3: Land cover/use map of Alicante province from Corine Land Cover 2000 (level I). Classes with (*) come from Corine Land Cover (level II) and represent the natural vegetation areas.

Figure 4.4: The six subclasses of forest and shrub from CORINE land-cover 2000

Figure 4.5: Metrics derived from MODIS-NDVI time-series (dashed line) using timesat. This time-series is from a single pixel in a forested area, and highlights the smoothing and curve-fitting (black line) methods with which Timesat derives LSP metrics.

Figure 4.6: frequency (%) of pixels where SOS or EOS occurs at a given M-date

Figure 4.7: Spatial variation of LSP metrics in Alicante. The mean SOS and EOS M-dates are used as thresholds and pixels are classified in three classes. Green and blue when SOS/EOS occurs before and after mean M-date respectively and yellow when it occurs on mean M-date.

Figure 4.8: LSP and Altitude relationships. SOS and EOS are expressed in M-dates and LOS is expressed in days.

Figure 4.9: Mean LSP metrics values in function of orientation. SOS and EOS are expressed in M-dates and LOS is expressed in days.

Figure 4.10: Percent of total pixels when SOS or EOS occurs depending on precipitation conditions. Accumulated precipitation of August and September used in the case of SOS and accumulated precipitation from January to April in the case of EOS.

Figure 4.11: Correlation matrix between LSP metrics and climate metrics in CORINE level II classes

Figure 4.12: Correlation matrix between LSP metrics and climate metrics in CORINE level III subclasses

Figure 4.13: Evolution of projected climate metrics determining LSP metrics in Alicante. Mean values of nine CMIP5 climate models under two RCP scenarios.

Annex4.1 Figure 1: The best fits between SOS and climate metrics. Y axis represents SOS expressed as M-dates. X axis represents climate metrics.

Annex4.1 Figure 2: The best fits between EOS and climate metrics. Y axis represents EOS expressed as M-dates. X axis represents climate metrics.

Annex4.2 Figure 1: LSP metrics projection in the CLC312 land cover class in function of precipitation and maximum temperature. SOS and EOS are expressed in M-dates and LOS is expressed in days. X axis represents the time in years.

Annex4.2 Figure 2: LSP metrics projection CLC321 land cover class in function of precipitation and maximum temperature. SOS and EOS are expressed in M-dates and LOS is expressed in days. X axis represents the time in years.

Annex4.2 Figure 3: LSP metrics projection CLC323 land cover class in function of precipitation and maximum temperature. SOS and EOS are expressed in M-dates and LOS is expressed in days. X axis represents the time in years.

Annex4.2 Figure 4: LSP metrics projection CLC324 land cover class in function of precipitation and maximum temperature. SOS and EOS are expressed in M-dates and LOS is expressed in days. X axis represents the time in years.

CAPÍTULO: 5

Figure 5.1: Location of the study area and the meteorological stations

Figure 5.2: Temporal and spatial distribution of the mean annual precipitations during the observed and projected periods. Frequency histograms (X-axis: annual precipitation mm); Y-axis: observed frequency (%)). Grey line shows the decrease of precipitations over time.

Figure 5.3: Temporal and spatial distribution of probability of exceeding 400 mm of annual precipitation during the observed and projected periods. Frequency histograms (X-axis: Probability of exceedance (%)); Y-axis: observed frequency (%)). Grey line shows the decrease of probability of exceeding 400 mm of annual precipitation over time.

Figure 5.4: Temporal and spatial distribution of the mean annual ETo during the observed and projected periods. Frequency histograms (X-axis: annual ETo mm); Y-axis: observed frequency (%)). Grey line shows the increase of ETo over time.

Figure 5.5: Frequency analysis of P exceeding half the ETo in the stations 8033 (left) and 8041A (right) during the observed and projected periods. (Blue area shows the decades when the frequency goes down 30%)

CAPÍTULO: 6

Figure 6.1: The four sites localization. Blue lines represent isohyets each 100 mm. Mean annual rainfall over the period 1953-2012.

Figure 6.2: Main flows simulated by HydrobalPCR. The vegetation with its vertical structure plays an important role regulating the water reaching the soil.

Figure 6.3: Adjustment of k factor in Mela site. Grey lines represent the SWC simulated running the model multiple times with randomly selected k factor sets. Thick line represents the best adjustment.

Figure 6.4: Model validation. Simulated SWC vs Observed SWC in forested areas in Mela Site over the period from October 2014 to September 2015.

Figure 6.5: Percent of change in the model outputs in the 30-year period 2070-2099 with respect to the period 2010-2039 in the four sites and two vegetation types under the two RCP scenarios and nine CMIP5 models. Pr: Precipitation, netPr: Net rainfall, Eto: reference evapotranspiration, Eta: actual evapotranspiration DP: deep percolation, SWC: soil water content.

Annex 6.3 Figure 1: Projected evolution of mean air temperatures ($^{\circ}\text{C}$) under the two RCP scenarios in the four sites in the period 2006-2099. Temperature time series (Thick lines) are averages of the nine projections from nine CMIP5 models. Thin lines represent the maximum and minimum of the nine CMIP5 models. X axis represents Tm ($^{\circ}\text{C}$) and Y axis represents time (years).

Annex 6.3 Figure 2: Projected evolution of Eto (mm) under the two RCP scenarios in the four sites in the period 2006-2099. Eto time series (Thick lines) are averages of the nine projections from nine CMIP5 models. Thin lines represent the maximum and minimum of the nine CMIP5 models. X axis represents Eto (mm) and Y axis represents time (years).

Annex 6.3 Figure3: Projected evolution of Pr (mm) under the two RCP scenarios in the four sites in the period 2006-2099. Pr time series (Thick lines) are averages of the nine projections from nine CMIP5 models. Thin lines represent the maximum and minimum of the nine CMIP5 models. X axis represents Pr (mm) and Y axis represents time (years).



LISTADO DE TABLAS

CAPÍTULO: 1

Tabla 1.1: Descripción de los nueve modelos climáticos CMIP5 usados en este trabajo

CAPÍTULO: 2

Tabla 2.1: los índices de extremos climáticos para la precipitación usados en este trabajo

Tabla 2.2: La media de los índices de extremos climáticos en los periodos 1953-2012, 1953-82 y 1983-2012

Tabla 2.3: La tendencia media de los índices de extremos climáticos en los periodos 1953-2012, 1953-82 y 1983-2012

CAPÍTULO: 3

Table 3.1: Changes in the significance of GWS peaks in 4-8 and 8-16 month bands between the two sub periods 1953-1982 and 1983-2012 in the ten clusters

Table 3.2: Trends per decade in the mean annual number of HREs, in mean annual volume of water produced by HREs and mean HREs size over the period 1953-2012. (The magnitude of change by linear regression and significance test by Mann-Kendall test)

Table 3.3: Change in the mean length of NARP in the second sub-period (1983-2012) with respect to the first sub-period (1953-1982) and trends over the entire observed period (1953-2012).

Table 3.4: Mean projected trends in HREs features over the period (2040-2099) under the two climate scenarios. Mean of the nine models and standard error.

CAPÍTULO: 4

Table 4.1: MODIS-NDVI 16-day composites dates (M-date) and the codes used in this work. We choose August 12 as date 0 because low values of precipitation (~0 mm) are registered in the two first weeks of this month. These codes will be used to determine the LSP metrics instead of the dates.

Table 4.2: Different CORINE land-cover 2000 (CLC level II) classes of Alicante.

Table 4.3: Natural vegetation areas from CORINE land-cover 2000. We selected Forest and shrub classes at CLC level II and three subclasses inside each class at level III.

Table 4.4: LSP metrics means in the natural vegetation classes CLC2000 level II. Mean \pm standard deviation over the period 2000-2012. For each LSP metric, the values followed by the same letter are not significantly different at $p < 0.05$

Table 4.5: LSP metrics means in the natural vegetation classes CLC2000 level III. Mean \pm standard deviation over the period 2000-2012. For each LSP metric, the values followed by the same letter are not significantly different at (Tukey HSD, $p < 0.05$). (*) differences not tested in these subclasses because of the low number of pixels in each one of them)

Table 4.6: Climate metrics used as explanatory variables for the LSP changes

Table 4.7: The regression equations used to project the LSP metrics under future climate change scenarios using precipitation and maximum temperature of August and

September (Pr8+9, Tx8+9) to project the SOS and precipitation from January to April (Pr1-4) and maximum temperature of April (Tx4) to project the EOS

Table 4.8: Mean projected trends of different LSP metrics in days/ decade over the period 2011-2099 under the two RCP scenarios. Mean values of the nine CMIP5 climate models. Significances tested by Mann-Kendall test.

CAPÍTULO: 5

Table 5.1: LGP in Marina Baixa using the 30% threshold of probability that P exceeds half the ETo. Start and end decades and duration in days. LGP start in a year and end in the next year.

CAPÍTULO: 6

Table 6.1: The ten possible combinations representing the vertical structure of vegetation in the four sites and its cover (%).

Table 6.2: Nearest meteorological stations to each site. Pr, T and distance represent Precipitation, Temperature and the distance to the nearest site respectively.

Table 6.3: Lapse rates ($^{\circ}\text{C}/100\text{m}$) used to correct the maximum and minimum monthly temperature.

Table 6.4: Soil parameters in the four sites and two vegetation types. WP: Wilting Point, FC: Field Capacity, Poros: Porosity, SWCi : intial Soil water content

Table 6.5: Commands used to call the PCRaster modules, numpy and HydrobalPCR functions module and to create a class named HydrobalPCR

Table 6.6: The initial section of HydrobalPCR main script

Table 6.7: The dynamic section of HydrobalPCR main script

Table 6.8: Mean projected trends in Tm, Eto and Pr over the period 2010-2099 in the four sites. The mean, min and max change values per decade from nine CMIP5 models under two RCP scenarios.

Table 6.9: NSE and RSR coefficients and the selected kmin and kmax values in the four sites and two vegetation types.

Table 6.10: Mean projected trends in the HydrobalPCR outputs over the period 2010-2099 under the two RCP scenarios, and the nine CMIP5 models in the forested and not forested areas in the four sites. Pr: Precipitation, netPr: Net rainfall, Eto: reference evapotranspiration, Eta: actual evapotranspiration DP: deep percolation, SWC: soil water content. All trends are expressed as mm/decade except SWC (%)/decade. * significant at 5%.

Annex 6.2 Table 1: Vegetation structure and cover (%) in Pine (forested) areas in the four sites. Nine classes + bare soil were differentiated (Grey cells). In some classes, different sub-classes were differentiated.

Annex 6.2 Table 2: Vegetation structure and cover (%) in shrub (not forested) areas in the four sites. Four classes + bare soil were differentiated (Grey cells). In some classes, different sub-classes were differentiated

Annex 6.3 Table 1: Mean Tm increment $^{\circ}\text{C}/\text{decade}$ over the period 2006-2099 in the four sites. Nine CMIP5 models and two RCP scenarios.

Annex 6.3 Table 2: Mean Eto increment mm/decade over the period 2006-2099 in the four sites. Nine CMIP5 models and two RCP scenarios.

Annex 6.3 Table 3: Mean Pr change mm/decade over the period 2006-2099 in the four sites. Nine CMIP5 models and two RCP scenarios.

Annex 6.4 Projected trends in the HydrobalPCR outputs over the period 2010-2099 under the two RCP scenarios, and the nine CMIP5 models in the forested areas in the four sites. Pr: Precipitation, netPr: Net rainfall, Eto: reference evapotranspiration, Eta: actual evapotranspiration DP: deep percolation, SWC: soil water content. All trends are expressed as mm/decade except SWC (%)/decade. * significant at 5%.

Annex 6.5 Projected trends in the HydrobalPCR outputs over the period 2010-2099 under the two RCP scenarios, and the nine CMIP5 models in the not forested areas in the four sites. Pr: Precipitation, netPr: Net rainfall, Eto: reference evapotranspiration, Eta: actual evapotranspiration DP: deep percolation, SWC: soil water content. All trends are expressed as mm/decade except SWC (%)/decade. * significant at 5%.

Annex 6.6 Water balance under the two RCP scenarios, average of the nine CMIP5 models in the forested areas in the four sites. Pr: Precipitation, netPr: Net rainfall, Eto: reference evapotranspiration, Eta: actual evapotranspiration DP: deep percolation, SWC: soil water content. All the variables are expressed as mm except SWC (%). Change is between the two 30-year periods 2010-2039 and 2070-2099.

Annex 6.7 Water balance under the two RCP scenarios, average of the nine CMIP5 models in the not forested areas in the four sites. Pr: Precipitation, netPr: Net rainfall, Eto: reference evapotranspiration, Eta: actual evapotranspiration DP: deep percolation, SWC: soil water content. All the variables are expressed as mm except SWC (%). Change is between the two 30-year periods 2010-2039 and 2070-2099.

Universitat d'Alacant
Universidad de Alicante

CAPÍTULO 1

INTRODUCCIÓN GENERAL

Universitat d'Alacant
Universidad de Alicante

1. Las previsiones del cambio climático sobre las temperaturas y precipitaciones

1.1. A escala global

A escala global, el quinto informe del Panel Intergubernamental sobre el Cambio Climático (IPCC, 2013) basándose en numerosos análisis científicos independientes de observaciones del sistema climático, archivos paleoclimáticos, estudios teóricos sobre los procesos climáticos y simulaciones que utilizan modelos climáticos ha puesto de manifiesto evidencias sobre el cambio climático. Según este informe el incremento en las temperaturas es inequívoco desde 1950, y desde 1983 al 2012 es posiblemente el periodo de 30 años más cálido de los últimos 1.400 años en el hemisferio Norte (IPCC, 2013). Los cambios en las temperaturas en las últimas décadas tienden hacia un aumento progresivo (Figura 1.1a), lo cual es un indicador del calentamiento global y uno de los efectos más evidentes del cambio climático. Un calentamiento generalizado debido al aumento en las temperaturas máximas y mínimas en la mayor parte del globo (Jones y Moberg, 2003, Vose et al., 2005) aunque con mayor aumento en el hemisferio norte en comparación con el sur (Vose et al., 2005).

A diferencia de las tendencias claras en las temperaturas, es difícil concretar los cambios en las precipitaciones debido a heterogeneidad de los resultados. A escala global las precipitaciones mostraron tendencias positivas en algunas regiones y negativas en otras con magnitudes diferentes (Figura 1.1b). Desde 1951 la disponibilidad y el nivel de confianza en los datos han aumentado y se ha observado un aumento en las precipitaciones en las latitudes medias del hemisferio Norte y tendencias negativas y positivas en otras latitudes con baja confianza (IPCC, 2014).

Las previsiones de cara al futuro no cambian de dirección ya que el quinto informe del IPCC (2013) pronostica un aumento en media global de entre de 0.3 °C a 1.7 °C bajo el escenario moderado RCP2.6, y de 2.6 °C a 4.8 °C bajo el escenario extremo RCP8.5 en el periodo 2081-2100 con respecto al periodo 1986-2005 (Figura 1.2a). Cuanto a las precipitaciones se espera un aumento en las latitudes altas, en el océano Pacífico ecuatorial y en muchas regiones húmedas de latitud media, y un descenso en muchas regiones secas de latitud media y subtropicales en el escenario RCP8.5 (Figura 2b).

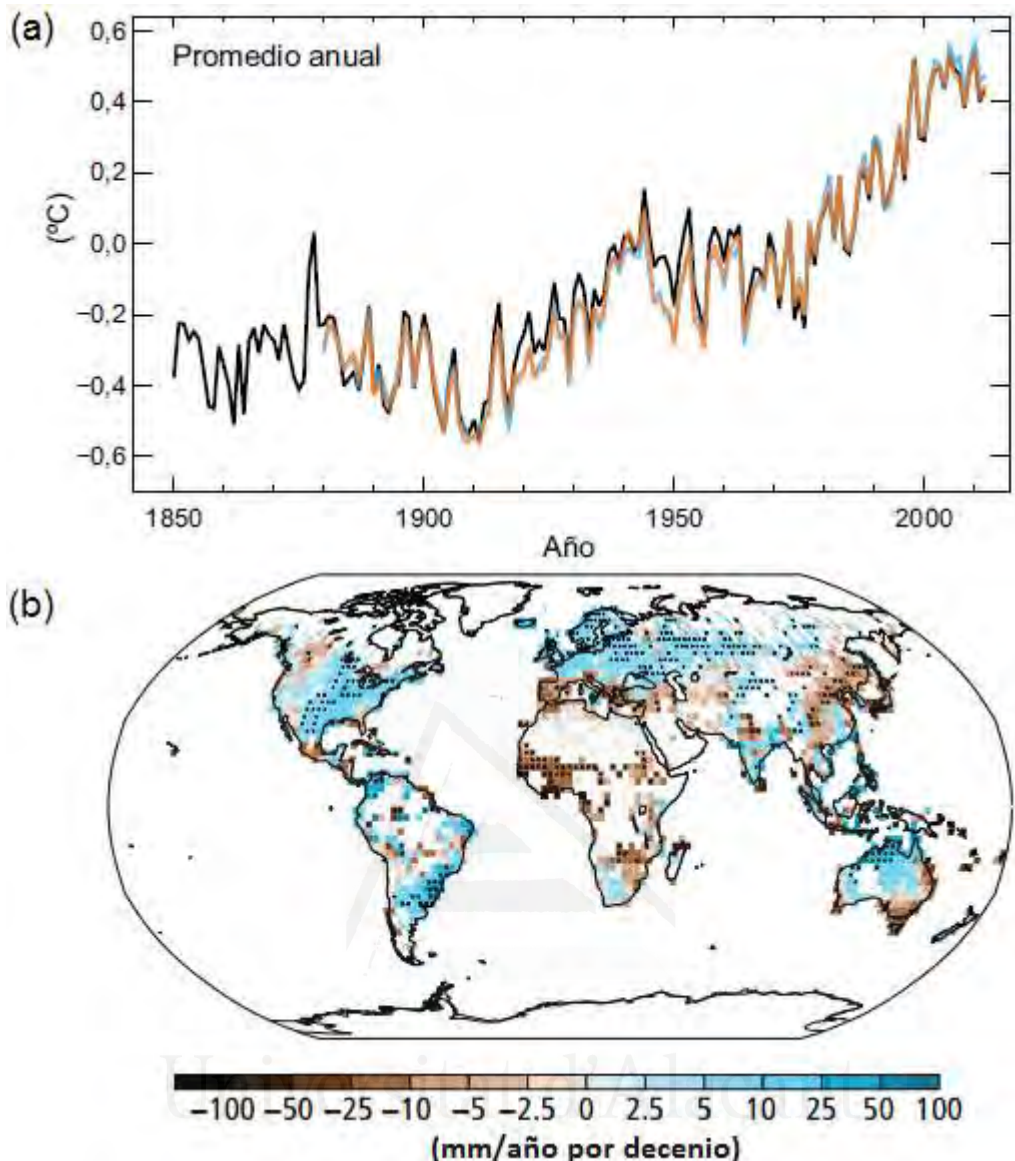


Figura 1.1: a) Anomalía observada en el promedio mundial de temperaturas en superficie, terrestres y oceánicas combinadas, 1850-2012. Las anomalías son relativas a la media del período 1961-1990. b) Mapa de los cambio observado en la precipitación entre 1951 y 2010 (Fuente: IPCC, 2014).

1.2. A escala regional

A escala regional varios trabajos han puesto de manifiesto el aumento de las temperaturas en el área mediterránea (Brunetti et al. 2009; Toreti et al., 2010; Hertig et al., 2010), y particularmente en la Península Ibérica donde se ha venido detectando uno de los aumentos más notables (Brunet et al., 2007, Gonzalez-Hidalgo et al., 2014) en las últimas décadas. Las precipitaciones en la zona del Mediterráneo mostraron tendencias de descenso en general (Figura 1b) (IPCC 2014). En la península ibérica no se observaron claras tendencias de cambio en general por la complejidad de los patrones

de las precipitaciones. Sin embargo, en el sur de la península y en las islas canarias se observaron tendencias negativas en la segunda mitad del siglo 20 (Moreno, 2005).

En el Mediterráneo, los cambios esperados son aún mayores ya que el último informe del (IPCC, 2013) señala a esta zona como una de las regiones que se verán especialmente afectadas por el cambio climático y donde las temperaturas seguirán aumentando a un ritmo mayor al detectado en las últimas décadas y las precipitaciones mostraran tendencias al descenso en general (Figura 1.2b). En la península ibérica se espera, que en el siglo 21, las temperaturas seguirán subiendo y las precipitaciones bajando según varios modelos globales de cambio climático (Moreno, 2005) profundizando el carácter extremo de las condiciones climáticas de la península, especialmente en las regiones del mediterraneo y del sur peninsular (Olcina Cantos, 2010).

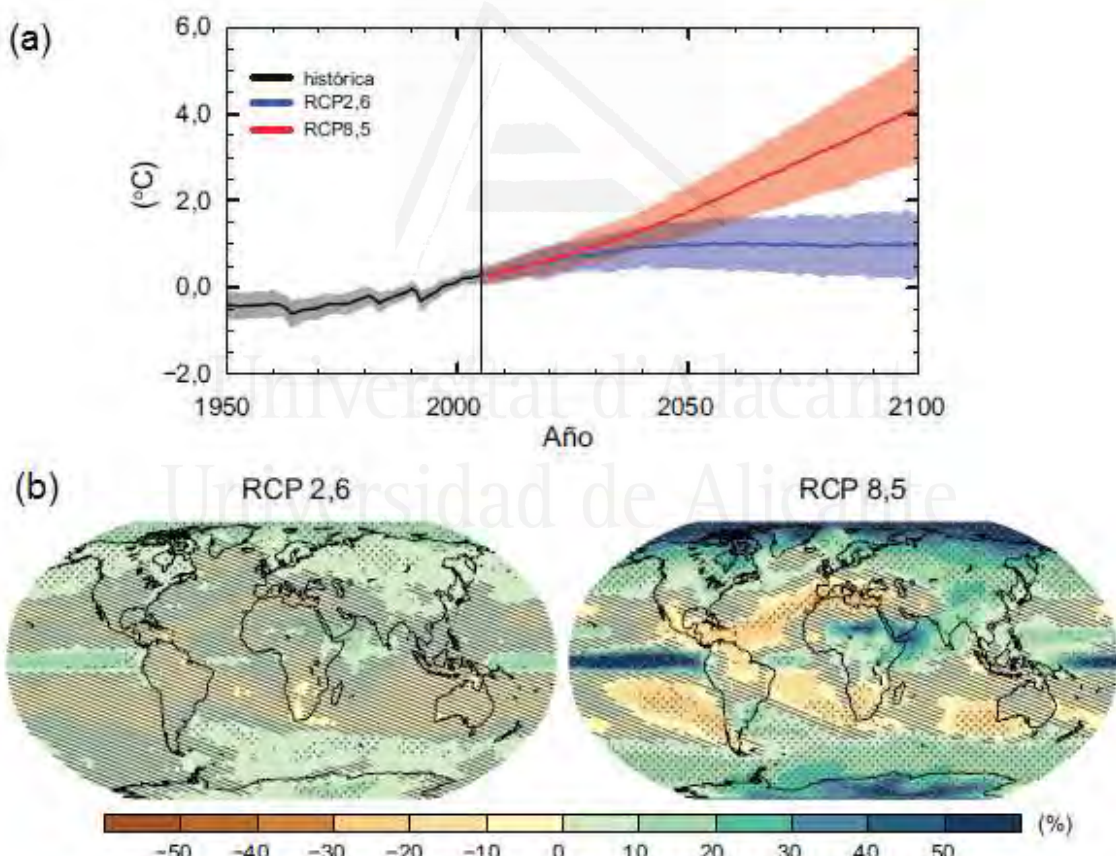


Figura 1.2: a) El cambio anual en la temperatura media global en superficie respecto de 1986-2005. Series temporales simuladas, basadas en modelos múltiples de la quinta fase del Proyecto de comparación de modelos acoplados (CMIP5) de los escenarios RCP2.6 y RCP8.5, entre 1950 y 2100. b) el cambio de la media porcentual de la precipitación media anual en el periodo 2081-2100 respecto de 1986-2005. Mapas de resultados medios de modelos múltiples de la quinta fase del Proyecto de comparación de modelos acoplados (CMIP5) de los escenarios RCP2.6 y RCP8.5 (Fuente: IPCC, 2013)

1.3. A escala local

1.3.1. Los indicios actuales del cambio climático en Alicante

La provincia de Alicante se encuentra en la costa mediterránea de la península ibérica y forma parte de la Comunidad Valenciana donde varios trabajos sobre el clima se llevaron a cabo en los últimos años (De Luis et al., 1997; 2000; González-Hidalgo et al., 2003; Vicente-Serrano et al., 2004). Estos trabajos han puesto de manifiesto la alta variabilidad espacial y temporal de las precipitaciones en esta zona.

En los últimos sesenta años hasta el 2012, la tendencia media de la precipitación en Alicante es negativa (-9.4 mm/década) (Tabla 1.1). Sin embargo, esa tendencia presenta una variabilidad espacial muy importante. En efecto, la precipitación mostrará tendencias positivas en la parte extremo norte y en la mitad sur y tendencias negativas en la parte sur de la mitad norte. No obstante, solo las tendencias negativas en esta zona de transición entre el clima mediterráneo seco y arido son significativas (Moutahir et al., 2014). Estas tendencias negativas han hecho que entre el periodo 1953-1982 y el periodo 1983-2012 los pisos bioclimáticos, según la clasificación de Rivas-Martínez (1983) se desplacen hacia el norte (Figura 1.3).

Al contrario de las precipitaciones, las temperaturas máximas y mínimas mostraron tendencias positivas (+0.16 y +0.20 °C/década respectivamente) y significativas en el periodo 1953-2012 (Tabla 1.1). Sin embargo, estas tendencias positivas no lo han sido todo el tiempo. En efecto, se ve una tendencia negativa hasta el año 1973 y luego una clara tendencia de aumento desde este año (Figura 1.4).

Tabla 1.1: Tendencias medias en la precipitación (Pr) anual (mm/década) y en las temperaturas (T) máxima, mínima y media (°C/década) en Alicante en el periodo 1953-2012. (Fuente: elaboración propia)

	Pr anual	T max	T min	T med
Tendencias	-9.4	0.16***	0.20***	0.18***

*, **, *** significativas al 5%, 1% y 0.1% respectivamente

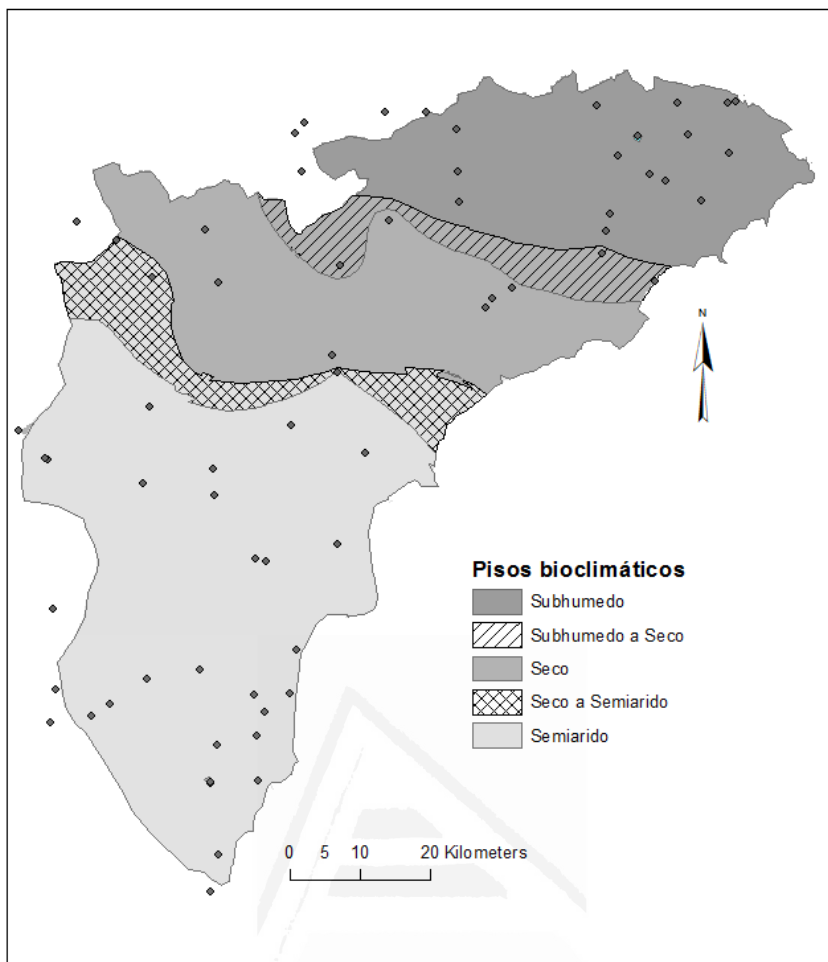


Figura 1.3: los pisos bioclimáticos en la provincia de Alicante según la clasificación de Rivas-Martínez (1983) y las zonas de transición entre los períodos 1953-1982 y 1983-2012. Los puntos representan las estaciones meteorológicas usadas (Fuente: elaboración propia)

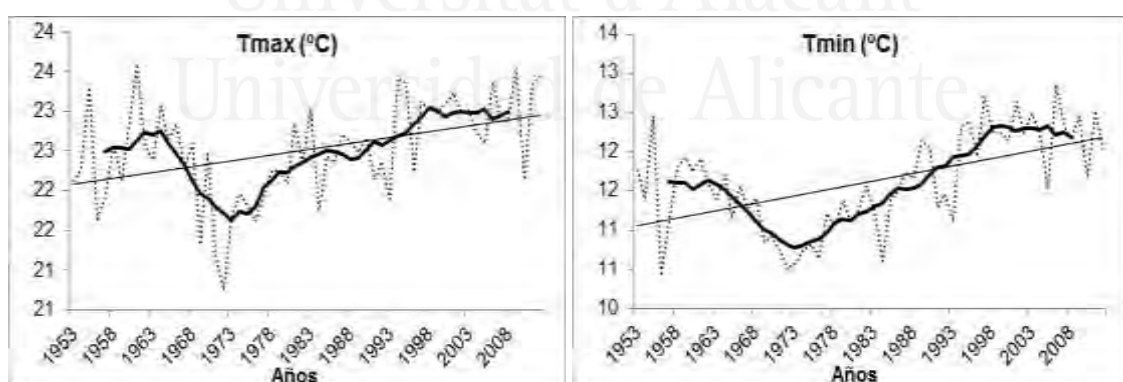


Figura 1.4: Evolución de las temperaturas máximas y mínimas en la provincia de Alicante en el periodo 1953-2012. La línea en negrita es media móvil cada 9 años (Fuente: elaboración propia)

1.3.2. Previsiones futuras

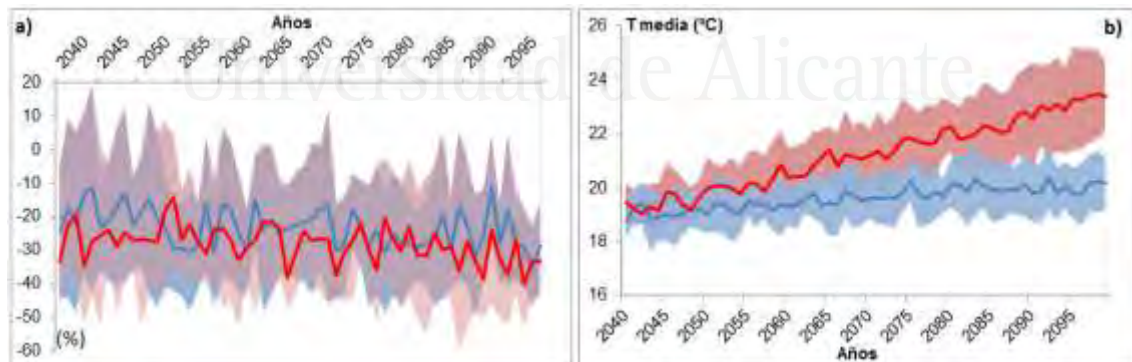
Según los datos de los nueve modelos múltiples de la quinta fase del Proyecto de comparación de modelos acoplados (CMIP5) utilizados en este trabajo (Anexo1.1:

Tabla 1), las precipitaciones seguirán disminuyendo (-6.1 ± 0.8 y -6.2 ± 0.6 mm/década en promedio bajo los escenarios RCP4.5 y RCP8.5 respectivamente) en el futuro (Tabla 1.2). Una reducción de hasta más 30% respecto del periodo 1953-2012 es probable bajo los dos escenarios de emisión RCP4.5 y RCP8.5 para el final del siglo 21 (Figura 1.5a). Las temperaturas seguirán subiendo en el futuro a un ritmo mayor bajo el escenario extremo RCP8.5 (0.73 ± 0.18 °C/década) en comparación con el escenario moderado RCP4.5 (0.2 ± 0.07 °C/década) (Tabla 2, Figura 1.5b).

Tabla 1.2: Tendencias proyectadas de la precipitación anual y la temperatura media anual en Alicante en el periodo 2040-2099 según nueve CMIP5 modelos y bajo dos escenarios. (Fuente: elaboración propia)

	Precipitación mm/década		Temperatura °C/década	
	RCP4.5	RCP8.5	RCP4.5	RCP8.5
BCC-CSM1-1	-20.9	-9.1	0.15**	0.58***
CanESM2	-6.4	-6.3	0.24***	0.82***
CNRM-CM5	-9.4	-8.0	0.18***	0.59***
GFDL-ESM2M	+6.3	-3.0	0.1*	0.58***
HADGEM2-CC	-5.7	-16.3	0.3***	1.04***
MIROC-ESM-CHEM	-2.4	+1.4	0.31***	0.99***
MPI-ESM-MR	-4.6	-7.5	0.13**	0.73***
MRI-CGCM3	-6.8	+0.6	0.2***	0.62***
NorESM1	-5	-7.8	0.2***	0.64***
Promedio	-6.1 ± 0.8	-6.2 ± 0.6	0.2 ± 0.07	0.73 ± 0.18

*, **, *** significativas al 5%, 1% y 0.1% respectivamente



2. Efectos probables del cambio climático

2.1. Los extremos climáticos

Los cambios en las medias de las temperaturas y precipitaciones no son los únicos cambios observados. En efecto, en el informe especial sobre los fenómenos climáticos extremos, el IPCC (2012) señala que es muy probable que se haya producido un descenso generalizado del número de días y noches fríos y un aumento generalizado del número de días y noches cálidos a escala mundial. Cuanto a las precipitaciones, se han observado tendencias significativas desde un punto de vista estadístico en el número de precipitaciones intensas en algunas regiones (Frich et al. 2002; Kostopoulou and Jones, 2005; Alexander et al., 2006; IPCC, 2012).

El cambio climático es probable que tenga un efecto intensificador en los fenómenos climáticos extremos. Un clima cambiante produce cambios en la frecuencia, la intensidad, la extensión espacial, la duración y las circunstancias temporales de los fenómenos meteorológicos y climáticos extremos, y puede dar lugar a fenómenos meteorológicos y climáticos extremos sin precedentes (IPCC, 2012). Numerosos trabajos científicos pronostican cambios en los extremos climáticos a escala mundial (Easterling et al., 2000; Arblaster and Alexander, 2005; IPCC, 2012; 2013) y a escala regional en la zona mediterránea (Sánchez et al., 2004; Goubanova and Li, 2007; IPCC, 2012) y particularmente en la península ibérica (Monjo et al., 2016). Todos estos trabajos coinciden en que los eventos extremos de temperaturas y precipitaciones van a aumentar en el futuro. Olas de calor, sequías frecuentes, inundaciones y tormentas son ejemplos de los efectos esperados de los posibles cambios en los extremos climáticos.

2.2. Efectos del cambio climático en la disponibilidad del agua

Según el IPCC (2013) es probable que las influencias antropógenas hayan afectado al ciclo global del agua desde 1960. Influencias que han contribuido a los cambios a escala global en los patrones de precipitación en la superficie terrestre y a la intensificación de precipitaciones fuertes. Estos cambios junto a los aumentos en las temperaturas que aumentan a su vez la evapotranspiración afectan a la disponibilidad del agua para el uso humano como para los ecosistemas.

En la zona mediterránea, los trabajos sobre el cambio climático pronostican un aumento en las temperaturas y un descenso en las precipitaciones (Sánchez et al., 2004; Bates et al., 2008; IPCC, 2013). Estos dos cambios afectaran a las principales componentes del balance hídrico que controlen la disponibilidad del agua. El aumento de las temperaturas aumentará la evapotranspiración que se traduce en una pérdida de agua del sistema por la vegetación o por la evaporación directa reduciendo la humedad del suelo que no se renueva por el descenso en las precipitaciones. A su vez la reducción en las precipitaciones se traduce en una reducción en la escorrentía superficial y en la recarga de los acuíferos. Sin embargo, el descenso de las precipitaciones es probable que esté acompañado con un aumento en la intensidad (IPCC, 2012; Monjo et al., 2016) lo que puede aumentar la escorrentía superficial en momentos puntuales con todas sus consecuencias socioambientales. La concentración de la lluvia en eventos puntuales alarga los periodos entre estos eventos y por lo tanto los periodos de sequía reduciendo la humedad en el suelo y la recarga de los acuíferos que pueden causar la llamada sequía de las aguas subterráneas (groundwater droughts) (Van Lanen and Peters, 2000; Mishra and Singh, 2010).

2.3. Efectos del cambio climático en la vegetación

Varios estudios se llevaron a cabo en los últimos años tratando de explorar los posibles efectos de los cambios del clima en la vegetación. Todos estos estudios coinciden en el hecho de que cambios en las precipitaciones y temperaturas han afectado y van a afectar a las plantas y la vegetación (Theurillat and Guisan, 2001; Bachelet et al., 2001; Gitay et al., 2002; Scheiter and Higgins, 2009; Ceccherini et al., 2014). Dichos cambios, sobre todo la subida de las temperaturas en algunas zonas, han afectado a la estación de la reproducción plantas, a la extensión de la estación de crecimiento, a la distribución de las especies y el tamaño de sus poblaciones, y a la frecuencia de las plagas y brotes de enfermedades.

Según el informe del IPCC (Gitay et al., 2002) sobre los impactos del cambio climático en la biodiversidad, se espera a que dicho cambio afecte a todos los aspectos de la biodiversidad. Se espera que el cambio climático afecte directamente a organismos individuales, a poblaciones, a la distribución de especies, y al funcionamiento de los ecosistemas e indirectamente aumentando la frecuencia de incendios forestales por ejemplo. La pérdida, modificación, fragmentación e incluso desplazamiento del hábitat,

y la introducción y extensión de especies no autóctonas son otros efectos esperados bajo el cambio climático.

En España, Fernández-González et al., (2005) indicaron que los impactos directos del cambio climático sobre la diversidad vegetal se producirán a través de dos efectos: el calentamiento, que alarga el período de actividad de las plantas e incrementa su productividad, y la reducción de las disponibilidades hídricas, que actúa en sentido contrario. La “mediterraneización” del norte peninsular y la “aridización” del sur son las tendencias más significativas durante el próximo siglo. En el sur y sobre todo en el suroeste peninsular, la mayor vulnerabilidad se prevé en los bosques y arbustadas caducifolios sensibles a la agudización de la sequía estival, los bosques esclerófilos y la vegetación litoral (Fernández-González et al., 2005).

3. Antecedentes de la presente investigación

En esta tesis doctoral se pretende analizar los posibles efectos del cambio climático en los recursos de agua y en la vegetación en la provincia de Alicante. Esta región forma parte de la zona mediterránea señalada como una de las zonas más vulnerables al cambio climático (IPCC, 2013), con un clima semiárido en la mayor parte de la provincia y una demanda de agua cada vez mayor. En este contexto, varios proyectos de investigación sobre los recursos de agua y la vegetación se llevaron a cabo, en el Dpto. de Ecología de la Universidad de Alicante, a diferentes escalas y con distintos objetivos para conocer el funcionamiento actual de nuestros ecosistemas más representativos y sus perspectivas de futuro.

Los primeros trabajos (década de los 90) estudiaron los procesos hidrológicos a escala de parcelas experimentales y mediante simulaciones de lluvia. Estos trabajos analizaron los diferentes componentes del balance hídrico bajo diferentes cubiertas vegetales. En ellos se intentó cuantificar la escorrentía superficial en función de la precipitación dependiendo de la cubierta vegetal (Derouiche, 1996; Abdelli, 1999). Se analizó el efecto de la vegetación en la evolución de la humedad en el suelo (Hernández, 1998), y se hizo una cuantificación de la transcolación y de la escorrentía cortical en función de la precipitación y de la vegetación (Abdelli, 1999; Chirino, 2003). Otros proyectos (entre 2000 y 2010) relacionados con los anteriores trataron de estudiar la escorrentía superficial y la erosión de los suelos a escala de ladera y microcuenca (Chirino et al.,

2006; Bautista et al., 2007; Mayor et al., 2007; Mayor, 2008) además del estudio de los patrones de distribución espacial de las plantas y la conectividad de las zonas de suelo desnudo fuentes de la escorrentía superficial y su efecto en la escorrentía y la erosión (Bautista et al., 2007; Mayor et al., 2008). En la década actual, se inició el estudio de los efectos de los balances hídricos sobre la recarga de los acuíferos, como tema principal, centrándose en el estudio del acuífero kárstico de la sierra del Ventós (Chirino, 2003; Touhami, 2007; Touhami et al., 2013, 2014, 2015), actualmente ampliado a 4 acuíferos de la provincia.

Como resultado de estos trabajos se ejaboró el modelo eco-hidrológico HYDROBAL con el objetivo de analizar las consecuencias de los cambios de la cubierta vegetal sobre el balance hídrico en el suelo y la recarga del acuífero. . (Bellot et al., 1999, Bellot and Chirino, 2013). Los estudios más recientes (Manrique-alba et al., 2015a; 2015b; Ruiz-Yanetti et al., 2015) aplicaron el HYDROBAL a cuatro acuíferos a lo largo de un gradiente climático en la provincia de Alicante, con resultados muy satisfactorios. Sin embargo, la incertidumbre es algo inherente a la aplicación de modelos de simulación, y en este caso, se ve aumentada por la dificultad derivada de las previsiones de los modelos de cambio climático.

En este contexto, se realizó la presente investigación, en la que se abordan los balances hídricos desde la perspectiva de los efectos del cambio climático. Para ello se cambió la escala del trabajo y se realizaron tres de los cinco estudios contenidos en ella a escala de toda la provincia de Alicante, uno a escala de una comarca y el último en cuatro acuíferos de la provincia.

4. Objetivos

Esta tesis doctoral tiene, como objetivo general, evaluar algunos de los posibles efectos del cambio climático en los recursos de agua y en la vegetación, a través del posible efecto en su periodo de crecimiento, en la provincia de Alicante. Para alcanzar este objetivo genenal se plantearon los siguientes objetivos específicos:

- 1) Analizar el clima (observado y proyectado) en la provincia de Alicante a través del análisis los cambios en las medias, las tendencias y los extremos climáticos,

2) Analizar los posibles cambios en la frecuencia y magnitud de los eventos grandes de lluvia que producen apreciables recargas de los acuíferos de la provincia.

3) Aplicar la técnica de análisis de los cambios en la fenología de superficie (LSP de las siglas en inglés Land Surface Phenology) en relación a las variables climáticas en las áreas con vegetación natural en Alicante en el periodo 2000-2012 y bajo los escenarios de cambio climático.

4) Analizar los posibles cambios en los periodos de crecimiento de los cultivos bajo los escenarios de cambio climático en una de las comarcas de la provincia de Alicante.

5) Usar una plataforma de modelización ambiental para optimizar la aplicación del modelo HYDROBAL, que permita su aplicación a múltiples zonas, años y estructuras vegetales, de un modo integrado y en un tiempo reducido.

Estos objetivos corresponden a los Capítulos 2 a 6 de esta memoria. Cada capítulo es independiente, ya que se presenta en un formato de artículo científico con sus diferentes partes: introducción, área de estudio, metodología, resultados, discusión, bibliografía y anexos propios de cada capítulo. En consecuencia, algunas partes pueden repetirse aunque en un contexto diferente y para objetivos distintos.

El análisis del clima observado y proyectado se hace en diferentes capítulos de esta tesis. En la introducción se hace una breve descripción del clima observado en los últimos 60 años hasta el 2012 y el proyectado hasta el final del siglo. En el primer capítulo se hace un análisis de los extremos de precipitaciones en la provincia de Alicante en los últimos 60 años. Finalmente, otros aspectos de las precipitaciones y las temperaturas se analicen en los otros capítulos según el objetivo de cada uno. Excepto en el caso del objetivo 4, los datos del cambio climático utilizados en los diferentes análisis corresponden a las proyecciones climáticas de la quinta fase del Proyecto de comparación de modelos acoplados (CMIP5). En este trabajo se utilizaron datos de nueve modelos CMIP5 presentados en la Tabla 1 en Anexo1.1 y por más detalle consultar Monjo et al. (2015).

Referencias bibliográficas

Abdelli F., (1999). Análisis comparativo de distintas comunidades vegetales a la distribución del agua de lluvia, a la conservación del agua en el suelo y a la recarga de

acuíferos en medios semiáridos. M.Sc. thesis dissertation, Instituto Agronómico Mediterráneo de Zaragoza (IAMZ). p. 160.

Alexander, L. V., Zhang, X., Peterson, T. C., Caesar, J., Gleason, B., Klein Tank, A. M. Haylock, G., M., Collins, D., Trewin, B., Rahimzadeh, F., Tagipour, A., Rupa Kumar, K., Revadekar, J., Griffiths, G., Vincent, L., Stephenson, D. B., Burn, J., Aguilar, E., Brunet, M., Taylor, M., New, M., Zhai, P., Rusticucci, M., J. L. Vazquez-Aguirre (2006). Global observed changes in daily climate extremes of temperature and precipitation. *Journal of Geophysical Research: Atmospheres*, 111(D5).

Arblaster, J., & Alexander, L. (2005). Extreme change: an analysis of past, present and future changes in global temperature and precipitation indices. *Bull Aust Met Ocean Soc*, 18, 125-130.

Bachelet, D., Neilson, R. P., Lenihan, J. M., & Drapek, R. J. (2001). Climate change effects on vegetation distribution and carbon budget in the United States. *Ecosystems*, 4(3), 164-185.

Bates, B.C., Z.W. Kundzewicz, S. Wu and J.P. Palutikof, Eds., 2008: Climate Change and Water. Technical Paper of the Intergovernmental Panel on Climate Change, IPCC Secretariat, Geneva, 210 pp.

Bautista, S., Mayor, A. G., Bourakhoudar, J., & Bellot, J. (2007). Plant spatial pattern predicts hillslope runoff and erosion in a semiarid Mediterranean landscape. *Ecosystems*, 10(6), 987-998.

Bellot, J., Sanchez, J. R., Chirino, E., Hernandez, N., Abdelli, F., Martinez, J. M. (1999). Effect of different vegetation type cover on the soil water balance in semi-arid areas of South Eastern Spain. *Physics and Chemistry of the Earth (B)*. Vol. 24: 353-357

Bellot, J., Chirino, E., (2013). Hydrobal: An eco-hydrological modelling approach for assessing water balances in different vegetation types in semi-arid areas. *Ecological Modelling*. 266.

Bentsen, M., Bethke, I., Debernard, J.B., Iversen, T., Kirkevåg, A., Seland, Ø., Drange, H., Roelandt, C., Seierstad, I.A., Hoose, C., Kristjánsson, J.E., 2012. The Norwegian Earth System Model, NorESM1-M – Part 1: Description and basic evaluation.

Geoscientific Model Development Discussion 5: 2843-2931. doi:10.5194/gmdd-5-2843-2012.

Brunet, M., P. D. Jones, J. Sigró, O. Saladié, E. Aguilar, A. Moberg, P. M. Della-Marta, D. Lister, A. Walther, and D. López (2007), Temporal and spatial temperature variability and change over Spain during 1850–2005, *J. Geophys. Res.*, 112, D12117, doi:10.1029/2006JD008249.

Brunetti, M., Lentini, G., Maugeri, M., Nanni, T., Auer, I., Boehm, R., & Schoener, W. (2009). Climate variability and change in the Greater Alpine Region over the last two centuries based on multi-variable analysis. *International Journal of Climatology*, 29(15), 2197-2225.

Ceccherini, G., Gobron, N., & Migliavacca, M. (2014). On the response of European vegetation phenology to hydroclimatic anomalies. *Remote Sensing*, 6(4), 3143-3169.

Chirino, E., (2003). Influencia de las precipitaciones y de la vegetación en el balance hídrico superficial y la recarga de acuíferos en clima semiárido. PhD Dissertation, Universidad de Alicante, Spain. <http://rua.ua.es/dspace/handle/10045/3386>.

Chirino, E., Bonet, A., Bellot, J., & Sánchez, J. R. (2006). Effects of 30-year-old Aleppo pine plantations on runoff, soil erosion, and plant diversity in a semi-arid landscape in south eastern Spain. *Catena*, 65(1), 19-29.

Chylek, P., Li, J., Dubey, MK., Wang, M., Lesins, G., 2001. Observed and model simulated 20th century Arctic temperature variability: Canadian Earth System Model CanESM2. *Atmos. Chem. Phys. Discuss.* 11: 22893-22907, doi:10.5194/acpd-11-22893-2011.

Clarke, L., J. Edmonds, H. Jacoby, H. Pitcher, J. Reilly, R. Richels, 2007. Scenarios of Greenhouse Gas Emissions and Atmospheric Concentrations. Sub-report 2.1A of Synthesis and Assessment Product 2.1 by the U.S. Climate Change Science Program and the Subcommittee on Global Change Research. Department of Energy, Office of Biological & Environmental Research, Washington, 7 DC., USA, 154 pp.

Collins, W.J., Bellouin, N., Doutriaux-Boucher, M., Gedney, N., Hinton, T., Jones, C.D., Liddicoat, S., Martin, G., O'Connor, F., Rae, J., Senior, C., Totterdell, I.,

Woodward, S., Reichler, T., Kim, J., Halloran, P., 2008. Evaluation of the HadGEM2 model. Hadley Centre Technical Note HCTN 74, Met Office Hadley Centre, Exeter, UK.

De Luis, M., González-Hidalgo, J. C., Raventós, J., Sánchez, J. R., & Cortina, J. (1997). Distribución espacial de la concentración y agresividad de la lluvia en el territorio de la Comunidad Valenciana. Cuaternario y Geomorfología, 11(3-4), 33-44.

De Luis, M. D., Raventós, J., González-Hidalgo, J. C., Sánchez, J. R., & Cortina, J. (2000). Spatial analysis of rainfall trends in the region of Valencia (East Spain). Int. J. Climatol, 20(12), 1451-1469.

Derouiche, A., (1996). Estimation et modélisation des composantes du bilan hidrique chez différentes firmatios arborees, arbustives et herbacees méditerranéennes. M.Sc. Thesis Dissertation, Instituto Agronómico Mediterráneo de Zaragoza (IAMZ), Departamento de Ecología. Universidad de Alicante. 158 pp.

Dunne, J.P., John, J.G., Adcroft, A.J., Griffies, S.M., Hallberg, R.W., Shevliakova, E., Stouffer, R.J., Cooke, W., Dunne, K.A., Harrison, M.J., Krasting, J.P., Malyshev, S.L., Milly, P.C.D., Phillipps, P.J., Sentman, L.T., Samuels, B.L., Spelman, M.J., Winton, M., Wittenberg, A.T., Zadeh, N., 2012. GFDL's ESM2 Global Coupled Climate-Carbon Earth System Models. Part I: Physical Formulation and Baseline Simulation Characteristics. *J. Clim.*, 25: 6646–6665. doi:10.1175/JCLI-D-11-00560.1.

Easterling, D. R., Meehl, G. A., Parmesan, C., Changnon, S. A., Karl, T. R., & Mearns, L. O. (2000). Climate extremes: observations, modeling, and impacts. *science*, 289(5487), 2068-2074.

Fernández-González, F., Loidi, J., Moreno, J. C., Del Arco, M., & Fernández-Cancio, A. (2005). Impactos sobre la biodiversidad vegetal. Evaluación preliminar de los impactos en España por efecto del cambio climático, 183-247.

Frich, P., L.V. Alexander, P. Della-Marta, B. Gleason, M. Haylock, A.M.G. Klein Tank, and T. Peterson (2002). Observed coherent changes in climatic extremes during the second half of the twentieth century, *Clim. Res.*, 19, 193-212.

Fujino, J., R. Nair, M. Kainuma, T. Masui, Y. Matsuoka, (2006). Multi-gas mitigation analysis on stabilization scenarios using AIM global model. Multigas Mitigation and Climate Policy. *The Energy Journal*, 3 (Special Issue).

Gitay, H., Suárez, A., Watson, R., & Dokken, D. J. (2002). Cambio climático y biodiversidad. Documento técnico V del IPCC.

González-Hidalgo, J. G., De Luis, M., Raventós, J., & Sánchez, J. R. (2003). Daily rainfall trend in the Valencia Region of Spain. *Theoretical and Applied Climatology*, 75(1-2), 117-130.

Gonzalez-Hidalgo, J.C., Peña-Angulo, D., Simolo, C., Brunetti, M., Cortesi, N., (2014). Variación espacial de las tendencias de los promedios estacionales de las máximas y de las mínimas en España (1951-2010). En: Fernández-Montes, S. y Rodrigo, F.S. (Eds). Cambio climático y cambio global. Publicaciones de la Asociación Española de Climatología (AEC). Serie A, nº9. Almería. ISBN: 978-84-16027-69-9. pp. 99-108.

Goubanova, K., & Li, L. (2007). Extremes in temperature and precipitation around the Mediterranean basin in an ensemble of future climate scenario simulations. *Global and Planetary Change*, 57(1), 27-42.

Hernández, N., (1998). Efecto del tipo de cubierta vegetal sobre la evolución temporal de la humedad del suelo. Tesis de licenciatura. Departamento de Ecología, Universidad de Alicante

Hertig, E., Seubert, S., and Jacobbeit, J., (2010). Temperature extremes in the Mediterranean area: trends in the past and assessments for the future, *Nat. Hazards Earth Syst. Sci.*, 10, 2039-2050, doi:10.5194/nhess-10-2039-2010.

Hijioka, Y., Y. Matsuoka, H. Nishimoto, M. Masui, and M. Kainuma, (2008). Global GHG emissions scenarios under GHG concentration stabilization targets. *Journal of Global Environmental Engineering* 13, 97-108.

IPCC, 2012: “Resumen para responsables de políticas” en el Informe especial sobre la gestión de los riesgos de fenómenos meteorológicos extremos y desastres para mejorar la adaptación al cambio climático [edición a cargo de C. B. Field, C. B., V. Barros, T. F. Stocker, D. Qin, D. J. Dokken, K. L. Ebi, M. D. Mastrandrea, K. J. Mach, G. -K.

Plattner, S. K. Allen, M. Tignor, y P. M. Midgley]. Informe especial de los Grupos de trabajo I y II del Grupo Intergubernamental de Expertos sobre el Cambio Climático, Cambridge University Press, Cambridge, Reino Unido y Nueva York, Nueva York, Estados Unidos de América, págs. 1-19.

IPCC, (2013): Climate Change 2013: The Physical Science Basis. Contribution of Working Group I to the Fifth Assessment Report of the Intergovernmental Panel on Climate Change [Stocker, T.F., D. Qin, G.-K. Plattner, M. Tignor, S.K. Allen, J. Boschung, A. Nauels, Y. Xia, V. Bex and P.M. Midgley (eds.)]. Cambridge University Press, Cambridge, United Kingdom and New York, NY, USA, 1535 pp, doi:10.1017/CBO9781107415324.

IPCC, (2014): Cambio climático 2014: Informe de síntesis. Contribución de los Grupos de trabajo I, II y III al Quinto Informe de Evaluación del Grupo Intergubernamental de Expertos sobre el Cambio Climático [Equipo principal de redacción, R.K. Pachauri y L.A. Meyer (eds.)]. IPCC, Ginebra, Suiza, 157 págs.

Iversen, T., Bentsen, M., Bethke, I., Debernard, J.B., Kirkevåg, A., Seland, Ø., Drange, H., Kristjánsson, J.E., Medhaug, I., Sand, M., Seierstad, I.A., 2012. The Norwegian Earth System Model, NorESM1-M – Part 2: Climate response and scenario projections. Geosci. Model. Dev. Discuss. 5: 2933-2998. doi:10.5194/gmdd-5-2933-2012.

Jones, P. D., and A. Moberg (2003), A hemispheric and large-scale surfaceair temperature variations: An extensive revision and an update to 2001, J. Clim., 16, 206–223.

Kostopoulou, E., & Jones, P. D. (2005). Assessment of climate extremes in the Eastern Mediterranean. Meteorology and Atmospheric Physics, 89(1-4), 69-85.

Manrique-Alba, A., Ruiz-Yanetti, S., Chirino, E., Moutahir, H., González, C., & Bellot, J. (2015a). El balance hídrico en el suelo de 4 pinares (*Pinus halepensis*) de repoblación de la provincia de Alicante. Cuadernos de la Sociedad Española de Ciencias Forestales, (41), 183–194.

Manrique-Alba, A., Ruiz-Yanetti, S., Moutahir, H., Chirino, E., Lledó, MJ. and Bellot, J., (2015b). Role of afforestation on soil water balance in Mediterranean areas. In Breil, P., (Ed). Measuring, Modeling and Managing of the natural processes related to water

flows - Social values of the linked ecosystem services. Book of abstracts of the international conference Ecohydrology, Lyon, France.

Marsland, S.J., Haak, H., Jungclaus, J.H., Latif, M., Roeske, F., 2003. The Max-Planck-Institute global ocean/sea ice model with orthogonal curvilinear coordinates. Ocean Modelling 5: 91-127. doi: 10.1016/S1463-5003(02)00015-X.

Mayor, A. G., Bautista, S., Llovet, J., & Bellot, J. (2007). Post-fire hydrological and erosional responses of a Mediterranean landscape: Seven years of catchment-scale dynamics. *Catena*, 71(1), 68-75.

Mayor, A. G., (2008). El papel de la dinámica Fuente-sumidero en la respuesta hidrológica, a varias escalas, de una zona mediterránea semiárida. Tesis doctoral, Universidad de Alicante, España, 173p

Mayor, Á. G., Bautista, S., Small, E. E., Dixon, M., & Bellot, J. (2008). Measurement of the connectivity of runoff source areas as determined by vegetation pattern and topography: a tool for assessing potential water and soil losses in drylands. *Water Resources Research*, 44(10).

Mishra, A. K., Singh, V. P. 2010. A review of drought concepts. *Journal of Hydrology*, 391(1), 202-216.

Moreno, J.M. (Ed). (2005). A Preliminary Assessment of the Impacts in Spain due to the Effects of Climate Change. ECCE Project-Final Report. Spanish Ministry of Environment-University of Castilla de la Mancha, Madrid, 786.

Monjo, R., Gaitán, E., Pórtoles, J., Ribalaygua, J., Torres, L., 2015. Changes in extreme precipitation over Spain using statistical downscaling of CMIP5 projections. *Int. J. Climatol.*

Monjo, R., Gaitán, E., Pórtoles, J., Ribalaygua, J., & Torres, L. (2016). Changes in extreme precipitation over Spain using statistical downscaling of CMIP5 projections. *International Journal of Climatology*, 36(2), 757-769.

Moutahir, H., De Luis, M., Serrano-Notivoli, R., Touhami, I., Bellot, J., (2014). Análisis de los eventos climáticos extremos en la provincia de Alicante, Sureste de España. En: Fernández-Montes, S. y Rodrigo, F.S. (Eds). Cambio climático y cambio

global. Publicaciones de la Asociación Española de Climatología (AEC). Serie A, nº9. Almería. ISBN: 978-84-16027-69-9. pp. 457-466.

OLCINA CANTOS, J. (2010) “Cambio climático y riesgos climáticos en España”, Investigaciones Geográficas, 49. Instituto Universitario de Geografía. Universidad de Alicante, pp. 197-220.

Raddatz, T.J., Reick, C.H., Knorr, W., Kattge, J., Roeckner, E., Schnur, R., Schnitzler, K.G., Wetzel, P., Jungclaus, J., 2007. Will the tropical land biosphere dominate the climate-carbon cycle feedback during the twenty first century? Climate Dynamics 29: 565-574. doi: 10.1007/s00382-007-0247-8.

Rao, S. & Riahi, K. (2006). The role of non-CO₂ greenhouse gases in climate change mitigation: Long-term scenarios for the 21st century. Multigas mitigation and climate policy. The Energy Journal. 3 (Special Issue), 177–200.

Riahi, K. Gruebler, A. and Nakicenovic N. (2007). Scenarios of long-term socio-economic and environmental development under climate stabilization. Technological Forecasting and Social Change 74, 7, 887-935. Available at <http://dx.doi.org/10.1016/j.techfore.2006.05.026>.

Rivas-Martínez, S., (1983). Pisos bioclimáticos de España. Lazaroa, 5: 33-43.

Ruiz-Yanetti, S., Manrique-Alba, A., Moutahir, H., Chirino, E., Lledó, MJ., Maturano, A. and Bellot, J. (2015). Soil water conservation and deep percolation in Mediterranean shrublands in a climatic gradient of southeast Spain. In Breil, P., (Ed). Measuring, Modeling and Managing of the natural processes related to water flows - Social values of the linked ecosystem services. Book of abstracts of the international conference Ecohydrology, Lyon. France.

Sánchez, E., Gallardo, C., Gaertner, M. A., Arribas, A., & Castro, M. (2004). Future climate extreme events in the Mediterranean simulated by a regional climate model: a first approach. Global and Planetary Change, 44(1), 163-180.

Scheiter, S., & Higgins, S. I. (2009). Impacts of climate change on the vegetation of Africa: an adaptive dynamic vegetation modelling approach. Global Change Biology, 15(9), 2224-2246.

Smith, S.J. and T.M.L. Wigley, 2006. Multi-Gas Forcing Stabilization with the MiniCAM. *The Energy Journal* (Special Issue #3) pp 373-391.

Theurillat, J. P., & Guisan, A. (2001). Potential impact of climate change on vegetation in the European Alps: a review. *Climatic change*, 50(1-2), 77-109.

Toreti, A., Desiato, F., Fioravanti, G., & Perconti, W. (2010). Seasonal temperatures over Italy and their relationship with low-frequency atmospheric circulation patterns. *Climatic Change*, 99(1-2), 211-227.

Touhami, I., (2007). Análisis comparativo entre varios métodos de estimación de recarga en ambientes semiáridos caso del acuífero Ventós-Castellar. Tesis Master, CIHEAM, Zaragoza, Spain, 176p.

Touhami, I., Andreu, J.M., Chirino, E., Sánchez, J.R., Moutahir, H., Pulido-Bosch, A., Martínez-Santos, P., Bellot, J. (2013). Recharge estimation of a small karstic aquifer in a semiarid Mediterranean region (southeastern Spain) using a hydrological model. *Hydrological Processes*. 27(2), 165-174.

Touhami, I., Andreu, J. M., Chirino, E., Sánchez, J. R., Pulido-Bosch, A., Martínez-Santos, P., Moutahir, H., & Bellot, J. (2014). Comparative performance of soil water balance models in computing semi-arid aquifer recharge. *Hydrological Sciences Journal*, 59(1), 193-203.

Touhami, I., Chirino, E., Andreu, J.M., Sánchez, J.R., Moutahir, H., Bellot, J. (2015). Assessment of climate change impacts on soil water balance and aquifer recharge in a semiarid region in south east Spain. *Journal of Hydrology*. 527, 619-629.

van Vuuren, D. P., Eickhout, B., Lucas, P. L. & den Elzen, M. G. J. 2006. Long-term multi-gas scenarios to stabilise radiative forcing — Exploring costs and benefits within an integrated assessment framework. *Multigas mitigation and climate policy*. *The Energy Journal*. 3 (Special Issue), 201–234.

van Vuuren, D., M. den Elzen, P. Lucas, B. Eickhout, B. Strengers, B. van Ruijven, S. Wonink, R. van Houdt, 2007. Stabilizing greenhouse gas concentrations at low levels: an assessment of reduction strategies and costs. *Climatic Change*. Available at <http://dx.doi.org/10.1007/s10584-006-9172-9>.

Vicente-Serrano, S. M., González-Hidalgo, J. C., de Luis, M., & Raventós, J. (2004). Drought patterns in the Mediterranean area: the Valencia region (eastern Spain). Climate Research, 26(1), 5-15.

Van Lanen, H. A. J., Peters, E. 2000. Definition, effects and assessment of groundwater droughts. In Drought and Drought Mitigation in Europe (pp. 49-61). Springer Netherlands.

Volodire, A., Sanchez-Gomez, E., Salas y Mélia, D., Decharme, B., Cassou, C., Sénési, S., Valcke, S., Beau, I., Alias, A., Chevallier, M., Déqué, M., Deshayes, J., Douville, H., Fernandez, E., Madec, G., Maisonnave, E., Moine, M.P., Planton, S., Saint-Martin, D., Szopa, S., Tyteca, S., Alkama, R., Belamari, S., Braun ,A., Coquart, L., Chauvin, F., 2013. The CNRM-CM5.1 global climate model: description and basic evaluation, Climate Dynamics 40: 2091-2121, doi: 10.1007/s00382-011-1259-y.

Vose,R. S., D. R. Easterling, and B. Gleason (2005), Maximum and minimum temperature trends for the globe: An update through 2004, Geophys. Res. Lett., 32, 23822, doi:10.1029/2005GL024379.

Watanabe, S., Hajima, T., Sudo, K., Nagashima, T., Takemura, T., Okajima, H., Nozawa, T., Kawase, H., Abe, M., Yokohata, T., Ise, T., Sato, H., Kato, E., Takata, K., Emori, S., Kawamiya, M., 2011. MIROC-ESM 2010: model description and basic results of CMIP5-20c3m experiments. Geoscientific Model Development 4, 845-872. doi:10.5194/gmd-4-845-2011.

Wise, MA, KV Calvin, AM Thomson, LE Clarke, B Bond-Lamberty, RD Sands, SJ Smith, AC Janetos, JA Edmonds. 2009. Implications of Limiting CO₂ Concentrations for Land Use and Energy. Science. 324:1183-1186.

Xiao-Ge, X., Tong-Wen, W., Jie, Z,. 2013. Introduction of CMIP5 Experiments Carried out with the Climate System Models of Beijing Climate Center. Advances in Climate Change Research 4: 41-49. doi: 10.3724/SP.J.1248.2013.041.

Yukimoto, S., Yoshimura, H., Hosaka, M., Sakami, T., Tsujino, H., Hirabara, M., Tanaka, T.Y., Deushi, M., Obata, A., Nakano, H., Adachi, Y., Shindo, E., Yabu, S., Ose, T., Kitoh, A., 2011. Meteorological Research Institute-Earth System Model Version 1 (MRI-ESM1) - Model Description. Technical Report of MRI, No. 64, 83 pp.

Anexo 1.1

Tabla 1: Descripción de los nueve modelos climáticos CMIP5 usados en este trabajo

Models	Institution	Country	Reference	Resolution (Lon×Lat)
BCC-CSM1-1	Beijing Climate Center (BCC),China Meteorological Administration	China	Xiao-Ge et al. (2013)	2.8° × 2.8°
CanESM2	Canadian Centre for Climate Modelling and Analysis (CC-CMA)	Canada	Chylek et al. (2011)	2.8° × 2.8°
CNRM-CM5	Centre National de Recherches Meteorologiques / Centre European de Recherche et Formation Avances en Calcul Scientifique (CNRM-CERFACS)	France	Voldoire et al. (2013)	1.4° × 1.4°
GFDL - ESM2M	Geophysical Fluid Dynamics Laboratory (GFDL)	USA	Dunne et al. (2012)	2° × 2.5°
HADGEM2-CC	Met Office Hadley Centre (MOHC)	United Kingdom	Collins et al. (2008)	1.87° × 1.25°
MIROC-ESM-CHEM	Japan Agency for Marine-Earth Science and Technology (JAMSTEC), Atmosphere and Ocean Research Institute (AORI), and National Institute for Environmental Studies (NIES)	Japan	Watanabe et al. (2011)	2.8° × 2.8°
MPI-ESM-MR	Max Planck Institute for Meteorology (MPI-M)	Germany	Raddatz et al. (2007) Marsland et al. (2003)	1.8° × 1.8°
MRI-CGCM3	Meteorological Research Institute (MRI)	Japan	Yukimoto et al. (2011)	1.2° × 1.2°
NorESM1-M	Norwegian Climate Centre (NCC)	Norway	Bentsen et al. (2012) Iversen et al. (2012)	2.5° × 1.9°

Tabla 2: Descripción de los cuatro RCPs (The Representative Concentration Pathways) (IPCC, 2013). RCPs 2.6, 4.5 y 6 considerados como moderados y el 8.5 como extremo.

	Description	IA Model	Publication – IA Model
RCP8.5	Rising radiative forcing pathway leading to 8.5 W/m ² in 2100.	MESSAGE	Riahi et al. (2007) Rao & Riahi (2006)
RCP6	Stabilization without overshoot pathway to 6 W/m ² at stabilization after 2100	AIM	Fujino et al. (2006) Hijioka et al. (2008) Smith and Wigley
RCP4.5	Stabilization without overshoot pathway to 4.5 W/m ² at stabilization after 2100	GCAM (MiniCAM)	(2006) Clarke et al. (2007) Wise et al. (2009)
RCP2.6	Peak in radiative forcing at ~ 3 W/m ² before 2100 and decline	IMAGE	van Vuuren et al. (2006; 2007)



Universitat d'Alacant
Universidad de Alicante



CAPÍTULO 2

**ANALISIS DE LOS EVENTOS CLIMÁTICOS EXTREMOS
EN LA PROVINCIA DE ALICANTE, SURESTE DE
ESPAÑA**

Universidad de Alicante



Universitat d'Alacant
Universidad de Alicante

ANALISIS DE LOS EVENTOS CLIMÁTICOS EXTREMOS EN LA PROVINCIA DE ALICANTE, SURESTE DE ESPAÑA

Resumen

En la zona del Mediterráneo el análisis de los extremos climáticos es muy importante para entender el comportamiento del clima sobre todo en un contexto de cambio climático. El conocimiento de este comportamiento es crucial para el diseño de políticas de adaptación a los potenciales cambios de clima en el futuro. En este trabajo se analizan las tendencias de las precipitaciones en la provincia de Alicante durante el periodo 1953-2012 y los dos sub-periodos 1953-1982 y 1983-2012. Para ello se ha preparado una base de datos de precipitación de resolución diaria, el control de calidad y la reconstrucción de datos se llevaron a cabo utilizando los registros disponibles de precipitaciones diarias de las estaciones meteorológicas de la provincia de Alicante y en una franja de 50 km a su alrededor. El análisis de los extremos climáticos se realizó calculando 11 índices de extremos climáticos correspondientes a las precipitaciones. Los resultados muestran que las tendencias de cambio varían en el tiempo y en el espacio.

1. Introducción:

El Grupo Intergubernamental de Expertos sobre el Cambio Climático (IPCC, 2013) señala a la zona del Mediterráneo como una de las regiones que se verán especialmente afectadas por el cambio climático. Las previsiones climáticas para esta zona hablan de un aumento de temperaturas y un descenso de precipitaciones que pueden tener grandes impactos a nivel ambiental como a nivel socioeconómico. Sin embargo, los cambios en las medias de las temperaturas y las precipitaciones no son la única preocupación en la zona. En efecto, cambios en la intensidad y frecuencia de eventos extremos son unos de los principales efectos esperados y estos últimos cambios pueden tener mayores impactos medioambientales y socioeconómicos que los cambios en las medias (Kunkel *et al.*, 1999).

Según el informe especial sobre eventos extremos (IPCC, 2012), un extremo climático es la ocurrencia de un valor de una variable meteorológica o climática por encima (o por

debajo) de un valor de umbral cercano al extremo superior (o inferior) de la horquilla de valores observados de la variable. Sin embargo, la literatura sobre los extremos climáticos, en general, se basa en los índices de extremos que a su vez se basan en la probabilidad de ocurrencia de unos valores o la excedencia de unos umbrales. El estudio de los extremos climáticos se basa en el cálculo y el análisis de estos índices.

En este trabajo se pretende realizar un análisis de los cambios en los extremos climáticos y sus tendencias en la provincia de Alicante. En esta región del Mediterráneo, los potenciales cambios en el clima suponen un alto riesgo para los ecosistemas naturales pero también para el desarrollo socioeconómico basado en el turismo donde cualquier cambio en el clima o en los extremos climáticos afectaría a las actividades turísticas por la pérdida del confort climático (Olcina Cantos, 2012). La representación de los índices de extremos climáticos se ha cartografiado para una mejor interpretación de la variabilidad espacial.

2. Zona de estudio

La provincia de Alicante, que se extiende sobre una superficie de 5816 km², está ubicada en la costa sureste de la Península Ibérica y es una de las provincias españolas con mayor presión demográfica, con una densidad de población que supera a los 330 hab/km². La economía alicantina se basó históricamente en la agricultura y desde hace cuatro décadas en el turismo principalmente, actividades que han provocado grandes cambios irreversibles en los usos del suelo, intensificadas por la presión agrícola y el crecimiento urbanístico (Bellot *et al.*, 2007). Predomina el clima mediterráneo con precipitaciones que siguen un gradiente latitudinal variando desde medias anuales inferiores a 250mm en el Sur de la provincia hasta más de 850 mm en el Norte. Las temperaturas medias oscilan entre 20°C en el Sur y 14°C en el Norte y las zonas montañosas (Pérez, 1994). La orografía alicantina es muy diversa y sus altitudes van desde los cero metros a nivel del mar hasta más de 1500m en la sierra de Aitana. La vegetación natural de la zona está dominada por espartales, matorrales dominados por coscojares y bosques dominados por pinares y carrascas.

3. Materiales y métodos

Para el cálculo de los índices climáticos se han reconstruido los observatorios disponibles en el periodo de estudio en la provincia de Alicante (243 estaciones) con el

apoyo de los ubicados en una franja 50 km alrededor de la misma (440 estaciones). Las estaciones utilizadas provienen en su mayoría de la red de observación de la Agencia Estatal de Meteorología (AEMET), aunque también se han utilizado las de la Confederación Hidrográfica del Júcar y de la Red del SiAR (Sistema de Información Agroclimática para el Regadío) del Ministerio de Agricultura, Alimentación y Medio Ambiente.

La reconstrucción de los observatorios se ha realizado a escala diaria, desde el 1 de enero de 1940 hasta el 31 de diciembre 2012. Para ello se han construido modelos polinomiales de segundo orden, individualizados para cada estación y día en función de la dependencia de cada dato de la latitud, la longitud, y la altitud respecto al conjunto de sus 10 vecinos más cercanos con observación registrada. Este método construye una serie de referencia para cada estación que se compara con la serie de observados. En el caso de que la relación de 1 a 10 entre observado y predicho se vea superada, se elimina el dato observado por considerarse anómalo, y los huecos se llenan con la serie de predichos previamente calculada. Al tratarse de una reconstrucción a escala diaria, e individualizada por observatorios, el dato de cada uno de ellos ya es comparado con sus 10 vecinos más cercanos, quienes tendrán un comportamiento climático al menos similar, por lo que la aparición de inhomogeneidades en la serie final es improbable. Con todo, cada serie de medias anuales ha pasado un test de homogeneidad para evitar variaciones no debidas a la propia variabilidad del clima. Se aplicó así pues, el test de SNHT (Alexandersson, 1986) a cada uno de los observatorios.

Los 11 índices de extremos de precipitaciones (Tabla 2.1) analizados en este trabajo vienen de una lista de 27 índices climáticos propuestos por el grupo de expertos en la detección del cambio climático y sus índices (ETCCDI) (Peterson, 2005). El cálculo de estos índices se hizo mediante el paquete de R “climdex.pcic” que es una implementación de las rutinas para el cálculo de los índices desarrollado por el “Pacific Climate Impacts Consortium” de la Universidad de Victoria en Canadá. Los mapas se han creado con el método Kriging Ordinario.

4. Resultados y discusión

El análisis de los índices de extremos climáticos en la provincia de Alicante se realizó analizando la variabilidad en el tiempo comparando los dos sub-periodos 1953-1982 y

1983-2012 sobre una serie media de todos los observatorios de la zona de estudio y en el espacio cartografiando las medias y tendencia de los índices de extremos climáticos en el periodo 1953-2012 para todos los observatorios. El análisis de las tendencias y su significancia se hizo mediante el ajuste de un modelo de regresión lineal. Para considerar las tendencias significativas se consideró un umbral de $\alpha = 0.05$.

Tabla 2.1: los índices de extremos climáticos para la precipitación usados en este trabajo

Nombre	Definición
1-Rx1day	Máximo mensual de precipitación en 1 día
2-Rx5day	Máximo mensual de precipitación en 5 días
3-SDII	Índice simple de intensidad diaria
4-R10mm	Número de días con precipitación $PRCP \geq 10\text{mm}$
5-R20mm	Número de días con precipitación $PRCP \geq 20\text{mm}$
6-Rnmm	Número de días con precipitación $PRCP \geq n\text{mm}$, nn es un umbral fijado por el usuario
7-CDD	Número máximo de días secos consecutivos con $RR < 1\text{mm}$
8-CWD	Número máximo de días húmedos consecutivos con $RR \geq 1\text{mm}$
9-R95pTOT	Precipitación Total Anual cuando $RR > 95\text{p}$
10-R99pTOT	Precipitación Total Anual cuando $RR > 99\text{p}$
11-PRCPTOT	Precipitación Total Anual en días húmedos $RR \geq 1\text{mm}$

4.1 La variabilidad temporal de los índices de extremos de precipitación

Los índices de extremos climáticos en la provincia de Alicante se analizaron a dos escalas temporales; por un lado a escala de un periodo de 60 años desde 1953 hasta 2012 para ver los cambios en un largo periodo de tiempo, y por otro a escala de dos sub-periodos de 30 años cada uno, de 1953 a 1982 y de 1983 a 2012 con el fin de comparar entre dos periodos de longitudes equivalentes. Los valores medios de los índices y sus tendencias para toda la zona en los 3 periodos estudiados se presentan en las tablas 2.2 y 2.3 sucesivamente. Además de los valores medios se hizo una comparación de las medias mediante el t-test y cálculo del cambio en porcentajes según la metodología propuesta por Frich *et al.* (2002).

La tabla 2.2 muestra una gran variabilidad en los valores medios de los índices y sus tendencias en los tres periodos estudiados. El índice PRCPTOT que representa la precipitación total anual es del orden de 477.1mm en el periodo largo pero esta media se ha visto reducida en más de 30 mm entre el primer sub-periodo y el segundo, pasando de 492.4 a 461.8mm. Esa misma tendencia negativa se observa en el caso del índice SDII que representa el índice simple de intensidad diaria. Al contrario del descenso

observado en los dos índices citados anteriormente, se observa un aumento en los índices R95ptot y R99ptot de los días muy húmedos y extremadamente húmedos al igual que el índice Rx1day que representa la cantidad máxima de precipitación en un día. El test de comparación de medias indicó que solo 3 índices (SDII, R10mm y R20mmm) mostraron diferencias significativas entre el periodo 1953-1982 y el periodo 1983-2012. Los mayores porcentajes de cambio se observaron en los mismos índices con diferencias significativas superando el 20% con signo negativo y en el índice R99ptot superando el 33% con un signo positivo.

La Tabla 2.3 recoge los valores medios de las tendencias de cambio en los índices para toda la zona. Una de las tendencias más destacadas es la inversión en la tendencia del índice de precipitación total (PRCPTOT). Mientras que se obtiene una tendencia negativa a escala del periodo 1953-2012 y del sub-periodo 1953-1982, la misma es positiva en el último (1983-2012) lo que señala que el descenso en el valor medio de la PRCPTOT entre el primer sub-periodo y el segundo es debido a años más secos al inicio del segundo sub-periodo (1983-2012) y que el final de este periodo es más húmedo. Otro aspecto destacado es la tendencia negativa en los índices Rx1day, Rx5day, R95ptot y R99ptot a pesar de la tendencia positiva en la precipitación total anual. Finalmente cabe destacar una tendencia negativa en el número de días secos consecutivos CDD en los tres periodos estudiados.

4.2 La variabilidad espacial de los índices de extremos de precipitación

Las figuras 2.1a-2.11a representan la distribución espacial de los índices de precipitaciones a escala de la provincia de Alicante mientras que las figuras 2.1b-2.11b muestran la variabilidad espacial de sus tendencias y donde esas tendencias son significativas (las estaciones señaladas con los triángulos negros).

Las precipitaciones medias anuales, como lo muestra el mapa del índice PRCPTOT (Figure 2.1a), siguen un gradiente latitudinal y van de menos de 300mm en el centro y el sur hasta más de 800mm en el norte y superando el umbral de 900mm en zonas puntuales. A pesar de que el valor medio de la tendencia del índice PRCPTOT es negativo para toda la zona (tabla 2.3) la tendencia no es la misma en todo el territorio alicantino (Figure 2.1b). En efecto, las tendencias negativas solo se concentran en la zona central y sobre todo en la zona sur de la mitad norte de la provincia en las mismas

comarcas donde se registraron bajadas significativas en la precipitación total anual entre los dos sub-periodos estudiados en este trabajo. En la parte sur y suroeste se registra una ligera tendencia positiva mientras que una tendencia positiva significativa se observa en la parte norte entre la comarca de la Marina Alta y el Comtat.

La distribución espacial de la mayoría de los índices y sus tendencias siguen los mismos patrones que el índice PRCPTOT con algunas diferencias. En efecto, las tendencias de índice SDII son negativas y significativas en el todo el territorio (Figure 2.6). Las tendencias del índice R1mm son positivas y significativas en la mayor parte de la provincia y las zonas de mayor aumento se concentran en el norte y en el oeste en la frontera con la provincia de Albacete y Murcia. Los días con precipitaciones mayores a 10mm y 20mm (R10mm y R20mm) también mostraron tendencias diferentes en el espacio con valores negativos y significativos en la parte sur de la mitad norte de la provincia.

El índice del número máximo de días secos consecutivos (CDD) que puede ser un indicador de la longitud de la estación seca puede ir de una media de 54.5 días consecutivos sin lluvia en el norte hasta 90 días en la parte sur en el límite con Murcia. La media de este índice es de 70 días y se registra en una gran parte del territorio. La tendencia de este índice es negativa y significativa en una gran parte del territorio y es positiva en las comarcas de Alacanti, del Bajo Vinalopó y del Bajo Segura.

Tabla 2.2: La media de los índices de extremos climáticos en los periodos 1953-2012, 1953-82 y 1983-2012

	Rx1day	Rx5day	SDII	R10mm	R20mm	R1mm	CDD	CWD	R95ptot	R99ptot	PRCPTOT
1953-2012	66.0	117.8	11.6	14.2	6.5	40.1	70.7	4.6	126.7	38.8	477.1
1953-1982	62.8	118.7	12.7	15.5	7.1	37.9	73.4	4.7	123.9	30.9	492.4
1983-2012	69.2	116.9	10.6	12.9	5.8	42.3	68.1	4.6	129.6	46.6	461.8
t-test p.value	0.26	0.88	0.0***	0.01**	0.03*	0.06	0.15	0.57	0.77	0.15	0.41
% cambio	+9.2	-1.5	-20.3	-20.7	-22.3	+10.4	-7.7	-2.8	+4.4	+33.6	-6.6

Tabla 2.3: La tendencia media de los índices de extremos climáticos en los periodos 1953-2012, 1953-82 y 1983-2012

	Rx1day	Rx5day	SDII	R10mm	R20mm	R1mm	CDD	CWD	R95ptot	R99ptot	PRCPTOT
1953-2012	0.08	-0.32	-0.07	-0.08	-0.04	0.17	-0.23	0.00	-0.09	0.19	-0.94
1953-1982	-0.19	-1.23	-0.10	-0.14	-0.09	0.02	-0.52	-0.02	-1.31	-0.32	-3.72
1983-2012	-0.43	-1.02	-0.05	0.07	0.04	0.43	-0.29	0.02	-0.56	-1.31	2.32

Los resultados obtenidos en este trabajo indican una tendencia de cambio en las precipitaciones variable en el espacio a escala de toda la provincia de Alicante en las últimas décadas. Sin embargo las tendencias negativas son las más significativas lo que coincide con los resultados obtenidos por De Luis *et al.* (2000) a escala de la Comunidad Valenciana y por el IPCC (2012) y Frich *et al.* (2002) a escala global.

La tendencia positiva observada en los índices R10mm y R20mm en el último subperiodo 1983-2012 coincide con otros trabajos que indicaron tendencias significativas desde un punto de vista estadístico en el número de precipitaciones intensas se han observado en algunas regiones en las últimas décadas (Frich *et al.* 2002; Kostopoulou and Jones, 2005; Alexander *et al.*, 2006; IPCC, 2012).

De cara al futuro es probable que esta tendencia de cambio en los extremos siga en la misma dirección ya que numerosos trabajos científicos pronosticaron cambios en los extremos climáticos a escala mundial (Easterling *et al.*, 2000; Arblaster and Alexander, 2005; IPCC, 2012; 2013) y a escala regional en la zona mediterránea (Sánchez *et al.*, 2004; Goubanova and Li, 2007; IPCC, 2012) y particularmente en la península ibérica (Monjo *et al.*, 2016). Todos estos trabajos coinciden en que los eventos extremos de temperaturas y precipitaciones van a aumentar en el futuro.

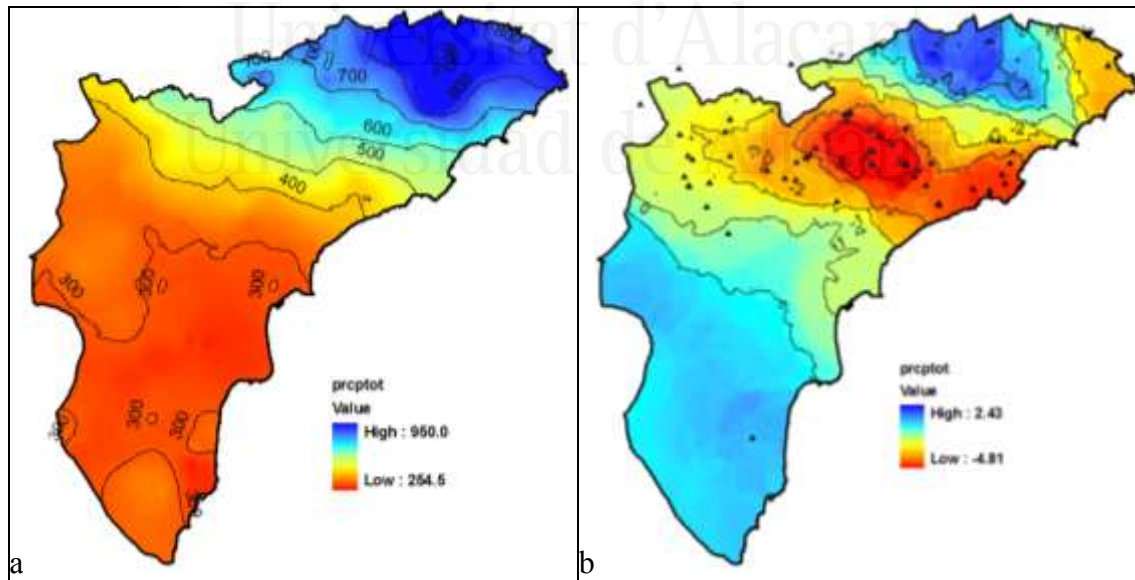


Figure 2.1: Mapa del índice PRCPTOT (a) y su tendencia (b)

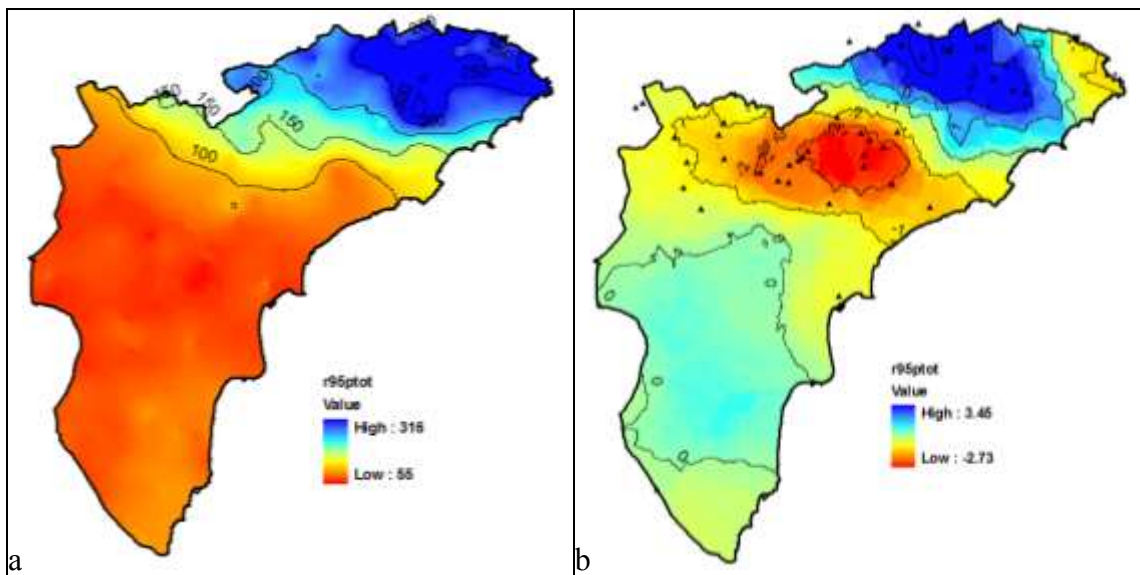


Figure 2.2: Mapa del índice R95ptot (a) y su tendencia (b)

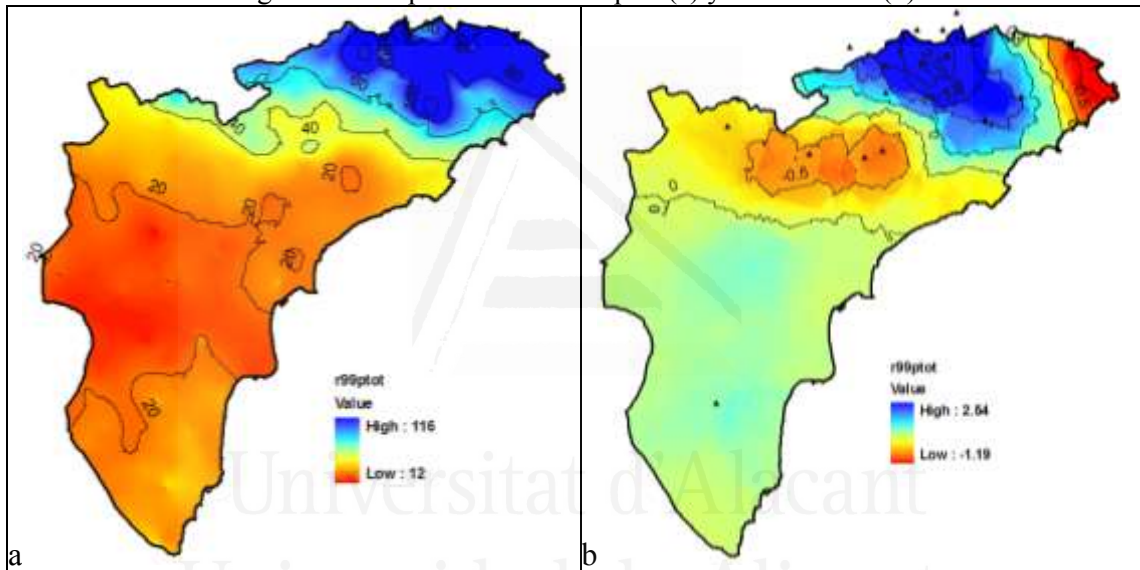


Figure 2.3: Mapa del índice R99ptot (a) y su tendencia (b)

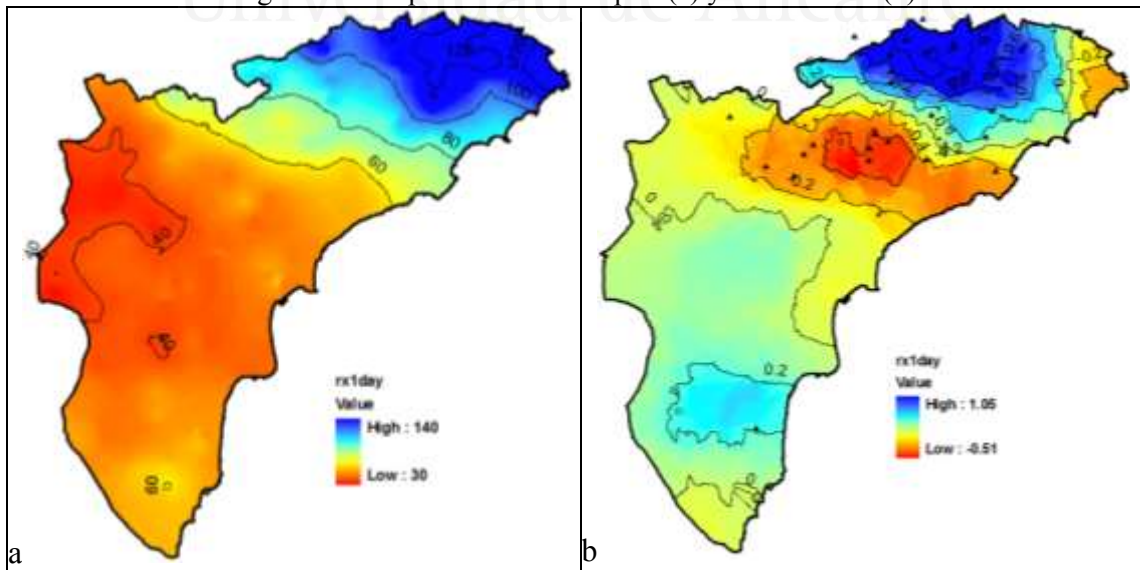


Figure 2.4: Mapa del índice Rx1day (a) y su tendencia (b)

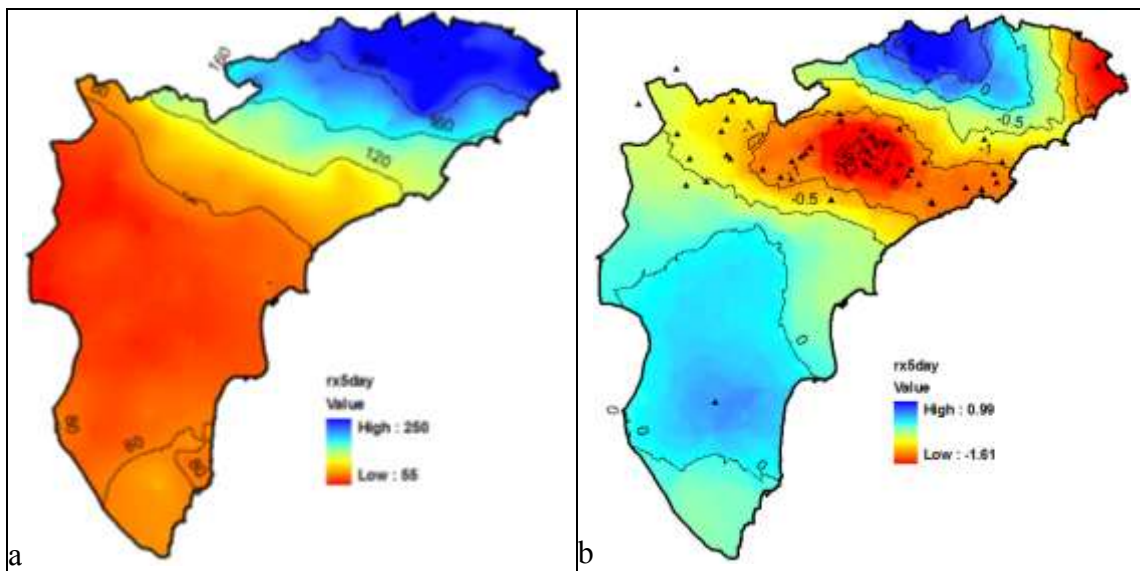


Figure 2.5: Mapa del índice Rx5day (a) y su tendencia (b)

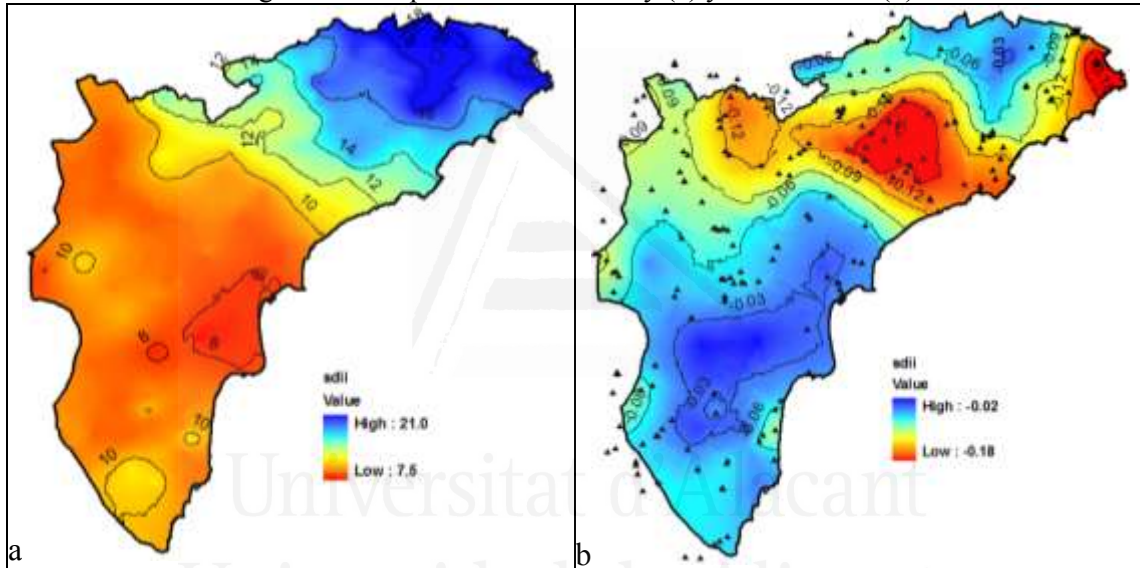


Figure 2.6: Mapa del índice SDII (a) y su tendencia (b)

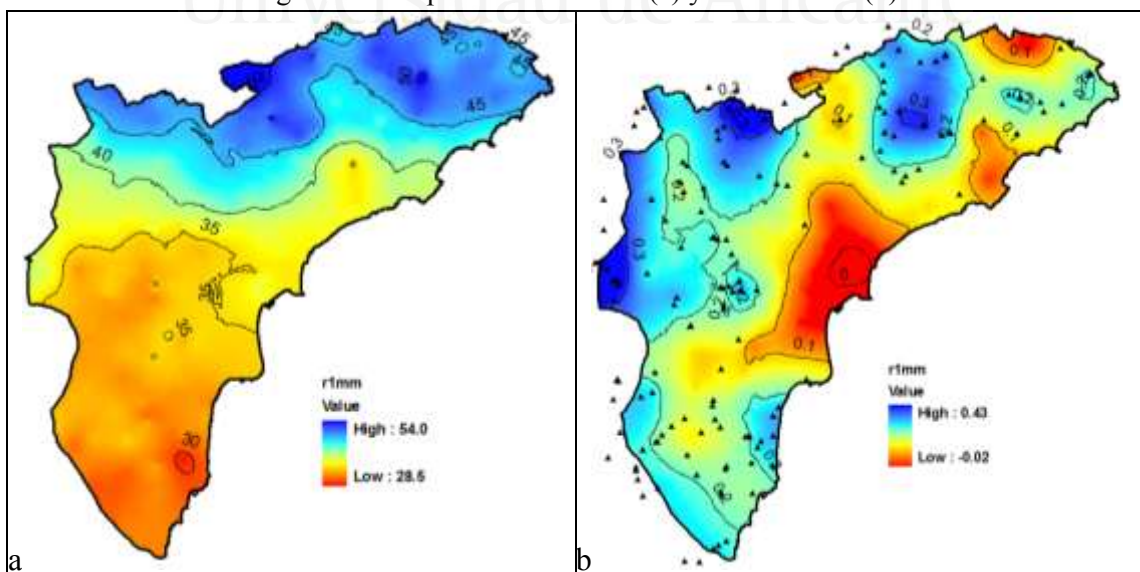


Figure 2.7: Mapa del índice R1mm (a) y su tendencia (b)

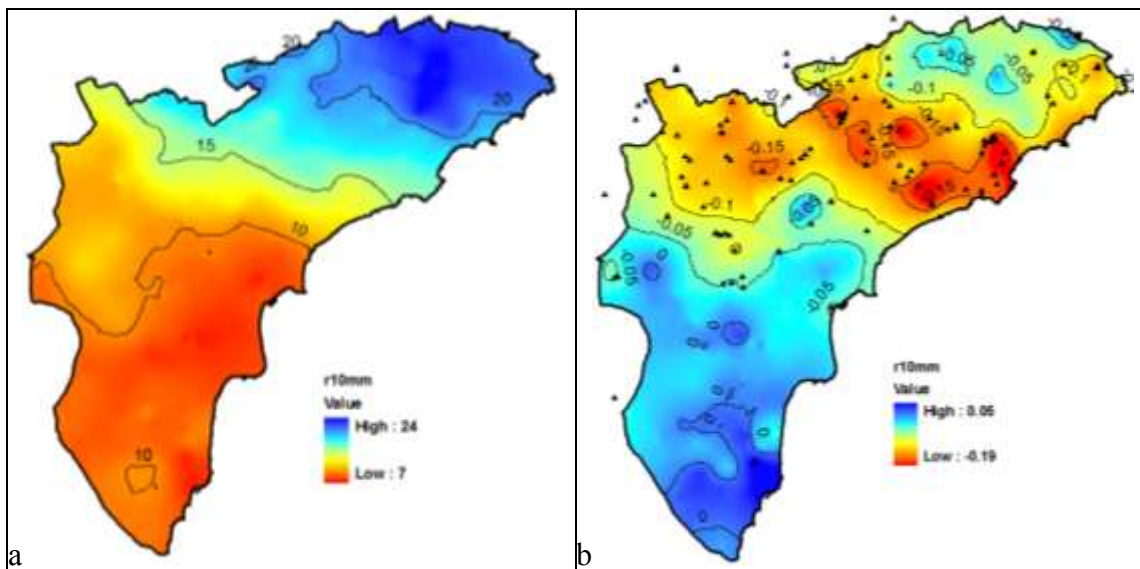


Figure 2.8: Mapa del índice R10mm (a) y su tendencia (b)

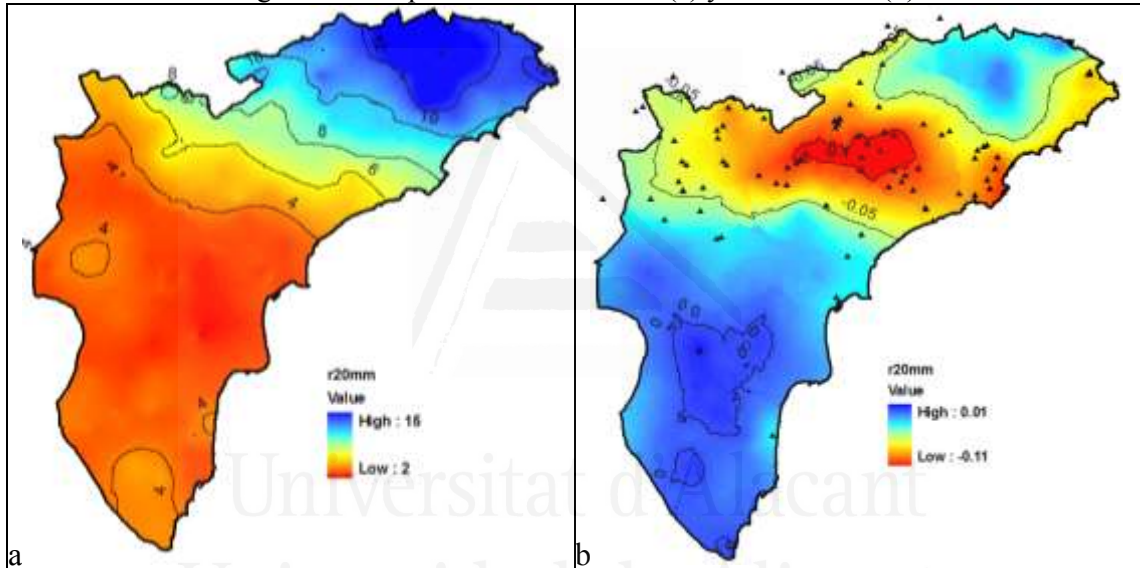


Figure 2.9: Mapa del índice R20mm (a) y su tendencia (b)

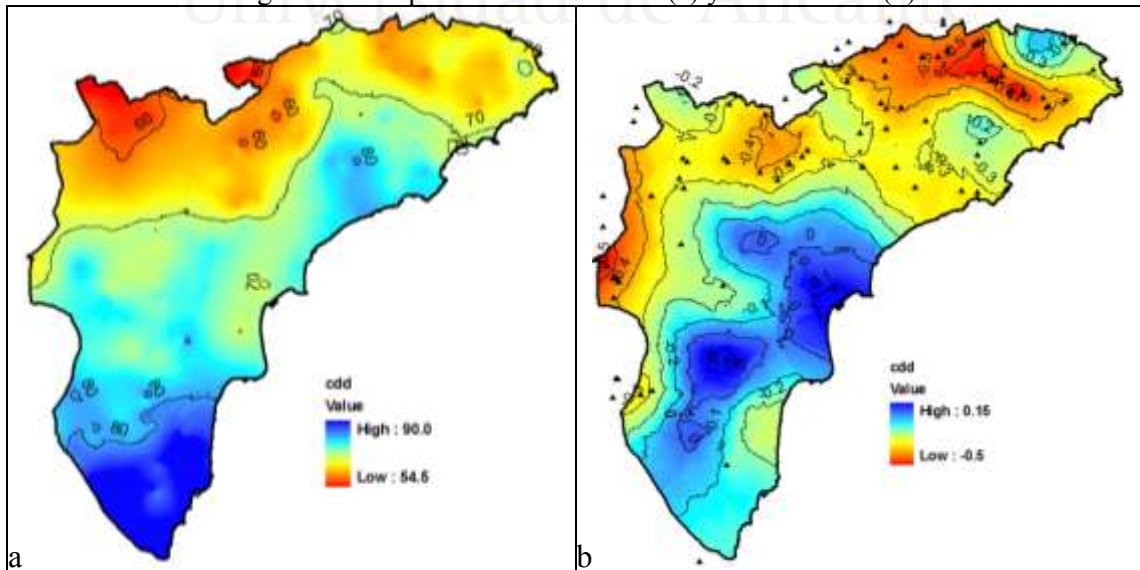


Figure 2.10: Mapa del índice CDD (a) y su tendencia (b)

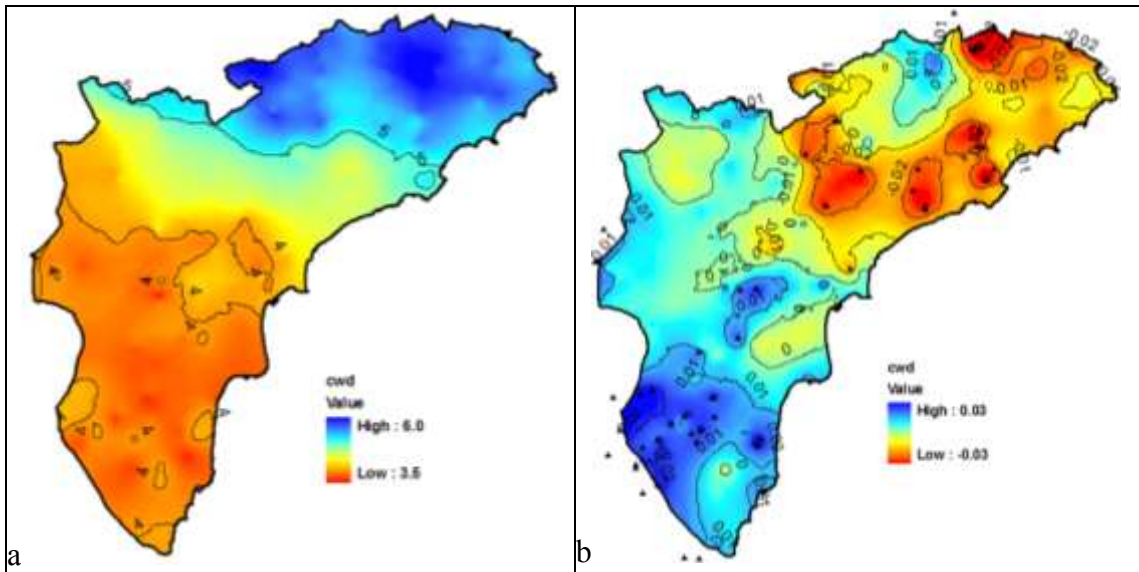


Figure 2.11: Mapa del índice CWD (a) y su tendencia (b)

5. Conclusiones

Los resultados obtenidos en este trabajo indican una tendencia de cambio en las precipitaciones variable en el espacio a escala de toda la provincia de Alicante en el tiempo a lo largo de las últimas décadas. El cambio de la escala temporal y espacial afecta a los resultados obtenidos. En efecto, las tendencias observadas a lo largo del periodo 1953-2012 no siempre coinciden con las tendencias observadas en los sub-periodos de 1953 a 1982 y de 1983 a 2012. En el espacio las tendencias varían de norte a sur y tendencias significativas se han visto concentradas en zonas limitadas del territorio para la mayoría de los índices de extremos analizados en este trabajo.

REFERENCIAS

Alexander, L. V., Zhang, X., Peterson, T. C., Caesar, J., Gleason, B., Klein Tank, A. M. Haylock, G., M., Collins, D., Trewin, B., Rahimzadeh, F., Tagipour, A., Rupa Kumar, K., Revadekar, J., Griffiths, G., Vincent, L., Stephenson, D. B., Burn, J., Aguilar, E., Brunet, M., Taylor, M., New, M., Zhai, P., Rusticucci, M., J. L. Vazquez-Aguirre (2006). Global observed changes in daily climate extremes of temperature and precipitation. *Journal of Geophysical Research: Atmospheres*, 111(D5).

Alexandersson, H. 1986. A homogeneity test applied to precipitation data, *J. Climatol.*, 6, 661–675.

Arblaster, J., & Alexander, L. (2005). Extreme change: an analysis of past, present and future changes in global temperature and precipitation indices. *Bull Aust Met Ocean Soc*, 18, 125-130.

Bellot, J., Bonet, A., Peña, J., et Sánchez, J.R (2007). Human impacts on land cover and water balances in a coastal Mediterranean county. *Environmental Management* , 39: 412–422.

De Luijs M, Raventós J, González-Hidalgo JC, Sánchez JR, Cortina J (2000). Spatial analysis of rainfall trends: a case study in Valencia Region (E Spain). *Int J Climatol* 20:1451–1469

Easterling, D. R., Meehl, G. A., Parmesan, C., Changnon, S. A., Karl, T. R., & Mearns, L. O. (2000). Climate extremes: observations, modeling, and impacts. *science*, 289(5487), 2068-2074.

Frich, P., L.V. Alexander, P. Della-Marta, B. Gleason, M. Haylock, A.M.G. Klein Tank, and T. Peterson (2002). Observed coherent changes in climatic extremes during the second half of the twentieth century, *Clim. Res.*, 19, 193-212.

Goubanova, K., & Li, L. (2007). Extremes in temperature and precipitation around the Mediterranean basin in an ensemble of future climate scenario simulations. *Global and Planetary Change*, 57(1), 27-42.

IPCC, (2012). Managing the Risks of Extreme Events and Disasters to Advance Climate Change Adaptation. A Special Report of Working Groups I and II of the Intergovernmental Panel on Climate Change [Field, C.B., V. Barros, T.F. Stocker, D. Qin, D.J. Dokken, K.L. Ebi, M.D. Mastrandrea, K.J. Mach, G.-K. Plattner, S.K. Allen, M. Tignor, and P.M. Midgley (eds.)]. Cambridge University Press, Cambridge, UK, and New York, NY, USA, 582 pp.

IPCC, (2013). Climate Change 2013: The Physical Science Basis. Contribution of Working Group I to the Fifth Assessment Report of the Intergovernmental Panel on Climate Change [Stocker, T.F., D. Qin, G.-K. Plattner, M. Tignor, S.K. Allen, J. Boschung, A. Nauels, Y. Xia, V. Bex and P.M. Midgley(eds.)]. Cambridge University Press, Cambridge, United Kingdom and New York, NY, USA, 1535 pp.

Kostopoulou, E., & Jones, P. D. (2005). Assessment of climate extremes in the Eastern Mediterranean. *Meteorology and Atmospheric Physics*, 89(1-4), 69-85.

Kunkel, K.E., Pielke, R.A., Changnon, S.A., (1999). Temporal fluctuations in weather and climate extremes that cause economic and human health impacts: a review. *Bull. Am. Meteorol. Soc.* 80, 1077 – 1098.

Monjo, R., Gaitán, E., Pórtoles, J., Ribalaygua, J., & Torres, L. (2016). Changes in extreme precipitation over Spain using statistical downscaling of CMIP5 projections. *International Journal of Climatology*, 36(2), 757-769.

Olcina Cantos, J., (2012). Turismo y cambio climático: una actividad vulnerable que debe adaptarse. *Investigaciones Turísticas*. N. 4 (jul.-dic. 2012). ISSN 2174-5609, pp. 1-34

Pérez Cueva A.J. (coordinador) (1994). *Atlas Climático de la Comunidad Valenciana*, Consejería de Obras Públicas, Urbanismo y Transporte, Generalitat Valenciana. 208 pp

Peterson, T.C., (2005). Climate Change Indices. *WMO Bulletin*, 54 (2), 83-86.

Sánchez, E., Gallardo, C., Gaertner, M. A., Arribas, A., & Castro, M. (2004). Future climate extreme events in the Mediterranean simulated by a regional climate model: a first approach. *Global and Planetary Change*, 44(1), 163-180.

Universitat d'Alacant
Universidad de Alicante



Universitat d'Alacant
Universidad de Alicante

CAPÍTULO 3

**LIKELY EFFECTS OF CLIMATE CHANGE ON
GROUNDWATER AVAILABILITY IN A
MEDITERRANEAN REGION OF SOUTHEASTERN
SPAIN**

Universitat d'Alacant
Universidad de Alicante



Universitat d'Alacant
Universidad de Alicante

Likely effects of climate change on groundwater availability in a Mediterranean region of Southeastern Spain

Abstract

Groundwater resources are typically the main fresh water source in arid and semi-arid regions. Natural recharge of aquifers is mainly based on rainfall; however, only heavy rainfall events (HREs) are expected to produce appreciable aquifer recharge in these environments. In this work we used daily rainfall and monthly water level time series from different locations over a Mediterranean region of Southeastern Spain to identify the critical threshold value to define HREs that lead to appreciable aquifer recharge in this region. Wavelet analysis and trend analysis were used to study the changes in the temporal distribution of the chosen HREs over the observed period 1953-2012 and its projected evolution by using eighteen downscaled climate projections (nine Coupled Model Intercomparison Project Phase 5 climate models under two Representative Concentration Pathways scenarios, RCP4.5 and RCP8.5) over the projected period 2040-2099. Results showed that HREs are above or equal to 20 mm day^{-1} for the study area. Wavelet analysis, applied to HREs time series grouped in ten clusters, showed that observed significant seasonal and annual peaks in global wavelet spectrum in the first sub-period (1953-1982) are no longer significant in the second sub-period (1983-2012) in the major part of the ten clusters. This change is due to the reduction of the mean HREs number, which showed a negative trend over the observed period in nine clusters and was significant in five of them. However, the mean size of HREs showed a positive trend in six clusters. A similar tendency of change is expected over the projected period. The expected reduction is two times higher under the high (RCP8.5) scenario than under the moderate (RCP4.5) scenario. The mean size of these events is expected to increase under the two scenarios. The groundwater availability will be affected by the reduction of HREs number which will increase the length of no aquifer recharge periods (NARP) accentuating the groundwater drought in the region.

1. Introduction

The Mediterranean is one of the most water scarce regions (Daccache *et al.*, 2014) where water demand is growing at an alarming rate (Frot *et al.*, 2007). In the Mediterranean coastal areas, such as southeastern Spain, global change scenarios

forecast an increase in water demand as a consequence of the expansion of irrigated lands, as well as the growth of urban and industrial areas, and tourist resorts (García-Ruiz *et al.*, 2011). Agriculture and tourism are a major source of income and employment in southeastern Spain; however, the pressure put on water resources have highlighted concerns regarding the environmental sustainability of these activities in the region, above all in the context of a changing climate that is expected to intensify the existing risks facing the agriculture in the Mediterranean (Iglesias *et al.*, 2011). Most climate models forecast an increase in temperature and a decrease in precipitation at the end of the 21st century for the Mediterranean region (IPCC, 2014). Declining inputs and rising outputs will increase the water deficit in this region which makes increased irrigation or any other economic activity based on a high water use an unviable option (Olesen *et al.*, 2011).

Groundwater is the main freshwater source in a number of Mediterranean catchments and is already under high pressure (Cudennec *et al.*, 2007; Ibáñez *et al.*, 2008; Daccache *et al.*, 2014). Its reliability is threatened by the likely increase in the frequency and intensity of droughts observed since 1950 (IPCC, 2014). Groundwater recharge is an important concern across the arid and semiarid regions of the Mediterranean. Therefore, in the Spanish Mediterranean coastal areas a growing number of studies are attempting to estimate and/or model groundwater recharge at different scales and characterize the mechanisms of recharge (Vias *et al.*, 2005; Bellot *et al.*, 2001; Andreo *et al.*, 2008; Martínez-Santos and Andreu, 2010; Touhami *et al.*, 2013, 2014).

Aquifer recharge is a complex process depending on different variables. In arid and semiarid regions, the recharge estimations from the regional water balance studies is often of low quality because of the limited recharge component. Not only climate but also geology, morphology, soil condition and land use have to be involved in the recharge estimations (Zagana *et al.*, 2007). In these environments climate variability and land use/land cover changes have an important effect on aquifer recharge (Scanlon *et al.*, 2006).

Aquifers in arid and semiarid regions are mainly recharged by precipitation. However, not all rainfall event types contribute to groundwater recharge. Indeed, recharge in these environments is often restricted to heavy rainfall events (Tweed *et al.*, 2011; Taylor *et al.*, 2013); light and moderate rainfall are not expected to contribute to the groundwater

recharge due to the evapotranspiration that would prevent infiltrating water from penetrating below the root zone (Frot *et al.*, 2007). In a small karstic aquifer in the southeastern Spain, Touhami *et al.*, (2013) concluded that the contribution of rainfall events of less than 15 mm to aquifer recharge is considered negligible, whereas Bellot and Chirino (2013) found that only rainfall events equal to or greater than 30 mm produced high enough infiltration to lead to an appreciable aquifer recharge in the same area.

Changes in the frequency and intensity of heavy rainfall events in the Mediterranean region will have a direct impact on groundwater systems. In fact, low precipitation in general or a decrease of rainfall events that produce aquifer recharge, possibly in combination with high evapotranspiration, will cause groundwater droughts (Mishra and Singh, 2010). This type of droughts has important effects on natural and socioeconomic systems (Van Lanen and Peters, 2000). Hence, the study of changes in the mean and trends in the frequency of heavy rainfall events is of direct concern to this region and other arid and semi-arid regions around the world.

As a contribution to the rising interest in impacts of climate change on groundwater (Green *et al.*, 2011), the main objectives of this paper are: (i) to define the Heavy Rainfall Events (HREs) that contribute in an appreciable manner to the aquifer recharge in a Mediterranean region in the southeastern Spain from 1953 through 2012, (ii) to identify observed changes and trends in the frequency and size of these HREs and (iii) to analyze expected future trends based on eighteen downscaled climate projections over the period 2040-2099, based on Coupled Model Intercomparison Project Phase 5 (CMIP5) climate models. Daily rainfall and monthly water level time series from different locations over the province of Alicante (SE Spain) are used to choose a critical threshold value to define the HREs. An application of wavelet analysis will be conducted in order to detect the main frequency components in the HREs time series over the period 1953-2012. Trend analysis will be used to study the evolution of these events over the observed and projected periods of time.

2. Study area

The province of Alicante is located in the southeast coast of the Iberian Peninsula and roughly covers an area of 5816 km². Alicante is mountainous, especially in the north as

part of the Subbaetic Mountain Range, whereas it is mostly flat in the south part (Figure 3.1). Elevation changes rapidly from 0 to more than 1000 m.a.s.l and it has an important influence on precipitations (Millán *et al.*, 1995). Mean annual rainfall values varies between 258 and 953 mm yr⁻¹, which follows a complex spatial pattern (N–S/E–W). Torrentiality is another characteristic of this region (González Hidalgo *et al.*, 2003). Daily maximum rainfall varies on average between 120 and 50 mm d⁻¹, and represents a mean of 17% (coastland) to 9% (inland) of annual rainfall (Vicente Serrano *et al.*, 2004). Precipitation in Alicante varies over time and space and it is marked by its seasonality. The major part of the annual precipitations is recorded in autumn months (40% of the annual amount) and reaches its maximum in October (more than 70 mm) (Figure 3.2). An important part (25%) is recorded in spring season with a peak in April. The standard deviation shows the high variability in time over the last 60 years. Regarding surface water resources the few major rivers in Alicante are Vinalopó, Serpis and Segura. Most of these rivers are seasonal and depend on the rainfalls which make ground water the main source of fresh water in this region. For decades, agriculture and tourism have been the main economic sectors in such Mediterranean environment leading to high pressure on groundwater resources. Indeed, more than 75% of the aquifers of Alicante are overexploited.

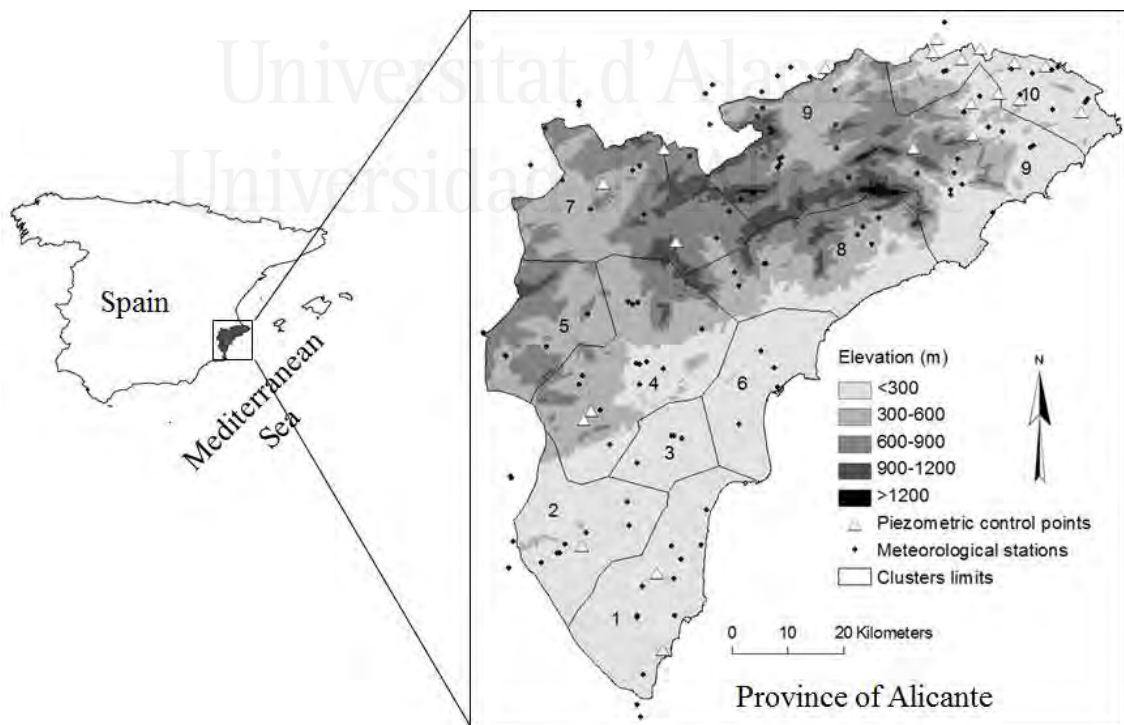


Figure 3.1: Study area location and used meteorological stations. Section numbers represent the ten clusters.

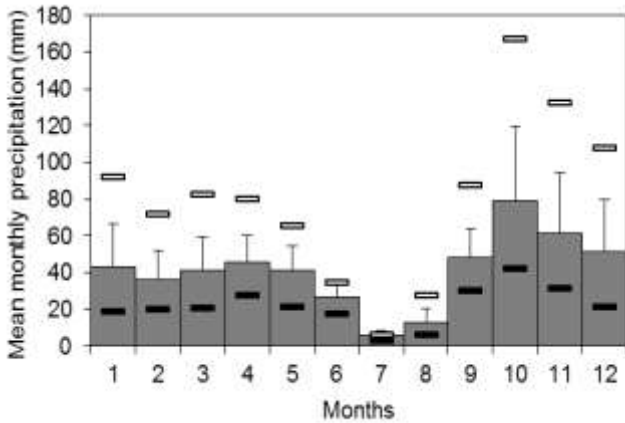


Figure 3.2: Mean (plain bars) and standard deviation (error bars) of the monthly precipitation for the entire province of Alicante over the period 1953-2012. Black and white bars represent the monthly mean precipitation of the driest and wettest weather stations respectively.

3. Data and methods

3.1 Observed rainfall data

Daily precipitation time series over the period 1953-2012 were taken from 111 meteorological observatories inside the province of Alicante limits and in a strip of 15 km around it (data provided by the Spanish Meteorological Agency, AEMET). The reconstruction of the series was performed and their homogeneity was checked using the Standard Normal Homogeneity Test (SNHT) in a previous work (Moutahir *et al.*, 2014). These 111 observatories were grouped in 10 clusters using the *hclust* function from the R “stats” package which allows performing hierarchical clustering. Similarities inside each cluster were assessed using Pearson correlations between rainfall time series. The delimitation of the different clusters was performed by the Thiessen polygons method. This method involves the construction of polygons around the stations and grouping them allows the delineation of the different clusters (Figure 3.1). The obtained clusters correspond to the topographic characteristics of Alicante where altitude, distance to the sea and latitude are the most important factors defining these clusters. Ten new average time series were obtained from different daily precipitation time series inside each cluster. The mean annual precipitation over the period 1953-2012 in the chosen ten clusters varies from north to south with high values in the clusters 10 and 9 (more than 800mm and 600mm respectively) located in the extreme northern part and mountainous areas. The annual precipitations in southern and central clusters vary between 300 and 400 mm (Figure 3.3).

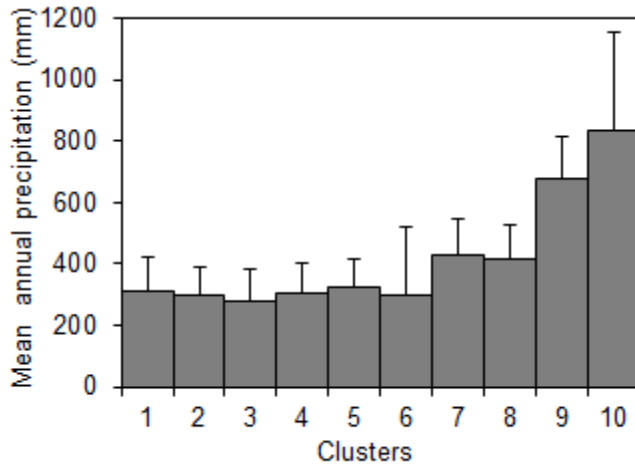


Figure 3.3: Mean annual precipitation (plain bars) and standard deviation (error bars) per cluster over the period 1953-2012

3.2 Projected rainfall data

We have used a data set of climate simulations from nine CMIP5 climate models (Anexo1.1: Table 1) downscaled to the 111 meteorological observatories used in this study. These simulations, based on the Program for Climate Model Diagnosis and Intercomparison (PCMDI) archives, are described and analyzed in Monjo *et al.* (2015). For these models, a ‘twentieth century’ simulation as the control run (the Historical simulation) and two future climate projections corresponding to the Representative Concentration Pathways RCP4.5 (moderate emissions scenario) and RCP8.5 (high emissions scenario) were used (Taylor *et al.* 2009).

Climate simulations were previously downscaled using a two-step analogue/regression statistical method developed by Ribalaygua *et al.* (2013). The first step is an analogue approach in which the n most similar days to the problem day are selected (Zorita and von Storch 1999). The similarity between the two days was measured using a weighted Euclidean distance between large-scale fields as predictors: speed and direction of the geostrophic wind at 1000 hPa and 500 hPa. In the second step, a nonlinear transfer function is applied between the analogous rainfalls and the rainfall of each problem day according to probability distribution of each problem month (Ribalaygua *et al.*, 2013; Monjo *et al.*, 2015).

3.3 Heavy Rainfall Events definition

As it was mentioned previously, not all rainfall events are involved in groundwater recharge in arid and semi-arid environments. Indeed, only heavy rainfall event (HREs) can lead to appreciable aquifer recharge. However, HREs are vaguely defined and depend on a given threshold. To choose the threshold that defines the HREs in the province of Alicante we used groundwater-level observations from a groundwater monitoring network operated by the Júcar River Basin and Segura River Basin authorities. From control points located inside the province of Alicante we used 21 monthly piezometric time series that have records during the period 2006-2012. In fact, we analyzed 36 borehole hydrographs but excluded 15 stations from further analysis due to inconsistencies and excessive gaps in their records.

The lack of information about groundwater extractions makes it difficult to relate variations in the piezometric level to the precipitation. It is why only monthly water level increments, which represent aquifers replenishment above extraction rates, were considered to be correlated to rainfall. In addition, the varying time of water table response to rainfall and the temporal resolution of piezometric data make it impossible to relate individual water level increments to its correspondent individual causing rainfall events. To overcome this problem we chose to correlate the number of water level increments to the number of rainfall events over the entire period 2006-2012 and entire region because of the low number of increments or rainfall events per year. Monthly piezometric level increments over the period 2006-2012 in each control point were counted and correlated to the number of rainfall events from the nearest precipitation station over the same period of time (taking into account only one event per month in the case that several events above the chosen threshold occur). The threshold to define a HRE is supported by sensitivity analysis in which this threshold was varied from 5 to 60 mm day⁻¹ in increments of 5 mm day⁻¹.

In contrast with the definition of HRE, No Aquifer Recharge Period (NARP) can be defined as the time period between two consecutive HREs, i.e., the time period (in days) when rainfall events that produce an appreciable aquifer recharge do not occur. In this work NARP will be considered as the maximum period between two consecutive HREs within a year.

3.4 Wavelet transform

Wavelet analysis is a common tool for performing a time-frequency localization of the characteristic time series features (Markovic and Koch, 2005). Developed by Grossmann and Morlet (1984), wavelet analysis has since been then applied in numerous fields including climatic research (Lau and Weng, 1995; Torrence and Compo, 1998; Markovic and Koch, 2005) and rainfall-runoff relation analysis (Nakken, 1999; Labat *et al.*, 2001). By decomposing a time series into time–frequency space, one is able to determine both the dominant modes of variability and how those modes vary in time (Torrence and Compo, 1998).

The continuous wavelet transform of a discrete sequence x_n is defined as the convolution of x_n with a scaled and translated version of a wavelet function $\psi_0(\eta)$:

$$W_n(s) = \sum_{n'=0}^{N-1} x_{n'} \Psi^* \left[\frac{(n'-n)\delta t}{s} \right] \quad (\text{Eq. 1})$$

where the (*) indicates the complex conjugate and δt is the time steps. The used $\psi_0(\eta)$ in this work is the Morlet wavelet, consisting of a complex wave modulated by a Gaussian:

$$\Psi_0(\eta) = \pi^{-1/4} e^{i\omega_0\eta} e^{-\eta^2/2} \quad (\text{Eq. 2})$$

where ω_0 is the nondimensional frequency, here taken to be 6 to satisfy the admissibility condition and η is a nondimensional “time” parameter.

By the convolution theorem, the wavelet transform is the inverse Fourier transform of the product:

$$W_n(s) = \sum_{k=0}^{N-1} \hat{x}_k \hat{\Psi}^*(s\omega_k) e^{i\omega_k n \delta t} \quad (\text{Eq. 3})$$

where (^) indicates the Fourier transform, n the localized translated time, k the frequency index and $\omega_k = \pm 2\pi k/N\delta t$ the angular frequency.

By sliding the wavelet along the time series, a new time series of the projection amplitude versus time can be constructed. Therefore, it is possible to get information on both the amplitude of any “periodic” signals within the series, and how this amplitude varies with time. Because the wavelet function is complex, the wavelet transform is also

complex and can be divided into the real part and imaginary part or amplitude, and phase. Finally, one can define the wavelet power spectrum as $|W_n(s)|^2$. The average of the wavelet power over all local wavelet spectra along the time axis is called the global wavelet spectrum (GWS) (Torrence and Compo, 1998).

$$\overline{W_n}^2(s) = \frac{1}{N} \sum_{n=0}^{N-1} |W_n(s)|^2 \quad (\text{Eq. 4})$$

Significance of the peaks observed in the GWS is tested by the χ^2 test (Torrence and Compo, 1998). Wavelet analysis was applied to time series of monthly number of HREs in each cluster.

3.5 Changes in the mean and trend analysis of HREs features

The frequency of occurrence of HREs, the HREs contribution to total annual rainfall and HREs sizes are some of HREs features that we will study in this work. Besides these features, changes in the length of No Aquifer Recharge Period (NARP) will be analyzed too.

To study the changes in the mean of HREs features a comparison between the two observed sub-periods (1953-1982 and 1983-2012) and between observed and projected periods was done and the significance of changes was tested by *t-test* method. To study the trends a linear trend was fitted to each time series using the least-squares regression method to derive the magnitude of trends while statistical significance was determined by Mann-Kendall (MK) test (Mann, 1945; Kendall, 1975). The MK, a non-parametric robust test against outliers, is widely used in detecting monotonic trends hydro-meteorological time series (Yue and Pilon, 2004).

4. Results and discussion

4.1 HREs threshold selection

The highest coefficient of determination relating HREs with water level increments was obtained with a threshold of 20 mm day^{-1} for the entire study area over the period 2006-2012 ($R^2 = 0.76$) (Figure 3.4a). The number of events above 10 mm day^{-1} threshold also showed a good correlation with water level increments ($R^2 = 0.64$). However, 87% of these $\geq 10 \text{ mm day}^{-1}$ events exceed 15 mm day^{-1} and more than 60% of cases when a water level increment concur with an event between 10mm and 15mm, this event is preceded

by at least an >5mm event in the five days before. It seems to be that water level increment occur after an >10mm event when the soil is saturated. The correlation between water level increments and rainfall events above or equal to 15 mm is closely similar to the correlation with 20mm threshold ($R^2 = 0.74$). Nevertheless, 94% of these ≥ 15 mm events that concur with a water level increment exceed 20mm. Therefore, we consider that the minimum value to define a HRE, which produces an appreciable aquifer recharge in the province of Alicante, is 20 mm day $^{-1}$. The selection of 20mm as a threshold is supported by the fact that the monthly distribution of rainfall events above 20mm shows the best fit with the monthly distribution of water level increments over the period 2006-2012 ($R^2 = 0.72$ against 0.55 and 0.57 in the case of events above 10mm and 15mm respectively) (Figure 3.4b).

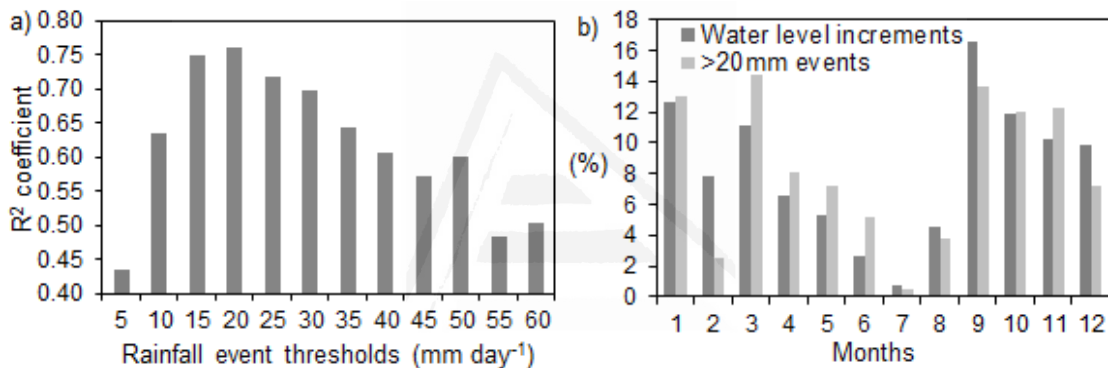


Figure 3.4: (a) Variation profile of the determination coefficient (R^2) from linear regression of monthly observed water level increments number against the number of rainfall events above a given threshold varied between 5 and 60 mm and incremented by 5 mm over the period 2006-2012. (b) the % of the total number of water level increments and of the number of ≥ 20 mm events occurred in each month over the period 2006-2012.

This value is closely similar to the threshold commented by Touhami *et al.* (2013) who concluded that the contribution of events less than 15 mm to aquifer recharge is considered negligible in small karstic aquifers in Alicante province. A bigger threshold was commented by Bellot and Chirino (2013) who mentioned that only rainfall events equal to or greater than 30 mm produced high infiltration values that led to appreciable recharge in the same aquifer. In the Upper Nile Basin of Uganda, Owor *et al.* (2009) commented that the best fit were realized with a threshold of 10 mm day $^{-1}$, nevertheless marginal improvements in the correlation were achieved by employing threshold of 20mm day $^{-1}$ in one of the 4 analyzed stations. A similar threshold was used by Ramírez and González, (2013) in Guadalupe Valley Aquifer in Mexico. They used 22 mm day $^{-1}$ to define the extraordinary rainfall events that produce a direct aquifer recharge.

Chosing 20mm day⁻¹ threshold, besides to the above justification, make us sure to be chosing a representative threshold for the entire province of Alicante due to the uncertainty in water level responses to lower threshold because of low temporal resolution of used data. In the next sections, HREs is referred to events above or equal to 20mm day⁻¹ (or \geq 20mm events). New time series were computed for each cluster. Only HREs occurred in more than 50% of the meteorological stations inside each cluster are counted in order to avoid that the same event will be counted two times when registered in different days in adjacent meteorological stations.

In this study we used 21 piezometric points over the entire province of Alicante. These points are located on different aquifers with different land uses. In the period of 7 years different climate conditions are represented besides the fact that there is a spatial gradient (N–S/E–W) where the mean annual rainfall values varies between 258 and 953 mm. Mean annual temperature which affect the evapotranspiration varies between 20°C and 14°C along this gradient. However, the chosen threshold, considered as representative, can change over time due to changes in climate conditions or in land use/land cover. Historical and projected analyses, in this paper, are made with the assumption that this threshold was valid in the past and will continue valid in the future.

4.2 Observed Changes in the HREs features

4.2.1 Wavelet Analysis results

Wavelet analysis is applied to time series of monthly number of HREs in each cluster. The analysis is focused on the actual oscillations of the individual wavelets, rather than just their magnitude. The (absolute value)² gives information on the relative power at a certain scale and a certain time. In particular, a concentration of power in the 4-8 (or 6±2) and 8-16 (or 12±4) month bands was observed as in the case of cluster 8 (Figure 3.5b, see dark areas). This can be confirmed by analyzing the global wavelet spectrum (GWS), where significant peaks around 6±2 and 12±4 month bands are observed (Figure 3.5c). Periods of low power concentration values (white color) at different scales are observed in the second half of the studied period. Similar results were observed in the northern clusters (7, 9 and 10) while in the southern clusters 1 to 5 a concentration of power were observed at the end of the first sub-period (1953-1982) and the beginning of the second sub-period (1983-2012).

By averaging the power over the entire studied time period we get the GWS which can highlight the dominant frequencies. Indeed, peaks above the 95% confidence level for the GWS (represented by the upper lines in figure 3.6) show the dominant frequencies in the time series. Figure 6 shows the GWS of clusters 1 to 10 over the period 1953-2012 and over the sub-periods 1953-1982 and 1983-2012 from wavelet analysis applied to monthly HREs number time series. The representation of the GWS over the two sub-periods allows the detection of changes in dominant frequencies over time. Significant peaks around 6 ± 2 and 12 ± 4 month bands are observed (Figure 3.5c). These peaks correspond respectively to the bimodal intra-annual regime (autumn - spring) and the annual cycle (autumn - autumn), as is typical of the studied region climate (Sumner *et al.*, 2001). Other peaks are found in clusters 1-5 around 90 ± 30 and 200 ± 50 month bands (i.e., around 8 and 16 years) (Figure 3.6), approximately corresponding to the multi-annual wet/dry cycles of the region (Estrela *et al.*, 2000; Vicente-Serrano *et al.*, 2004).

The most important change observed in the second sub-period (1983-2012) is that in six clusters the significant peak for 6 ± 2 month frequency is no longer significant. The same change observed for the annual peak (12 ± 4 month band) in some clusters.

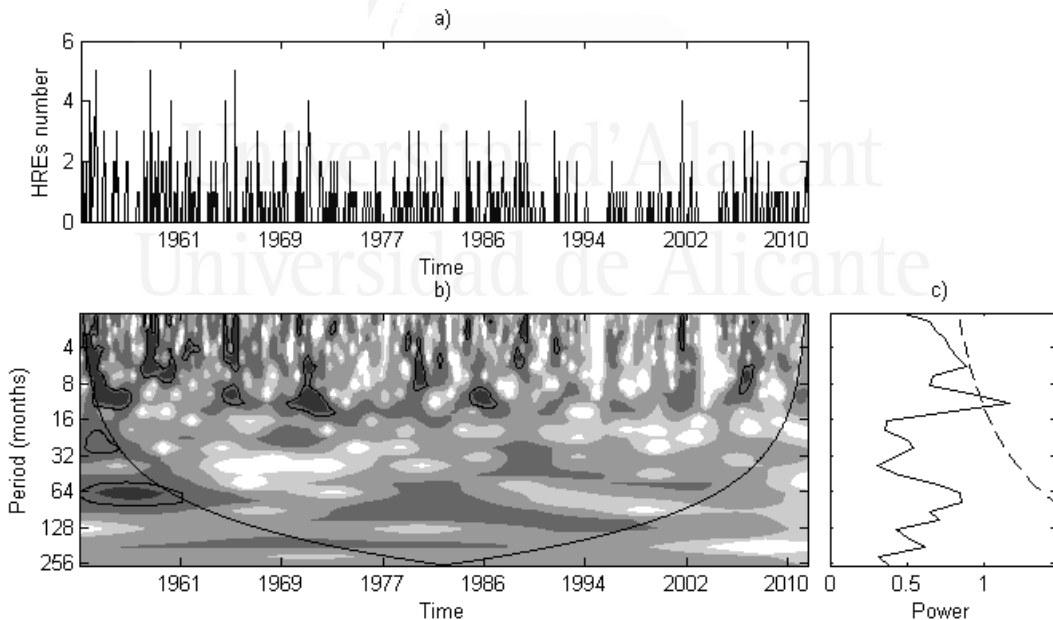


Figure 3.5: (a) Monthly number of HREs in the Cluster 8. (b) The wavelet power spectrum (white areas represent the low values). The region under the cone line is the cone of influence, where zero padding has reduced the variance. Black contour is the 5% significance level, using a white-noise background spectrum. (c) The global wavelet spectrum. The dashed line is the significance for the global wavelet spectrum, assuming the same significance level and background spectrum as in (b)

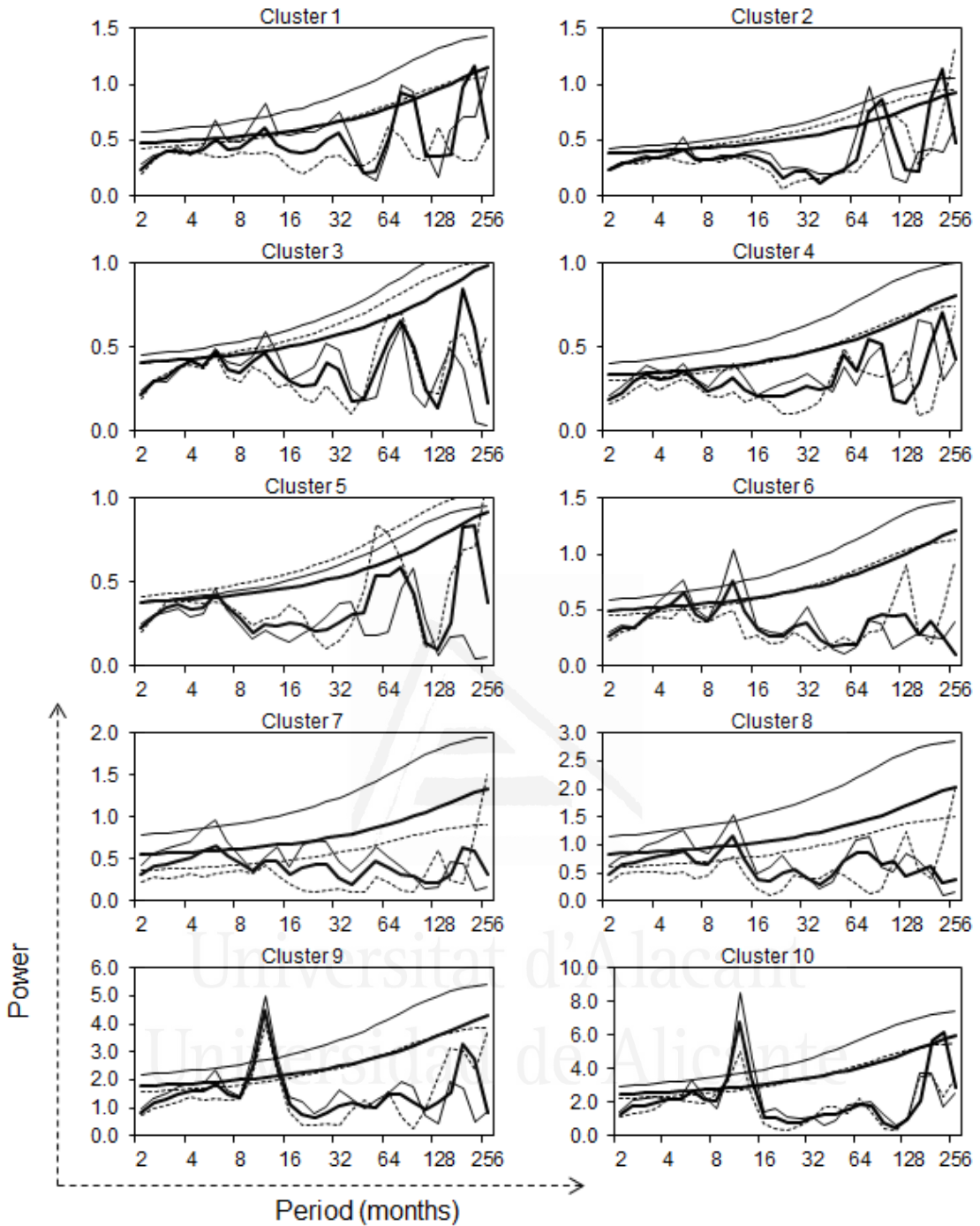


Figure 3.6: The GWS of clusters 1 to 10 from wavelet analysis applied to HREs time series over the period 1953-2012 (thick line) and sub-periods 1953-1982 (thin line) and 1983-2012 (dashed line). (Upper thick, thin and dashed lines are the 95% significance levels for global power spectrum over the three periods respectively)

The main changes in the significance of GWS peaks in the 6 ± 2 and 12 ± 4 month bands between the two sub periods 1953-1982 and 1983-2012 for HREs are summarized in Table 3.1. With the exception of cluster 3, 4 and 9, all other clusters showed significant GWS peaks in the 6 ± 2 month band in the first sub period 1953-1982 which turned not

significant in the second sub period 1983-2012. Significant annual peaks (12 ± 4 month band) were observed in both sub periods in the case of clusters 8, 9 and 10. However, annual peaks were significant in first sub-period and turned not significant in the second sub period in the case of clusters 1, 3 and 6. In the rest of clusters (2, 4, 5 and 7) the annual peaks are not significant in both sub periods.

Table 3.1: Changes in the significance of GWS peaks in 4-8 and 8-16 month bands between the two sub periods 1953-1982 and 1983-2012 in the ten clusters

Months band	Entire period		Sub-periods			
	1953-2012		1953-1982		1983-2012	
	4-8	8-16	4-8	8-16	4-8	8-16
cluster1	s.	s.	s.	s.	n.s.	n.s.
cluster2	s.	n.s.	s.	n.s.	n.s.	n.s.
cluster3	s.	s.	n.s.	s.	n.s.	n.s.
cluster4	s.	n.s.	n.s.	n.s.	n.s.	n.s.
cluster5	s.	n.s.	s.	n.s.	n.s.	n.s.
cluster6	s.	s.	s.	s.	s.	n.s.
cluster7	s.	n.s.	s.	n.s.	n.s.	n.s.
cluster8	s.	s.	s.	s.	n.s.	s.
cluster9	n.s.	s.	n.s.	s.	n.s.	s.
cluster10	s.	s.	s.	s.	n.s.	s.

s.: significant at 5%, n.s.: not significant

4.2.2. Changes in the mean of HREs features

The mean annual number of HREs in the province of Alicante varies from more or less 3 events in the southern clusters to 11 events in the cluster 10 located in the extreme northeast of the study area over the period 1953-2012 (Figure 3.7a). This area with maximum number of HREs coincides with the area with the highest precipitation concentration index (CI) of Spain (De Luis *et al.*, 1997; Martin-Vide, 2004). The HREs number decreased between the two sub-periods (1953-1982 and 1983-2012) in nine clusters with significant decreases in 4 clusters (6, 7, 8 and 10) where the number of HREs decreases a 30%. The major decrease was observed in cluster 8 with 2.5 events less in the second sub-period which represents a change of -37% with respect to the first sub-period. Similar results were observed when analyzing the evolution of extreme events over the same period in a previous study in the same region by Moutahir *et al.* (2014) using 20 mm day^{-1} as a threshold to define precipitation extreme events.

Touhami *et al.*, (2015) also reported that a reduction of events above 15mm is expected over the period 2011-2099 in small region inside our study area.

As it is expected the decrease of HREs number produces a decrease in the total volume of water produced by these events. Indeed, the volume of water produced by HREs decreases in 6 of the ten clusters with significant changes between the two sub-periods in three clusters (Figure 3.7b). Significant negative changes ($p<0.10$) were observed in three clusters with an important reduction of HREs total water (-33% with respect to the sub-period 1953-1982). As in the case of the number of HREs, the major and most significant reduction of water between the two sub-periods was observed in the cluster 8 (-88 mm which represents -36% with respect to the first sub-period (1953-1982)).

The expected decrease in the total volume of water produced by HREs is not proportional to the expected decrease in the number of these events. In fact, among the nine clusters where the number of HREs number has decreased, the mean size of events increased 8% in seven clusters with respect to the first observed sub-period (Figure 3.7c). This change was significant at 5% in only the cluster 9 located in the northeast of Alicante (+5 mm/event which represents +12% with respect to the first sub-period 1953-1982). This finding is the main result of the comparison between the two sub-periods. This result matches with the prediction of climate models for the Mediterranean region where the increase of extreme events is expected to be one of the major climatic changes (IPCC, 2012, Rajczak *et al.*, 2013).

4.2.3 Trends in the HREs features

A negative trend in the number of HREs is observed in nine clusters over the period 1953-2012. However, only the northern clusters (7, 8, 9 and 10) and the cluster 6 located the middle of the coastal area of Alicante province showed significant trends (Table 2). The highest change rate in the number of HREs was observed in the cluster 8 ($-0.8 \text{ events decade}^{-1}$). A close rate ($-0.6 \text{ events decade}^{-1}$) was observed in the clusters 7, 9 and 10. A negative linear trend of -0.8 events per decade in the cluster 8 means a reduction of 4.8 HREs in 60 years which represent 70% of the mean number of HREs over the first sub-period (1953-1982).

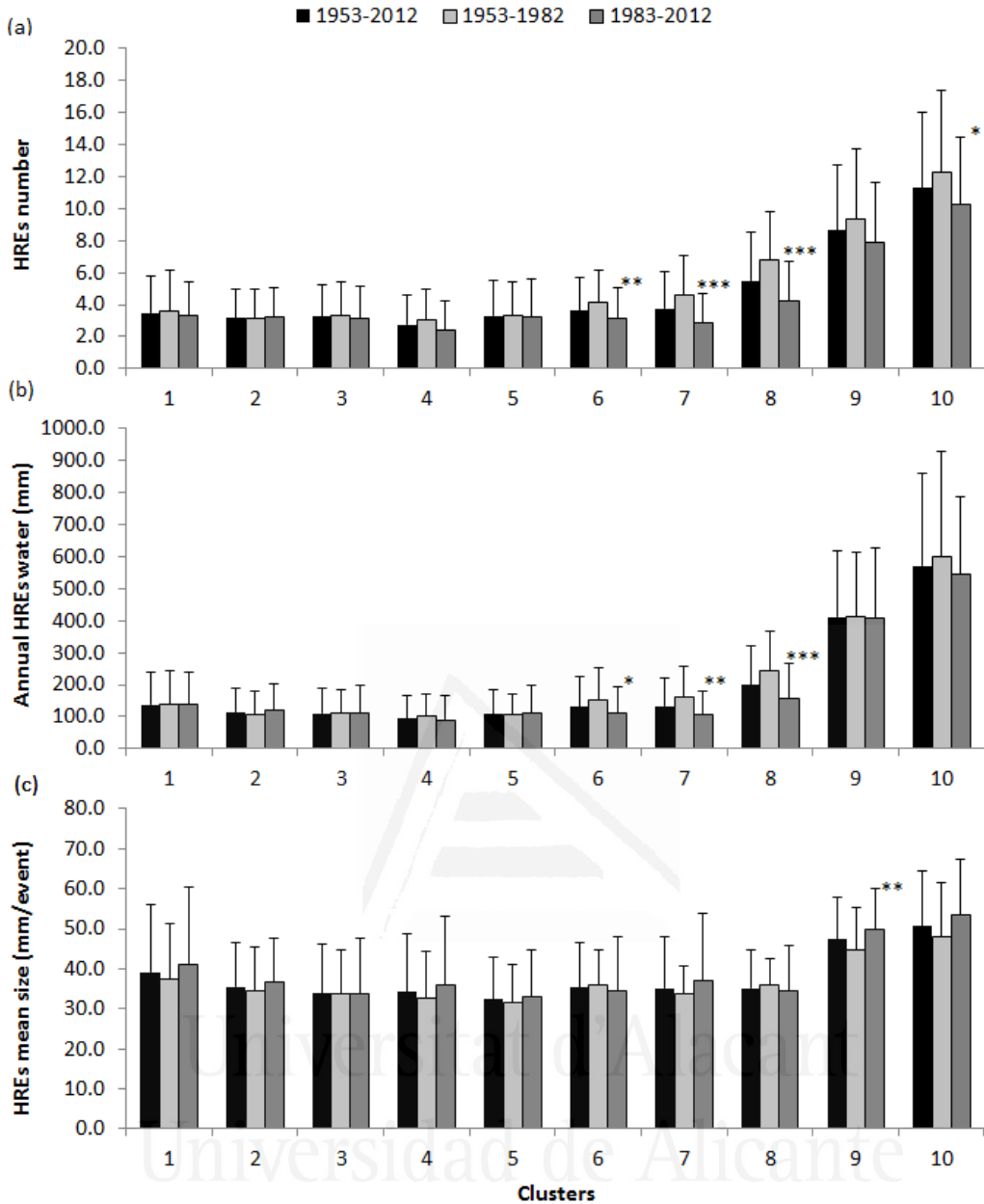


Figure 3.7: Mean annual number of HREs (a), Mean annual volume of water produced by HREs (b) and Mean size of events (mm/event) (c) over the period 1953-2012 and the two sub-periods 1953-1982 and 1983-2012. The difference with respect to the first sub-period is *significant at 10%, **significant at 5%, ***significant at 1%.

The total annual water produced by HREs also showed a negative trend in the nine clusters where HREs number reduction was observed (Table 3.2). Nonetheless, only 3 clusters showed significant negative trends. The most important negative trends were observed in clusters 6, 7 and 8 with values of -9.5, -18.9 and -26.5 mm per decade respectively. These rates mean a reduction between -60 and -160 mm in 60 years in these clusters. Other important negative not significant trends in HREs water were observed in clusters 9 and 10 (-10.4 and -25.7 mm decade⁻¹ respectively). The decrease

in the HREs contribution to total annual rainfall matches with the decrease in the annual rainfall observed by Moutahir *et al.* (2014). This decrease could be the important factor in the reduction observed in total annual rainfall because extreme events in the Valencia Region represent on average 50% of annual rainfall (De Luis *et al.*, 2000).

Trends on the HREs mean size go in the opposite way to the HREs number and total annual water trends. Actually the mean size of HREs showed a positive trend in six clusters (Table 3.2). The most important positive trend is observed in clusters 4, 9 and 10 (+1 mm decade⁻¹); however, it is not statistically significant. This positive trend in the mean size of HREs is leading to high concentration of precipitation expressed as an increase in the frequency of extreme events.

Despite the fact that changes in the HREs number showed significant trends over the period 1953-2012 it was not the case all time. Clusters 6 to 9 showed significant to very significant negative trends in the number of HREs per decade over the studied period of time. However, if we change the temporal scale and use a moving 30-years window over the period 1953-2012 we can see that the sign of trend and magnitude is changing over time (Figure 3.8). Indeed, in the cluster 9 the trend was negative and significant at the beginning of the studied period of time and became positive and not significant at the end. In the clusters 6 to 8 trends are negative and significant in the second part of the studied period and the magnitude is decreasing.

Table 3.2: Trends per decade in the mean annual number of HREs, in mean annual volume of water produced by HREs and mean HREs size over the period 1953-2012. (The magnitude of change by linear regression and significance test by Mann-Kendall test)

	Trends per decade in:		
	number of HREs	Total HREs water (mm)	Size of HREs (mm/event)
cluster01	-0.1	-2.1	-0.1
cluster02	0.0	+1.4	+0.3
cluster03	-0.1	-1.4	-0.1
cluster04	-0.2	-3.5	+0.9
cluster05	-0.1	-2.9	+0.5
cluster06	-0.2*	-9.5**	-0.4
cluster07	-0.6***	-18.9***	+0.4
cluster08	-0.8***	-26.5***	-0.2
cluster09	-0.6*	-10.4	+1.0
cluster10	-0.6*	-25.7	+1.0

*significant at 10%, **significant at 5%, ***significant at 1%

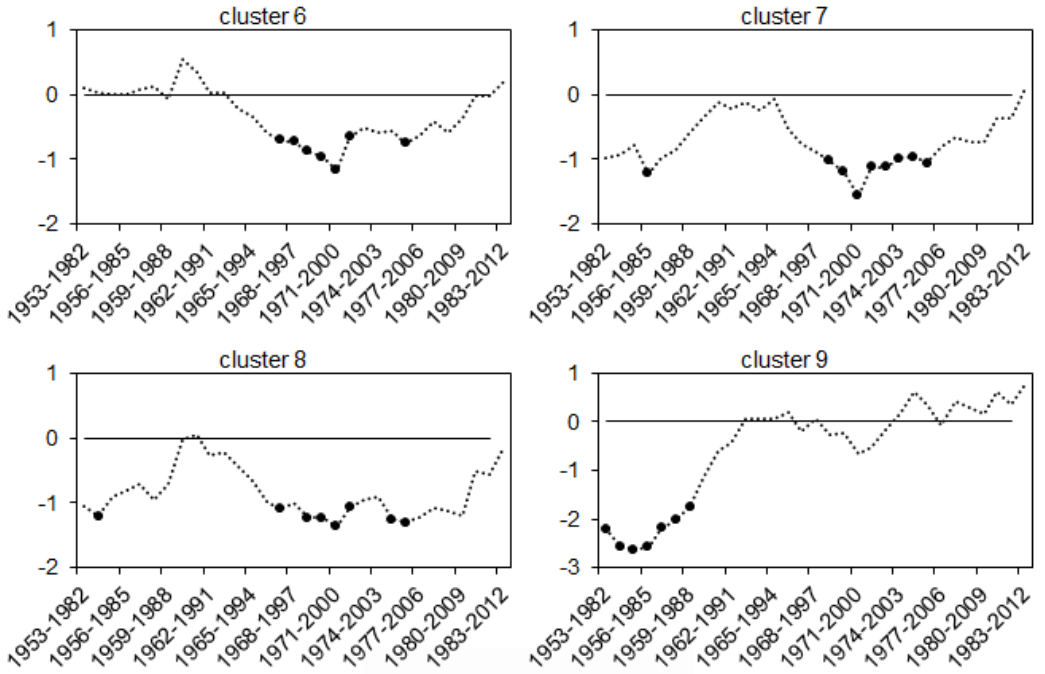


Figure 3.8: Evolution of the trend direction and of the magnitude of change (event per decade) in the number of HREs over a moving 30-year window over the period 1953-2012. Black dots show the significant trends at 5%.

Negative trends observed in the number of HREs over the period 1953-2012 in the region of Alicante is similar to results obtained by Moutahir *et al.* (2014) when analyzing trends in extreme events over the same period of time in the same area. Nonetheless, these results don't match with results observed at Valencian community scale (González-Hidalgo *et al.*, 2003) and at regional and global scales (Frich *et al.*, 2002; IPCC, 2012). In fact, the previous cited works talk about an increase in extreme events in the 2th half of 20th century. This difference is due in part to spatial and temporal scales used. The time window used is different and as it is illustrated in Figure 8 the sign and magnitude of trends depend on the chosen time window. In fact, Moutahir *et al.* (2014) observed a non-significant increase in extremes rainfall events over the sub-period 1983-2012. Another factor which could explain this difference is the threshold used to define the extreme events. Actually González-Hidalgo *et al.* (2003) used the 10 high values per year method. This can match with the fact that results showed that the HREs size is increasing.

4.2.4 Changes in the mean and trends in the length of NARP

In this work NARP is considered as the maximum period of time (in days) between two consecutive HREs within a year. This period of time between increases when the frequency of HREs decreases. The mean length of NARP increased on average 21 days in the 2th sub-period with respect to the first sub-period (1953-1982) in eight clusters; however, the increase was significant in only two clusters (Table 3.3). NARP showed a negative non-significant change in the extreme southern clusters 1 and 2. The two high and significant increases in NARP were observed in clusters 7 and 8 (39 and 34 days respectively). Another high increment in NARP was observed in cluster 4 (33 days) but it was not significant.

A positive trend in the mean length of NARP was observed in eight clusters (Table 3.3). Significant trend was observed only in the cluster 7. In this cluster the NARP has increased by 11.5 days per decade. Negative and non-significant trends were observed in clusters 1 and 2.

The maximum length of NARP is observed in the summer months. The increment in the length of NARP is, in part, due to the decrease in HREs number in general and to the decrease of HREs number in the months from April to August. Indeed, in these months the number of HREs decreased 15% in the second sub-period with respect the first sub-period in the entire region which makes the NARP exceeds the limits of summer to May and April. This result coincides with the changes observed in the wavelet analysis. In fact, the analysis of the GWS showed that significant peaks in the 4-8 month band in the first sub period 1953-1982 are no longer significant in the second sub period 1983-2012. This situation is expected to continue in the future. Indeed, Frei *et al.*, (2006) indicated that, in the Iberian Peninsula, the x1d.5 (return value of one-day precipitation intensity with a return period of 5 years) will decrease in spring and change marginally in autumn. An increase in NARP will cause groundwater droughts which generally occur on a time scale of months to years (van Lanen and Peters, 2000)

Table 3.3: Change in the mean length of NARP in the second sub-period (1983-2012) with respect to the first sub-period (1953-1982) and trends over the entire observed period (1953-2012).

	Change with respect to the sub-period (1953-1982) (days)	Trends in NARP length (days/decade)
cluster01	-11.1	-7.2
cluster02	-7.4	-5.4
cluster03	+8.9	+3.9
cluster04	+32.6	+7.2
cluster05	+19.7	+5.9
cluster06	+19.6	+1.8
cluster07	+38.6**	+11.5*
cluster08	+34.2*	+5.4
cluster09	+2.0	+0.4
cluster10	+11.3	+1.6

*significant at 10%, **significant at 5%

4.3 Projected Changes in the HREs features

4.3.1 Changes in the mean with respect to the observed period

According to the nine CMIP5 models studied, the same tendency of changes detected in HREs features over the observed period (1953-2012) is expected under the two RCP scenarios over the last 60 years of the 21st century. With the exception of the NorESM1 model, a decrease in the number of HREs is expected in the major part of clusters under the other eight models. The reduction in the mean number of HREs, in the entire region, under the high RCP8.5 scenario is expected to be about two times the reduction under the moderate RCP4.5 scenario with respect to the observed period (-15% and -8% respectively) (Figure 3.9).

The mean number of HREs is expected to decrease in the ten clusters under the two RCP scenarios by the end of the 21st century (Figure 3.10a); nonetheless, the major changes are expected under the high scenario. The highest decreases are expected in clusters 6 to 9 (-19, -23, -18 and -22% respectively under the RCP8.5 scenario with respect to the observed period 1953-2012). However, the highest change in absolute value will be observed in cluster 9 (-2 events as an average of the nine models and up to 2.6 events under three models). These high and significant change values are expected

in the northern clusters located in a wet region in comparison with the southern clusters. In fact, in the southern clusters the number of HREs is low and the changes are not significant.

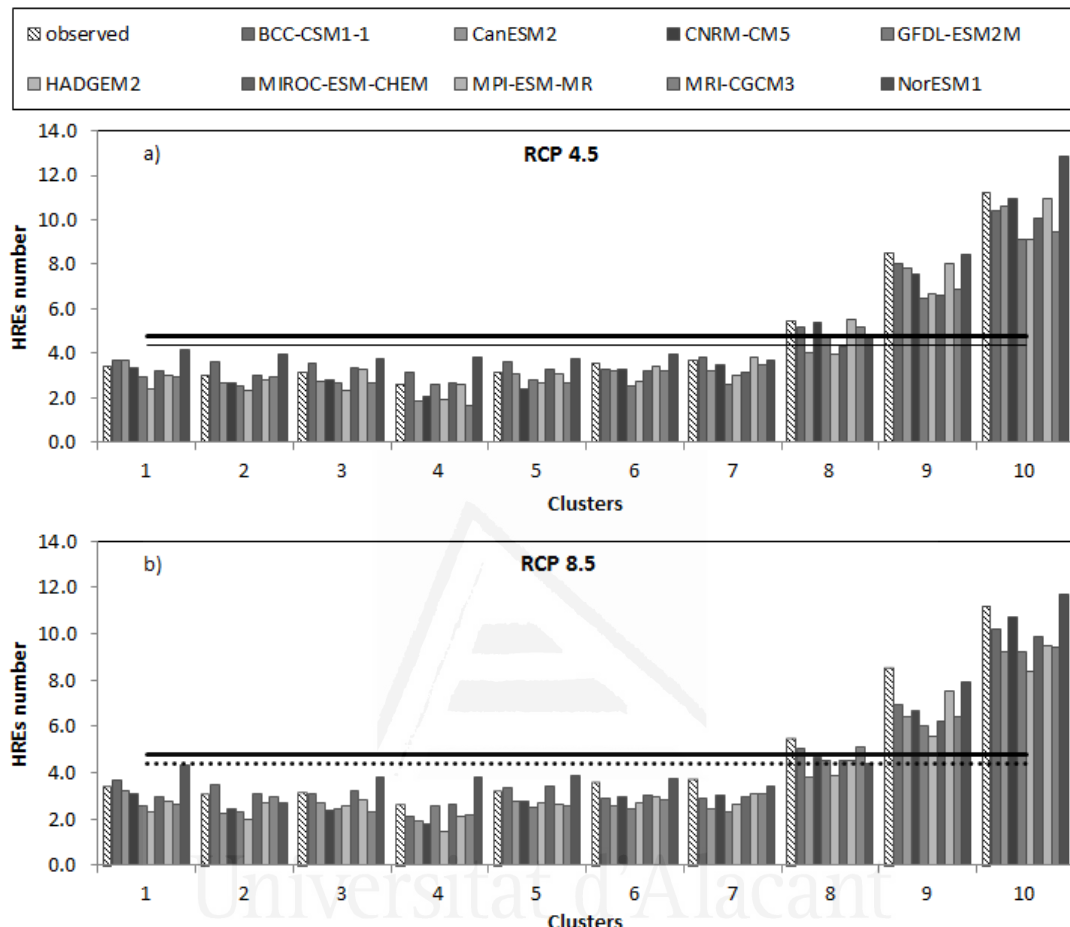


Figure 3.9: Projection of the expected mean annual number of HREs by the nine CMIP5 models under RCP4.5 (a) and RCP8.5 (b) scenarios for the period (2040-2099). Thick, thin and dashed lines are the observed, RCP4.5 and RCP8.5 mean numbers of HREs for the entire region and the nine models respectively.

A similar tendency of change is expected in the total water produced by HREs with major decreases with respect to the observed period under the RCP8.5 scenario (-13% on average in the ten clusters in comparison with only -6% under the RCP4.5) (Figure 3.10b). Indeed, the major and significant decreases in the total HREs water are expected in the northern clusters 7 to 10 (-22, -15, -24 and -12% respectively) and in the coastal cluster number 6 (-17%). The maximum absolute reduction will be observed in clusters 9 and 10 (-98 and -73 mm with respect to the observed period). This reduction is largely bigger than the reduction in the southern clusters (≤ 15 mm).

On the contrary of the tendency of change expected in the mean HREs number and total water, the mean size of HREs is expected to increase under the two RCP scenarios in the entire region with the exception of clusters 9 and 10 (Figure 3.10c). The major and significant increases ($p<0.05$) are expected in the clusters 4, 5 and 8 (+13, +9 and +8% under the RCP4.5 scenario and +14, +11 and +6% under the RCP8.5 scenario respectively).

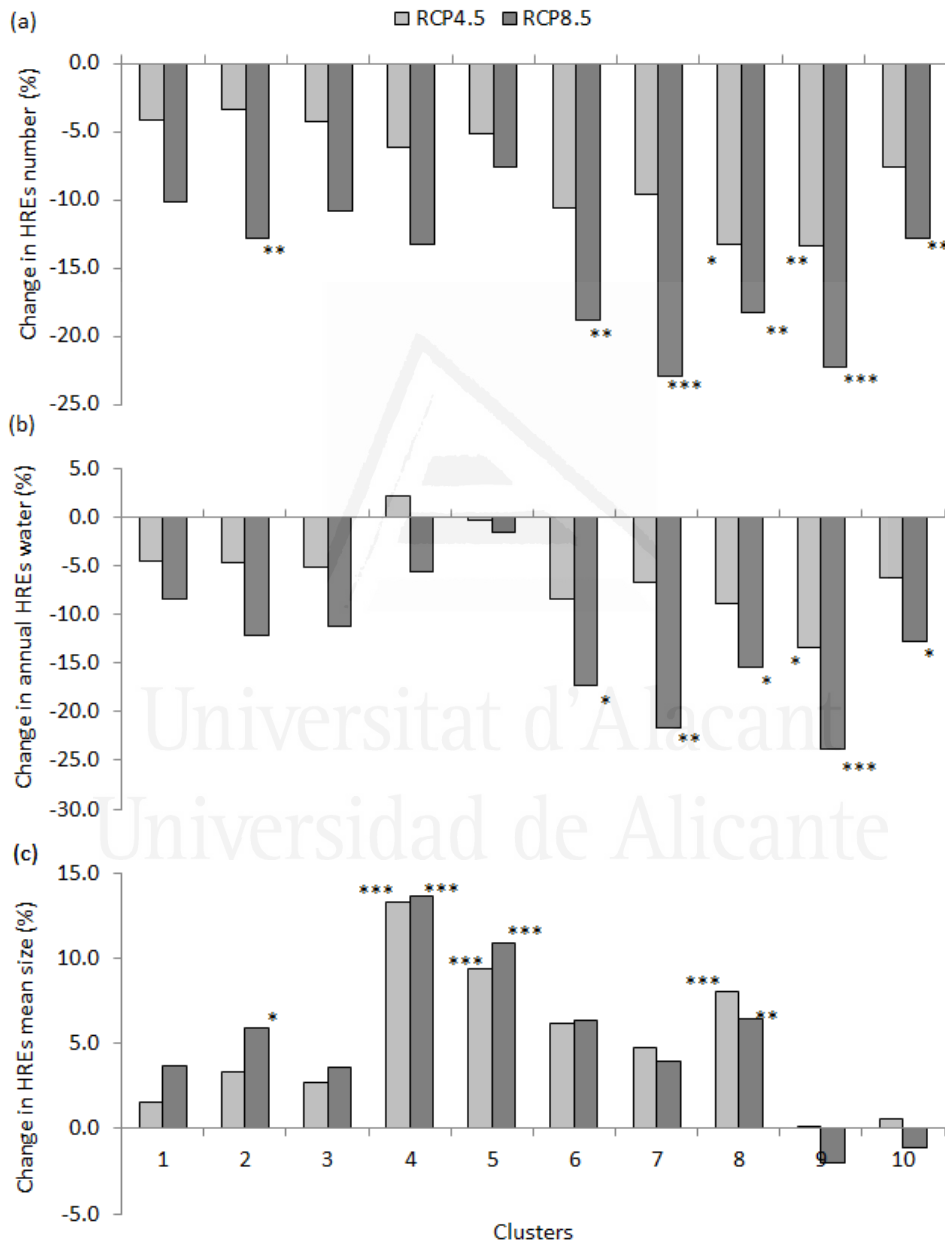


Figure 3.10: Projected change in mean values under the nine CMIP5 models and the two RCP scenarios with respect to the observed period of the expected (a) mean annual number of HREs; (b) mean annual volume of water produced by HREs; and (c) the mean size of HREs. The difference with respect to the observed period is *significant at 10%, **significant at 5%, ***significant at 1%.

4.3.1 Trends in the HREs features over the projected period

A summary of the mean projected trends in HREs features, under the two RCP scenarios and nine CMIP5 models, is presented in table 3.4. Mean HREs number showed no trends or negative not significant trends in nine clusters under the RCP4.5 scenario. However, it showed significant negative trends in four clusters under the RCP8.5 scenario. In the opposite way, the total HREs water showed more negative and significant trends under the RCP4.5. The major part of negative trends in HREs number and total water were observed in the northern clusters. The mean HREs size showed positive trends under the RCP8.5 while they were negative or null under the RCP4.5. In general, changes in HREs features are expected to continue in the same direction as in the observed period above all under the high scenario.

The expected decrease in HREs number and total HREs water will be reflected in a decrease of annual precipitation. Actually, extreme events in the Valencia Region represent on average 50% of annual rainfall (De Luís *et al.*, 2000). Many studies focusing on precipitation changes agree on the fact that precipitation, in the Mediterranean area, is decreasing and will continue decreasing in the future (Frei *et al.*, 2006; Beniston, *et al.* 2007; Rajczak *et al.*, 2013; IPCC, 2014).

The decrease in frequency and total HREs water is partly compensated for by an increase in HREs size. The increase of HREs size means an increase of precipitations concentration which is expected in the major part of the province of Alicante. Higher decreasing in low intensities and significant increases in heavy precipitation is also found by Rajczak *et al.* (2013) for the Mediterranean basin, according with several regional climate models from the ENSEMBLES project (van der Linden and Mitchell, 2009). According to Monjo *et al.* (2015), a high uncertainty is found in the projected changes for the extreme precipitation due to its natural variability and its non-linear behavior. For example, although a priori more significant changes could be expected under the RCP8.5, they can be diluted by the natural cycles and even smoothed by a non-linear compensating mechanism regarding a minor radiative forcing (e.g. under the RCP4.5; Mitchell and Hulme, 1999).

Table 3.4: Mean projected trends in HREs features over the period (2040-2099) under the two climate scenarios. Mean of the nine models and standard error.

	Trends per decade in:					
	Number of HREs		Total HREs water (mm)		Size of HREs (mm/event)	
	RCP4.5	RCP8.5	RCP4.5	RCP8.5	RCP4.5	RCP8.5
cluster01	0.01 ±0.01	-0.04 ±0.01	0.4 ±0.68	0.16 ±0.54	0.02 ±0.06	0.45 ±0.06
cluster02	-0.03 ±0.02	0.04 ±0.02	-1.81 ±0.79	2.05 ±0.75	-0.29 ±0.06	0.17 ±0.03
cluster03	-0.07 ±0.02*	0 ±0.02	-2.79 ±0.56*	0.33 ±0.58	-0.12 ±0.03	-0.06 ±0.06
cluster04	0.02 ±0.02	0.04 ±0.02	0.64 ±0.91	1.34 ±0.67	0 ±0.04	-0.15 ±0.05
cluster05	-0.03 ±0.01	0.02 ±0.02	-1.14 ±0.4	1.34 ±0.65	-0.01 ±0.03	0.23 ±0.03
cluster06	-0.07 ±0.01	-0.05 ±0.01	-3.75 ±0.57**	-1.3 ±0.44	-0.33 ±0.05*	0.28 ±0.04
cluster07	-0.05 ±0.01	-0.09 ±0.02*	-2.92 ±0.65	-3.23 ±0.69*	-0.21 ±0.04	0.07 ±0.04
cluster08	-0.1 ±0.02	-0.14 ±0.03**	-4.53 ±0.71*	-4.83 ±1.07*	-0.13 ±0.03	0.04 ±0.06
cluster09	-0.11 ±0.03	-0.3 ±0.02***	-8.49 ±1.64*	-13.78 ±1.06***	-0.36 ±0.05*	0.08 ±0.05
cluster10	-0.13 ±0.03	-0.18 ±0.04**	-8.59 ±1.67	-6.55 ±1.74	-0.02 ±0.05	0.13 ±0.07

*significant at 10%, **significant at 5%, ***significant at 1%

5. Conclusion

Aquifer recharge is facing an important decrease in the province of Alicante. Results obtained in this work showed that the number of heavy rainfall events which produce appreciable aquifer recharge has experienced a significant decrease in the last 60 years until 2012. This decrease is expected to be accentuated by climate change by the end of the 21st century. Indeed, according to the nine CMIP5 models studied, the mean number of HREs may have a significant decrease in Alicante province especially under the high (RCP8.5) scenario. The highest percentages of reduction of HREs number are expected in the northern clusters; however, this reduction maybe more important in southern clusters. In fact, in the southern clusters there is a significant water deficit and any reduction will affect the ecosystems functioning. The reduction in aquifer recharge due to the decrease in HREs number seems to be partly compensated for by an increase in HREs size; however, this will have negative environmental and socio-economic consequences. The decrease of the number of HREs is causing an increase in the length of no aquifer recharge periods which will accentuate the groundwater droughts in the region. Although some of the observed trends are significant over the 60-years window it is not the case when analyzing these trends over a 30-years moving window. Actually the significance, magnitude and sign of these trends are changing depending on the selected time window. Decision makers in Alicante should take into account such

results when planning economic activities to manage groundwater resources in a sustainable way.

References

- Andreo, B., Vías, J., Durán, J. J., Jiménez, P., López-Geta, J. A., Carrasco, F., 2008. Methodology for groundwater recharge assessment in carbonate aquifers: application to pilot sites in southern Spain. *Hydrogeology Journal*, 16(5), 911-925.
- Bellot, J., Bonet, A., Sanchez, J.R., Chirino, E., 2001. Likely effects of land use changes on the runoff and aquifer recharge in a semiarid landscape using a hydrological model. *Landscape and Urban Planning*, 55(1), 41-53.
- Bellot, J., & Chirino, E., 2013. Hydrobal: An eco-hydrological modelling approach for assessing water balances in different vegetation types in semi-arid areas. *Ecological Modelling*, 266, 30-41.
- Beniston, M., Stephenson, D. B., Christensen, O. B., Ferro, C. A. T., Frei, C., Goyette, S., Halsnaes, K., Holt, T., Jylhä, K., Koffi, B., Palutikof, J., Schöll, R., Semmler, T., Wothonen, K., 2007. Future extreme events in European climate: An exploration of regional climate model projections, *Climatic Change*, 81, 71–95, doi:10.1007/s10584-006-9226-z.
- Cudennec, C., Leduc, C., Koutsoyiannis, D., 2007. Dryland hydrology in Mediterranean regions—a review, *Hydrological Sciences Journal*, 52:6, 1077-1087, DOI: 10.1623/hysj.52.6.1077
- Daccache, A., Ciurana, J S., Rodriguez Diaz, J A., Knox, J W., 2014. Water and energy footprint of irrigated agriculture in the Mediterranean region. *Environ. Res. Lett.* 9 124014 [doi:10.1088/1748-9326/9/12/124014](https://doi.org/10.1088/1748-9326/9/12/124014)
- De Luis, M., González-Hidalgo, J. C., Raventós, J., Sánchez, J. R., & Cortina, J., 1997. Distribución espacial de la concentración y agresividad de la lluvia en el territorio de la Comunidad Valenciana. *Cuaternario y Geomorfología*, 11(3-4), 33-44.
- De Luis, M., Raventós, J., González-Hidalgo, J.C., Sánchez, J.R., Cortina, J., 2000. Spatial analysis of rainfall trends: a case study in Valencia Region (E Spain). *Int. J. Climatol* 20:1451–1469

- Estrela, M.J., Peñarrocha, D., Millán, M. 2000. Multi-annual drought episodes in the Mediterranean (Valencia region) from 1950–1996. A spatio-temporal analysis. *Int. J. Climatol.*, 20: 1599–1618.
- Frich, P., Alexander, L.V., Della-Marta, P., Gleason, B., Haylock, M., Klein Tank, A.M.G., Peterson, T., 2002. Observed coherent changes in climatic extremes during the second half of the twentieth century, *Clim. Res.*, 19, 193-212.
- Frei, C., R. Scholl, S. Fukutome, J. Schmidli, and P. L. Vidale 2006. Future change of precipitation extremes in Europe: Intercomparison of scenarios from regional climate models, *J. Geophys. Res. Atmos.*, 111(D6), doi:10.1029/2005jd005965.
- Frot, E., van Wesemael, B., Vandenschrick, G., Souchez, R., Solé Benet, A., 2007. Origin and type of rainfall for recharge of a karstic aquifer in the western Mediterranean: a case study from the Sierra de Gador–Campo de Dalias (southeast Spain). *Hydrological Processes*, 21: 359–368. doi: 10.1002/hyp.6238
- García-Ruiz, J.M., López-Moreno, J.I., Vicente-Serrano. S.M., Lasanta Martínez, T., Beguería, S., 2011. Mediterranean water resources in a global change scenario *Earth-Sci. Rev.* 105121–39
- González-Hidalgo, J. G., De Luis, M., Raventós, J., & Sánchez, J. R., 2003. Daily rainfall trend in the Valencia Region of Spain. *Theoretical and Applied Climatology*, 75(1-2), 117-130.
- Green, T. R., Taniguchi, M., Kooi, H., Gurdak, J. J., Allen, D. M., Hiscock, K. M., Treidel, H., Aureli, A. (2011). Beneath the surface of global change: Impacts of climate change on groundwater. *Journal of Hydrology*, 405(3), 532-560.
- Grossmann, A., Morlet, J., 1984. Decomposition of Hardy functions into square integrable wavelets of constant shape. *SIAM journal on mathematical analysis*, 15(4), 723-736.
- Ibáñez, J., Martínez Valderrama, J., Puig de fábregas, J., 2008. Assessing overexploitation in Mediterranean aquifers using system stability condition analysis. *Ecological Modelling*, Volume 218, Issues 3–4, 10: 260-266, ISSN 0304-3800, <http://dx.doi.org/10.1016/j.ecolmodel.2008.07.004>.

Iglesias, A., Mougou, R., Moneo, M., Quiroga, S. 2011. Towards adaptation of agriculture to climate change in the Mediterranean. *Regional Environmental Change*, 11(1), 159-166.

IPCC, 2012: Managing the Risks of Extreme Events and Disasters to Advance Climate Change Adaptation. A Special Report of Working Groups I and II of the Intergovernmental Panel on Climate Change [Field, C.B., V. Barros, T.F. Stocker, D. Qin, D.J. Dokken, K.L. Ebi, M.D. Mastrandrea, K.J. Mach, G.-K. Plattner, S.K. Allen, M. Tignor, and P.M. Midgley (eds.)]. Cambridge University Press, Cambridge, UK, and New York, NY, USA, 582 pp.

IPCC, 2014: Climate Change 2014: Impacts, Adaptation, and Vulnerability. Part B: Regional Aspects. Contribution of Working Group II to the Fifth Assessment Report of the Intergovernmental Panel on Climate Change [Barros, V.R., C.B. Field, D.J. Dokken, M.D. Mastrandrea, K.J. Mach, T.E. Bilir, M. Chatterjee, K.L. Ebi, Y.O. Estrada, R.C. Genova, B. Girma, E.S. Kissel, A.N. Levy, S. MacCracken, P.R. Mastrandrea, and L.L. White (eds.)]. Cambridge University Press, Cambridge, United Kingdom and New York, NY, USA, 688 pp.

Kendall, M.G., 1975. Rank Correlation Methods. Griffin, London, UK.

Labat, D., Ababou, R., Mangin, A., 2001. Introduction of Wavelet Analyses to Rainfall/Runoffs Relationship for a Karstic Basin: The Case of Licq-Atherey Karstic System (France). *Groundwater*, 39(4), 605-615.

Lau, K.M., Weng, H., 1995. Climate signal detection using wavelet transform: How to make a time series sing. *Bull. Am. Met. Soc.*, 76(12), 2391-2402.

Mann, H.B., 1945. Nonparametric tests against trend. *Econometrica* 13 (3), 245–259.

Markovic, D., Koch, M., 2005. Wavelet and scaling analysis of monthly precipitation extremes in Germany in the 20th century: Interannual to interdecadal oscillations and the North Atlantic Oscillation influence, *Water Resour. Res.*, 41, W09420, doi:[10.1029/2004WR003843](https://doi.org/10.1029/2004WR003843).

Martin-Vide, J., 2004. Spatial distribution of a daily precipitation concentration index in peninsular Spain. *Int. J. Climatol.*, 24: 959–971. doi: 10.1002/joc.1030

- Martínez-Santos, P., Andreu, J. M., 2010. Lumped and distributed approaches to model natural recharge in semiarid karst aquifers. *Journal of hydrology*, 388(3), 389-398.
- Millán, M., Estrela, M. J., Caselles, V., 1995. Torrential precipitations on the Spanish east coast: the role of the Mediterranean sea surface temperature. *Atmospheric Research*, 36(1), 1-16.
- Mishra, A. K., Singh, V. P. 2010. A review of drought concepts. *Journal of Hydrology*, 391(1), 202-216.
- Monjo, R., Gaitán, E., Pórtoles, J., Ribalaygua, J., Torres, L., 2015. Changes in extreme precipitation over Spain using statistical downscaling of CMIP5 projections. *Int. J. Climatol.*
- Moutahir, H., De Luis, M., Serrano-Notivoli, R., Touhami, I., Bellot, J., 2014. Análisis de los eventos climáticos extremos en la provincia de Alicante, Sureste de España. En: Fernández-Montes, S. y Rodrigo, F.S. (Eds). Cambio climático y cambio global. Publicaciones de la Asociación Española de Climatología (AEC). Serie A, nº9. Almería. ISBN: 978-84-16027-69-9. pp. 457-466.
- Nakken, M., 1999. Wavelet analysis of rainfall-runoff variability isolating climatic from anthropogenic patterns. *Environmental Modelling & Software*, 14(4), 283-295.
- Olesen, J.E., Trnka, M., Kersebaum, K.C., Skjelvåg, A.O., Seguin, B., Peltonen-Sainio, P., Rossi, F., Kozyra, J., Micale, F., 2011. Impacts and adaptation of European crop production systems to climate change. *European Journal of Agronomy*, 34(2), 96-112.
- Owor, M., Taylor, R.G., Tindimugaya, C., Mwesigwa, D., 2009. Rainfall intensity and groundwater recharge: empirical evidence from the Upper Nile Basin. *Environ. Res. Lett.*, 4(3), 035009.
- Rajczak J, Pall P, Schär C. 2013. Projections of extreme precipitation events in regional climate simulations for Europe and the Alpine Region. *J. Geophys. Res.* 118: 2169–8996, doi: 10.1002/jgrd.50297.
- Ramírez, J., González, R., 2013. Modeling of the Water Table Level Response Due to Extraordinary Precipitation Events: The Case of the Guadalupe Valley Aquifer.

International Journal of Geosciences, Vol. 4 No. 6, 2013, pp. 950-958. doi: 10.4236/ijg.2013.46088.

Ribalaygua, J., Torres, L., Pórtoles, J., Monjo, R., Gaitán, E., Pino, M.R., 2013.

Description and validation of a two-step analogue/regression downscaling method.

Theoretical and Applied Climatology 114: 253-269. doi:10.1007/s00704-013-0836x.

Scanlon, B. R., Keesee, K. E., Flint, A. L., Flint, L. E., Gaye, C. B., Edmunds, W. M. and Simmers, I.: Global synthesis of groundwater recharge in semiarid and arid regions, Hydrological Processes, 20(15), 3335–3370 doi: <http://dx.doi.org/10.1002/hyp.6335>

Sumner, G., Homar, V., Ramis C. 2001. Precipitation seasonality in eastern and southern coastal Spain. Int. J. Climatol. 21: 219–247.

Taylor, K.E., Stouffer, R.J., Meehl, G.A., 2009. A summary of the CMIP5 experiment design. PCDMI Rep. http://cmip-pcmdi.llnl.gov/cmip5/docs/Taylor_CMIP5_design.pdf (accessed 10th April 2015).

Taylor, R., Todd, M., Kongola, L., Maurice, L., Nahozya, E., Sanga, H., *et al.* 2013. Evidence of the dependence of groundwater resources on extreme rainfall in East Africa. Nature Climate Change, 3: 374-378.

Torrence, C., Compo, G.P., 1998. A practical guide to wavelet analysis. Bull. Am. Met. Soc., 79 (1), 61-78.

Touhami, I., Andreu, J.M., Chirino, E., Sánchez, J.R., Moutahir, H., Pulido-Bosch, A., Martínez-Santos,P., Bellot, J., 2013. Recharge estimation of a small karstic aquifer in a semiarid Mediterranean region (southeastern Spain) using a hydrological model. Hydrological Processes, 27(2), 165-174.

Touhami, I., Andreu, J. M., Chirino, E., Sánchez, J. R., Pulido-Bosch, A., Martínez-Santos, P., Moutahir, H., Bellot, J., 2014. Comparative performance of soil water balance models in computing semi-arid aquifer recharge. Hydrological Sciences Journal, 59(1), 193-203.

Touhami, I., Andreu, J.M., Chirino, E., Sánchez, J.R., Pulido-Bosch, A., Martínez-Santos, P., Moutahir, H., Bellot, J. 2015. Assessment of climate change impacts on

soil water balance and aquifer recharge in a semiarid region in south east Spain. Journal of Hydrology 527 (2015) 619–629.

Tweed, S., Leblanc, M., Cartwright, I., Favreau, G., Leduc, C., 2011. Arid zone groundwater recharge and salinisation processes; an example from the Lake Eyre Basin, Australia. Journal of Hydrology, 408(3), 257-275.

Van der Linden, P., and Mitchell, J. F. B., 2009. ENSEMBLES: Climate Change and Its Impacts: Summary of Research and Results From the ENSEMBLES Project, 160 pp., MetOffice Hadley Centre, Exeter.

Van Lanen, H. A. J., Peters, E. 2000. Definition, effects and assessment of groundwater droughts. In Drought and Drought Mitigation in Europe (pp. 49-61). Springer Netherlands.

Vias, J.M., Andreo, B., Perles, M.J., Carrasco, F., 2005. A comparative study of four schemes for groundwater vulnerability mapping in a diffuse flow carbonate aquifer under Mediterranean climatic conditions. Environmental Geology, 47(4), 586-595.

Vicente-Serrano, S.M., González-Hidalgo, J.C., Luis, M.D., Raventós, J., 2004. Drought patterns in the Mediterranean area: the Valencia region (eastern Spain). Climate Research, 26(1), 5-15.

Yue, S., Pilon, P., 2004. A comparison of the power of the t test, Mann-Kendall and bootstrap tests for trend detection/Une comparaison de la puissance des tests t de Student, de Mann-Kendall et du bootstrap pour la détection de tendance. Hydrological Sciences Journal, 49(1), 21-37.

Zagana, E., Kuells, Ch., Udluft, P., Constantinou, C., 2007. Methods of groundwater recharge estimation in eastern Mediterranean--a water balance model application in Greece, Cyprus and Jordan. Hydrological Processes 21, 2405–2414

Zorita E, Von Storch H., 1999. The analog method as a simple statistical downscaling technique: comparison with more complicated methods. J. Clim. 12: 2474–2489.

CAPÍTULO 4

**LAND SURFACE PHENOLOGY (LSP) CHANGES IN
RELATION TO CLIMATIC VARIABLES IN THE
MEDITERRANEAN NATURAL VEGETATION AREAS,
SOUTHEASTERN SPAIN: OBSERVED AND PROJECTED
CHANGES**

Universitat d'Alacant
Universidad de Alicante



Universitat d'Alacant
Universidad de Alicante

Land surface phenology (LSP) changes in relation to climate variables in the Mediterranean forest and shrub areas, Southeastern Spain: observed and projected changes

Abstract

The Mediterranean is one of the most sensitive regions to global change, particularly climate change. Advances in synoptic monitoring and evaluation can help decision makers project trends and prevent or reduce negative effects on regional ecosystems. In particular, vegetation phenology derived from remotely sensed multi-temporal satellite imagery can be used as a bio-indicator for climate change. Land surface phenology (LSP) is the seasonal pattern of variation in vegetated land surfaces observed from remote sensing. The ready availability of time-series satellite imagery and associated analytical tools makes possible the monitoring of LSP over extended periods of time. In this work we used the Moderate Resolution Imaging Spectroradiometer (MODIS) 16-day composite NDVI time series to derive several phenological metrics in order to assess LSP changes in relation to climate variables in the Mediterranean forest and shrub areas in the province of Alicante (southeastern Spain) over the period of 2000 to 2012. The best-fit regression results when comparing phenological metrics and climate variables were then used to predict the future changes in LSP under eighteen climate change projections for the period of 2011 through 2099. The results show that autumn and spring precipitation and maximum temperature are the climate variables that best explain the changes in LSP. A decrease in the precipitation and an increase in the maximum temperature may result in a shorter length of growing season (LOS) due principally to earlier end of season (EOS) and slightly delayed start of season (SOS).

1. Introduction

The Mediterranean is indicated as one of the regions that will be particularly affected by climate change according to the Intergovernmental Panel on Climate Change (IPCC) fifth report (IPCC, 2013). Most climate models forecast an increase in temperature and a decrease in precipitation at the end of the 21st century for this region (IPCC, 2014). These changes will have different effects on vegetation and particularly on vegetation phenology which is highly sensitive to climate change (Cleland et al., 2007; Richardson et al., 2013).

Vegetation phenology describes seasonal characteristics of plants, such as emergence and senescence, which are closely related to seasonally varying weather patterns and may be used as indicators of climate change (Reed et al., 1994; Spano et al., 1999; Cleland et al., 2007). The IPCC fourth assessment report on climate change indicated that perhaps phenology is the simplest process with which to track changes in the ecology of species in response to climate change (Parry et al., 2007). This is supported by numerous studies documenting a progressively earlier spring, changes in length of growing season or changes in the timing of spring events (Menzel and Fabian, 1999; Kramer et al., 2000; Parmesan and Yohe, 2003; Menzel, et al., 2006; Cleland et al., 2007; Gordo and Sanz, 2010).

In contrast with the traditional notion of plant phenology, land surface phenology (LSP) is defined as the seasonal pattern of variation in vegetated land surfaces observed from remote sensing (de Beurs and Henebry 2004; Friedl et al., 2006; Morisette et al., 2008). Due to the spatial resolution of satellite sensors, LSP deals with mixtures of land covers which make it different from the traditional notion of plant phenology (Friedl et al. 2006). LSP monitors phenological events such as vegetation growth and senescence at regional to continental scales, facilitating the comparison of broad-scale climatic drivers with the phenological response of ecosystems (Zhang et al., 2003).

Vegetation phenology can be detected by satellites and other remote sensing systems due to the unique seasonal and spectral reflectance and transmittance characteristics of canopy, plants and leaves (Justice et al., 1985; Reed et al., 1994). LSP is derived from a time-series of satellite-based vegetation indices (VI). VIs have been developed to enhance vegetation signals from remote sensing measurements using ratios of different

spectral bands mostly in the visible and near infrared regions of the electromagnetic spectrum (Viña et al., 2011). A widely used VI is the Normalised Difference Vegetation Index ($NDVI = (NIR - RED) / (NIR + RED)$) (Rouse et al., 1974) where RED and NIR are reflectances in their respective electromagnetic bands. The NDVI is less sensitive to topographic effect than other VIs (Moreira et al., 2016).

The availability of 16-day MODIS composite images of a variety of vegetation indices since 2000 for the entire globe facilitated the realization of several studies about the LSP of different regions (De Beurs and Henebry, 2004; Funk and Budde, 2009; Van Leeuwen et al., 2010a; Davison et al., 2011; Qiu et al., 2013; Rodriguez-Galiano et al., 2015a). Most of these studies were carried out on global or regional scales which do not necessarily reflect changes at local scales. In this context, we carried out this study in the province of Alicante aiming to assess the LSP in different vegetation types at a local scale taking advantage of the availability of updated land use maps. The main objectives of this are to: (1) describe and examine the variation of the LSP of different vegetation types across the Mediterranean landscape of Alicante province as a function of climatic and topographic variables, (2) highlight the relative importance of these variables in influencing phenology over time and (3) analyze the likely effects of projected changes in climate on LSP.

2. Study area

The province of Alicante is located in the southeast coast of the Iberian Peninsula and roughly covers an area of 5816 km². Alicante is mountainous in the north as part of the Subbaetic Mountain Range, whereas it is mostly flat in the southern part (Figure 4.1). Altitude ranges from 0 to more than 1000 m.a.s.l. which has an important influence on the local climate. The Mediterranean climate predominates in the region with annual rainfall varying between 258 and 953 mm yr⁻¹. Precipitation in Alicante varies over time and space and it is marked by its seasonality. The major part of the annual precipitation is recorded in autumn months (40% of the annual amount) and reaches its maximum in October (more than 70 mm). An important part (25%) is recorded in spring with a peak in April. Mean temperatures vary between 20°C in the south and 14°C in the northern and mountainous areas (Pérez, 1994). Natural vegetation covers 35% of Alicante territory and is mainly dominated by shrublands and grasslands (78%). Forested ecosystems are dominated by coniferous pine forests which represent 95% of forested

area. Alicante is one of the most populous Spanish provinces (330 inhabitant/km²), leading to high pressure on natural ecosystems. The province of Alicante has suffered major land cover and land use changes. These changes consist mainly in 1) the abandonment of farming in less productive soils which are then colonized by natural vegetation (Bonet, 2004), 2) agricultural intensification and 3) urban growth stimulated by the tourism attraction of the area (Bellot et al., 2007).

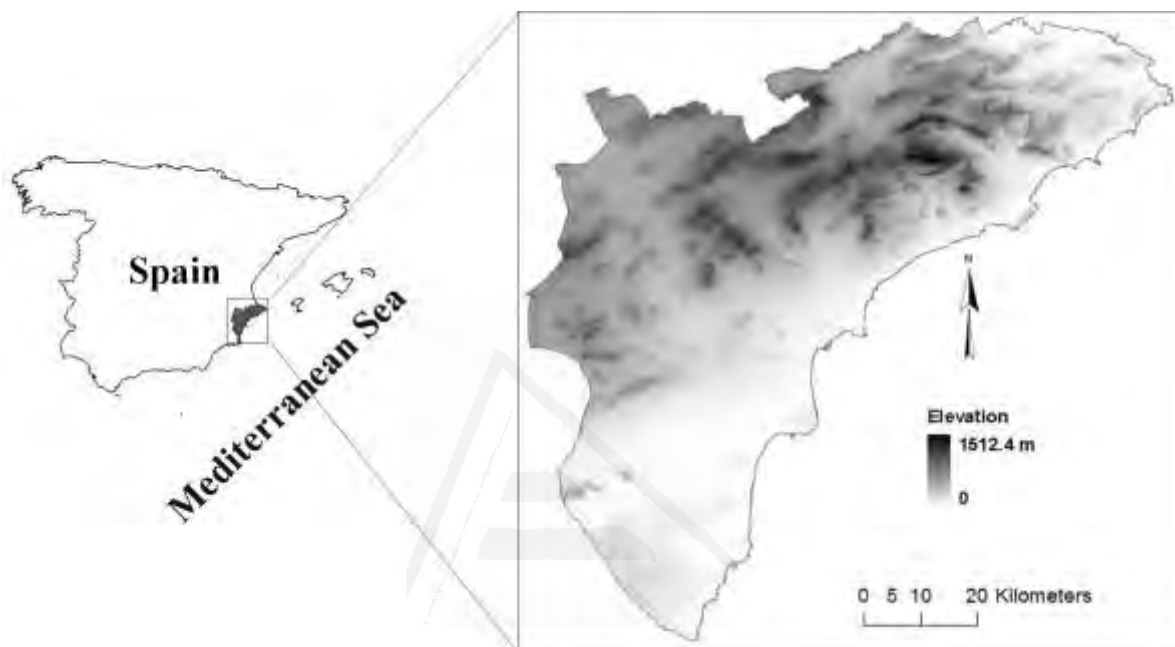


Figure 4.1: Study area location and elevation map.

3. Data and analysis

3.1 MODIS-NDVI data

To derive the LSP metrics we used NDVI data at 250 m resolution and 16-day composite intervals from the Moderate Resolution Imaging Spectroradiometer (MODIS) Vegetation Index Product Series Collection 5, acquired by MODIS on the Terra platform (MOD13Q1). These NDVI data were downloaded from the United States Geological Survey (USGS) for the period from March 2000 through May 2013. MOD13Q1 data are composited every 16 days such that each NDVI image is composed of pixels from different dates within the 16-day time interval providing 23 NDVI images per year (table 4.1). MOD13Q1 composites balance the highest NDVI value with the optimal view angle for each pixel minimizing atmospheric contamination and favoring observations closest to nadir (Huete et al., 2002; Didan and Huete, 2006).

A total of 612 NDVI images (306 x 2; because we needed two images to cover the entire Alicante territory) and associated quality assurance (QA) data (Justice et al., 1998) were downloaded and processed from the Data Pool using MODIS R-package (Mattiuzzi et al., 2014). The R-package can be used for download, re-projection, resample, mosaic, format conversion, SDS-extraction, bit-encoding and filtering/smoothing capabilities. In this work downloaded data were mosaicked and re-projected to UTM zone 30, WGS84 using the MODIS Reprojection Tool (MRT) called through the MODIS R-package using the R script in Apéndice 1.

Table 4.1: MODIS-NDVI 16-day composites dates (M-date) and the corresponding codes used in this work. We choose August 12 as date 0 because low values of precipitation (~0 mm) are registered in the two first weeks of this month. These codes will be used to determine the LSP metrics instead of the dates.

M-	12	28	13	29	15	31	16	2	18	1	17	2	18	5	21	6	22	5	24	9	25	11	27
date	Aug	Aug	Sep	Sep	Oct	Nov	Dec	Dec	Jan	Jan	Feb	Feb	Mar	Mar	Apr	Apr	May	May	Jun	Jun	Jul	Jul	
Code	0	1	2	3	4	5	6	7	8	9	10	11	12	13	14	15	16	17	18	19	20	21	22

3.2 Climate data

In order to assess variability in LSP metrics across the study area we evaluated them as a function of precipitation (Pr), temperature (T), and reference evapotranspiration (Eto). We used daily precipitation and air temperatures (maximum and minimum) time series over the period 2000-2012. These times-series come from several meteorological observatories (111 for precipitation and 67 for temperature) inside the province of Alicante and in adjacent areas (to avoid the border effect) within a 15 km strip (Figure 4.2). The original climate data were provided by the Spanish Meteorological Agency (AEMET). The reconstruction of the precipitation series was performed and their homogeneity was checked using the Standard Normal Homogeneity Test (SNHT) in a previous work (Moutahir et al., 2014). The reconstruction and homogenization of the temperature series was conducted by means of the “CLIMATOL” R contributed package (Guijarro, 2006; 2011) (see APENDICE 2). Daily Eto was calculated using Hargreaves and Samani (1982) method using temperature and solar radiation.

For the projected climate data we used a data set of climate simulations from nine CMIP5 climate models (Anexo1.1: Tabla 1) downscaled to the scale of data obtained from the AEMET meteorological observatories for the period 2006-2099 under two climate scenarios. These simulations, based on the Program for Climate Model

Diagnosis and Intercomparison (PCMDI) archives, are described and analyzed in Monjo et al. (2015). The two future climate scenarios correspond to the Representative Concentration Pathways RCP4.5 (moderate emissions scenario) and RCP8.5 (high emissions scenario) (Taylor et al. 2009) (Taylor et al. 2009).

New time series of climate data were computed at different time resolutions. Besides the annual and monthly series, two new 16-day period series that fit the MODIS-dates (M-date) were computed. The first series were the precipitation and the mean air temperature of each 16 days before the M-date. The second series was the accumulated precipitation from the M-date 0 until each M-date. In order to determine the accumulated precipitation before the start of the season (for example), SOS dates were adjusted such that they represented the number of 16-day periods from the beginning of the typical precipitation period (M-date 0) rather than the beginning of the calendar year. The beginning of precipitation was established at the 15th period from the beginning of the calendar year for each year of data, corresponding with the beginning of August (Table 4.1). In the case of temperature, the series is the mean temperature of the entire period from M-date 0 until each M-date. The accumulated Eto time series fitted the temperature time resolutions. Time series of ratios of Eto to Pr (Eto/Pr) and T to Pr (T/Pr) also were computed to explore the combined effect of precipitation and temperature on LSP. These new climate time series at different time resolution will be used as climate metrics in the next sections. The most important climate metrics, used in this work, are summarized in table 4.2.

The climate variables were organized to fit with MODIS-NDVI dates and gridded using the inverse distance weighting (IDW) method. Climate grids were resampled to fit the MODIS spatial resolution and extent. A map for each time-step in the MODIS time-series (306 maps total) was created for each variable using Python scripts and ArcGIS geoprocessing tools.

Table 4.2: The most important climate metrics used as explanatory variables for the LSP changes. Pr is precipitation, Tx, Tn and Tm are maximum, minimum and mean temperatures and Eto is the reference evapotranspiration.

	SOS	EOS	
Pr_Mdate3	Accumulated precipitation until M-date 3	Pr_Mdate10-16	Accumulated precipitation from M-date 10 to 16
Pr8, Pr9	Precipitation of August and September	Pr_Mdate11-16	Accumulated precipitation from M-date 11 to 16
Pr8+9	Precipitation of Aug + Sept	Pr4, Pr1-4	Precipitation of Apr and from Jan to Apr
Tx_Mdate3	Mean max temperature until M-date 3	Tx_Mdate16, 17	Mean max temperature of M-date 16 and 17
Tx8, Tx9	Mean max temperature of Aug and Sept	Tx_Mdate16-17	Mean max temperature of M-date 16 to 17
Tx8+9	Mean max temperature from Aug to Sept	Tx4	Mean max temperature of Apr
Tn_Mdate3	Mean min temperature until M-date 3	Tn_Mdate16	Mean min temperature of M-date 16
Tn9	Mean min temperature of Sept	Tn_Mdate17	Mean min temperature of M-date 17
Tn8+9	Mean min temperature from Aug to Sept	Tn_Mdate16-17	Mean min temperature of M-date 16 to 17
Tm8+9	Mean temperature from Aug to Sept	Eto4	Eto from Apr
Eto8+9	Eto from Aug to Sept	Eto4/Pr4	Ratio Eto4 and Pr4
Eto8+9/Pr8+9	Ratio Eto8+9 and Pr8+9	Tx4/Pr4	Ratio Tx4 and Pr4
Tx8+9/Pr8+9	Ratio Tx8+9 and Pr8+9	Tx4/Pr1-4	Ratio Tx4 and Pr1-4

3.3 Vegetation cover and topographic data

To delimit the natural vegetation areas in the province of Alicante we used cartographic information from the CORINE Land-cover 2000 (CLC2000) database of the European Environmental Agency. CLC2000 provides information about the European Union land-cover for the year 2000. CLC2000 describes land cover (and partly land use) according to a nomenclature of 44 classes organized hierarchically in three levels (EEA, 2006).

In this study we used a hierarchical approach to analyze LSP in forest and shrub areas. In the first case we analyzed the LSP for both classes using natural vegetation areas to refer to these two classes together. In the second case we analyzed the LSP in each class separately and in the last case LSP was analyzed in three subclasses inside each class. In the first and second cases we used the two classes “CLC31” and “CLC32” (which represent forests and shrub lands respectively) from CLC2000 level II (Figure 4.3,

Table 4.3). In the last case we used six classes (CLC311, CLC312, CLC313, CLC321, CLC323 and CLC324) from Level III (Figure 4.4, Table 4.4). We stratify the analysis in order to compare between the two vegetation classes and their subclasses.

A digital elevation model (DEM) at 200 m resolution was used. The DEM and CLC2000 (as vector layer) cartography were downloaded from the Spanish National Geographic Institute website (<http://www.ign.es/>). The vector layers were rasterized and cartographic data were resampled at 250 m resolution using the same coordinate system and spatial extent as MODIS series. The study area was divided into 100 m altitude classes and the mean LSP metrics were calculated for each class.

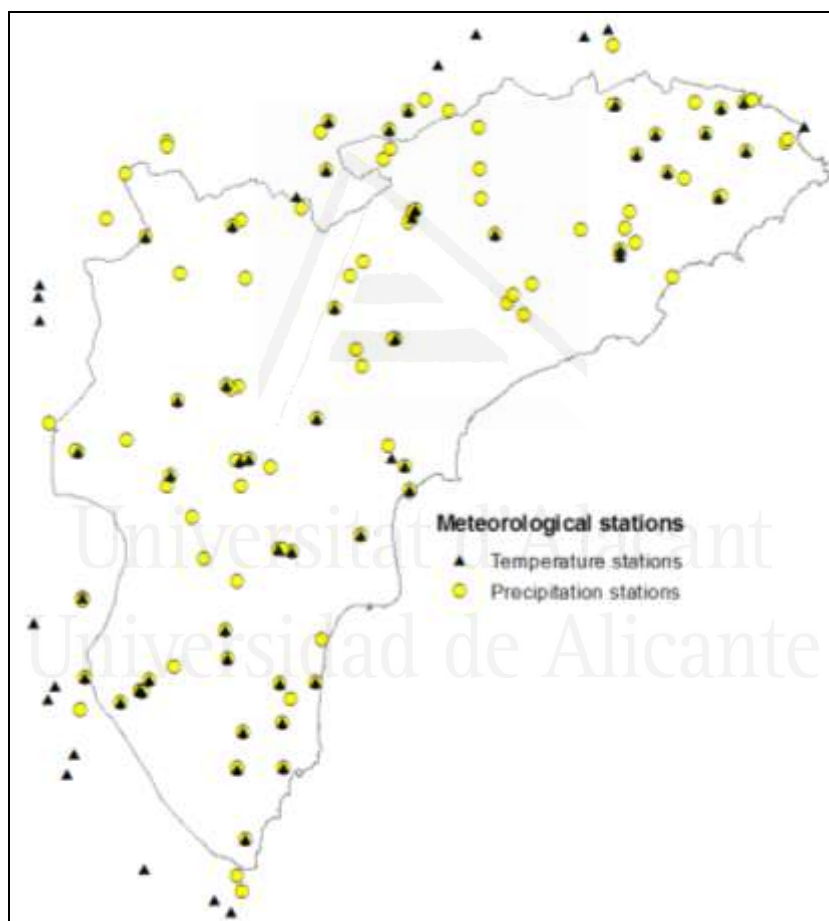


Figure 4.2: Temperature and precipitation stations. Stations outside the province of Alicante were used to ovoid the border effect.

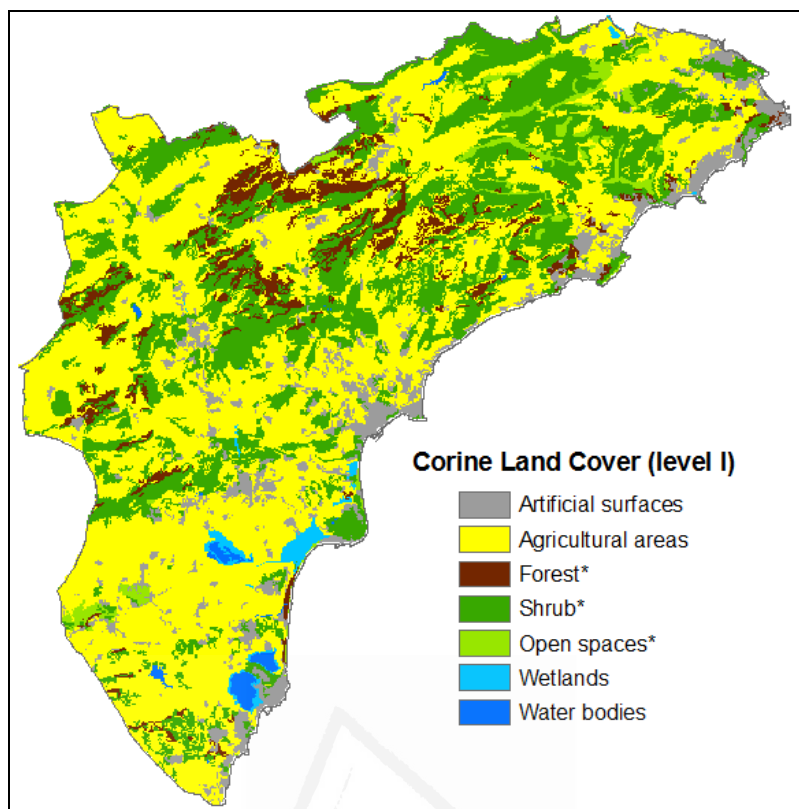


Figure 4.3: Land cover/use map of Alicante province from Corine Land Cover 2000 (level I). Classes with (*) come from Corine Land Cover (level II) and represent the natural vegetation areas.

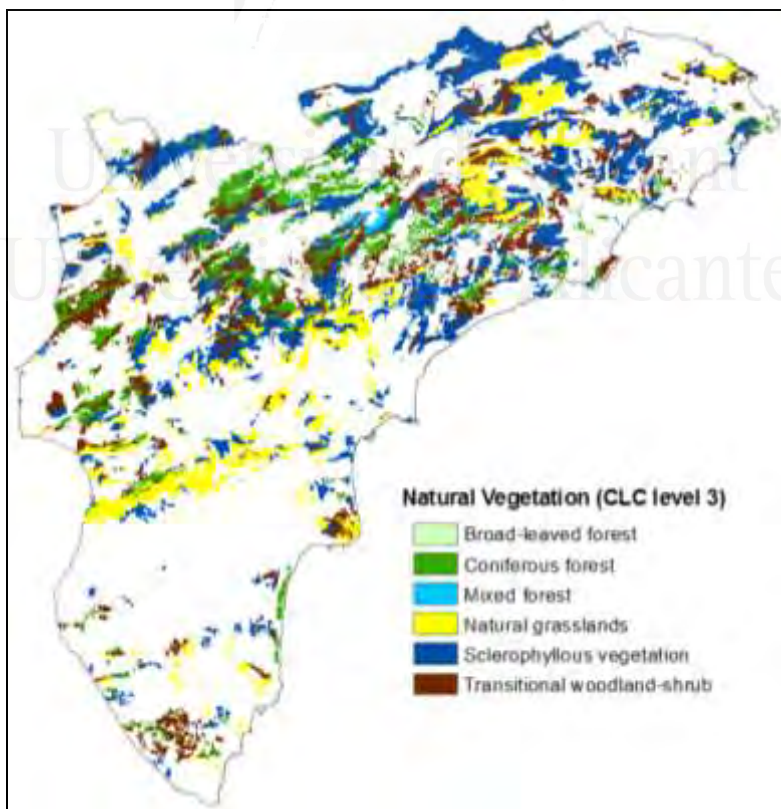


Figure 4.4: Natural vegetation areas from Corine Land Cover 2000 (level III). The first three land covers are subclasses of forest and the last three are subclasses of shrub class.

Table 4.3: Different CORINE land-cover 2000 (CLC level II) classes of Alicante. The two classes in bold which represent forest and shrub classes are used in this work.

CLC II Code	Land-covers	Area (km2)	(%)
CLC11	Urban	329.6	5.7
CLC12	Industrial, commercial and transport unit	51.8	0.9
CLC13	Mine, dump and construction sites	45.8	0.8
CLC14	Artificial, non-agricultural vegetated	10.7	0.2
CLC21	Arable land	293.6	5.1
CLC22	Permanent crops	1251.6	21.5
CLC24	Heterogeneous agricultural areas	1569.3	26.9
CLC31	Forest	355.6	6.1
CLC32	Shrub and/or herbaceous vegetation associations	1684.7	28.9
CLC33	Open spaces with little or no vegetation	126.7	2.2
CLC41	Inland wetlands	5.3	0.1
CLC42	Coastal wetlands	47.5	0.8
CLC51	Inland water	11.6	0.2
CLC52	Marine waters	30.7	0.5
Total		5814.7	

Table 4.4: The six subclasses of forest and shrub from CORINE land-cover 2000.

CLC II classes	CLC III subclasses	CLC III Code	AREA (km2)	(%)
Forest	Broad-leaved forest	CLC311	7.2	0.4
	Coniferous forest	CLC312	336.6	16.5
	Mixed forest	CLC313	11.8	0.6
Shrub	Natural grasslands	CLC321	388.0	19.0
	Sclerophyllous vegetation	CLC323	795.0	39.0
	Transitional woodland-shrub	CLC324	501.8	24.6

3.4 LSP metrics derivation

LSP metrics were established using Timesat time-series analysis software (Jonsson and Eklundh 2004) by removing noise from the time series and representing each season of time-series data using a series of piecewise logistic functions as suggested by Zhang et al. (2003). Noise was removed from the data using MOD13Q1 pixel reliability data as a mask whereby data were weighted 0.5 for records that were flagged as marginal data. Timesat was then used to derive the start of season (SOS), end of season (EOS) and length of season (LOS) from the NDVI time-series over the period 2000-2012 (Figure

4.5). The three LSP metrics were established for: (1) SOS as the time at which the seasonal greenup reached 20% of the total amplitude for the season (2) EOS as the time at which senescence reached 20% of the amplitude and (3) LOS as the time from the start to the end of the season.

The timing of SOS and EOS were coded with value from 0 to 22 giving the value 0 to the first 16-day NDVI composite of August (Table 4.1). A value of 300 was assigned to these pixels where no LSP metrics was determined. The annual pattern spans across calendar years. Hence SOS occurs in one year and EOS occurs in the next year. If no LSP metric is determined for a pixel in a particular year over the period 2000-2012, the pixel is excluded from the analysis.

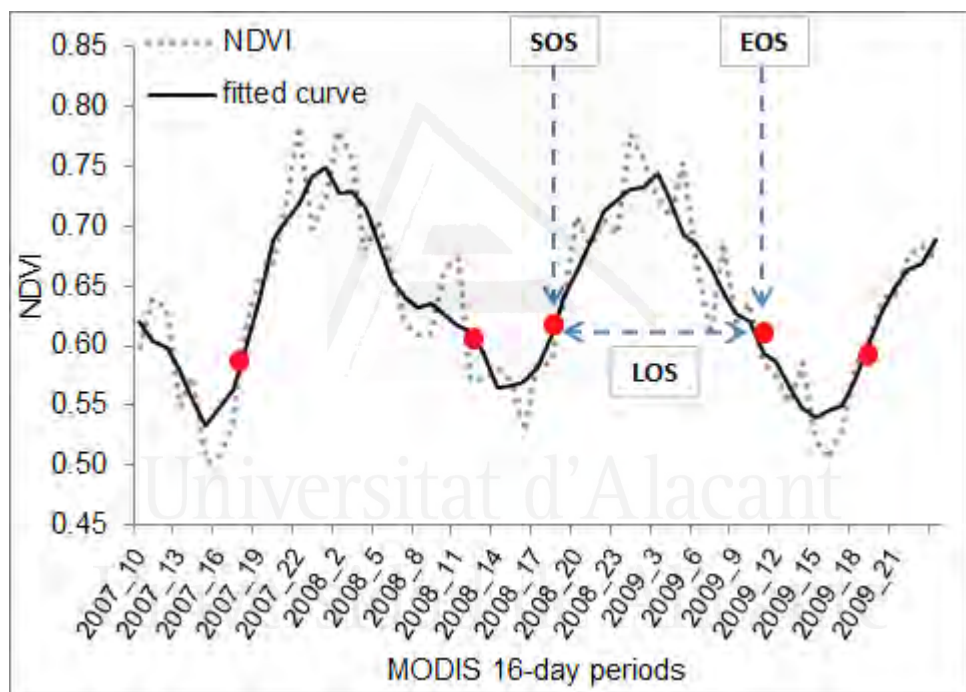


Figure 4.5: Metrics derived from MODIS-NDVI time-series (dashed line) using timesat. This time-series is from a single pixel in a forested area, and highlights the smoothing and curve-fitting (black line) methods with which Timesat derives LSP metrics.

3.5 Data analysis

The two CLC2000 level maps were used to extract the LSP metrics and climate variables values for forest and shrub areas in the first level and for the six sub-classes of forest and shrub areas in the second level. The mean annual value of LSP metrics and climate variables in each class was calculated as the average of all pixel values in this class. This was done to avoid using arithmetic means which do not reflect the spatial

distribution of different variables. For example, in the case of the spatial distribution of forests, the major part is located in the northern and mountain areas of the Alicante territory where precipitation is higher. The mean value of each variable is a weighted average by the number of pixels.

A comparison between the LSP metrics of the different natural vegetation sub-classes was done by testing for differences in the mean of each metric using ANOVA and adjusting for multiple comparisons by calculating the Tukey Honest Significant Difference (Tukey HDS) tests at the 95% confidence level. The analysis of the spatial variability of LSP in Alicante province was done by reclassifying the different LSP metrics maps using the mean value as a threshold and comparing these metrics with altitude and aspect.

Simple regressions were used to search the best fit between LSP metrics and observed climate variables. The best-fit regression results were then used to predict the future changes in LSP under eighteen climate change projections for the period of 2011 through 2099. To study the future trends on LSP metrics a linear trend was fitted to each time series using the simple regression method to derive the magnitude of trends while statistical significance of these trends was tested by Mann-Kendall (MK) test (Mann, 1945; Kendall, 1975). The MK, a non-parametric robust test against outliers, is widely used in detecting monotonic trends hydro-meteorological time series (Yue and Pilon, 2004).

Python programming language and ArcGis geoprocessing tools were used to create all the climatic maps. R language was used to extract climate metric values for each vegetation type (by pixels) and to perform the statistical analysis by means of different scripts and packages.

4. Results

The two forest subclasses (CLC311 and CLC313) which represent the broad-leaved forest and mixed forest areas, respectively, were excluded from the analysis. These two subclasses contain a small number of pixels where some were excluded because no LSP metrics were determined and some represented mixed pixels along the boundary with other land cover types, and were therefore excluded because of the border effect. Mean

LSP metrics values in these two subclasses are presented in table 4.5 but not analyzed in the next sections.

4.1 Mean LSP metrics in natural vegetation areas

The mean date for the SOS, over the period 2000-2012 in natural vegetation areas in Alicante province is around M-date 4, which corresponds to October 15. SOS mean date is similar between forests and shrublands (Table 4.5, Figure 4.6) and it is also similar between the four CLC level III subclasses where no significant differences were observed (Table 4.6).

The EOS in natural vegetation areas occurs around M-date 16 which corresponds to April 22. However the peak of pixels where EOS occurs is around M-date 18 which corresponds to May 24 (Figure 6). Contrary to SOS, EOS is significantly different ($p<0.05$) between forests and shrublands (15.2 and 16.1 respectively) (Table 4.5). Inside the shrub class, EOS in sclerophyllous vegetation (CLC323) is not significantly different from EOS in natural grasslands (CLC321) or transitional woodland-shrub (CLC324); however, EOS is significantly different between these last two subclasses (Table 4.6).

The LOS depends on SOS and EOS. The mean LOS in natural vegetation areas is about 191.5 days and it is significantly different between forest and shrub (Table 4.5). However, there are no significant differences between the CLC312 and CLC324 subclasses. Inside the shrub class there is no significant differences in LOS between the three subclasses (Table 4.6).

LSP metrics, except SOS, in natural vegetation areas showed differences between forest and shrub classes. Nevertheless, similarities between CLC312 (coniferous forests) and CLC324 (woodland-shrub) were observed.

Table 4.5: LSP metrics means in the natural vegetation classes CLC2000 level II. Mean \pm standard deviation over the period 2000-2012. For each LSP metric, the values followed by the same letter are not significantly different at $p < 0.05$

	SOS (M-date)	EOS (M-date)	LOS (days)
Forest	3.9 ± 0.6 a	15.2 ± 0.9 a	181.4 ± 11.8 a
Shrub	4.0 ± 0.7 a	16.1 ± 1 b	193.9 ± 14.3 b
Natural Vegetation	4.0 ± 0.7	16.0 ± 1	191.5 ± 13.4

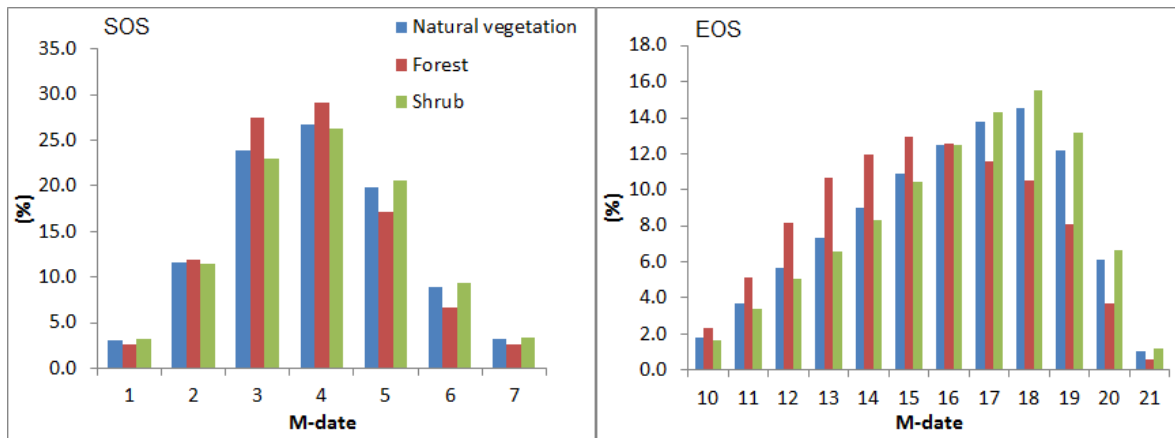


Figure 4.6: frequency (%) of pixels where SOS or EOS occurs at a given M-date

Table 4.6: LSP metrics means in the natural vegetation classes CLC2000 level III. Mean \pm standard deviation over the period 2000-2012. For each LSP metric, the values followed by the same letter are not significantly different at (Tukey HSD, $p < 0.05$). (*These two subclasses were removed from subsequent analysis because of the low number of pixels in each one of them and differences were not tested in them)

Class	Sub-class	SOS (M-date)	EOS (M-date)	LOS (days)
Forest	Broad-leaved forest*	4.7 ± 0.8	14.7 ± 1.2	160.1 ± 22.8
	Coniferous forest	$3.9 \pm 0.6a$	$15.3 \pm 0.9a$	$182.2 \pm 11.7a$
	Mixed forest*	3.7 ± 0.6	13.9 ± 1.1	161.8 ± 17.1
Shrub	Natural grasslands	$4.3 \pm 0.9a$	$16.7 \pm 1.1b$	$198.2 \pm 15.8b$
	Sclerophyllous vegetation	$4.0 \pm 0.7a$	$16.3 \pm 1.1ab$	$197.7 \pm 16b$
	Transitional woodland-shrub	$3.9 \pm 0.6a$	$15.5 \pm 0.9a$	$185.9 \pm 12.3ab$

4.2 Spatial variation of LSP metrics

Mapping the mean LSP metrics over the period 2000-2012 in Alicante showed spatial variability between northern and southern regions and between different vegetation types. We used the mean values of SOS and EOS (4 and 16 respectively) in natural vegetation areas as a threshold to classify the pixels of the map to three classes; where yellow pixels represent LSP metric measurements falling on the mean M-date (the threshold class), pixels in green representing when the LSP metric occurs before the mean value, and blue when it occurs after the mean value (Figure 4.7). SOS typically occurs before or on M-date 4 in the northern areas while the majority of pixels where SOS occurs after M-date 4 are located in the southern half of Alicante (Figure 7a). When analyzing forests and shrubs separately we observed that the majority of pixels when SOS occurs after M-date 4 are in shrub areas (Figure 4.7b and c). Similarly, with EOS the majority of pixels where the growing season ends after M-date 16 are located

in shrub areas (Figure 4.7f) while EOS typically occurs before M-date 16 in forests (Figure 4.7e). Earlier EOS is observed in southern and interior pixels (Figure 4.7d).

4.3 LSP and topographic variables relationships

A strong negative correlation between SOS and altitude was observed ($R^2 = 0.89$). SOS occurs earlier at high altitudes and later at low altitudes (Figure 4.8a). Unlike SOS, EOS occurred earlier at low and high altitudes and later at intermediate altitudes with a peak between 400 and 600m a.s.l.; however, EOS at high altitudes occurs much earlier than in low altitudes (Figure 4.8b). LOS has the same behavior as EOS (Figure 4.8c). The above described behavior of LSP metrics in relation to altitude is similar in both forest and shrub classes. LSP metrics in relation to altitude in the sub-classes (CLC312, CLC321, CLC323 and CLC324) showed the same behavior as in forest and shrub classes.

LSP metrics vary between north-northwest and south-southeast facing slopes. In both forest and shrub classes (level II), SOS and EOS occur earlier in north and northwest facing slopes than in south and southeast facing slopes (Figure 4.9a). At the CLC level III scale, the CLC312, which represents the coniferous forest, shows the same behavior as level II forest because it covers 95% of the surface of this class. The SOS in CLC321, which represents the grasslands, showed a clear difference between north facing slopes and south facing slope. SOS in this subclass occurs more or less one week (0.6 of the 16-day period) earlier for north facing slopes than in south facing slopes. In the other subclasses the difference was less than one week (0.2 of the 16-day period) (Figure 4.9b).

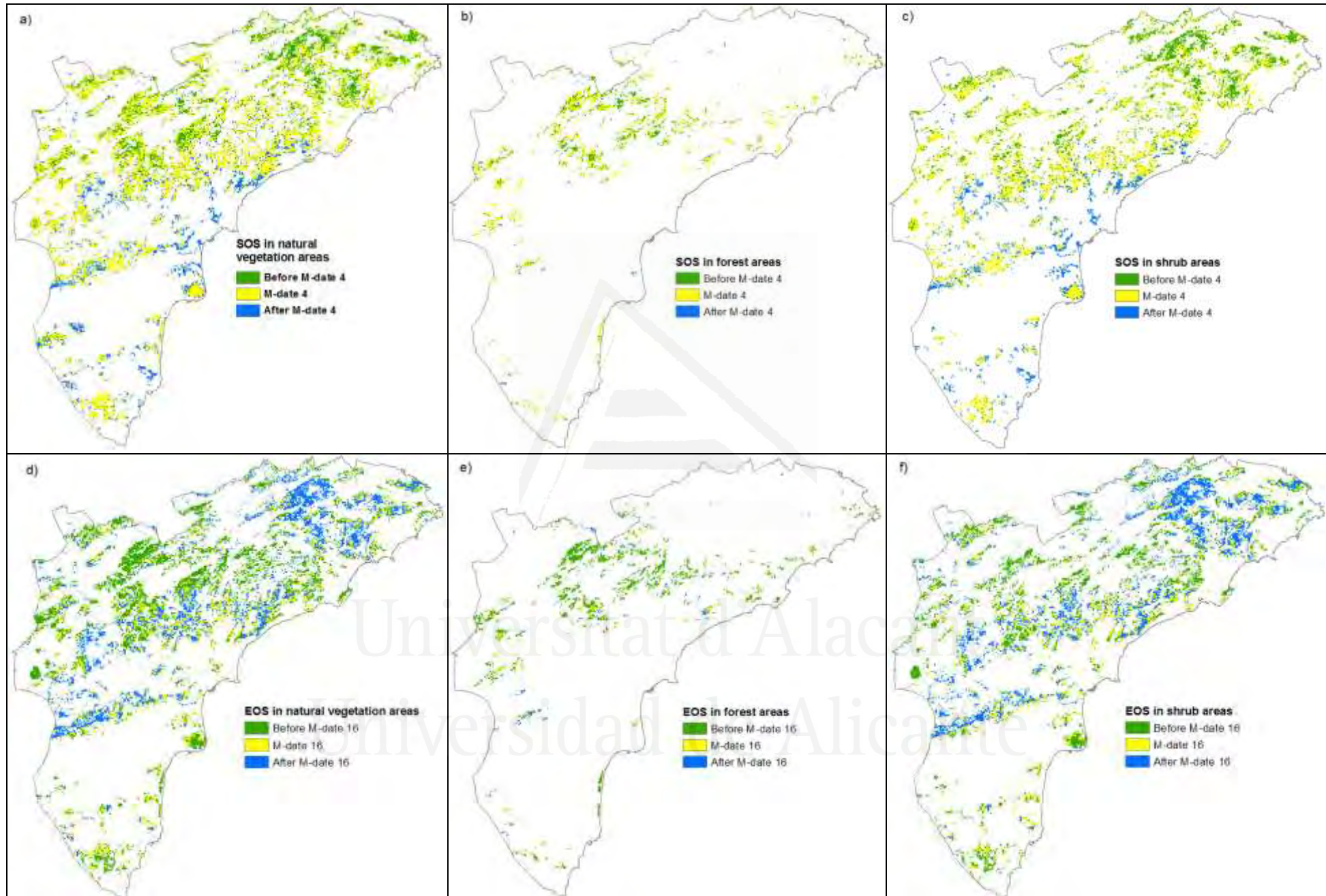


Figure 4.7: Spatial variation of LSP metrics in Alicante. The mean SOS and EOS M-dates are used as thresholds and pixels are classified in three classes. Green and blue when SOS/EOS occurs before and after mean M-date respectively and yellow when it occurs on mean M-date.

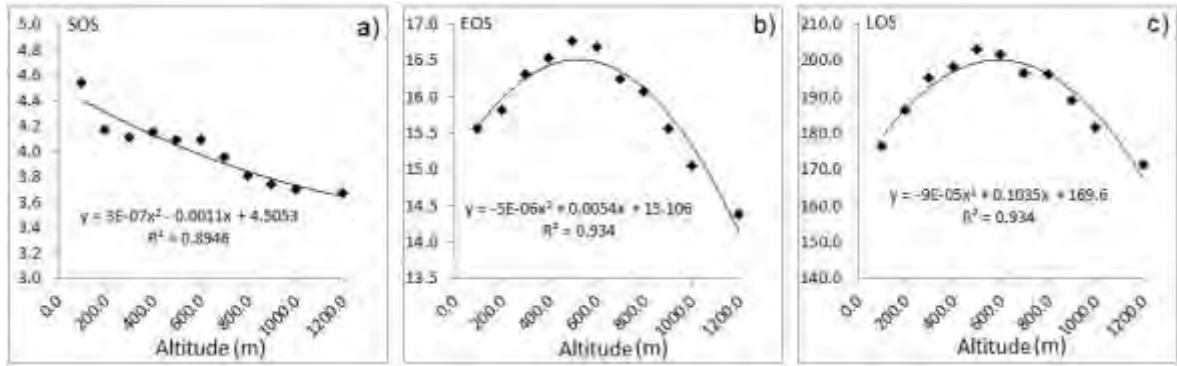


Figure 4.8: LSP and Altitude relationships. SOS and EOS are expressed in M-dates and LOS is expressed in days.

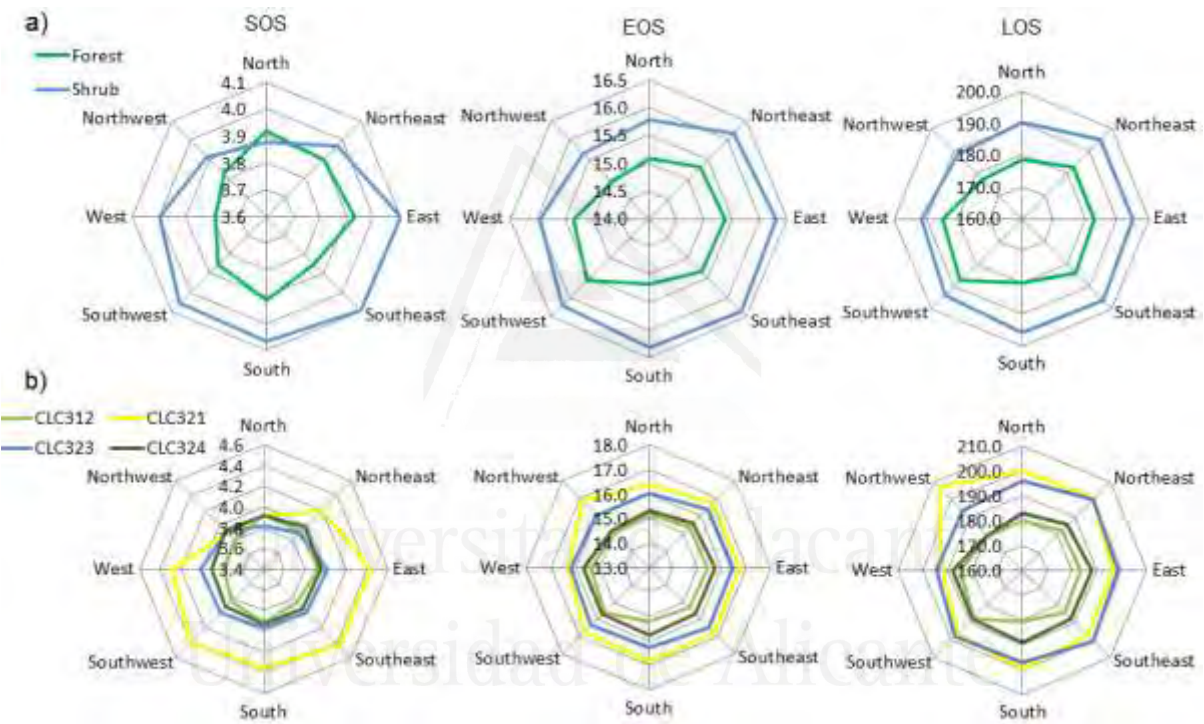


Figure 4.9: Mean LSP metrics values in function of orientation. SOS and EOS are expressed in M-dates and LOS is expressed in days.

4.4 LSP and climate relationships

The comparison between LSP metrics and climate metrics over the period 2000-2012 showed strong relations between LSP and climate. The occurrence of SOS and EOS depended on previous climatic conditions. Figure 10 shows that SOS and EOS depends on the precipitation level of August-September and of the period from January to April

respectively. Under wet conditions, when the accumulated precipitation in August-September is high, the peak of SOS occurs before the mean value (M-date 4) and it occurs after this date when the accumulated precipitation in these months is low (dry conditions). In the same way when the accumulated precipitation in the period January-April is high, the peak of EOS occurs after the mean value (M-date 16) and the contrary happens under dry conditions.

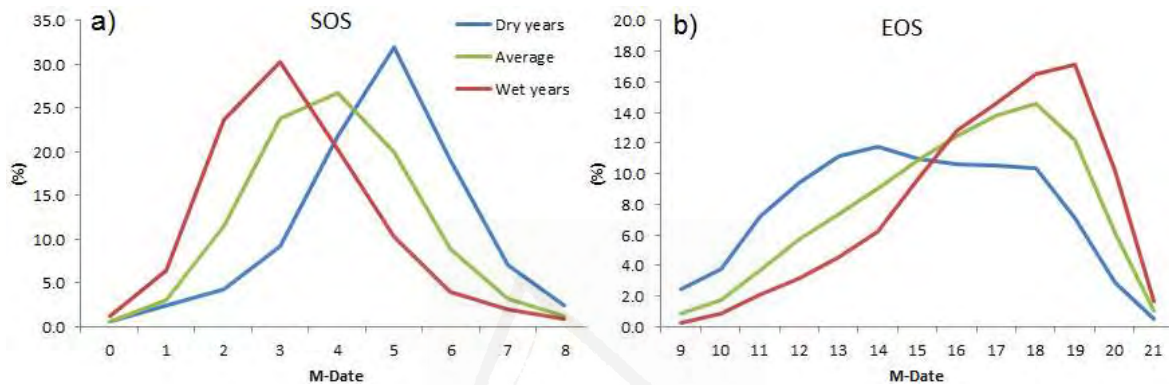


Figure 4.10: Percent of total pixels when SOS or EOS occurs depending on precipitation conditions. Accumulated precipitation of August and September used in the case of SOS and accumulated precipitation from January to April in the case of EOS.

On the one hand SOS in natural vegetation areas (with its different CLC classes and subclasses) showed strong negative correlations with accumulated precipitation until M-date 3 (Pr_Mdate3) and with August-September precipitations (Pr8+9). On the other hand SOS showed strong positive correlations with maximum temperature and potential evapotranspiration for the same periods of time (Figure 4.11a and 4.12a). SOS also showed strong negative correlations with ratio of Eto to precipitation (Eto8+9/Pr8+9) and Tx to precipitation (Tx8+9/Pr8+9). Other high negative and positive correlations with precipitation and temperature of different periods of time between August and September were observed (Figure 4.11a and 4.12a).

Unlike SOS, EOS showed positive correlations with precipitation and negative correlations with temperature (Figure 4.11b and 4.12b). Indeed, strong positive correlations between EOS and precipitation of the period from January to April (Pr1-4), between EOS and Pr_Mdate10-16 and between EOS and Pr_Mdate11-16 were observed. However, strong

negative correlations between EOS and Tx of April (Tx4), between EOS and Tx_Mdate16-17 and between EOS and Eto of April (Eto4) were observed. Strong negative correlations also were observed with Eto4/Pr4, Tx4/Pr4 and Tx4/Pr1-4 ratios. In the same way high correlations were observed with precipitation and temperature of different intervals of time in the period from January to April (Figure 4.11b and 4.12b).

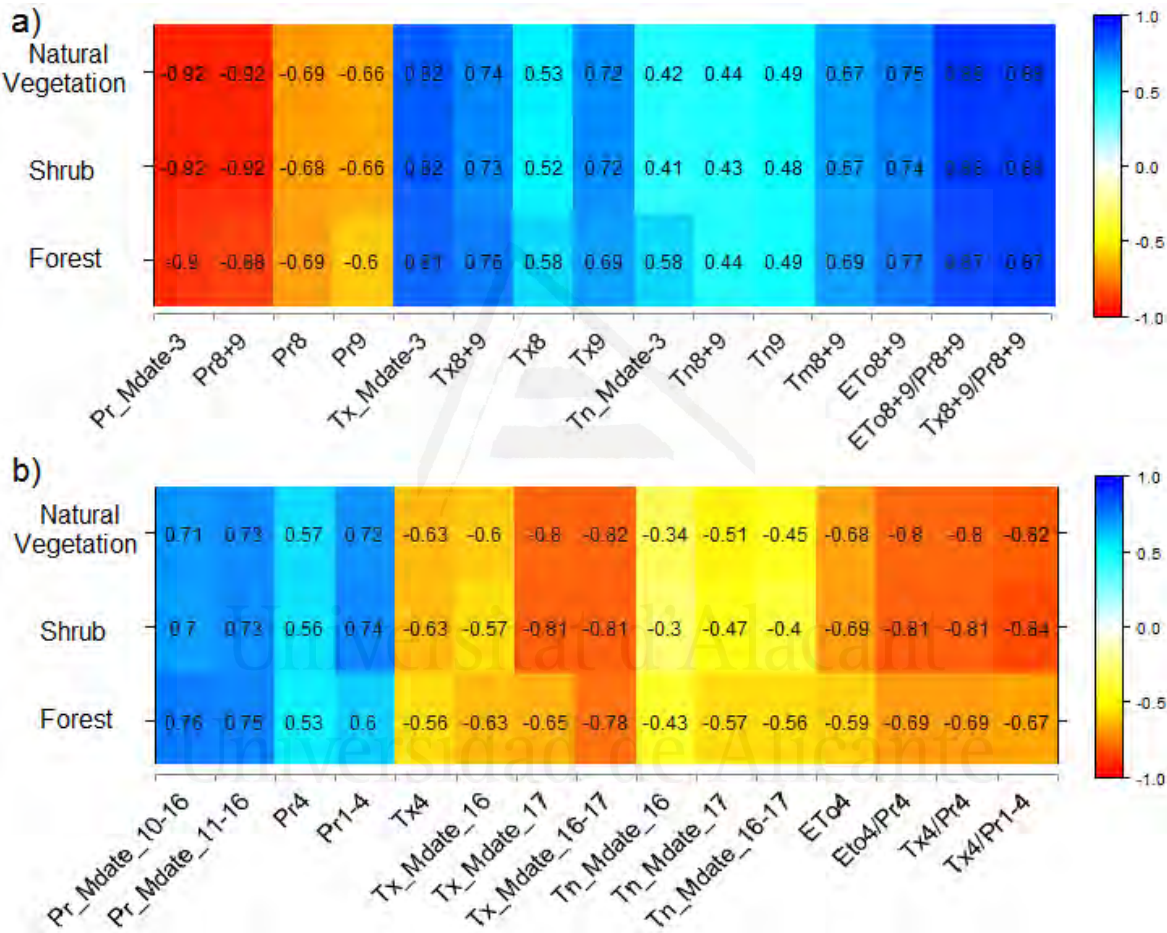


Figure 4.11: Correlation matrix between LSP metrics (a) SOS and b) EOS) and climate metrics in CORINE level II classes. See table 4.2 for meaning of each climate metric.

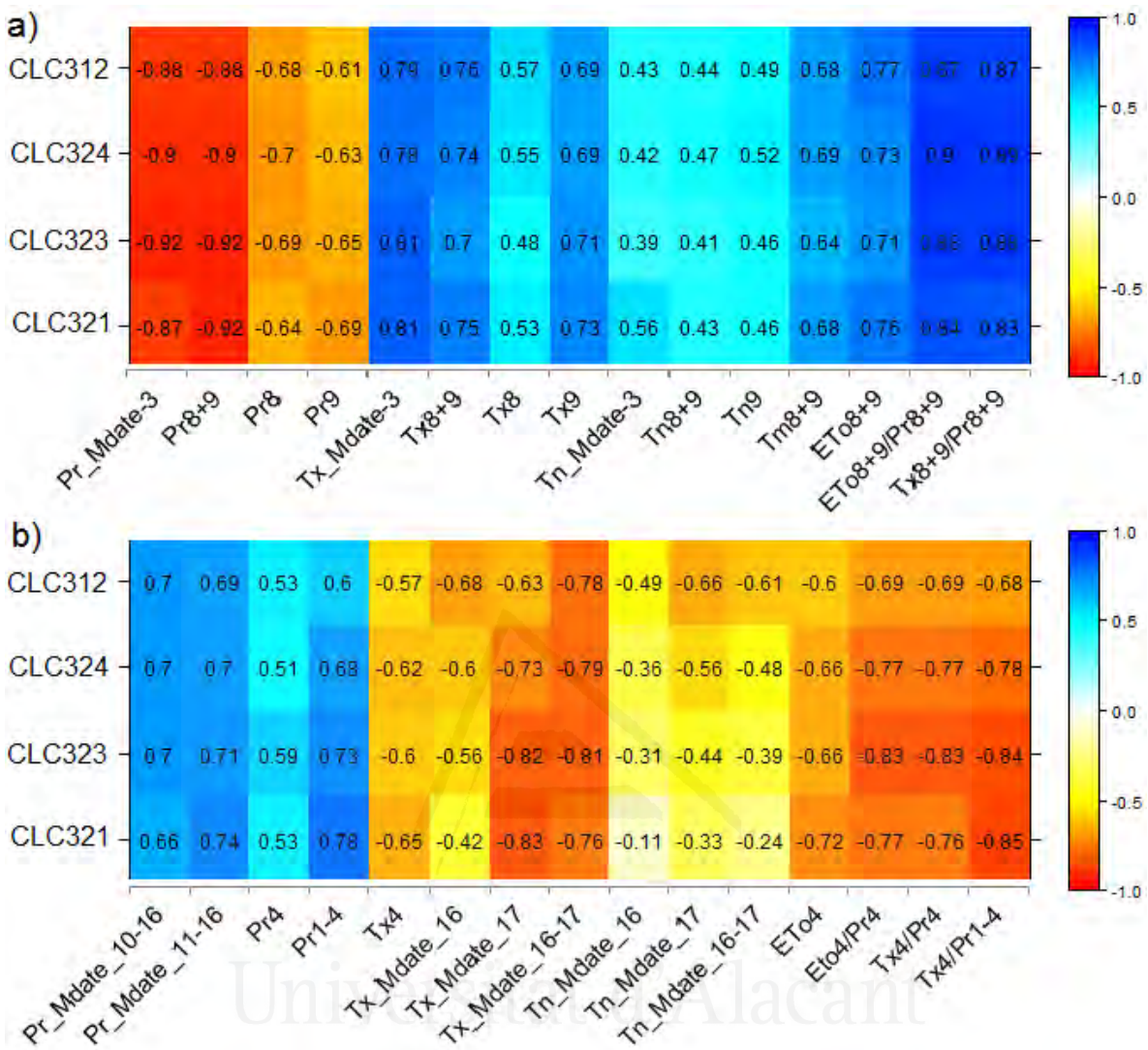


Figure 4.12: Correlation matrix between LSP metrics (a) SOS and b) EOS) and climate metrics in CORINE level III subclasses. See table 4.2 for meaning of each climate metric.

Positive and negative correlations with precipitation and temperature show that favorable climatic conditions in September stimulate an earlier SOS while favorable climatic conditions in the period from January to April extend the growing season and the EOS occurs later. In contrast, lack of precipitation or higher temperatures in September cause a later SOS and adverse climatic conditions in the period from January to April cause an earlier EOS.

Advancement or delay in SOS and in EOS will cause shorter or longer growing season (LOS). Therefore, climate variables affecting SOS and EOS also affect LOS. In fact, good fits were observed between LOS and the sum of Pr8+9 and Pr1-4 in the different natural vegetation classes ($0.5 < R^2 < 0.7$).

4.5 Projected changes in LSP metrics

We selected the six climate metrics that showed the best fits with LSP to explore the likely effects of climate change on LSP in the future. We used precipitation (Pr) and maximum temperature (Tx) for August, September and the period from January to April from nine CMIP5 climate models under two RCP scenarios. Figure 13 shows future projections of these climate metrics in Alicante. The graphs show the mean value of nine CMIP5 climate models under the moderate scenario (RCP4.5) and under the high scenario (RCP8.5). The Pr8+9 and Pr1-4 variables show a negative trend over the period 2011-2099 while Tx8+9 and Tx4 show a positive trend. The ratios Tx8+9/Pr8+9 and Tx4/Pr1-4 also showed a positive trend due the effect of Tx. However, not all trends are significant: Pr8+9 and Tx8+9/Pr9+8 did not show significant negative trends.

Precipitation is expected to decrease under the two RCP scenarios over the period 2011-2099, above all the Pr1-4. Pr1-4 is expected to decrease two times faster under the high scenario RCP8.5 in comparison with the moderate scenario RCP4.5 (-3.5mm/decade and -1.8mm/decade respectively). Pr8+9 is expected to decrease slightly under the two scenarios. In contrast, Tx is expected to increase in both periods of time under the two RCP scenarios. Nevertheless, Tx is expected to increase at higher rate under the RCP8.5 scenario. In the same way Tx8+9 is expected to increase at a higher rate than Tx4 under the two RCP scenarios (+0.8 against +0.5°C/decade under the RCP8.5 and +0.3 against +0.2°C/decade under the RCP4.5 respectively) (Figure 4.13).

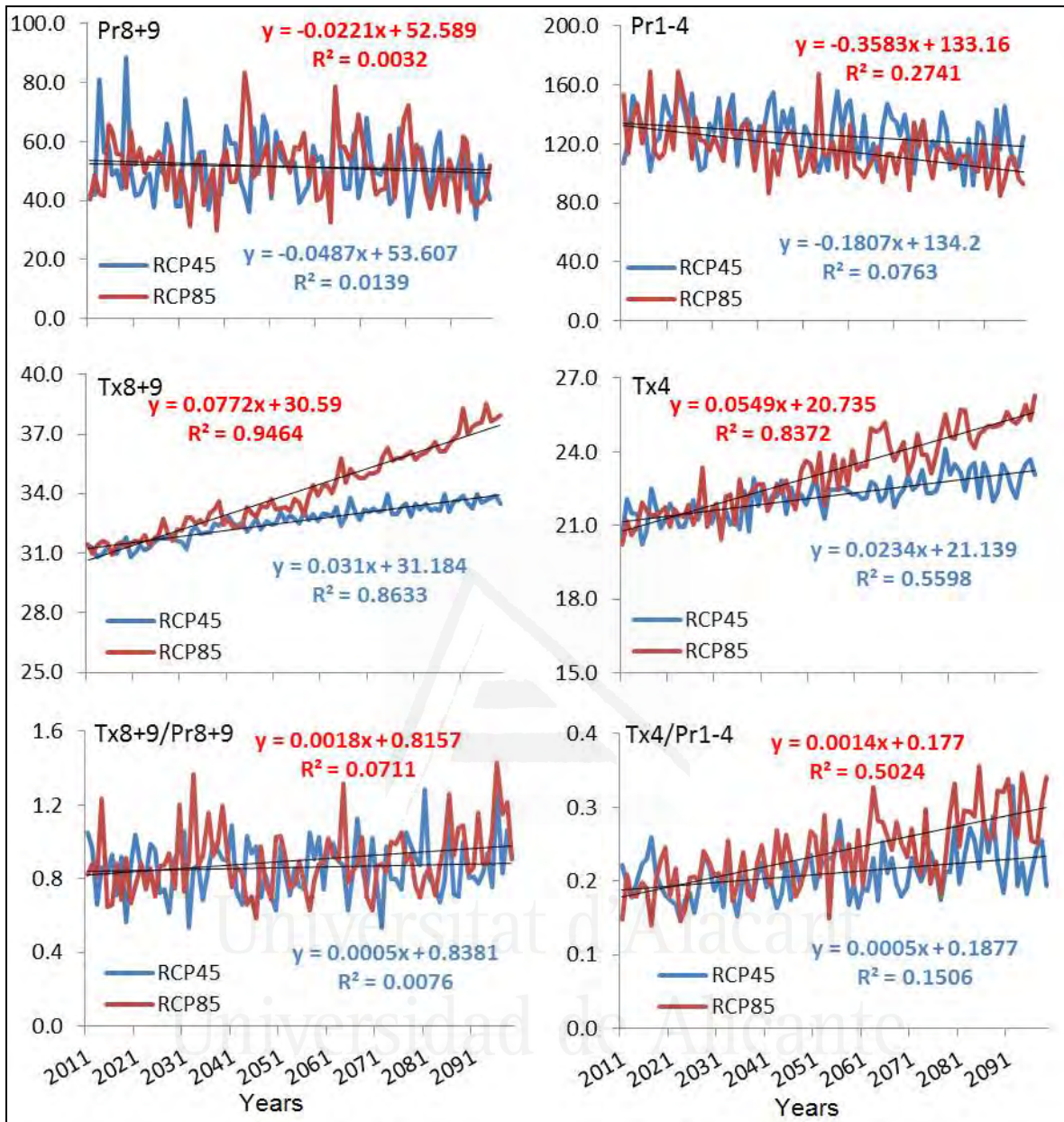


Figure 4.13: Evolution of projected climate metrics determining LSP metrics in Alicante. Mean values of nine CMIP5 climate models under two RCP scenarios. Pr8+9 and Tx8+9 represent precipitation and maximum temperature of August and September respectively, Pr1-4 represents precipitation from January to April (Pr1-4) and Tx4 represents maximum temperature of April.

To project the LSP metrics under future climate change scenarios using precipitation and maximum temperature we used the regression equations that were developed via linear

regression between LSP metrics and the chosen climate variables (Table 4.7, Annex4.1: Figures 1 and 2). Maximum temperature was used as a proxy of Eto due to the high correlation between these two variables ($R^2=0.90$). The ratio Tx/Pr was used as a proxy of Eto/Pr to evaluate the likely effects of climate change on LSP.

Table 4.7: The regression equations used to project the LSP metrics under future climate change scenarios using precipitation and maximum temperature of August and September (Pr8+9, Tx8+9) to project the SOS and precipitation from January to April (Pr1-4) and maximum temperature of April (Tx4) to project the EOS

Pr8+9				Tx8+9				Tx8+9/Pr8+9			
	a	b	R ²	a	b	R ²	a	b	R ²		
SOS	CLC312	-0.014	4.675	0.77	0.548	-12.740	0.57	0.753	3.229	0.75	
	CLC321	-0.022	5.650	0.85	0.824	-20.602	0.57	1.095	3.444	0.69	
	CLC323	-0.019	5.082	0.84	0.660	-16.008	0.49	0.993	3.146	0.78	
	CLC324	-0.015	4.843	0.82	0.580	-13.631	0.55	0.841	3.229	0.80	
Pr1-4				Tx4				Tx4/Pr1-4			
	a	b	R ²	a	b	R ²	a	b	R ²		
EOS	CLC312	0.010	13.482	0.37	-0.428	24.291	0.33	-6.149	16.124	0.46	
	CLC321	0.014	14.294	0.61	-0.547	28.425	0.42	-8.624	18.094	0.71	
	CLC323	0.014	13.892	0.53	-0.538	27.802	0.36	-9.093	17.722	0.71	
	CLC324	0.011	13.549	0.46	-0.481	25.784	0.38	-7.396	16.672	0.61	

Anticipated shifts in climate variables under the different climate scenarios demonstrate significant changes on LSP. In fact, the majority of trends expected in LSP metrics are significant at $p=0.05$ (Table 4.8). A delayed SOS, an earlier EOS and a shorter LOS are expected in natural vegetation areas. The rate of change depends on the specific LSP metrics, climate variables and vegetation type (Table 4.8, Annex4.2: Figures 1 to 4).

SOS showed positive trends under the two RCP scenarios over the period 2011-2099 in the four CLC land cover subclasses independently of the climate variable used. However, the highest rates of change are expected when using only Tx8+9 under the RCP8.5 high climate scenario (between +6.7 and +10.2 days/decade) which are higher than two times the rates under the moderate scenario RCP4.5. Pr8+9 seems not to produce big changes in SOS due to the low changes expected on this variable (<+0.5 days/decade). A combined effect

of Tx and Pr on SOS is expected. In fact, depending on the changes in Tx8+9/Pr8+9 a delay of SOS is expected under the two RCP scenarios. The trend is only significant under the RCP8.5 and in all cases is not expected to exceed +0.5 days/decade.

Unlike SOS, an earlier EOS is expected under the two scenarios and in the four natural vegetation types. When used alone, Tx seems to be the climate variable that will produce the largest change in EOS (between -3.7 and -4.8days/decade) under the high RCP scenario two times higher than under the moderate RCP scenario. Changes in Pr1-4 are expected to produce significant changes on EOS when used separately and more when combined with Tx4. In fact, changes in the ratio Tx4/Pr1-4 are expected to produce important change in EOS (between -1.4 and -2 days/decade) under the RCP8.5 two times higher than under the RCP4.5 scenario.

The evaluation of the effect of climate variables on LOS was done by analyzing the changes in the difference between EOS and SOS. Expected delay of SOS and advancement of EOS will cause a shortening of LOS. Indeed, the major change is expected when using Tx separately (between -10.5 and -15days/decade and between -4.3 and -6.1days/decade under RCP8.5 and RCP4.5 scenarios respectively). Important combined effects of Pr and Tx on LOS are expected too. Changes in the ratio Tx/Pr are expected to produce important changes in LOS (between -1.6 and -2.3 days/decade) under the RCP8.5 – two times higher than under the RCP4.5 scenario.

A comparison of the expected changes in the LSP metrics between the different natural vegetation types showed that the higher change rates are expected in the CLC321 and CLC323 subclasses. These two subclasses belong to the shrub class and represent the grasslands and the sclerophyllous vegetation respectively. Absolute higher rates of change are expected in the grasslands areas (Table 4.8). Similarities were observed between CLC312 and CLC324 because CLC324 represents transitional woodland-shrub which are expected to be converted to forests.

Table 4.8: Mean projected trends of different LSP metrics in days/ decade over the period 2011-2099 under the two RCP scenarios. Mean values of the nine CMIP5 climate models. Significances tested by Mann-Kendall test. Pr8+9 and Tx8+9 represent precipitation and maximum temperature of August and September respectively, Pr1-4 represents precipitation from January to April (Pr1-4) and Tx4 represents maximum temperature of April.

			CLC312	CLC321	CLC323	CLC324
SOS (days/decade)	Pr8+9	RCP45	+ 0.1	+ 0.2	+ 0.1	+ 0.1
		RCP85	+0.04	+ 0.1	+ 0.1	+0.02
	Tx8+9	RCP45	+ 2.7***	+ 4.1***	+ 3.3***	+ 2.9***
		RCP85	+ 6.7***	+ 10.2***	+ 8.2***	+ 7.1***
	Tx8+9/Pr8+9	RCP45	+ 0.1	+ 0.1	+ 0.1	+ 0.1
		RCP85	+ 0.2**	+ 0.3**	+ 0.3*	+ 0.2**
EOS (days/decade)	Pr1-4	RCP45	-0.3**	-0.4*	-0.4**	-0.3*
		RCP85	-0.6***	-0.8***	-0.8***	-0.7***
	Tx4	RCP45	-1.6***	-2.1***	-2***	-1.8***
		RCP85	-3.7***	-4.8***	-4.7***	-4.3***
	Tx4/Pr1-4	RCP45	-0.5***	-0.7***	-0.7***	-0.6***
		RCP85	-1.4***	-1.9***	-2***	-1.6***
LOS (days/decade)	Pr	RCP45	-0.4*	-0.6*	-0.6*	-0.5*
		RCP85	-0.6***	-0.9***	-0.9***	-0.7***
	Tx	RCP45	-4.3***	-6.1***	-5.3***	-4.7***
		RCP85	-10.5***	-15***	-12.9***	-11.4***
	Tx/Pr	RCP45	-0.6***	-0.8***	-0.8***	-0.7***
		RCP85	-1.6***	-2.2***	-2.3***	-1.9***

*Significant at 5%, ** significant at 1%, *** significant at 0.1%

5. Discussion

The LSP analysis performed in this study demonstrates that SOS in natural vegetation areas in Alicante occurs after the first important rains of autumn around October 15. This mean SOS date is similar among the different forest and shrub subclasses. The results also suggest that the growing season in the Alicante territory ends around April 22, with the majority of the region characterized by an EOS of May 24 depending on Jan-April precipitation. However, other LSP studies in the European and Mediterranean regions indicated that the onset of growing season occurs in the spring and EOS in autumn (Han et al., 2013; Rodriguez-Galiano et al., 2015a, 2015b). This is supported by numerous phenological (traditional phenology) studies delimiting the growing season in the period

between spring and autumn (Menzel and Fabian, 1999; Menzel, et al., 2006; Cleland et al., 2007; Gordo and Sanz, 2010) and dendrochronological studies indicating that early wood is produced in spring and late wood in autumn (de Luis et al., 2007; Camarero et al., 2009; Novak et al., 2013). These differences can be explained in part by the definition of the phenology metrics themselves. in this study SOS/EOS were determined from the MODIS-NDVI times series as the time at which the seasonal greenup/senescence reached 20% of the total amplitude for the season. This methodology were proposed by Eklundh and Jonsson (2011) and used in numerous studies (van Leeuwen et al., 2010a, 2010b; Han et al., 2013). The analysis of greenup in our study area using a time-series of vegetation index data indicates an SOS with the period between M-date 3 and 5 which match with the period between September 29 and October 31. This is similar to a study in drylands of Southeastern Spain demonstrated by Cabello et al., (2012) which showed that the beginning of the growing season coincides with mid-autumn. The senescence coincides with period between M-date 15 and 20 which match with the period between April 6 and June 25 (table 4.1, Figure 4.5). LSP is distinct from traditional notion of phenology and LSP metrics also are distinct from the traditional phenological timing and depend on vegetation types, scales and geographic localization (Stöckli and Vidale, 2004; Rodriguez-Galiano et al., 2015a).

In this study, we tried to adjust the LSP data to the hydrological year instead of the calendar year. The growing season starts after the first important rains of autumn and ends at the beginning of the summer drought period. SOS depends on the August-September precipitation and temperature. SOS also showed strong correlations with climate metrics of the period from M-date 0 to 3. Gordo and Sanz (2010) had similar results, indicating that climate during the weeks leading up to phenophase occurrences had the greatest impact on plants. Cabello et al. (2012) indicated that the earlier arrival of the first rains after summer drought and the cooler temperatures during late-summer/early-autumn marks the beginning of the growing season. Espigares and Peco (1995) indicated that the first rains of autumn initiate germination and regrowth of Mediterranean grasslands. In the same way, EOS depends on the Jan-April precipitation and April temperature which corresponds to research suggesting that climate during the February–April quarter affects the spring events (Gordo and Sanz, 2010).

Taking advantage of the good correlations between some climate metrics and LSP metrics, we analyzed the likely effects of climate change on LSP in Alicante. Our results showed that SOS is not expected to change dramatically under both climate scenarios. Trends in SOS, when using a combined effect of temperature and precipitation, were only significant under the high RCP scenario. However, EOS showed significant trends under the two RCP scenarios (in the majority of cases $p < 0.001$). This is similar to results obtained by Gordo and Sanz (2010) in their study in the Mediterranean ecosystems showing that spring events are changing more than autumn events. According to the nine CMIP5 climate models used, both temperatures of August-September and of April are expected to increase under the two RCP scenarios while only the precipitation in January-April showed significant decrease under the two RCP scenarios (Figure 4.13). Expected decreases of spring precipitation in Spain were reported in a study using CMIP3 models data (De Castro et al., 2005). These predictions are not expected to change under CMIP5 for the Mediterranean region (Baker and Huang, 2014). De Castro et al., (2005) also reported a slight increase in autumn precipitation.

According to our results SOS is not expected to change due to the slight changes in August-September precipitation (58mm observed over the period 2000-2012 against 51.3 and 51.5mm under RCP4.5 and RCP8.5 scenarios respectively). This happens when using precipitation alone or combined with temperature. In contrast, EOS is expected to occur earlier due the combined effect of increasing temperature and decreasing precipitation. Earlier EOS will shorten the LOS in the Alicante province. This result is distinct to results observed in northern Europe where the temperature is a limiting factor and any increase in it is expected to lengthen the growing season (Gordo and Sanz, 2010). However, in semi-arid regions the limiting factor is water and this is confirmed by the small changes in SOS despite the high increase of temperature and stable levels of precipitation. This matches with results of Kramer et al., (2000) indicating that the phenology of Mediterranean coniferous forests is mainly driven by water availability affecting the development of leaf area.

6. Conclusions

The use of LSP metrics to describe vegetation response to climate variables under historical conditions allows the exploration of potential future changes in these metrics under different climate change scenarios. When applied to the Mediterranean forest and shrub areas in the province of Alicante, results suggest that a decrease in the precipitation and an increase in the maximum temperature may result in a shorter growing season (LOS). This is due principally to earlier end of season (EOS) caused by a decrease in the precipitation of the period from January to Abril and an increase in the maximum temperature of Abril. Importantly, the impact of climate change is expected to be distinct for different vegetation types. The effect of climate change on LSP also will depend on spatial distribution of forest and shrub areas in the province of Alicante. The rate of change in precipitation and temperature is projected to be distinct between the northern part and the southern part of Alicante. Decision makers should take into account these potential effects of climate change on LSP towards a better management of forest and shrub areas.

References

- Baker, N. C., & Huang, H. P. (2014). A comparative study of precipitation and evaporation between CMIP3 and CMIP5 climate model ensembles in semiarid regions. *Journal of Climate*, 27(10), 3731-3749.
- Bellot, J., Bonet, A., Peña, J., Sánchez, J.R (2007). Human impacts on land cover and water balances in a coastal Mediterranean county. *Environmental Management*, 39: 412–422.
- Bonet, A. (2004). Secondary succession of semi-arid Mediterranean old-fields in south-eastern Spain: insights for conservation and restoration of degraded lands. *Journal of Arid Environments*, 56: 213-233
- Cabello, J., Alcaraz-Segura, D., Ferrero, R., Castro, A. J., & Liras, E. (2012). The role of vegetation and lithology in the spatial and inter-annual response of EVI to climate in drylands of Southeastern Spain. *Journal of Arid Environments*, 79, 76-83.

Camarero, J.J., Olano, J.M. and Parras, A. 2009 Plastic bimodal xylogenesis in conifers from continental Mediterranean climates. *New Phytol.* 185, 471–480

Cleland, E. E., Chuine, I., Menzel, A., Mooney, H. A., & Schwartz, M. D. (2007). Shifting plant phenology in response to global change. *Trends in ecology & evolution*, 22(7), 357-365.

Davison, J. E., Breshears, D. D., Van Leeuwen, W. J., & Casady, G. M. (2011). Remotely sensed vegetation phenology and productivity along a climatic gradient: on the value of incorporating the dimension of woody plant cover. *Global Ecology and Biogeography*, 20(1), 101-113.

De Beurs, K.M., and G.M. Henebry. (2004). Land surface phenology, climatic variation, and institutional change: Analyzing agricultural land cover change in Kazakhstan. *Remote Sensing of Environment* 89:497-509; doi:10.1016/j.rse.2003.11.006.

De Castro, M., Martín-Vide, J., & Alonso, S. (2005). The climate of Spain: past, present and scenarios for the 21st century. A preliminary general assessment of the impacts in spain due to the effects of climate change. Spanish Ministry of Environment, Madrid, 162.

De Luis, M., Gričar, J., Čufar, K., & Raventós, J. (2007). Seasonal dynamics of wood formation in *Pinus halepensis* from dry and semi-arid ecosystems in Spain. *Iawa Journal*, 28(4), 389-404.

Didan, K., & Huete, A. (2006). MODIS vegetation index product series collection 5 change summary. TBRS Lab, The University of Arizona. Available online:

http://landweb.nascom.nasa.gov/QA_WWW/forPage/MOD13_VI_C5_Changes_Document_06_28_06.pdf

EEA (2006), Land accounts for Europe 1990–2000. Towards integrated land and ecosystem accounting. EEA Report No 11/2006. Luxembourg LU, Office for Official Publications of the European Communities. ISBN 92-9167-888-0

Eklundh, L. and Jönsson, P., 2011, Timesat 3.1 Software Manual, Lund University, Sweden.

Espigares, T., & Peco, B. (1995). Mediterranean annual pasture dynamics: impact of autumn drought. *Journal of Ecology*, 135-142.

Friedl MA, Henebry G, Reed B et al. (2006) Land surface phenology: a community white paper requested by NASA.

ftp://ftp.iluci.org/Land_ESDR/Phenology_Friedl_whitepaper.pdf

Funk, C., & Budde, M. E. (2009). Phenologically-tuned MODIS NDVI-based production anomaly estimates for Zimbabwe. *Remote Sensing of Environment*, 113(1), 115-125.

Gordo, O., & Sanz, J. J. (2010). Impact of climate change on plant phenology in Mediterranean ecosystems. *Global Change Biology*, 16(3), 1082-1106.

Guijarro, J.A. (2006). Homogenization of a dense thermo-pluviometric monthly database in the Balearic Islands using the free contributed Rpackage CLIMATOL. WMO Fifth Seminar for Homogenization and Quality Control in Climatological Databases. Budapest, Hungary, 2006; WCDMP-No. 68, WMO-TD No. 1434, 2008.

Guijarro, J.A. (2011). User'sguide to Climatol. Instituto Nacional de Meteorología, Centro Meteorológico en Illes Balears.

Han, Q., Luo, G., & Li, C. (2013). Remote sensing-based quantification of spatial variation in canopy phenology of four dominant tree species in Europe. *Journal of Applied Remote Sensing*, 7(1), 073485-073485.

Hargreaves, G.H. and Samani, Z.A., (1982). Estimating reference evapotranspiration. Tech. Note. *Journal of Irrigation and Drainage Engineering*, ASCE, 108 (3), 225–230.

Huete, A., Didan, K., Miura, T., Rodriguez, E.P., Gao, X. & Ferreira, L.G. (2002). Overview of the radiometric and biophysical performance of the MODIS vegetation indices. *Remote Sensing of Environment*, 83, 195–213.

IPCC, (2013): Climate Change 2013: The Physical Science Basis. Contribution of Working Group I to the Fifth Assessment Report of the Intergovernmental Panel on Climate Change [Stocker, T.F., D. Qin, G.-K. Plattner, M. Tignor, S.K. Allen, J. Boschung, A. Nauels, Y.

Xia, V. Bex and P.M. Midgley (eds.)]. Cambridge University Press, Cambridge, United Kingdom and New York, NY, USA, 1535 pp, doi:10.1017/CBO9781107415324.

IPCC, (2014): Climate Change 2014: Impacts, Adaptation, and Vulnerability. Part B: Regional Aspects. Contribution of Working Group II to the Fifth Assessment Report of the Intergovernmental Panel on Climate Change [Barros, V.R., C.B. Field, D.J. Dokken, M.D. Mastrandrea, K.J. Mach, T.E. Bilir, M. Chatterjee, K.L. Ebi, Y.O. Estrada, R.C. Genova, B. Girma, E.S. Kissel, A.N. Levy, S. MacCracken, P.R. Mastrandrea, and L.L. White (eds.)]. Cambridge University Press, Cambridge, United Kingdom and New York, NY, USA, 688 pp.

Jonsson, P., and L. Eklundh. (2004). TIMESAT - a program for analyzing time-series of satellite sensor data. *Computers & Geosciences* 30:833-845.

Justice, C.O., Townshend, J.R.G., Holben, B.N., Tucker, C.J., (1985). Analysis of the phenology of global vegetation using meteorological satellite data. *Int. J. Remote Sens.*, 6, 1271-1318.

Justice, C.O., Vermote, E., Townshend, J.R.G., Defries, R., Roy, D.P., Hall, D.K., Salomonson, V.V., Privette, J.L., Riggs, G., Strahler, A., Lucht, W., Myneni, R.B., Knyazikhin, Y., Running, S.W., Nemani, R.R., Wan, Z.M., Huete, A.R., van Leeuwen, W., Wolfe, R.E., Giglio, L., Muller, J.P., Lewis, P., Barnsley, M.J. (1998). The Moderate Resolution Imaging Spectroradiometer (MODIS): Land remote sensing for global change research. *Geoscience and Remote Sensing, IEEE Transactions on*, 36(4), 1228-1249.

Kendall, M.G., (1975). Rank Correlation Methods. Griffin, London, UK.

Kramer, K., Leinonen, I., & Loustau, D. (2000). The importance of phenology for the evaluation of impact of climate change on growth of boreal, temperate and Mediterranean forests ecosystems: an overview. *International Journal of Biometeorology*, 44(2), 67-75.

Mann, H.B., (1945). Nonparametric tests against trend. *Econometrica* 13 (3), 245–259.

Mattiuzzi, M., Verbesselt, J., Stevens, F., Mosher, S., Hengl, T., Klisch, A., Evans B., and Lobo A., (2014). MODIS: MODIS acquisition and processing package. R package version 0.10-11/r471. <http://R-Forge.R-project.org/projects/modis/>

Menzel, A., Fabian, P., (1999). Growing season extended in Europe. *Nature*, 397, p. 659

Menzel, A., Sparks, T. H., Estrella, N., Koch, E., Aasa, A., Ahas, R., ... & Chmielewski, F. M. (2006). European phenological response to climate change matches the warming pattern. *Global change biology*, 12(10), 1969-1976.

Monjo, R., Gaitán, E., Pórtoles, J., Ribalaygua, J., Torres, L., (2015). Changes in extreme precipitation over Spain using statistical downscaling of CMIP5 projections. *International Journal of Climatology*.

Moreira, E. P., Valeriano, M. D. M., Sanches, I. D. A., & Formaggio, A. R., (2016). TOPOGRAPHIC EFFECT ON SPECTRAL VEGETATION INDICES FROM LANDSAT TM DATA: IS TOPOGRAPHIC CORRECTION NECESSARY?. *Boletim de Ciências Geodésicas*, 22(1), 95-107. <https://dx.doi.org/10.1590/S1982-21702016000100006>

Morisette, J.T., A.D. Richardson, A.K. Knapp, J.I. Fisher, E. Graham, J. Abatzoglou, B.E. Wilson, D.D. Breshears, G.M. Henebry, J.M. Hanes, and L. Liang. (2008). Unlocking the rhythm of the seasons in the face of global change: Challenges and opportunities for phenological research in the 21st Century. *Frontiers in Ecology and the Environment*.

Moutahir, H., De Luis, M., Serrano-Notivoli, R., Touhami, I., Bellot, J., (2014). Análisis de los eventos climáticos extremos en la provincia de Alicante, Sureste de España. En: Fernández-Montes, S. y Rodrigo, F.S. (Eds). *Cambio climático y cambio global. Publicaciones de la Asociación Española de Climatología (AEC). Serie A, nº9*. Almería. ISBN: 978-84-16027-69-9. pp. 457-466.

Novak, K., de Luis, M., Raventós, J. and Cufar, K. (2013) Climatic signals in tree-ring widths and wood structure of *Pinus halepensis* in contrasted environmental conditions. *Trees* 27, 927–936.

Parry, M. L. (Ed.). (2007). Climate change 2007-impacts, adaptation and vulnerability: Working group II contribution to the fourth assessment report of the IPCC (Vol. 4). Cambridge University Press.

Parmesan, C., & Yohe, G. (2003). A globally coherent fingerprint of climate change impacts across natural systems. *Nature*, 421(6918), 37-42.

Pérez Cueva A.J. (coordinador) (1994). Atlas Climático de la Comunidad Valenciana, Consejería de Obras Públicas, Urbanismo y Transporte, Generalitat Valenciana. 208 pp

Qiu, B., Zhong, M., Tang, Z., & Chen, C. (2013). Spatiotemporal variability of vegetation phenology with reference to altitude and climate in the subtropical mountain and hill region, China. *Chinese Science Bulletin*, 58(23), 2883-2892.

Reed, B.C.; Brown, J.F.; Vanderzee, D.; Loveland, T.R.; Merchant, J.W.; Ohlen, D.O., (1994). Measuring phenological variability from satellite imagery. *J. Veg. Sci.* 5, 703-714.

Richardson, A. D., Keenan, T. F., Migliavacca, M., Ryu, Y., Sonnentag, O., & Toomey, M. (2013). Climate change, phenology, and phenological control of vegetation feedbacks to the climate system. *Agricultural and Forest Meteorology*, 169, 156-173.

Rodriguez-Galiano, V. F., Dash, J., & Atkinson, P. M. (2015a). Characterising the Land Surface Phenology of Europe Using Decadal MERIS Data. *Remote Sensing*, 7(7), 9390-9409.

Rodriguez-Galiano, V. F., Sanchez-Castillo, M., Dash, J., and Atkinson, P. M. (2015b). Modelling anomalies in the spring and autumn land surface phenology of the European forest, *Biogeosciences Discuss.*, 12, 11833-11861, doi:10.5194/bgd-12-11833-2015,

Rouse, J.W., Hass, R.H., Schell, J.A., Deering, D.W., (1974). Monitoring Vegetation Systems in the Great Plains with ERTS. In Proceedings Third Earth Resources Technology Satellite-1 Symposium, Washington, DC, USA, , pp. 3010-3017.

Spano D, Cesaraccio C, Duce P, Snyder RL (1999) Phenological stages of natural species and their use as climate indicators. *Int J Biometeorol* 42:124–133

Stöckli, R., & Vidale, P. L. (2004). European plant phenology and climate as seen in a 20-year AVHRR land-surface parameter dataset. International Journal of Remote Sensing, 25(17), 3303-3330.

Taylor, K.E., Stouffer, R.J., Meehl, G.A., (2009). A summary of the CMIP5 experiment design. PCDMI Rep. http://cmip-pcmdi.llnl.gov/cmip5/docs/Taylor_CMIP5_design.pdf (accessed 10th April 2015).

Van Leeuwen, W. J., Davison, J. E., Casady, G. M., & Marsh, S. E. (2010a). Phenological characterization of desert sky island vegetation communities with remotely sensed and climate time series data. Remote Sensing, 2(2), 388-415.

van Leeuwen, W. J., Casady, G. M., Neary, D. G., Bautista, S., Alloza, J. A., Carmel, Y., Wittenberg, L. Malkinson G, D., Orr, B. J. (2010b). Monitoring post-wildfire vegetation response with remotely sensed time-series data in Spain, USA and Israel. International Journal of Wildland Fire, 19(1), 75-93.

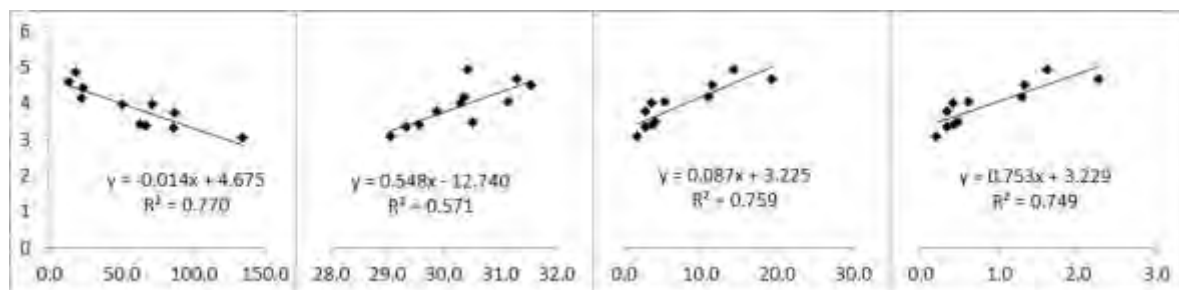
Viña, A., Gitelson, A. A., Nguy-Robertson, A. L., & Peng, Y. (2011). Comparison of different vegetation indices for the remote assessment of green leaf area index of crops. Remote Sensing of Environment, 115(12), 3468-3478.

Yue, S., Pilon, P., (2004). A comparison of the power of the t test, Mann-Kendall and bootstrap tests for trend detection/Une comparaison de la puissance des tests t de Student, de Mann-Kendall et du bootstrap pour la détection de tendance. Hydrological Sciences Journal, 49(1), 21-37.

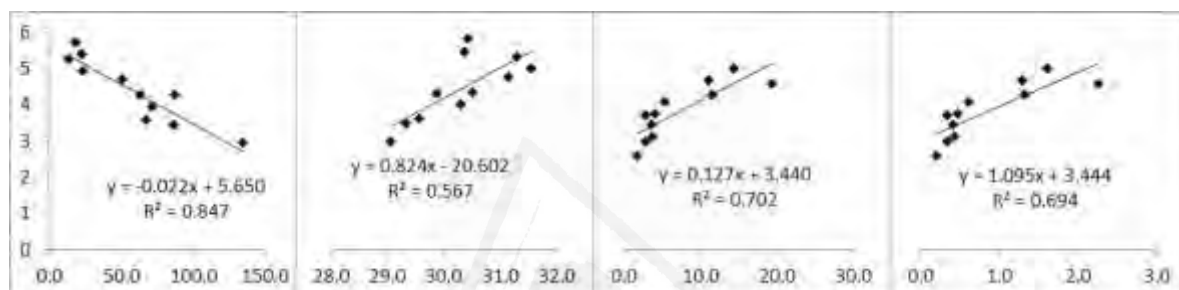
Zhang, X. Y., Friedl, M. A., Schaaf, C. B., Strahler, A. H., Hodges, J. C., Gao, F., Reed, B. C. & Huete, A. (2003). Monitoring vegetation phenology using MODIS. Remote sensing of environment, 84(3), 471-475.

Annex4.1: The best fits between LSP metrics and climate metrics

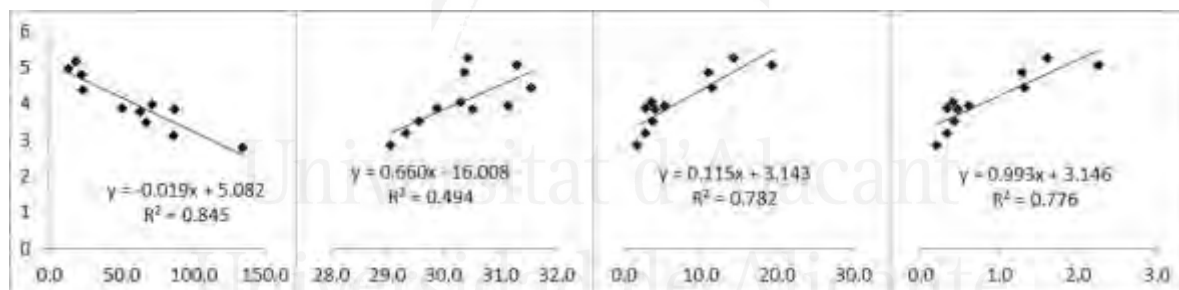
CLC312



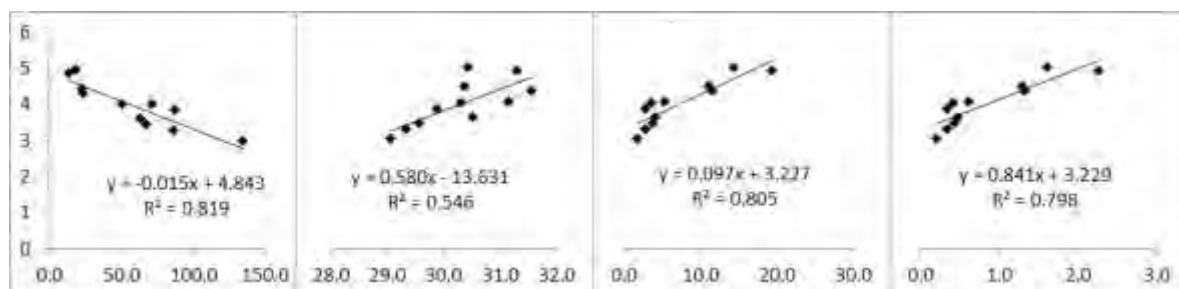
CLC321



CLC323



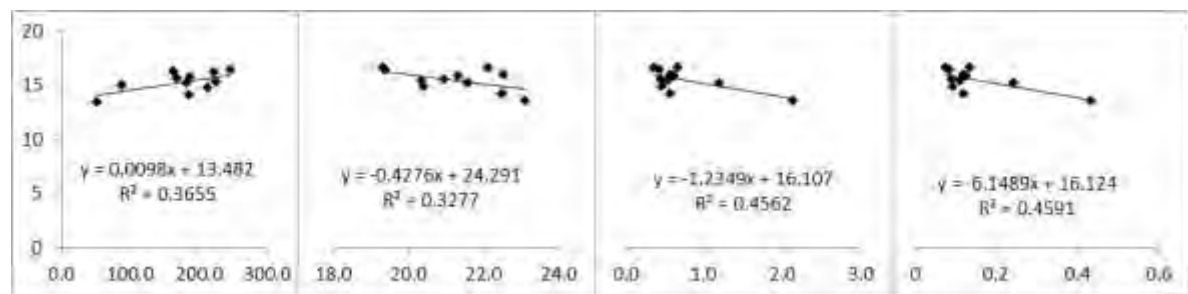
CLC324



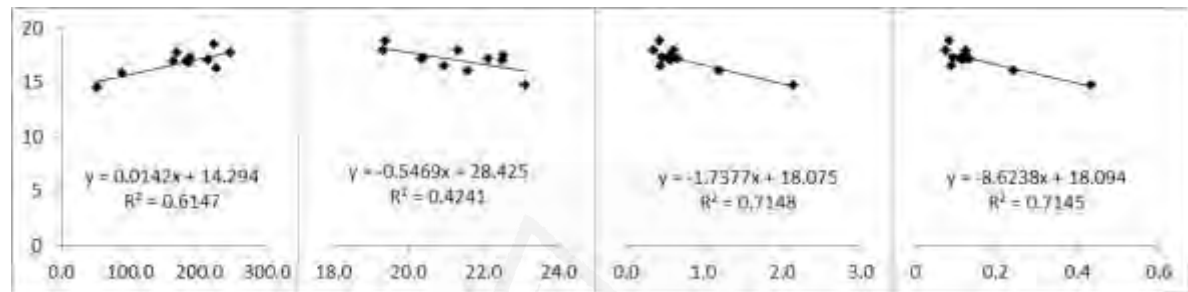
Pr8+9	Tx8+9	Eto8+9/Pr8+9	Tx8+9/Pr8+9
-------	-------	--------------	-------------

Figure 1: The best fits between SOS and climate metrics. Y axis represents SOS expressed as M-dates. X axis represents climate metrics.

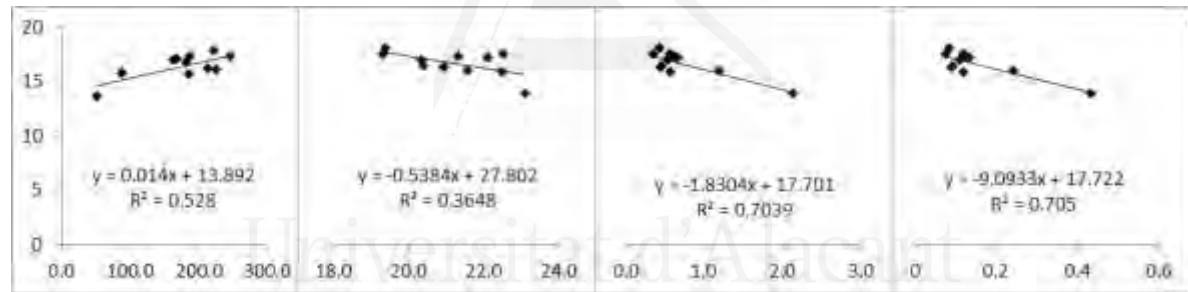
CLC312



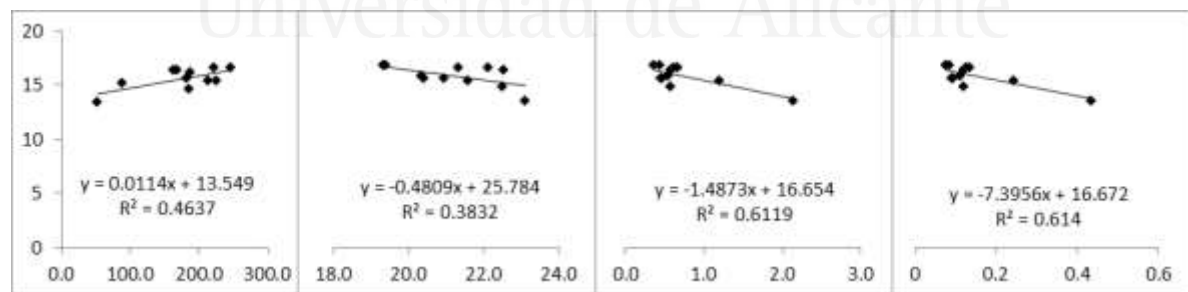
CLC321



CLC323



CLC324



Pr1-4	Tx4	Eto4/Pr1-4	Tx4/Pr1-4
-------	-----	------------	-----------

Figure 2: The best fits between EOS and climate metrics. Y axis represents EOS expressed as M-dates. X axis represents climate metrics.

Annex4.2: LSP metrics projections in the different CLC level III land cover classes in function of precipitation and maximum temperature. Mean values of nine CMPI5 climate models under two RCP scenarios.



Universitat d'Alacant
Universidad de Alicante

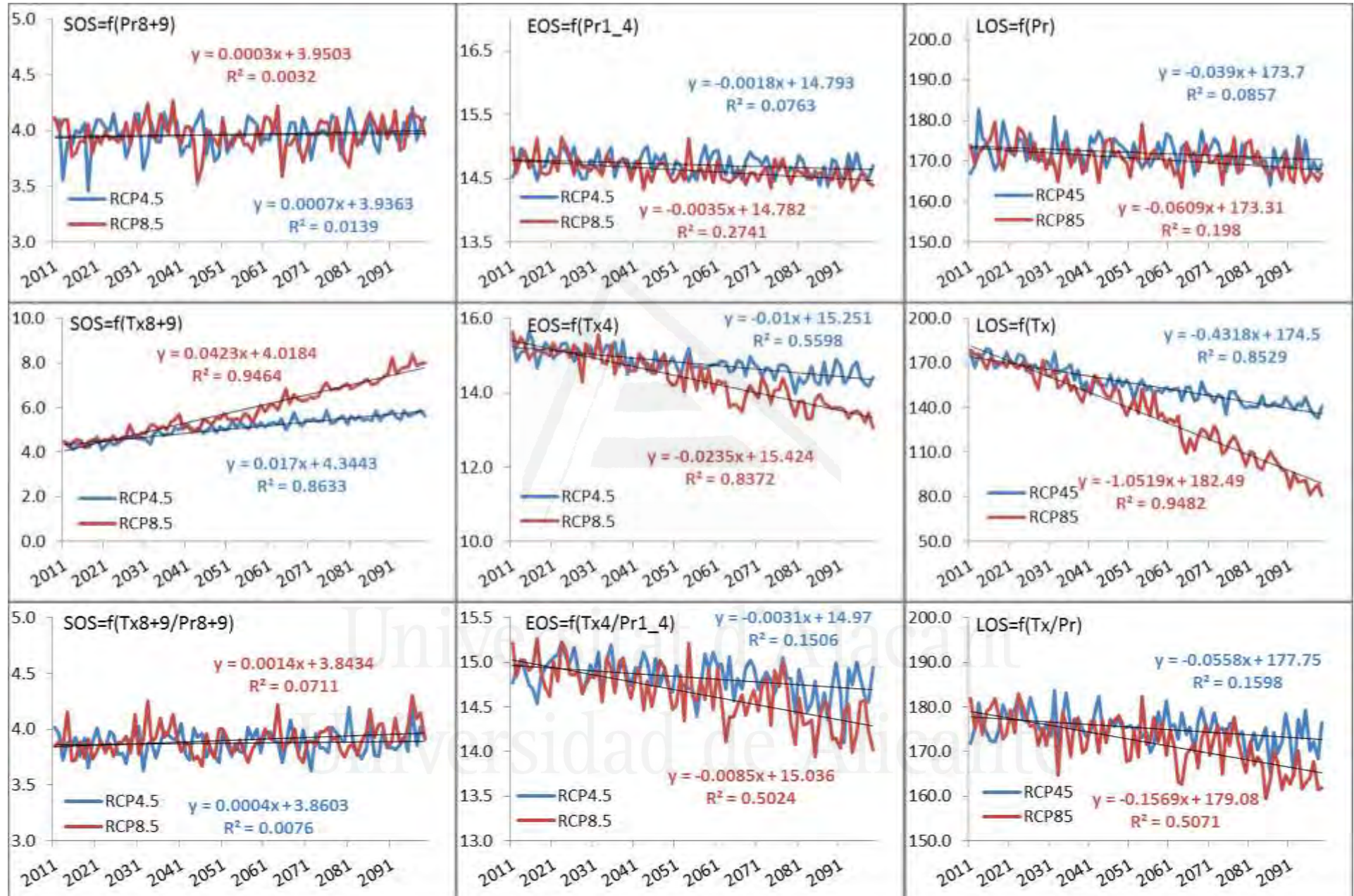


Figure 1: LSP metrics projection in the CLC312 land cover class in function of precipitation and maximum temperature. SOS and EOS are expressed in M-days and LOS is expressed in days. X axis represents the time in years.

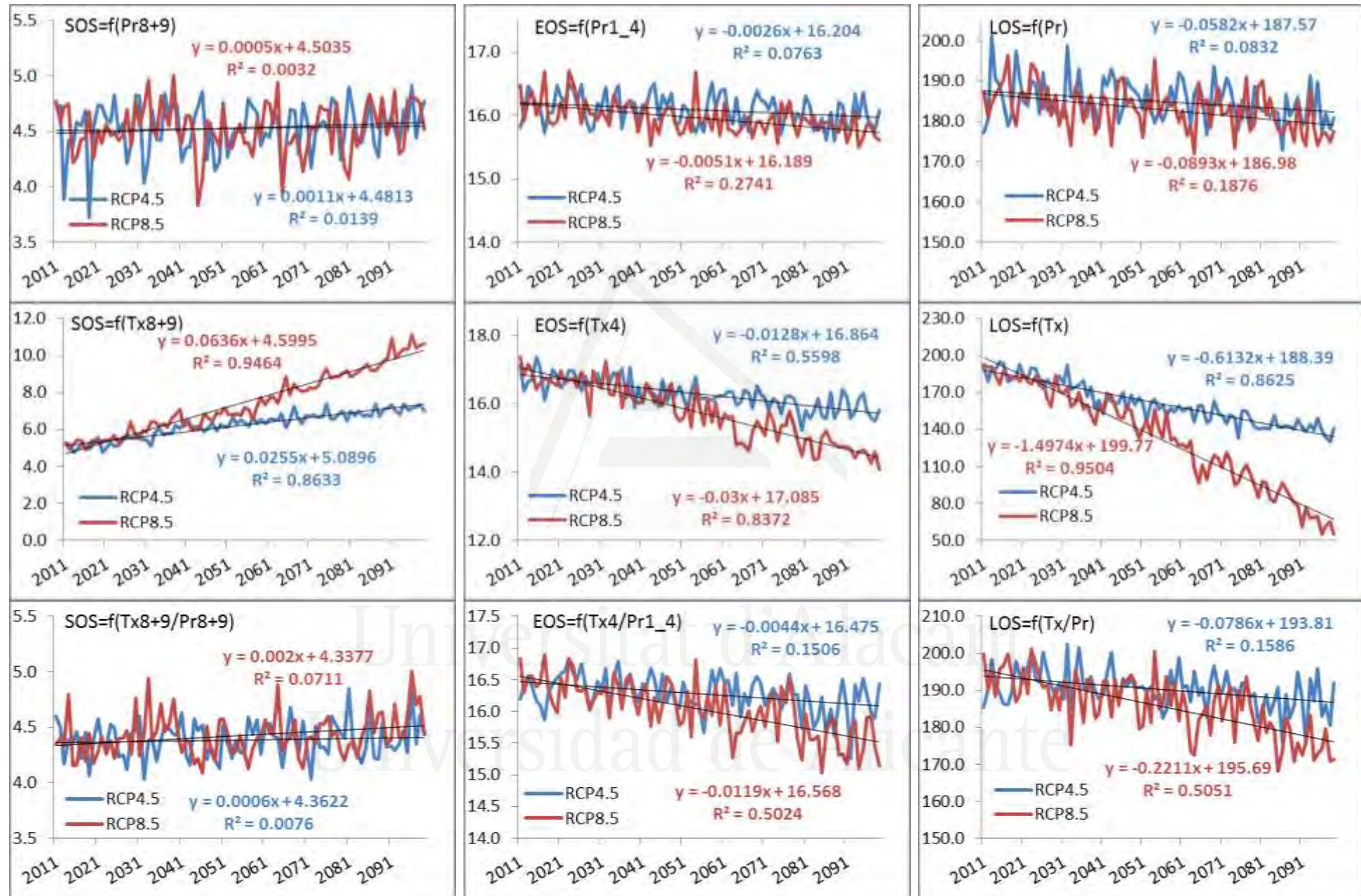


Figure 2: LSP metrics projection CLC321 land cover class in function of precipitation and maximum temperature. SOS and EOS are expressed in M-dates and LOS is expressed in days. X axis represents the time in years.

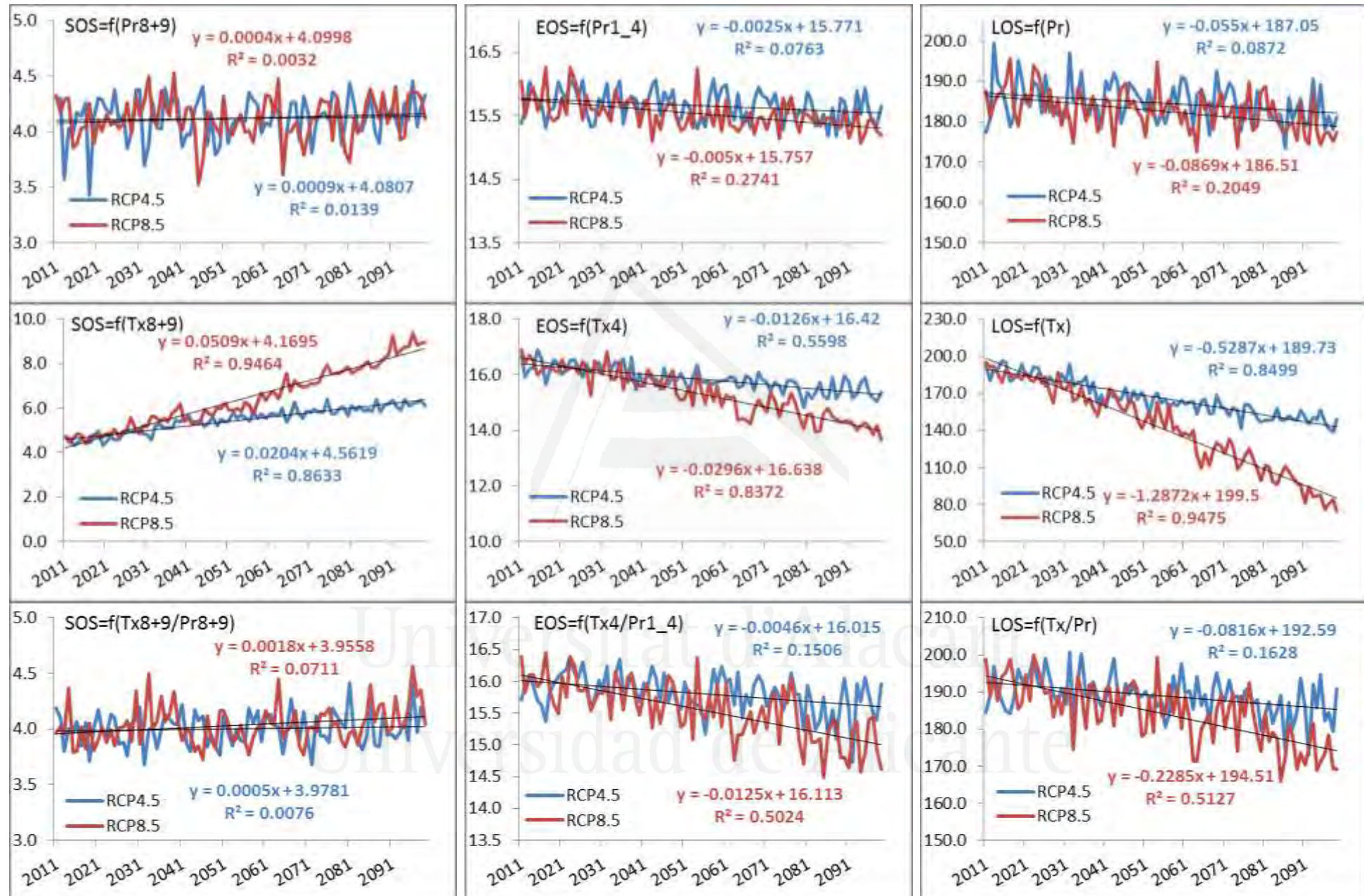


Figure 3: LSP metrics projection CLC323 land cover class in function of precipitation and maximum temperature. SOS and EOS are expressed in M-dates and LOS is expressed in days. X axis represents the time in years.

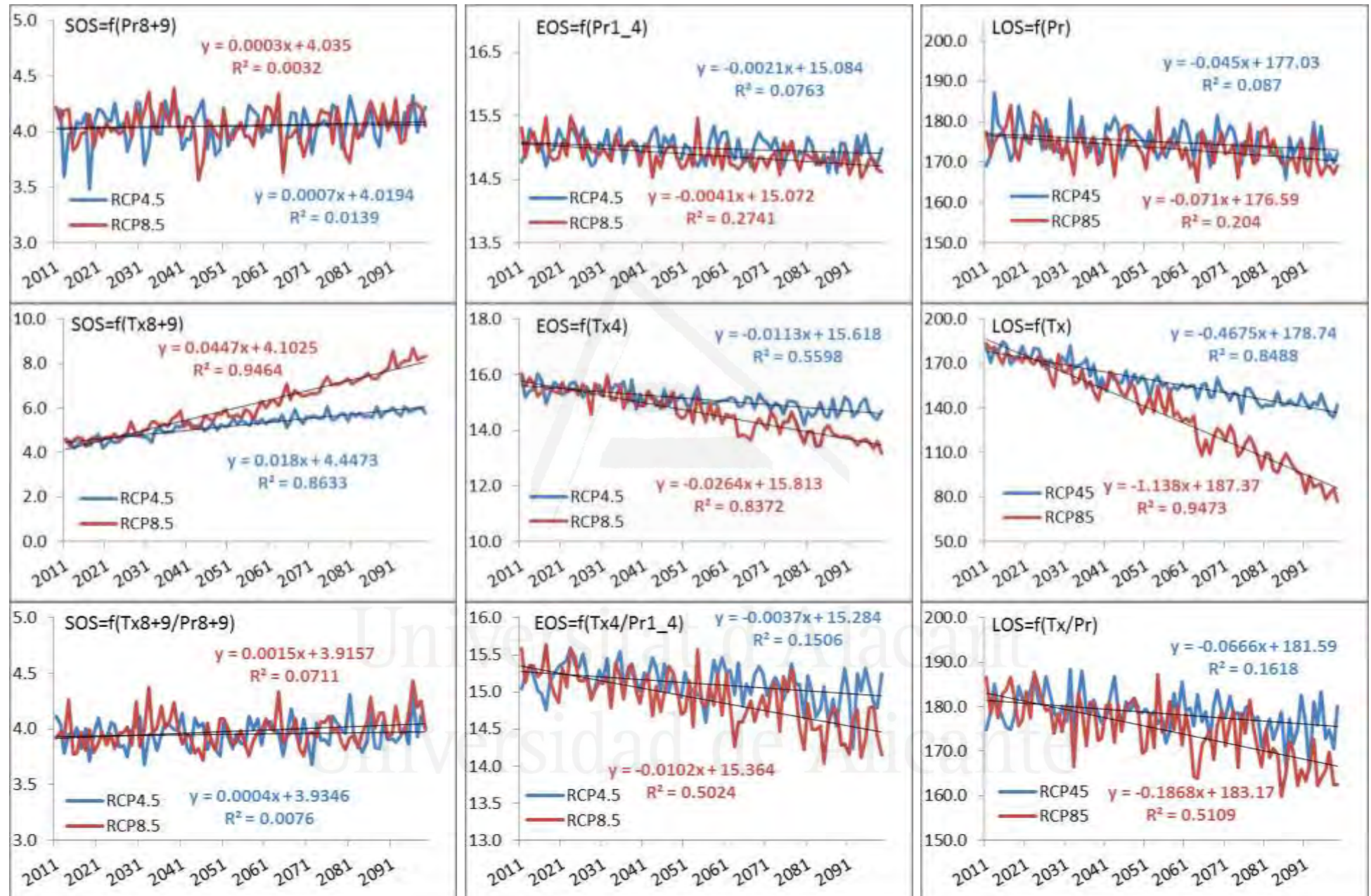


Figure 4: LSP metrics projection CLC324 land cover class in function of precipitation and maximum temperature. SOS and EOS are expressed in M-dates and LOS is expressed in days. X axis represents the time in years.



Universitat d'Alacant
Universidad de Alicante

CAPÍTULO 5

**ASSESSING THE CROP GROWING PERIOD
ACCORDING TO THE CLIMATE CHANGE FORECASTS
FOR MARINA BAIXA (SE SPAIN)**

Universitat d'Alacant
Universidad de Alicante



Universitat d'Alacant
Universidad de Alicante

Assessing the crop growing period according to the climate change forecasts for Marina Baixa (SE Spain)

Abstract

The present work aims to assess the likely effects of climate change on the length of growing period (LGP) of crops in Marina Baixa (SE, Spain). LGP can be assessed by a balance between precipitation and reference evapotranspiration. Less rainfall and an increased evapotranspiration, forecast by Global Climate Models (GCMs), are considered a high risk for agriculture. This area is located in a semiarid climate region where water is a very limited resource. It is a typical example of areas where the agricultural sector has to compete for water with the tourism industry. In this context, using observed and projected precipitation data set (model HadCM3, Scenario A2), calculating reference evapotranspiration (ETo), and applying the frequency analysis of a probability-type method, we estimated the growing period length in the observed period (1961-1990) and three 30-years future periods (2011-40, 2041-70 and 2071-99) in the study area. The results show a drop in annual precipitations (-30%) and an increased ETo (+18%) towards the end of this century with respect to the observed period (mean annual rainfall: 356 mm; mean ETo: 1476 mm). The results also show a decrease in the number of decades (10 days) when precipitation exceeds half the ETo, which means shorter growing periods as the 21st century advances. This expected reduction in growing period length towards the end of the present century will imply that many rainfed crops, like olives, almonds and cereals, will require a higher irrigation water supply to maintain suitable growth and performance levels. The results are an early warning to manage water resources in Marina Baixa in a sustainable way.

1. Introduction

Global Climate Change is an unquestionable process. From the 1950s to the present-day, it has been scientifically demonstrated that the atmosphere and ocean have warmed, volumes of snow and ice have decreased, the sea level has risen, and concentrations of greenhouse gases have increased. On a global scale, an increase of $0.6 \pm 0.2^\circ\text{C}$ in the mean air temperature has been observed since 1861 and forecasts predict an increase of $2\text{-}4^\circ\text{C}$ over the next 100 years. More frequent intense and extreme weather events (including drought and floods) are also expected (IPCC, 2007; 2013).

The scientific community has reached a broad consensus about the impact and consequences of climate change on plant biodiversity (Aber et al, 1995; Churkina et al., 1999; Davi et al., 2006), particularly on agriculture. Climate change will produce changes in the spatial plant distribution on a regional scale as a result of changes in rainfall and air temperature. Long-lasting climatic changes are likely to cause geographical shifts of the main plant species and even of the ecosystems (Ozenda and Borel, 2000).

In the Mediterranean region, an increase of 2°C in mean air temperatures in the second half of this century is expected (Smith et al., 2001, Giannakopoulos et al., 2009). A decrease in precipitations and more frequent long-lasting extreme weather events including severe droughts, heat waves and heavy rainfall events are also expected in this region. These changes in the climatic conditions will affect the agricultural production which is one of the main economic activities in the Mediterranean area. Indeed, prolonged periods of time with less precipitation and high reference evapotranspiration (ETo) rates, due to rising temperatures, will affect the crop growing period. Shorter growing period means reduced crops productivity. Studies and programmes of adaptation to climate change will be an adequate way to mitigate the damage that climate change could cause. For this purpose, assessments of future climatic changes based on Global Climate Models (GCMs) can help to define early warning systems to prevent climate change effects. The Intergovernmental Panel on Climate Change (IPCC) provides a set of GCMs (e.g., HadCM3, ECHAM 4, CGCM2, etc.) with a well standardised group of scenarios (e.g., A1B, A2, B1, B2, etc.) for climate impact studies. The database of these models presents certain levels of uncertainty due to multiple factors.

A change in the variance of a distribution will have a larger effect on the frequency of extremes than a change in the mean (Katz and Brown 1992). An analysis of climatic data dedicated to detect trends on extreme events, may not be the appropriate analysis due to the fortuitous behavior of these events. Therefore, it is recommended to establish the frequency of occurrence of these events and to correlate it with their observed variability, instead of adopting the mean values of climatic variables. In this context, the objectives of this study are: (1) to assess the temporal and spatial variation of the climatic conditions in the Marina Baixa region from the observed period (1961-1990) to

the end of the 21st century, using the Agroclim-Map® software; (2) to assess the potential effect of climate change forecasts on the length of crop growing period (LGP) in the study area.

2. Materials and Methods

2.1. Study area

The study was conducted in the Marina Baixa region in the province of Alicante, SE Spain (Figure 5.1). This region covers an area of 578.7 km² and encloses 18 municipalities. Climate is characterised by high inter-annual variability of rainfall. The predominant soil type in the region is the Entisol which shows erosion processes and insufficient vegetation cover affected by torrential rain (Peña, 2007). Altitudes in the region go from more than 1500 (Sierra Aitana: 1558) to 0 m.a.s.l. in the coastline. This topography produces strong climatic contrasts between continental inland and the Mediterranean coastal areas. This region includes three watersheds (Algar River, 216.2 km², Guadalest River, 122.5 km² and Amadorio River, 205.2 km²) and three aquifer systems (Sierra Bernia, 90 km², Serrella-Aixorta, 40 km² and Sierra de Aitana, 255 km²). Agriculture and tourism have been the main economic activities in the region for decades. Farmlands in Marina Baixa cover 8582 ha and more of the half of this area is covered by rainfed crops (4775 ha), where non-citrus fruit trees, olives and cereals cover 3093 ha, 1400 ha and 282 ha respectively. Irrigated crops (3807 ha) are dominated by citrus (1820 ha) and non-citrus fruit trees (1550 ha.).

2.2. Data

To conduct this study, we used daily precipitation data, and the maximum and minimum temperatures, of eleven weather stations located inside (6 stations) and outside (5 stations) the study area (Figure 5.1). These data derive from a database of climate forecasts available on the Spanish State Meteorology Agency website (<http://escenarios.aemet.es/>), which collects data from different GCMs. However, only three GCMs have regionalised data in weather stations. These data, generated by three GCMs (ECHAM4 (the atmosphere-ocean-coupled model of the Max Plan Meteorology Institute (Germany), version 4), CGCM2 (the atmosphere-ocean-coupled model of the Canadian Climate Centre, version 2), HadCM3 (the atmosphere-ocean-coupled model of the Hadley Centre (UK), version 3), have been regionalised by two empirical

methods: the FIC analogues (method of Climate Research Foundation) to regionalise the data of models ECHAM4 and CGCM2, and the SDSM (Statistical DownScaling Method) regression method for the HadCM3 model data (Brunet et al., 2009). It was considered sufficient to use only HadCM3 model data because it presents similar simulation data as the ECHAM4 model. CGCM2 model was discarded given the worse fit that it provided to reconstruct the observed period climate data in Marina Baixa. Indeed, a recent study carried out in a nearby area (Touhami et al, 2015) concluded that from the above cited CGMs the HadCM3 model presented the most similar database (precipitation and air temperature) when the same years selected from the observed period were compared. Another former study carried out in Iran came to a similar conclusion (Samadi et al., 2010).

The impact of climate change forecasts on the Marina Baixa region was assessed for emission Scenario A2. Scenario A2 forecasts high population growth and slow economic and technological development, where local solutions prevail with a moderate employment of energy for future time series (2011-40, 2041-70 and 2071-99). Scenario A2 was selected based on the assumption that the demographic development and growth model to follow, and its relation with the natural environment, would continue with no significant changes, particularly as far as the sustainability of ecosystems is concerned.

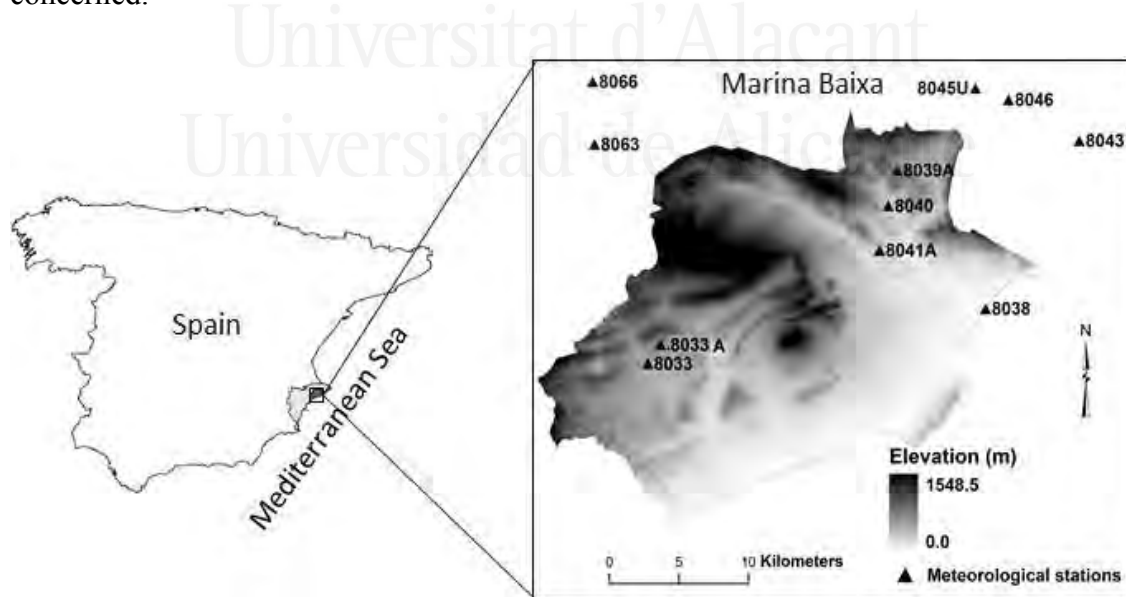


Figure 5.1: Location of the study area and the meteorological stations

2.2. Data analysis

In order to study the change dynamics of precipitations in Marina Baixa, a temporal and spatial analysis was done for the observed and projected periods. The mean annual precipitation during each projected period was calculated and compared to the observed period (1961-1990). The same analysis was done with the reference evapotranspiration ETo calculated by Hargreaves and Samani method (1985), using observed and projected air temperature data.

To complete the analysis of precipitations in the study area, an analysis of the probability of exceedance of a threshold was done. The probability of exceedance (Pe , %, Equation 1) was calculated according to the distribution of Weibull (1961) and Gulinova (1974):

$$Pe = \frac{m}{n+1} * 100 \quad (1)$$

where m is the order number of each observed value, with $m=1$ for the higher value and $m=n$ for the lower one, and n is the number of observations. The study of probability of exceedance considered the 400 mm threshold (80% of the average annual precipitation registered in the eleven stations used over the observed period 1961-1990).

In order to assess the likely effects of climate change on agriculture, the crop growing period length (LGP) for each climatic period was estimated. The growing period is the period of the year when both moisture and temperature conditions are favorable for crop growth (FAO, 1996; Eldin and Rojas, 1983). LGP can be assessed by a simple moisture balance of precipitation (P) and reference evapotranspiration (ETo) when the temperature is not a limiting factor ($T > 5^\circ\text{C}$) (FAO, 1996). In Marina Baixa crops are grown in low altitudes where temperatures rarely go down 5°C . The growing period (GP) is the period of consecutive decades (10-day periods) when P is higher or equal to the half ETo. The choice of 10-day periods as a time base for analysing water balance derives from the ability of a soil to hold rainwater and to have it available to the crop (Eldin and Rojas, 1983). New decadal (10-days) time series of precipitation and ETo were computed to carry out this analysis. Climate model data have only 360 days; it is why only 36 decades were computed by year. Besides the decadal analysis, an exploratory analysis of LGP at a daily basis was done.

To analyse this information, applying probability methods like a frequency analysis (FA, Equation 2) (Eldin and Rojas, 1983) was prioritised. This method evaluates the probability of precipitation exceeding half the ETo of each decade as a percentage. With the obtained results, the growing period was obtained, and was defined as the time interval in which precipitation exceeded half the ETo for a probability of 75% or more.

$$FA(\%) = \frac{n}{N} * 100 \quad (2)$$

where n is the number of times that $\geq \frac{ETo}{2}$; N is the number of years in the data series.

The attributes of the LGP lie in precipitation acquiring ecological properties since its performance relates to being able to meet the water requirements of crops. A risk assessment is also indicated when conditioning the period to meet the conditions of exceeding 75% of probability, which is a guarantee for the crop in question. Frequency over 30% in any of the scenarios is taken as a comparison measure.

The whole database was processed by the Agroclim-Map® software (Herrera, 2000; Herrera and González, 2007; González et al., 2012), which allowed the computation of various agroclimatic models and indices. The output variables of these models were used as input variables for post-processing methods (statistic and geostatistic processing). The final products were tables, graphs and maps created using the Inverse Distance Weighted (IDW) interpolation method, which provided a better interpretation of the results.

3. Results and Discussion

3.1. Temporal and spatial dynamics of precipitations

The spatial distribution of precipitations in Marina Baixa shows a NE-SW gradient. High precipitation values (green and yellow areas on the map) are observed in the NE of the study area and low values (red and orange areas) in the SW (Figure 2). The temporal dynamics analysis of precipitation from the observed period to the end of the present century showed a negative trend. The reduction in the mean annual precipitation, for the entire region, expected in the first projected period is less marked (-5% with respect to the observed period). However, the decrease is expected to be more evident in the 2041-70 and 2071-99 periods (-14 and -30 % with respect to the observed period

respectively). Frequency histograms show the percentage of the Marina Baixa territory with precipitations in a given range (Figure 5.2). In the observed period 20% of the territory showed precipitation values above 400 mm, with areas reaching values above 600 mm near the town of Altea located in the NE. During the 2041-70 and 2071-99 periods, these areas are expected to be reduced to 10% and only 2% of the territory, respectively. These results coincide with those reported by Tatarinov and Cienciala (2009) in Central Europe and at a global scale by IPCC (2014).

The spatial analysis of precipitation in Marina Baixa and its expected changes in the future showed that the rate of change is space-dependent. Actually, despite the fact that the mean rates of change were -5, -14 and -30% in the 2011-40, 2041-70 and 2071-99 periods with respect to the observed period respectively, these rates were different depending on the space. Few differences found between the observed period and 2011-40 exceed 60 mm; however, the most frequent differences were concentrated between 0 and 30 mm. The differences found in the 2041-70 period exceeded 210 mm, although 90% of the area showed differences below 100 mm. In the period 2071-99 infrequent differences reached values above 300 mm in reduced areas while in the major part of the territory these differences fluctuated within the 50-250 mm range. Between the period 2041-70 and the period 2071-99 the areas affected by high change rates passed from 10 to 40% which coincides with results reported by Jones (1996) and Whetton (2001), who reported more shortages in precipitations and changes in their annual distribution. The resulting reduction in precipitations became a factor that can have serious effects on the growth of different species, as reported by several authors (Tatarinov et al., 2005; Vygodskaya et al., 2004; Aber et al., 1995). In some regions, as is the case crop growing regions of Russia, the frequency of food production shortfalls could triple by the 2070s (Alcamo et al., 2007).

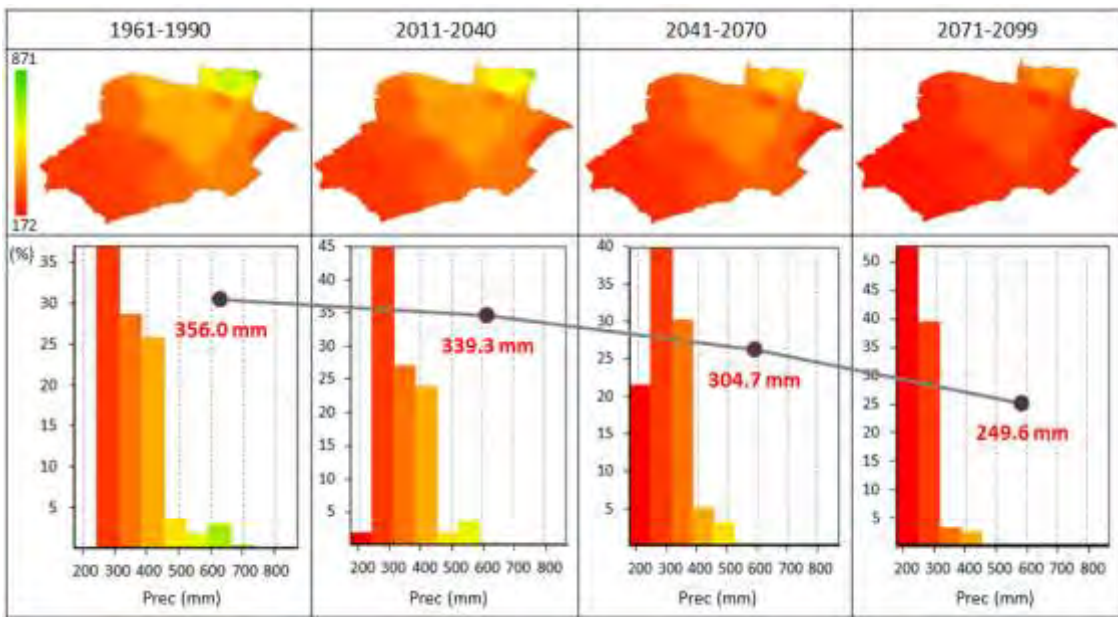


Figure 5.2: Temporal and spatial distribution of the mean annual precipitations during the observed and projected periods. Frequency histograms (X-axis: annual precipitation mm); Y-axis: observed frequency (%)). Grey line shows the decrease of precipitations over time.

3.2. Probability of exceeding the 400 mm threshold of annual precipitation

The mean probability of exceeding the 400 mm threshold (Pe_{400}) of annual precipitation in Marina Baixa was 29% in the period 1961-1990. This probability is expected to decline to 9% by the end of the 21st century (Figure 5.3). The maps in the Figure 5.3 show the spatial distribution of the Pe_{400} where green and yellow indicate high values and red and orange low values. The histograms show the percentage of the territory with a given probability. The results of the comparison of the Pe_{400} in the projected periods with the observed one indicate that there will be more areas with little Pe_{400} , while the areas with a great probability tend to lower by the end of the 21st century (Figure 5.3). Probability that equalled or exceeded 60% were only significant during the observed period 1961-90 and the first projected period, whereas areas that reached this threshold was negligible in the 2041-70 period, and null in the last period 2071-99 (Figure 5.3). Similar results were reported by Alcamo *et al.* (2007). The spatial analysis of the territorial distribution of the probability of exceedance in the study area is essential. If not, extreme values can be confusing when making comparisons because they can obtain higher or lower values, but in small areas. This became evident when comparing the observed period with the period 2011-2040, where the distribution of the

values provided a more exact image of the true effect of territory, even when values appeared with similar magnitudes.

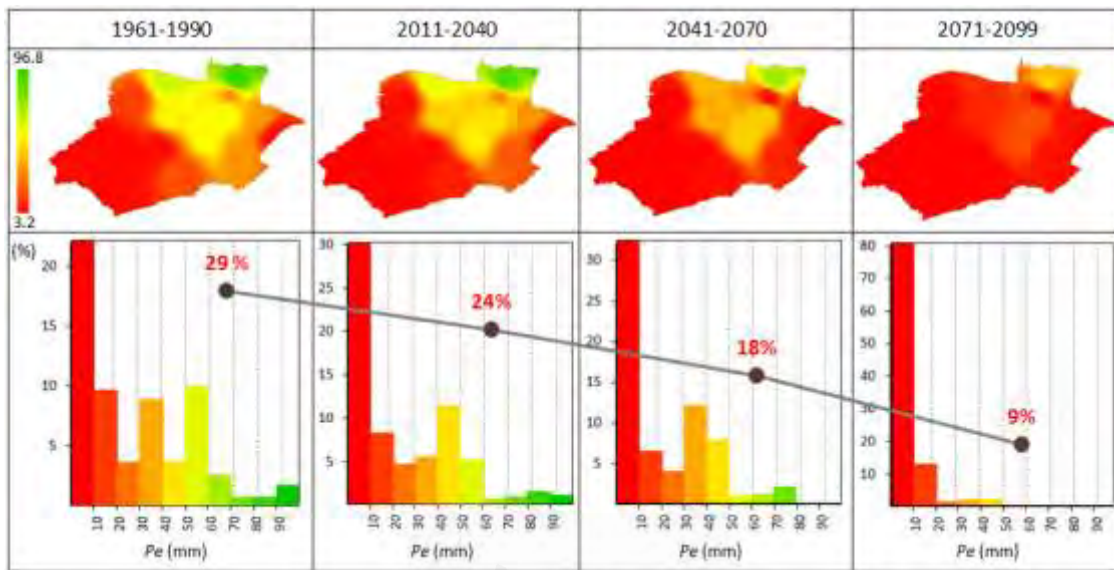


Figure 5.3: Temporal and spatial distribution of probability of exceeding 400 mm of annual precipitation during the observed and projected periods. Frequency histograms (X-axis: Probability of exceedance (%)); Y-axis: observed frequency (%)). Grey line shows the decrease of probability of exceeding 400 mm of annual precipitation over time.

3.3. Temporal and spatial dynamics of reference evapotranspiration (ETo)

The spatial distribution of the reference evapotranspiration follows the same distribution as temperature, low values in the northern and coastal areas and high values in the southern and inland areas (Figure 5.4). Over time the ETo showed inverse trends in comparison with precipitation. In fact, the expected increment in air temperature will cause an increase in ETo (Figure 4). The observed mean value of ETo for the entire region is about 1476 mm. This value is expected to rise more slightly in the first projected period (+4% with respect to the observed period) and with higher rates in the second and third projected periods (+10 and +18% with respect to the observed period respectively). These changes are expected to show some homogeneity throughout the study area where no contrasts are obtained in the obtained in the reference evapotranspiration values shown in the maps. These results are similar to those obtained by Whetton (2001), who considered that lack of humidity would increase, along with a rise in temperatures, a trend that is related with increased evapotranspiration. In some experiments, the increase of 3.5 °C found by some models could determine an increase in evapotranspiration of 13.8% (Finnerty and Ramirez 1995).

3.4. Analysis of the length of the growing period (LGP)

3.4.1. Balance between precipitation and ETo at a daily basis

The LGP can be computed as the consecutive periods of time when P exceeds half the ETo with a probability of 75%. As an exploratory analysis we analysed the balance between P and ETo at a daily basis computing the days when P exceeds half the ETo with a probability of 75%. The balance showed very low values, which ranged from 0 to 10 days. The resulting balance between precipitation and reference evapotranspiration was negative for more than 90% of the days of the year. Although rainfall in a certain number of years was higher than the ETo, it does not exceed the probability of 75% of the population ($30 \times 0.75 = 22.5$ years) due the torrential regime of precipitation and their high inter-annual variability in the region (Hidalgo et al., 2003). The spatial and temporal analysis of the balance between P and ETo, in Marina Baixa showed low values varying between 0 and 10 days in the observed period with high values in the north part and very low values in the south part. In the periods 2011-40 and 2041-70 the balance showed values between 1 and 2 days, whereas in the last projected period (2071-99) there were null days throughout the study area.

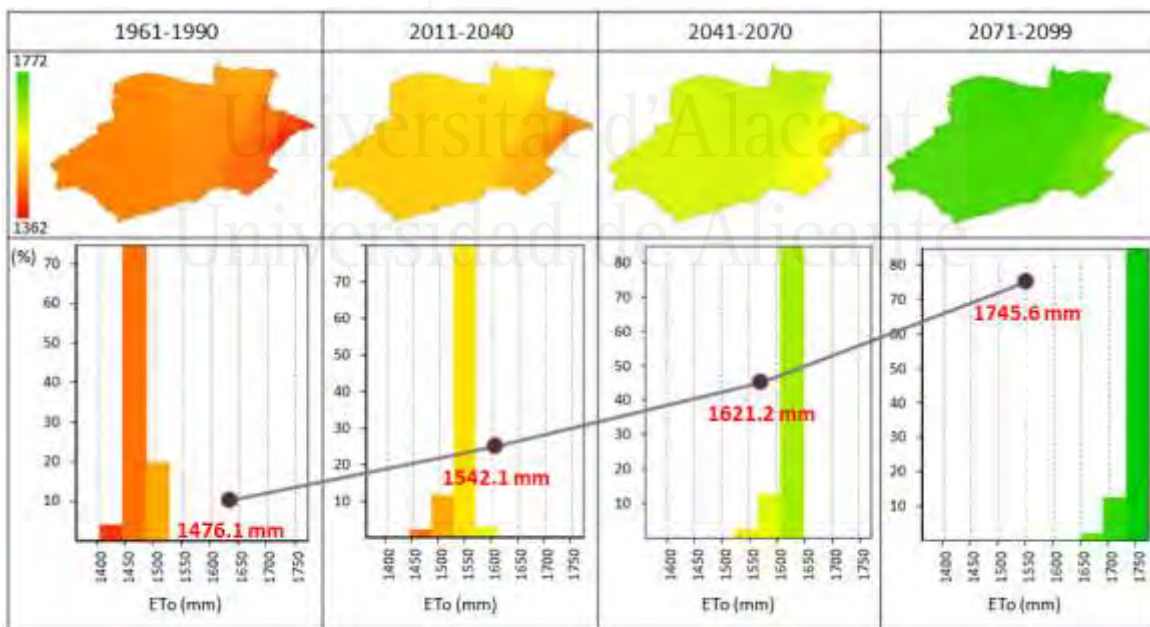


Figure 5.4: Temporal and spatial distribution of the mean annual ETo during the observed and projected periods. Frequency histograms (X-axis: annual ETo mm); Y-axis: observed frequency (%)). Grey line shows the increase of ETo over time.

3.4.2. Analysis of the length of the growing period (LGP) and its projected evolution

In this section the LGP was computed as the consecutive decadal periods (10-day periods) when P exceeds half the ETo. However, as in the case of the daily basis, the probability that P exceeds half the Eto reached the 75% threshold only in very few decades in just one of the eleven meteorological stations used. Therefore, the use of the 75% probability threshold to assess LGP in Marina Baixa was not feasible. After exploring the use of other threshold, we chose the 30% threshold because it marks the beginning and end of the rainy season in the region. On the one hand when the probability that P exceeds half the Eto starts going up 30% between the 26th and 29th decade (September to October) this marks the start of the autumn rainfalls. On the other hand when this probability starts going under 30% between the 7th and 13th decade (March to May) it marks the end of the spring rainfalls. The growing period starts in a year and end in the next year in the Mediterranean region which coincide with the hydrological year.

Figure 5.5 presents the FA graphs in two weather stations inside Marina Baixa limits, 8033 and 8041A for the observed and projected periods. These two stations, situated in the SW and NE respectively, are representative of the regional climatic conditions. In the two stations the probability that P exceeds half the ETo never reaches the 75% threshold in the four periods. Station 8033 showed a large interval of time with low frequencies in general and very low frequencies (<30%) between the 6th decade and 29th decade in the observed period which means a shorter LGP (blue area in the left graphs in Figure 5). Station 8041A, in comparison with station 8033, showed a short interval of time with low frequencies (<30%) in the observed period (from the 13th decade to the 26th) which means a larger LGP (blue area in the right graphs in Figure 5). This interval of time is expected to increase in the projected periods in both stations with a slight high rate of change in station 8041A in comparison with the station 8033. This means that the LGP is expected to be shorter by the end of the 21st century.

Table 5.1 summarises all the FA results and the LGP at the six stations inside the study area limits, and for all the simulation periods. The observed LGP starts in the beginning of the last quarter of a year (26th to 29th decades) and end in the next year (7th to 13th decade) taking into account that in this work the year has 360 days and 36 decades. In

the observed period the mean value of LGP varies between SW and NE (150 and 230 days respectively). The LGP is shorter (150-180 days) in SW and coastal stations and larger (220-230) in the NE stations with the exception of station 8040. The LGP is expected to decrease by the end of the 21st century in the six stations. Indeed, in the SW and coastal stations the LGP is expected to decrease by 60 to 70 days in the last projected period (2071-99) while in NE stations the reduction will be about -40 to -50 days. The contrast between NE and SW is due the differences in precipitations and ETo between the two regions. Precipitations are higher and temperatures are lower in the NE and changes in LGP will be proportional to change in these two climatic variables.

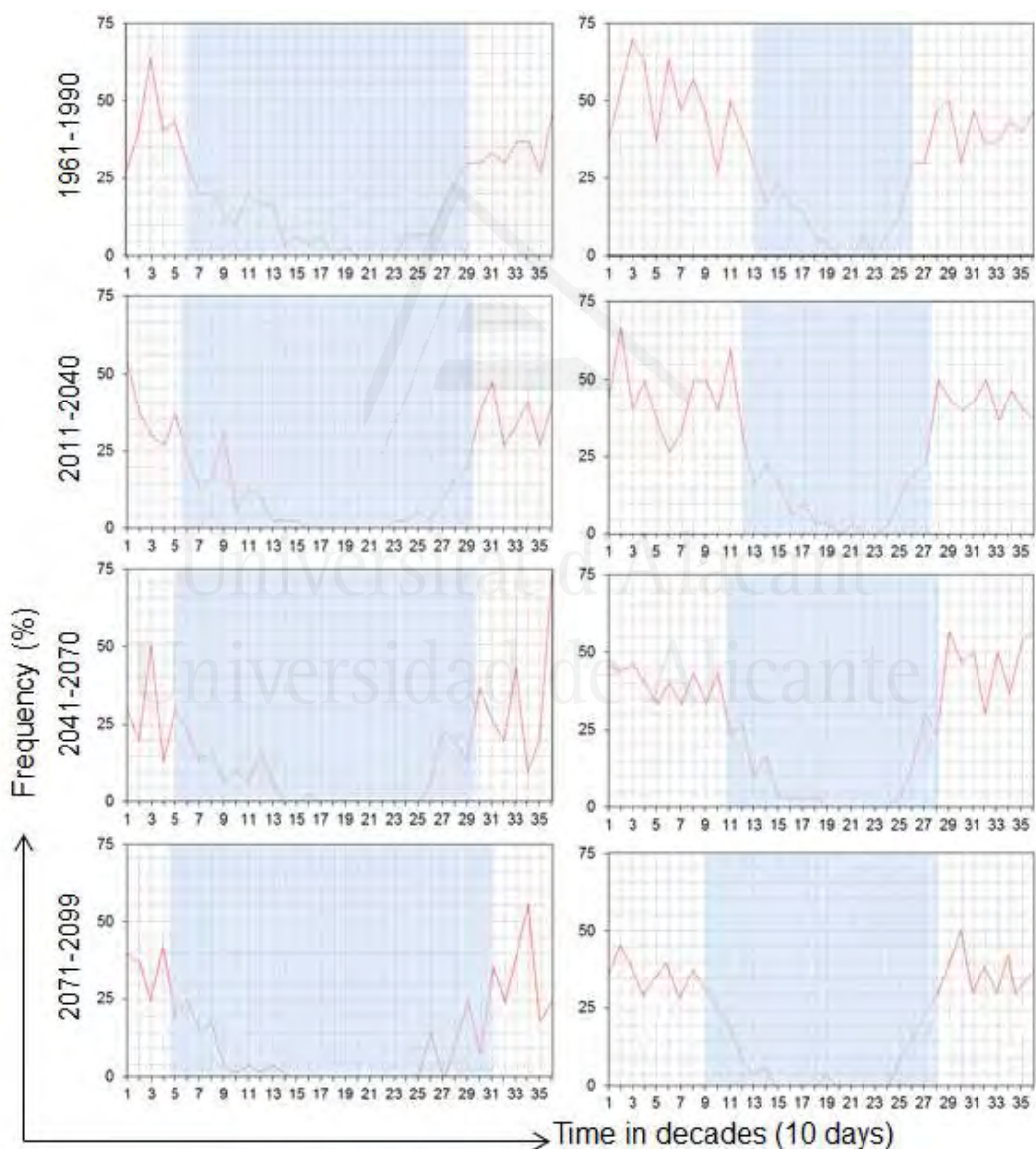


Figure 5.5: Frequency analysis of P exceeding half the ETo in the stations 8033 (left) and 8041A (right) during the observed and projected periods. (Blue area shows the decades when the frequency goes down 30%)

Table 5.1: LGP in Marina Baixa using the 30% threshold of probability that P exceeds half the ETo. Start and end decades and duration in days. LGP start in a year and end in the next year.

Meteorological Stations	LGP start and end decades and duration in days			
	1961-90	2011-40	2041-70	2071-99
8033	29 - 8 (150)	30 - 6 (120)	30 - 6 (120)	31 - 4 (90)
8033A	28 - 10 (180)	26 - 12 (220)	28 - 6 (140)	29 - 5 (120)
8038	28 - 7 (150)	29 - 10 (170)	28 - 6 (140)	32 - 4 (80)
8040	28 - 9 (170)	27 - 10 (190)	28 - 6 (140)	28 - 7 (150)
8039A	26 - 13 (230)	26 - 14 (240)	28 - 12 (200)	27 - 10 (190)
8041A	26 - 12 (220)	27 - 12 (210)	28 - 9 (170)	28 - 9 (170)

4. Conclusions

The results show that a decrease in the annual total precipitation is expected towards the end of this century (-30% in the period 2071-99 with respect to the observed period (1961-1990)). Besides this change in the mean, the probability of exceeding the 400 mm threshold of annual precipitation is expected to decrease from 29% in the observed period to 9% in the last projected period. In contrast, an increase of +18% in the ETo is expected. Therefore these forecasts in the climatic conditions will produce a reduction in the crop growing period length assessed by a balance between precipitation and ETo. This result indicates that the region of Marina Baixa will face a big challenge in terms of water insufficiency in the future, which can only be overcome through mitigation and adaptation actions. A possible alternative could be, to consider the use varieties of crops with short growing season and to design infrastructures for irrigation to meet the water needs of crops of interest.

References

- Aber, J.D., Ollinger, S.V., Federer, C.A., Reich, P.B., Goulden, M.L., Kicklighter, D.W., Melillo, J. M. and Lathrop, R. G. (1995) Predicting the Effects of Climate Change on Water Yield and Forest Production in the Northeastern United States. *Climate Research*, 5, 207-222. <http://dx.doi.org/10.3354/cr005207>
- Alcamo, J., Dronin, N., Endejan, M., Golubev, G. and Kirilenko, A. (2007) A New Assessment of Climate Change Impacts on Food Production Shortfalls and Water Availability in Russia. *Global Environmental Change*, 17, 429-444. <http://dx.doi.org/10.1016/j.gloenvcha.2006.12.006>

Brunet, M., Casado, M.J., de Castro, M., Galán, P., López, J.A., Martín, J.M., Pastor, A., Petisco, E., Ramos, P., Ribalaygua, J., Rodríguez, E., Sanz, I. and Torres, L. (2009) Generación de escenarios regionalizados de cambio climático para España. Ministerio de Medio Ambiente y Medio Rural y Marino, Agencia Estatal de Meteorología, Madrid, 158 p.

Churkina, G., Running, S.W., Schloss, A.L., and the Participants of the Potsdam NpP. Model Intercomparison (1999) Comparing Global Models of Terrestrial Net Primary Productivity (NPP): The Importance of Water Availability. *Global Change Biology*, 5, 46-55. <http://dx.doi.org/10.1046/j.1365-2486.1999.00006.x>

Davi, H., Dufrêne, E., Francois, C. , Le Maire, G., Loustau, D., Bosc, A., Rambal, S. , Granier, A., and Moors E. (2006) Sensitivity of Water and Carbon Fluxes to Climate Changes from 1960 to 2100 in European Forest Ecosystems. *Agricultural and Forest Meteorology*, 141, 35-56. <http://dx.doi.org/10.1016/j.agrformet.2006.09.003>

Eldin, M. and Rojas, O. (1983) A System of Agroclimatic Zoning to Evaluate Climatic Potential for Crop Production. In: Cusak, D.F., Ed., *Agroclimatic Information for Development: Reviving the Green Revolution*, Westview, Boulder, 83-91.

FAO (1996). Agro-Ecological Zoning Guidelines. FAO Soils Bulletin 73. Soil Resources, Management and Conservation Service. FAO Land and Water Development Division. Food and Agriculture Organization of the United Nations. Rome

Finnerty, B. and Ramirez, J.A. (1995) Impact Assessment Study of Climate Change on Evapotranspiration and Irrigated Agriculture in the San Luis Valley, Colorado. Proceedings of the AWRA 31st Annual Conference and Symposia, Houston, 5-9 November 1995, <http://www.nws.noaa.gov/oh/hrl/papers/area/sanluisb.htm>

Giannakopoulos, C., Le Sager, P., Bindi, M., Moriondo, M., Kostopoulou, E., and Goodess, C. M. (2009) Climatic changes and associated impacts in the Mediterranean resulting from a 2 °C global warming. *Global and Planetary Change*, 68(3), 209-224.

González, C.A., Moutahir, H., Herrera, M., Zayas, L., Touhami, I. and Bellot, J.F. (2012) Agroclim-Map, a GIS Application for Agroclimatic Systems Analysis. Proceedings of the International Conference of GIS Users, Taza GIS-Days, Morocco, 23-24 May 2012, 491-493.

Gulinova, N.V. (1974) Métodos Agroclimáticos de Elaboración de las Observaciones. Guidrometeoizdat, Leningrado, 151 p.

Hargreaves, G.H. and Samani, Z.A. (1985) Reference Crop Evapotranspiration from Temperature. Applied Engineering in Agriculture, 1, 96-99. <http://dx.doi.org/10.13031/2013.26773>

Herrera, M. and González, C. (2007) AgroClim: Un software para la ciencia y la docencia. Premio Relevanteen Fórum Provincial, Ciudad Habana, Cuba.

Herrera, M.S. (2000) Contribución metodológica a la zonificación agroclimática de la caña de azúcar: Caracterización agroclimática de las áreas cañeras de la provincia La Habana. Tesis en opción al grado de Doctor en Ciencias Agrícolas. Universidad Agraria de la Habana, La Habana.

Hidalgo, J.G., De Luis, M., Raventós, J. and Sánchez, J.R. (2003) Daily Rainfall Trend in the Valencia Region of Spain. Theoretical and Applied Climatology, 75, 117-130.

IPCC (2007) Tercer Informe de Evaluación. Cambio Climático 2007, la base científica.

IPCC (2013) Informe de Evaluación. Cambio Climático 2013, la base científica.

IPCC (2014) Climate Change 2014: Impacts, Adaptation, and Vulnerability. Part A: Global and Sectoral Aspects. Contribution of Working Group II to the Fifth Assessment Report of the Intergovernmental Panel on Climate Change. Cambridge University Press, Cambridge and New York, 1132 p.

Jones, R. (1996) Climate Change Scenarios for the Australian Region. CSIRO Atmospheric Research, Aspendale.

Katz, R.W. and Brown, B.G. (1992) Extreme Events in a Changing Climate: Variability Is More Important than Averages. Climatic Change, 21, 289-302. <http://dx.doi.org/10.1007/BF00139728>

Ozenda, P. and Borel, J.-L. (2000) An Ecological Map of Europe: Why and How? Comptes Rendus de l'Académie des Sciences—Series III—Sciences de la Vie/Life Sciences, 323, 983-994.

Peña, J. (2007) Efectos ecológicos de los cambios de coberturas y usos del suelo en la Marina Baixa (Alicante). Tesis presentada en opción al título de Doctor en Ciencias, Universidad de Alicante, España.

Samadi, S.Z., Sagareswar, G. and Tajiki, M. (2010) Comparison of General Circulation Models: Methodology for Selecting the Best GCM in Kermanshah Synoptic Station, Iran. International Journal of Global Warming, 2, 347-365. <http://dx.doi.org/10.1504/IJGW.2010.037590>

Smith, J.B., et al. (2001) Vulnerability to Climate Change and Reasons for Concern: A Synthesis. In: McCarthy, J.J., Canziani, O.F., Leary, N.A., Dokken, D.J., White, K.S., Eds., Climate Change 2001: Impacts, Adaptation, and Vulnerability: Contribution of Working Group II to the Third Assessment Report of the Intergovernmental Panel on Climate Change, Cambridge University Press, Cambridge, 913-967.

Tatarinov, F. and Cienciala, E. (2009) Long-Term Simulation of the Effect of Climate Changes on the Growth of Main Central-European Forest Tree Species. Ecological Modelling, 220, 3081-3088.

Tatarinov, F., Bochkarev, Y., Oltchev, A., Nadezhina, N. and Cermak, J. (2005) Effect of Contrasting Water Supply on the Diameter Growth of Norway Spruce and Aspen in Mixed Stands: A Case Study from the Southern Russian Taiga. Annals of Forest Science, 62, 807-816. <http://dx.doi.org/10.1051/forest:2005086>

Touhami, I., Chirino, E., Andreu, J.M., Sánchez, J.R., Moutahir, H. and Bellot, J. (2015) Assessment of Climate Change Impacts on Soil Water Balance and Aquifer Recharge in a Semiarid Region in South East Spain. Journal of Hydrology, 527, 619-629. <http://dx.doi.org/10.1016/j.jhydrol.2015.05.012>

Vygodskaya, N.N., et al. (2004) Long-Term Dynamics of Soil Moisture and Drying of Spruce Trees in Spruce Forests of the Southern Taiga. Russian Forest Sciences (Lesovedenie), 1, 3-22. (In Russian)

Weibull, W. (1961) Fatigue Testing and Analysis of Results. Pergamon, Oxford, 225.

Whetton, P. (2001) Climate Change: Projections for Australia. CSIRO Atmospheric Research Report, Aspendale.

CAPÍTULO 6

**HYDROBALPCR: A MODEL BASED ON AN ENVIRONMENTAL
MODELLING FRAMEWORK TO EVALUATE OF THE LIKELY EFFECTS
OF CLIMATE CHANGE ON WATER BALANCE UNDER DIFFERENT
VEGETATION COVERS**

Universitat d'Alacant
Universidad de Alicante



Universitat d'Alacant
Universidad de Alicante

HydrobalPCR: a model based on an environmental modelling framework to evaluate of the likely effects of climate change on water balance under different vegetation covers

Abstract

Environmental modelling frameworks based on higher level programming languages are suitable tools for model construction for domain experts, such as hydrologists, without expert knowledge in programming. The implementation of the model in a high-level scripting language allows the iteration over large data sets in simple loop syntax. In this work, we used the PCRaster-Python framework to build a modified version of the eco-hydrological HYDROBAL model. The HydrobalPCR was then used to evaluate the likely effects of climate change on water balance using data from nine CMIP5 climate models under two RCP scenarios over the period 2010-2099. The analysis was performed on two vegetation cover types in four sites along a climate gradient in Alicante province. The calibration and validation of HydrobalPCR were done by adjusting the k factor and minimizing the RMSE between observed and simulated soil water content (SWC) over the period 2012-2015. The evaluation of HydrobalPCR showed acceptable performance. Results showed that negative trends are expected in the main water flows simulated by HydrobalPCR under the projected climate change conditions in the four sites and two vegetation types. These negative trends are due to the expected reduction in rainfall and the increase in reference evapotranspiration caused by the increase in temperature. Comparing the last 30-year projected period 2070-2099 to the first period 2010-2039, the results showed that the major change is expected in the aquifer recharge (more than -30% in average between the four sites and the two vegetation types with respect to the period 2010-2039).

1. Introduction

Evaluating the likely effects of climate change, land use change or the combined effect of both of them on water balance requires the use of tools that integrate multiple processes and help predict changes in water balance components. Hydrological models, a simplified representation of a part of the hydrologic cycle, are often used for understanding hydrologic processes and for hydrologic prediction (Moradkhani et al., 2005). Hydrological models differ in their structure, complexity, spatial and temporal

resolution and are applied with different purposes (Kremer and Running, 1996; Gracia et al., 1999; Beeson et al., 2001; Bellot et al., 2001; Ajami et al., 2007; Blöschl et al., 2008; Delgado et al., 2010; Sood and Smakhtin, 2015). Another point of difference between hydrological models is the programming technique used in their construction. Although the low-level system programming languages present several advantages, higher level environmental modelling language is better in the sense that it operates at the conceptual level of the hydrologist (Karssenberg, 2002). Several modelling frameworks have been developed for the purpose of model construction (Reed et al., 1999; Pullar, 2004; Kraft et al., 2011; PCRaster, 2016; MATLAB, 2016).

In this context, we used the PCRaster modelling framework (van Deursen, 1995, Karssenberg and de Jong, 2005; PCRaster, 2016) to build a modified version of the eco-hydrological HYDROBAL model (Bellot et al., 2001; Bellot and Chirino, 2013). The original version of HYDROBAL is based on C++ and Quickbasic software and any modification on it requires specific programming knowledge. The HYDROBAL graphic interface is easy to handle; however, it is difficult to work with large sets of data which is the case when iteration over several global climate models (GCM) daily data under different emission scenarios are needed to evaluate the effect of climate change on water balance in different sites and vegetation types over one hundred years.

PCRaster is a collection of software targeted at the development and deployment of spatio-temporal environmental models (Van Deursen, 1995; PCRaster, 2016). PCRaster model construction framework was extended by adding new components using Python programming language (Python, 2016). PCRaster-Python framework is an integrated framework that provides tools for both model construction and optimization; in this case optimization means data assimilation and model calibration (Karssenberg et al., 2007; 2010). Performing both operations with the same software is one of the advantages of using PCRaster-Python framework (Karssenberg et al., 2010). PCRaster is a toolbox with more than 200 applications for environmental cartographic and dynamic modelling. It includes a rich set of model building blocks and analytical functions for manipulating raster GIS maps which allows users to perform several GIS tasks using PCRaster alone. PCRaster contains a scripting model development environment which allows users to develop their own simulation models. Scripting languages supported include PCRcalc and Python (PCRaster, 2016). The earth scientists can design their

own models without specialized knowledge in programming (Karssenberg and de Jong 2005; Karssenberg et al., 2007).

HYDROBAL is an ecohydrological model that integrates the meteorological conditions, vegetation characteristics and soil processes to simulate water balances at plot scale in ecosystems dominated by different vegetation types (Bellot et al., 2001; Bellot and Chirino, 2013). HYDROBAL was applied in different studies to simulate the effect of vegetation type and rainfall amount on the soil–water balance (Bellot et al., 1998, Bellot et al., 2001, Bellot et al., 2005, Bellot and Chirino, 2013, Manrique-Alba et al., 2015a; 2015b; Ruiz-Yanetti et al., 2015), on aquifer recharge (Touhami et al., 2013; 2014) and to assess the effect of climate change on aquifer recharge (Touhami et al., 2015). A detailed description of HYDROBAL can be found in Bellot and Chirino (2013). A description of different components of HYDROBAL will be presented in the next sections.

This work describes the HydrobalPCR model which is a modified version of HYDROBAL based on PCRaster-Python framework. The general structure of HydrobalPCR is presented and the major differences with HYDROBAL highlighted. Finally HydrobalPCR was applied to assess the likely effects of climate change on the water balance using data from nine CMIP5 climate models under two RCP scenarios over the period 2010-2099. This analysis was performed in two vegetation types in four sites along a climate gradient in Alicante province.

2. Study area

This study was performed in four sites located along a climate gradient in the province of Alicante, Southeastern Spain (Figure 6.1). The four sites are located in the recharge “window” into four aquifers: Mela, Cabeço d’or, Ventós and Águilas stated from north to south respectively. The overall climate is Mediterranean and varies from dry Mediterranean in the northern site Mela (rainfall: 650 mm and temperature: 11.7°C) to semiarid Mediterranean in the southern two sites Águilas and Ventós (rainfall: 300 mm and temperature: 17.3°C). Caboço d’or is located in a transitional area between both dry and semiarid climates (rainfall: 400 mm and temperature: 13.2°C). Natural areas cover 35% of Alicante territory and are mainly dominated by shrublands and grasslands (78%). Forested ecosystems are dominated by coniferous pine forests which represent

95% of forested area. Afforested Pine (*Pinus halipensis*) is a common land cover in the four sites with different tree ages and densities.

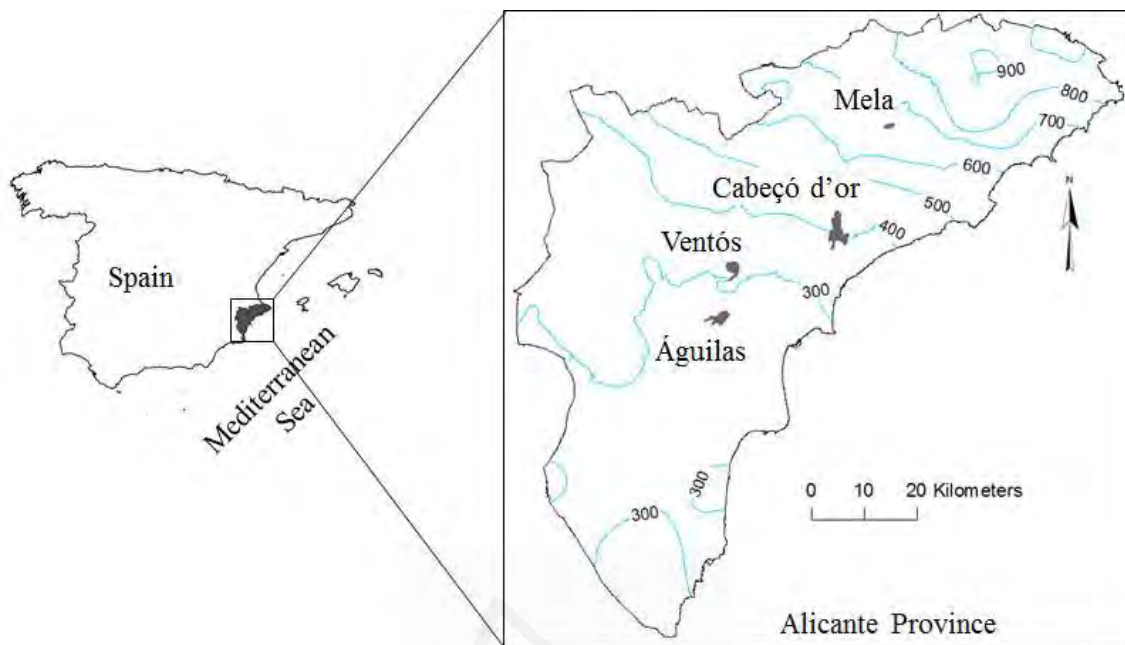


Figure 6.1: The four sites localization. Blue lines represent isohyets each 100 mm.
Mean annual rainfall over the period 1953-2012.

3. Vegetation types and structure

To characterize the vegetation structure in the study area, six plots (100m^2) were selected in each site; three in pine areas (Manrique-Alba et al., 2015a; 2015b) and three in shrub areas (Ruiz-Yanetti et al., 2015). An inventory of all plant species and their covers was carried out in each site per vegetation type. Vegetation cover in the study area was classified into two types: forested and not forested areas. Within each type, different vegetation classes and subclasses were differentiated and the spatial and vertical structures were determined. The spatial structure is the simple distribution of the different subclasses inside each class and plot. The vertical structure is the vertical organization of the different vegetation strata. In the forested areas, the vertical structure is composed by the pine trees and its accompanying understory vegetation (shrub, grass, alpha grass or a combination of these vegetation types). Nevertheless, inside the forested areas some subclasses do not have pine trees (Annex 6.2: Table 1). In the not forested areas, the higher layer is the shrub species and the understory can be grass or alpha grass (Annex 6.2: Table 2). The shrub species were grouped in a unique class called shrub mixture (MixShrub). Ten possible combinations, representing the

vertical structure in the study area, between the different vegetation types were established (Table 6.1).

Table 6.1: The ten possible combinations representing the vertical structure of vegetation in the four sites and its cover (%).

Class	Forested areas				Not forested areas			
	Ventós	Águilas	Cabeço	Mela	Ventós	Águilas	Cabeço	Mela
1-Pine	7.1	11.9	17.1	36.2	-	-	-	-
2-Pine+MixShrub	11.0	3.3	10.5	20.5	-	-	-	-
3-Pine+MixShrub+Grass	16.7	6.7	6.7	7.6	-	-	-	-
4-Pine+Steppe	0.5	2.9	11.4	-	-	-	-	-
5-Pine+Grass	14.3	35.7	10.0	21.0	-	-	-	-
6-MixShrub	21.9	5.7	14.3	5.2	15.2	23.3	12.4	17.2
7-MixShrub+Grass	11.4	5.2	3.3	2.4	12.4	23.3	49.6	48.6
8-Steppe	3.8	0.5	12.4	-	23.8	-	-	-
9-Grass	6.7	17.1	1.0	4.8	6.2	22.4	22.4	18.6
10-BareSoil	6.7	11.0	13.3	2.4	42.4	31.0	8.6	15.7

4. Data

4.1. Observed and projected climate data

Daily rainfall, maximum and minimum air temperatures and solar radiation were registered during the period 2012-2015 in the four sites. Data from nearest meteorological stations, from the Meteorological State Agency network (AEMET), to each experimental site were used to fill gaps and to correct errors in the registered data (Table 6.2).

To assess the likely effects of climate change on water balance in the four sites we used eighteen projected climate data sets. Climate simulations from nine CMIP5 climate models (Annex 1.1: Table 1) downscaled to the nine meteorological observatories used (Table 6.4) for the period 2010-2099 under two climate scenarios. The two future climate projections correspond to the Representative Concentration Pathways RCP4.5 (moderate emissions scenario) and RCP8.5 (high emissions scenario) (Taylor et al. 2009). The used simulations are based on the Program for Climate Model Diagnosis and Intercomparison (PCMDI) archives, are described and analyzed in Monjo et al. (2015). New time series from these stations were computed. Precipitation time series were computed using the inverse distance weighting method and air temperature time series were corrected using the mean altitude of each site and applying a monthly lapse rate ($^{\circ}\text{C}/100\text{m}$) (Table 6.3).

Table 6.2: Nearest meteorological stations to each site. Pr, T and distance represent Precipitation, Temperature and the distance to the nearest site respectively.

Site	Station code	Longitude	Latitude	Altitude (m)	Distance (km)	Variable
Mela	8060	-0.33°	38.67°	739	5.7	Pr and T
	8063	-0.35°	38.72°	545	7.4	Pr
Cabeço	8029	-0.50°	38.54°	415	9.9	Pr and T
	8029A	-0.50°	38.54°	450	10.2	Pr
	8033	-0.31°	38.58°	429	9.2	Pr
	8033E	-0.28°	38.56°	260	10.1	Pr
Ventós	8021A	-0.64°	38.43°	376	2.9	Pr and T
Aguilas	8014I	-0.72°	38.37°	250	6.1	Pr
	8013	-0.77°	38.38°	241	10.5	T

Table 6.3: Lapse rates ($^{\circ}\text{C}/100\text{m}$) used to correct the maximum and minimum monthly temperature.

Months	1	2	3	4	5	6	7	8	9	10	11	12
T max	0.73	0.68	0.58	0.51	0.32	0.17	0.004	0.08	0.32	0.57	0.69	0.74
T min	0.63	0.63	0.60	0.61	0.58	0.56	0.54	0.60	0.63	0.67	0.67	0.65

4.2. Soil water content (SWC) and parameters

During the period 2012-2015, SWC ($\text{cm}^3 \text{ cm}^{-3}$) was monitored from 0 to 30 cm of soil depth using two methods. (1) continuous measuring, hourly with eight soil moisture sensors per site (10HS Decagon devices, Inc. Pullman, WA, USA) connected to a datalogger (EM50 Decagon devices, Inc. Pullman, WA, USA), and (2) periodically measuring with the Time Domain Reflectometry Method (TDR100, Campbell scientific, Inc. Logan, Utah, USA), by means of 18 TDR probes per site (Manrique-Alba et al., under review). SWC was measured under patches (Pine trees or shrubs) and in bare soil inter-patches in the both pine and shrub vegetation types. Field capacity (FC) was estimated according to laboratory analyses and Fuentes and Cruz (1990) equations. Wilting point (WP) was taken as the minimum SWC value observed over the three years of measurements. The initial SWC value is the observed SWC value in the day used as the start of simulations (Table 6.4).

Table 6.4: Soil parameters in the four sites and two vegetation types. WP: Wilting Point, FC: Field Capacity, Poros: Porosity, SWCi : intial Soil water content

		WP (%)	FC (%)	Poros (%)	SWCi (%)	Depth (mm)
Forested	Ventós	5	21	42	14	300
	Águilas	4	20	48	15	480
	Cabeço	5	20	46	11	300
	Mela	8	30	47	16	500
Not forested	Ventós	2	21	41	13	300
	Águilas	5	22	42	12	480
	Cabeço	2	20	42	11	400
	Mela	2	20	41	11	500

5. HydrobalPCR: a modified version of HYDROBAL based on PCRaster-Python framework

The water balance simulated by HydrobalPCR is based on the main flows represented in figure 6.2. A fraction of rainfall (Pr) is intercepted by vegetation and evaporated directly while the other fraction reaches the soil flowing through the vegetation as throughfall (ThF) and stemflow (StF). The fraction of rainfall reaching the soil is divided into infiltration (Inf) and runoff (Roff). The infiltration increases the available soil water content (SWC) and a part of it percolates to the under soil recharging the aquifer. Deep percolation (DP) is not the only loss of water from the soil layer; the actual evapotranspiration (Eta) is the water used by plants which depends on SWC, the reference evapotranspiration (Eto) and the vegetation structure.

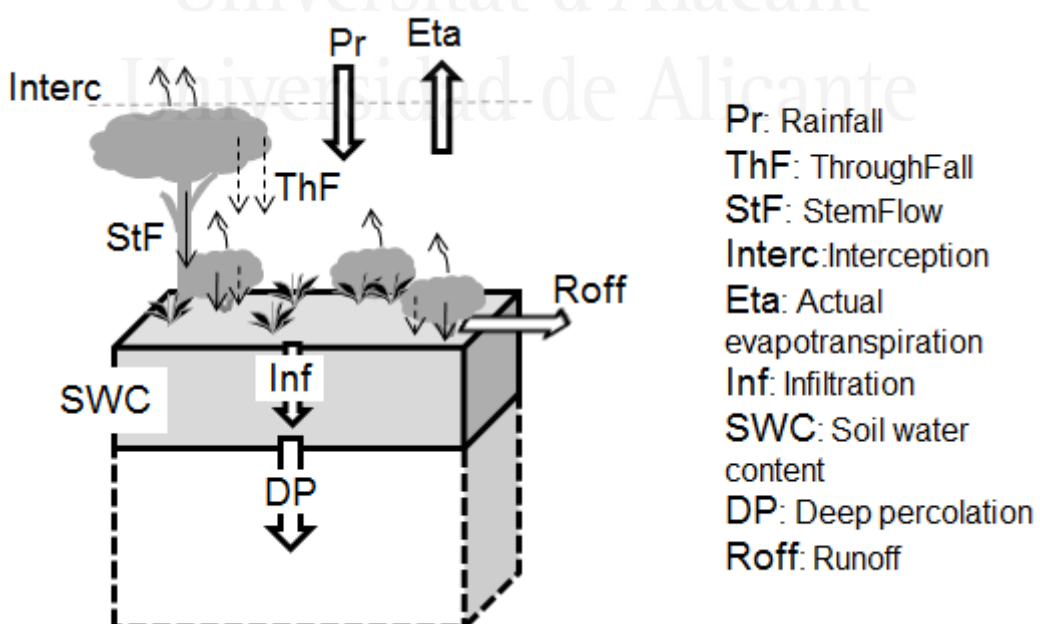


Figure 6.2: Main water flows simulated by HydrobalPCR. The vegetation with its vertical structure plays an important role by regulating the water reaching the soil.

To simulate all these water flows at a daily basis we used PCRaster-Python framework to build the dynamic HydrobalPCR model which is composed of three parts: (1) The main script, (2) The functions script and (3) The run scripts.

5.1. The main HydrobalPCR script

The PCRaster-Python framework provides templates for the custom construction of model components. These templates are Python classes that organize the execution of static and dynamic models.

We used the dynamic model template to create the main HydrobalPCR script. To start this script we called the modules that store all the functions and tools needed (Table 6.5). *pcraster* and *pcraster.framework* modules store all PCRaster functions and communication tools between the Python language and the PCRaster code. *numpy* is an extension to the Python language adding support for large multi-dimensional arrays and matrices. *HydrobalPCRfunctions* is a module containing different functions that allow the calculation of the different HydrobalPCR water balance flows. Finally we created the class *HydrobalPCR* that inherits properties from the *DynamicModel* class.

Table 6.5: Commands used to call the PCRaster modules, numpy and HydrobalPCR functions module and to create a class named HydrobalPCR

```
from pcraster import *
from pcraster.framework import *
import HydrobalPCRfunctions as hpf
import numpy as np

class HydrobalPCR(DynamicModel):
    def __init__(self, cloneMap):
        DynamicModel.__init__(self)
        setclone(cloneMap)
        setglobaloption("matrictable")
```

Inside the HydrobalPCR class, two methods were implemented:

The *initial()* method represents the initial section which contains operations to initialize the state of the model at time step 0 (Table 6.6). These operations are executed once. In this section, the input data (Tables containing soil and cover parameters, precipitation and evapotranspiration time series) are read. The initial states of input variables can be read from disk or created directly in this section. Finally, the output variable names are assigned in this section.

The *dynamic()* method represents the dynamic section which contains the operations that are executed consecutively each time step (Table 6.7). Results from a previous time step can be used as input for the current time step and the state of a model variable at time t is defined by its state at t-1 and a function f (Equation 1) (Karssenberg and De Jong, 2005):

$$Z_{1\dots m}(t) = f(Z_{1\dots m}(t-1), I_{1\dots n}(t), Z_{1\dots l}) \quad (1)$$

The model state variables $Z_{1\dots m}$ belong to coupled processes and have feedback in time. $I_{1\dots n}$ denote the inputs to the model, $P_{1\dots l}$ are model parameters, and f transfers the model state from time step t-1 to t.

HydrobalPCR simulates the different water flows at a daily basis. In the dynamic section, the Pr and Eto of each day are read and used in the calculation of other flows by means of different functions as illustrated in table 6.7. The order of execution of the different functions and calculations in the dynamic section is very important. The soil water content (SWC) is the main simulated water-balance variable and it is used to calibrate and validate the model. The SWC is updated in each iteration when it is used by a function to calculate a flow depending on the current SWC state. The final state of SWC at the end of each iteration is updated as in equation (2):

$$\text{SWC}(t) = \text{SWC}(t-1) + \text{Inf}(t) - \text{Eta}(t) - \text{DP}(t) - \text{SI}(t) \quad (2)$$

where Inf is infiltration, Eta is actual evapotranspiration, DP is deep percolation and SI is slow infiltration in time step t.

5.2. The functions script:

The functions used in the dynamic section to calculate the main water flows simulated by HydrobalPCR are stored in the *Functions script* which is called in the main script as a module with the name *hpf*. All these functions are called as *hpf.name of the function*. In this section both the different water flows and its correspondent functions are described:

5.2.1. Net rainfall (netPr):

Net rainfall is the part of rainfall that reaches the soil through the vegetation. As in HYDROBAL model (Bellot and Chirino, 2013), HydrobalPCR starts with the gross rainfall (Pr) received by the vegetation, then distributes it across the vegetation structure as throughfall (ThF) and stemflow (StF), which are differentiated according to the canopy stratification of each vegetation type. However, in HydrobalPCR the vertical structure of vegetation was reduced to ten possible combinations grouping the different shrub species in the same class (Table 6.1). The vertical vegetation structure is very important by regulating the water reaching the soil. The different layers of vegetation act as multiple filters. For example, in the case of three vegetation layers structure (tree-shrub-grass), a fraction of ThF from the tree layer is intercepted by the shrub layer. The other fraction (ThF from shrub) reaches the grass layer where a part of it is intercepted too. Light rainfall is intercepted by vegetation except if the canopy is saturated by a previous rainfall event.

The ThF and StF were estimated using a linear model ($a + b*Pr$; Pr is daily rainfall) obtained from field measurements in the hydrological plots and laboratory measurements for different vegetation types (Derouiche, 1996; Bellot and Escarré, 1998; Abdelli, 1999 and Chirino, 2003).

The netPr was calculated as the sum of ThF + StF using the function in equation (3) which uses as arguments the rainfall and the coefficient of linear model that allows the calculation of ThF and StF. This function can be modified to add more vegetation structures.

$$netPr = hpf.netPr(Pr, CoefC) \quad (3)$$

5.2.2. Surface runoff (Roff):

In addition to the method used in HYDROBAL to calculate the Roff based on a linear model (Roff in function of precipitation), HydrobalPCR gives the user the possibility to use another method. Roff can be calculated by the two following methods:

-by a linear model as function of daily rainfall ($a + b*Pr$) using the equations obtained previously in the hydrological plots by Abdelli (1999) and Chirino (2003) for different vegetation types. This method is the same used by HYDROBAL and it is implemented

in the HydrobalPCR as the function in equation (4) which uses as arguments the rainfall and the coefficients of the linear model.

$$Roff = hpf.RoffEq(Pr, c1, c2, c3) \quad (4)$$

-by the Soil Conservation Service curve number CN method (SCS, 1972; USDA, 1986) (equation 5) modified by Huang et al., (2006) by incorporating the slope as factor into the CN method (equation 6). The function in equation (7) is used. This function uses the daily netPr of the current day and the rainfall of the 5 previous day (Pr5PD) to choose between using the CN under wet and dry conditions depending on the antecedent moisture conditions (CNwet and CNdry respectively). The mean slope in the study area is used.

$$Q = \frac{(P - 0.2S)^2}{P + 0.8S} \text{ for } P > 0.2S \text{ and } Q = 0 \text{ for } P \leq 0.2S \quad (5)$$

where Q (mm) is surface runoff, P (mm) is rainfall, and S (mm) is the retention parameter ($S = (25400/CN) - 254$).

$$CN_\alpha = CN \frac{322.79 + 15.63\alpha}{\alpha + 323.52} \quad (6)$$

where α is the slope (m/m) which should range between 0.14 and 1.4

$$Roff = hpf.RoffCN(Pr5PD, CNwet, CNdry, slope, netPr) \quad (7)$$

CN can be used as a parameter of calibration in HydrobalPCR.

5.2.3. Soil water infiltration (Inf):

Inf is calculated, to a variable soil depths read from soil parameters table, using the daily values of net rainfall and the runoff at a plot level using equation (8) in the same way as in HYDROBAL.

$$Inf(t) = netPr(t) - Roff(t) \quad (8)$$

where t is time in days

Table 6.6: The initial section of HydrobalPCR main script

```

def initial(self):
    #to read the Soil params table
    self.ParamS=np.genfromtxt('InputData/ParamsSoil.csv', delimiter=',')
    
    #to give a name to each the soil params variable
    self.HH=self.ParamS[8] # Soil depth (mm)
    self.c1=self.ParamS[12] # Runoff coeffitients
    self.c2=self.ParamS[13]
    self.c3=self.ParamS[14]
    self.FC=scalar(self.ParamS[2]*self.HH/100) # Field capacity (%)
    self.SWC=scalar(self.ParamS[5]*self.HH/100) # initial soil water content (%)
    self.WP=scalar(self.ParamS[1]*self.HH/100) # wilting point (%)
    self.Poros=scalar(self.ParamS[4]*self.HH/100) # porosity (%)
    self.Km=self.ParamS[6] # min value of k factor
    self.Kx=self.ParamS[7] # max value of k factor
    self.CNdry=self.ParamS[15] # curve number under dry conditions
    self.CNwet=self.ParamS[16] # curve number under wet conditions
    self.slope=self.ParamS[17] # slope in m/m

    # to read the cover params table: throughfall and stemflow Coefficients
    self.CoefC=np.genfromtxt('InputData/ParamsCover.csv', delimiter=',')
    
    # to read the vegetation cover table(as fractions of 1)
    self.FractC=np.genfromtxt('InputData/CoverFract.csv', delimiter=',')
    
    self.Prtss = "InputData/Precipitation.tss" # Precipitation mm/day
    self.Etotss = "InputData/Eto.tss" # reference Evapotranspiration mm/day
    self.outlet = readmap("InputData/punto.map") # A pcraster map with one pixel
                                                #repesenting the Hydrobal plot
    self.PD=-1. # a counter
    self.PrPD=np.genfromtxt(self.preciptss, delimiter=' ')
    self.PrPD=self.PrPD[:,1]
    self.PrSPD=0.
    
    self.TimeStepInHours = 1.0 # time step in days

    # Output variable names
    self.PrStTss = TimeoutputTimeseries("resulttss/PrSt.tss", self, self.outlet,)
    self.netPrTss = TimeoutputTimeseries("resulttss/netPr.tss", self, self.outlet)
    self.RoffTss= TimeoutputTimeseries("resulttss/Roff.tss",self,self.outlet)
    self.EtoTss=TimeoutputTimeseries("resulttss/Eto.tss", self, self.outlet)
    self.EtaTss=TimeoutputTimeseries("resulttss/Eta.tss", self, self.outlet)
    self.SWCTss=TimeoutputTimeseries("resulttss/SWC.tss", self, self.outlet)
    self.KKTss=TimeoutputTimeseries("resulttss/KK.tss", self, self.outlet)
    self.DPTss=TimeoutputTimeseries("resulttss/DP.tss", self, self.outlet)

```

Table 6.7: The dynamic section of HydrobalPCR main script

```

def dynamic(self):
    # Reading the precipitation file and ET0 # mm/timestep
    self.Pr = spatial(timeinputscalar(self.Prtss,1)*self.TimeStepInHours)
    self.Eto = spatial(timeinputscalar(self.Etotss,1)*self.TimeStepInHours)
    # Net precipitation (mm)
    self.netPr=scalar(hpf.netPr(self.Pr, self.CoefC))
    # Interception (mm)
    self.Int = self.Pr-self.netPr
    # Runoff (mm) using the RunoffEq() or RunoffCN() equation
    self.Roff=scalar(ifthenelse(self.Roffp=1,
        hpfc.RoffEq(self.Pr, self.c1, self.c2, self.c3),
        hpfc.RoffCN(self.Pr5PD,self.CNwet,self.CNdry,self.slope,
        self.netPr)))

    # Infiltration (mm)
    self.Inf = ifthenelse(self.netPr>0,self.netPr-self.Roff,0)
    # k factor
    self.kk = scalar(hpf.kk(self.FC, self.WP, self.SWC, self.kkm, self.kkx))
    # Actual evapotranspiration (mm)
    self.Eta = scalar(hpf.Eta(self.WP, self.SWC, self.kk, self.Eto))

    # Deep percolation (mm)
    self.DP= scalar(hpf.DP(self.Inf, self.FC, self.WP, self.Pr, self.Pr5PD,
        self.Poros))

    # Updating the SWC value 1st time
    self.SWC = self.SWC+self.Inf-self.Eta-self.DP
    #slow Infiltration (mm)
    self.SI=scalar(hpf.SI(self.SWC, self.FC))
    # Updating the SWC value 2nd time
    self.SWC=self.SWC-self.SI
    # Updating the DP value 2nd time
    self.DP=self.DP+self.SI
    # Transforming SWC from mm to %
    self.SWC1 = self.SWC*100/self.HH
    # # Precipitation of the 5 previous days
    self.PD=scalar(self.PD+1.)
    self.Pr5PD=scalar(hpf.PrPD(self.PD,self.PrPD))
    #Outputs
    self.PrStTss.sample(self.Pr)
    self.netPrTss.sample(self.netPr)
    self.RoffTss.sample(self.Roff)
    self.EtaTss.sample(self.Eta)
    self.SWCTss.sample(self.SWC1)
    self.EtoTss.sample(self.Eto)
    self.KKTss.sample(self.KK)
    self.DPTss.sample(self.DP)

```

5.2.4. Actual evapotranspiration (Eta):

In HYDROBAL, Eta is calculated in function of Eto, SWC and the evaporative coefficient (k factor). The k factor in HYDROBAL expresses the transpiration rate capacity characteristic of each vegetation type, as a function of the plant cover and structure, and soil water availability (Bellot and Chirino, 2013). It is a dynamic factor that changes daily, ranging between a minimum value (kmin) for the driest days and a maximum (kmax) for the wettest days and it is calculated by the equation (9):

$$k(t)=k_{\max} \cdot SWCa_coef(t) \quad (9)$$

where $SWCa_coef(t)$ is the coefficient of soil water availability at time (t) which is function of SWC, field capacity (FC) and wilting point (WP) and is calculated by equation (10):

$$SWCa_coef(t) = 1 - \frac{FC - SWC(t)}{FC - WP} \quad (10)$$

The implementation of the function calculating the k factor each time step was done as in the equation (11)

$$k = hpf.kk(FC, WP, SWC, kmin, kmax) \quad (11)$$

Eta is the main water loss in the semi-arid soil-plant system and strongly determines the SWC, which is a critical variable for water availability to vegetation and the resulting degree of water stress (Bellot and Chirino, 2013). Eta is calculated in the same way as in HYDROBAL. Eta is determined from a combined modification of the Nizinski and Saugier (1989) and Specht (1972) equations, in which Eta is a fraction of Eto, and the forcing variables are the current value of the stored SWC and LAI, represented by the k factor evaporative coefficient (Equation 12). The calculation of Eta is implemented in HydrobalPCR as the function in equation (13) which takes as arguments SWC, Eto and k factor.

$$Eta(t) = Eto(t) * (1 - e^{(-k * SWC(t))}) \quad (12)$$

where t is time in days

$$Eta = hpf.Eta(SWC, kk, Eto) \quad (13)$$

5.2.5. Deep percolation (DP):

Based on field observations, many hydrologists suggest that some infiltration water percolates downwards before the soil's field capacity is reached (Samper, 1997). HydrobalPCR uses the equation (14) proposed by Samper (1997) to calculate the deep percolation and it is implemented in the model as the function in equation (15).

$$DP(t) = Inf(t) * \left(1 - e^{\left(-3 * \frac{SWC(t) - \left(\frac{2Ru}{3} + WP\right)}{Poros - \left(\frac{2Ru}{3} + WP\right)}\right)}\right) \quad (14)$$

where Ru is the usable reserve (FC-WP) and Poros is the soil porosity.

$$DP = hpf.DP(Inf, FC, WP, Pr, Pr5PD, Poros) \quad (15)$$

In a previous work, Moutahir et al., (Under review) showed that, in the province of Alicante, appreciable aquifer recharge occurs with rainfall events equal or greater than 20 mm day^{-1} . This threshold can be lowered to 10 mm day^{-1} depending on the rainfall of previous days which controls the state of the soil saturation. This was implemented in HydrobalPCR by allowing the DP only when the rainfall (Pr) of the current day is greater than 10mm or the rainfall (Pr5PD) of the 5 previous days is greater than 10 mm too. This function can be modified to use another threshold or none.

5.2.6. Slow infiltration (SI):

The SI occurs when the SWC is over the FC (Bellot and Chirino, 2013) and it is calculated by the equation (16) implemented in HydrobalPCR as the function in equation (17):

$$SI = SWC - FC \quad (16)$$

$$SI = hpf.SI(SWC, FC) \quad (17)$$

5.2.7. Reference evapotranspiration (Eto):

This function is not used directly in HydrobalPCR but it can be used to prepare the Eto input files. This function calculates the Eto according to Hargreaves and Samani (1982) method using temperature and solar radiation. The Eto function can be called from an external script that calculates the Eto and saves it in the PCRaster file format.

5.3. The run scripts

The annex 6.1 presents a quick start to the use of HydrobalPCR. In this quick start the directory structure of HydrobalPCR is described. In the zip file of HydrobalPCR there are two input data folders; one for the user and the other one used by the model. The run scripts read the input files in the user input folder and copy them to the model inputs folder and run the model the number of time we need. The multiple run script allows the iteration over large sets of data. The run scripts also organize the output data in a csv format file.

5.4. Model calibration and validation

HydrobalPCR uses k factor as a parameter of calibration. This operation is performed by the Automatic Model Optimization Reference Implementation framework (AMORI, 2009) by running the model multiple times with randomly selected k_{\min} and k_{\max} values within a range fixed previously. The adjustment of the k_{\min} and k_{\max} is done by means of Montecarlo simulations minimizing the root mean square error (RMSE) between the simulated and observed soil water content. The validation of the model is done by comparing the simulated and observed SWC data that was not used in the calibration step. The performance of the model was evaluated by calculating two indices:

- The Nash–Sutcliffe model efficiency (NSE) coefficient (Nash and Sutcliffe, 1970); equation (18):

$$NSE = 1 - \frac{\sum_{t=1}^T (\theta_o^t - \bar{\theta}_o)^2}{\sum_{t=1}^T (\theta_s^t - \bar{\theta}_o)^2} \quad (18)$$

where: $\bar{\theta}_o$ is the mean observed SWC, θ_o^t is the observed SWC at time t and θ_s^t is the simulated SWC at time t.

NSE can range from $-\infty$ to 1, with NSE =1 being the optimal value. Values between 0.0 and 1.0 are generally viewed as acceptable levels of performance (Moriasi et al., 2007).

- The RMSE-observations standard deviation ratio (RSR) developed by Moriasi et al. (2007). RSR is a model evaluation statistic which standardizes RMSE using the observations standard deviation; equation (19):

$$RSR = \frac{RMSE}{STDEV_o} = \frac{\sqrt{\sum_{t=1}^T (\theta_o^t - \theta_s^t)^2}}{\sqrt{\sum_{t=1}^T (\theta_o^t - \bar{\theta}_o)^2}} \quad (19)$$

Where: $STDEV_o$ is the observations standard deviation, $\bar{\theta}_o$ is the mean observed SWC, θ_o^t is the observed SWC at time t and θ_s^t is the simulated SWC at time t.

RSR can range from 0 to $+\infty$, with RSR =0 being the optimal value. Low values approaching 0 indicate good performance (Moriasi et al., 2007).

6. Application of HydrobalPCR

HydrobalPCR was used to evaluate the likely effects of climate change on water balance in two dominant vegetation covers in Alicante province. Forested class represents the pine forests dominated by *Pinus halepensis* with other accompanying species. Not forested class represents different shrubland communities dominated by a mixture of sclerophyllous vegetation with other accompanying species too. To evaluate the likely effects of climate change on the water balance in the study area we assumed that the vegetation cover is not going to change in the future.

To evaluate the expected changes in the water balance components under the climate change scenarios in the study area trend analysis was performed over the period 2010-2099. To study the trends a linear model was fitted to each time series using the least-squares regression method to derive the magnitude of trends while statistical significance was determined by Mann-Kendall (MK) test (Mann, 1945; Kendall, 1975). In addition to the trend analysis, we analyzed the changes in the mean between the two projected 30-year periods 2010-2039 and 2070-2099.

6.1. HydrobalPCR calibration and validation in the study area

In the study area, daily SWC observations over three hydrological years from October 2012 to September 2015 were used for the model calibration and validation. Data over two years were used for calibration and the third year for a post validation. Figure 6.3 represents multiple model runs (grey lines) and the simulation that represents the best fit with the observed data (thick line vs dashed line) in the forested area in Mela site. This operation is repeated for each vegetation type and site using the AMORI (2009)

framework minimizing the RMSE between the simulated and observed soil water content.

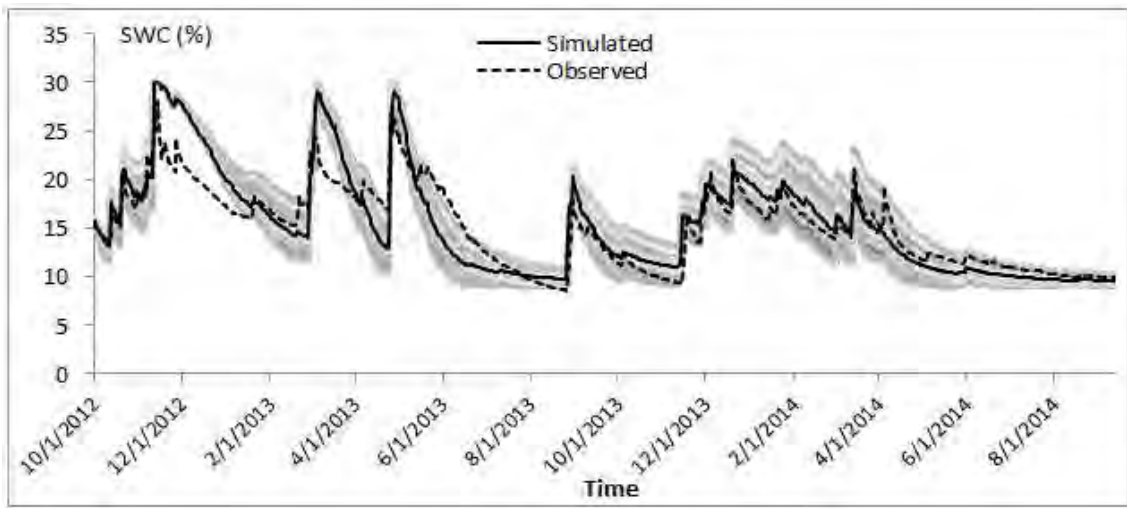


Figure 6.3: Adjustment of k factor in Mela site. Grey lines represent the SWC simulated running the model multiple times with randomly selected k factor sets. Thick line represents the best adjustment.

The simulated SWC over the period from October 2014 to September 2015 compared to observed SWC for the same period showed a good fit. Figure 6.4 shows an example of the fit observed between simulated and observed SWC in the forested area of Mela site. Despite differences observed in some peaks, the model showed good results. Table 6.8 shows the NSE and the RSR values between observed and simulated SWC in the four sites and the two vegetation types. NSE showed values between 0.34 and 0.70 in the four sites. These values are viewed as acceptable levels of performance (Moriasi et al., 2007) which indicates the acceptable performances of the model in the study area. RSR showed relatively low values in the four sites (between 0.56 and 0.95) indicating a lower RMSE and a better simulation performance.

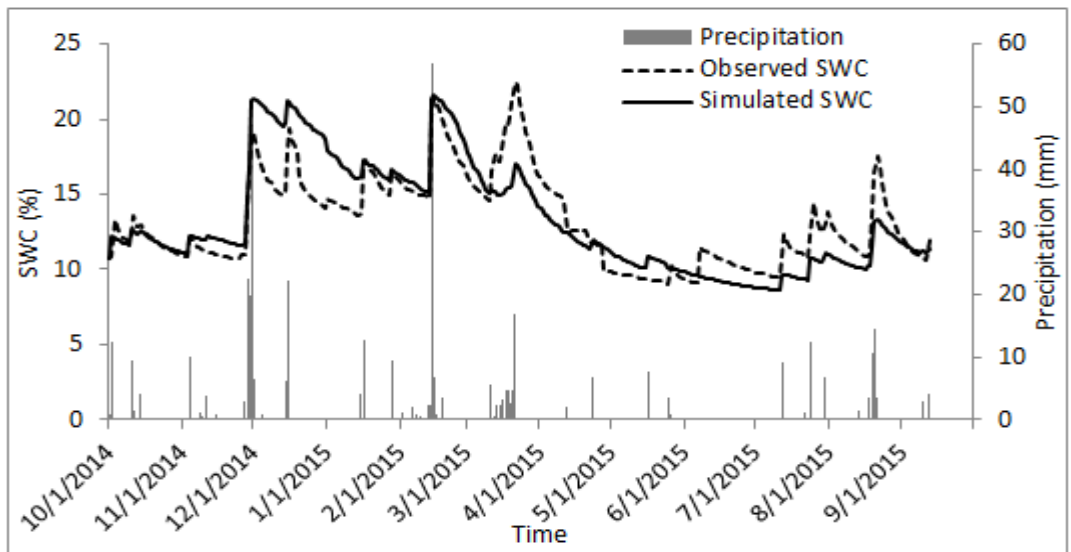


Figure 6.4: Model validation. Simulated SWC vs Observed SWC in forested areas in Mela Site over the period from October 2014 to September 2015.

Table 6.8: NSE and RSR coefficients and the selected k_{\min} and k_{\max} values in the four sites and two vegetation types.

Site	Vegetation type	Nash-Sutcliffe	RSR	Kmin	kmax
Ventós	Forested	0.68	0.57	0.007	0.03
	Not forested	0.53	0.62	0.004	0.09
Águilas	Forested	0.34	0.82	0.006	0.02
	Not forested	0.56	0.95	0.009	0.02
Cabeço	Forested	0.70	0.56	0.007	0.07
	Not forested	0.58	0.65	0.009	0.03
Mela	Forested	0.57	0.63	0.005	0.05
	Not forested	0.65	0.83	0.009	0.08

6.2. Projected trends in climate variables

According to the mean values from the nine CMIP5 models used, an increase in mean air temperature (T_m) and in reference evapotranspiration (Eto) is expected over the period 2010-2099 in the four sites under the two RCP scenarios while rainfall (Pr) is expected to decrease over the same projected period (Table 6.9, Annex 6.3: Figure 1 to 3). In the case of T_m and Eto , positive trends are expected under the two RCP scenarios and the nine models, however; rainfall showed negative trends in the majority of cases and positive trends in some CMIP5 models in the four sites (Annex 6.3: Table 1 to 3). Under the high climate scenario (RCP8.5), trends of increase in T_m and Eto are about two times higher than under the moderate scenario (RCP4.5). The higher increase in T_m and Eto are expected in Mela site under the RCP8.5 scenario ($+0.66^{\circ}\text{C}/\text{decade}$ and

+27.7 mm/decade respectively). The increase in Tm and Eto is expected to be accompanied by a decrease in rainfall in the four sites. The higher decrease is expected in Mela site under the RCP8.5 (-12 mm/decade). Tm and Eto showed significant trends at 5% level in the nine CMIP5 models and under the two RCP scenarios.

Table 6.9: Mean projected trends in Tm, Eto and Pr over the period 2010-2099 in the four sites. The mean, min and max change values per decade from nine CMIP5 models under two RCP scenarios.

		Tm (°C/decade)	Eto (mm/decade)	Pr (mm/decade)	
RCP4.5	Ventós	+0.25 (+0.17,+0.38)	+10.1 (+6.7,+15.6)	-0.3 (-4.4,+3.6)	
	Águilas	+0.27 (+0.19,+0.41)	+10.4 (+7.3,+15.7)	-2.3 (-6.1,+2.8)	
	Cabeço	+0.25 (+0.18,+0.38)	+10.3 (+7.2,+15.4)	-2.3 (-6.2,+0.7)	
	Mela	+0.28 (+0.19,+0.42)	+11.2 (+7.3,+17)	-7.8 (-14.6,-0.3)	
RCP8.5	Ventós	+0.58 (+0.46,+0.85)	+23.9 (+18.6,+35.2)	0.4 (-6.1,+5.3)	
	Águilas	+0.64 (+0.51,+0.91)	+25.4 (+19.5,+34.7)	-4.4 (-9.5,-0.6)	
	Cabeço	+0.58 (+0.46,+0.83)	+24.5 (+19.4,+33.4)	-3.4 (-7.9,+1.0)	
	Mela	+0.66 (+0.52,+0.92)	+27.7 (+20.9,+38.1)	-12.0 (-17.8,-4.5)	

6.3. Projected changes in the water balance

Changes in Pr and Tm are expected to affect the water balance in the study area. Table 6.10 shows the mean projected trends in HydrobalPCR outputs from nine CMIP5 models and under two RCP scenarios over the period 2010-2099 (more details of trends under each CMIP5 model are presented in Annex 6.4 and 6.5). Negative trends are expected in the different water balance components because of the increase in Eto and the decrease in Pr. Less water, as net rainfall (netPr), is expected to reach the soil. At the same time, the Eta is expected to decrease because of the decrease in the available soil water for plants. In fact, Eta, in absolute values, will decrease but it will increase as a percent of netPr (because of the increase in Eto) which will cause a reduction in deep percolation (DP) and soil water content (SWC).

The major decreases are expected in Mela site under the high RCP8.5 scenario (-8.2, -5.3, -2.9 mm/decade in netPr, Eta and DP respectively in the forested area and -10.3, -4.1, -6.2 mm/decade respectively in the not forested area). In this site and under the same RCP scenario, major reductions in SWC are also expected (-0.3 and -0.2 (%)/decade in forested and not forested areas respectively). This is due to the major reduction in Pr and major increase in Eto expected in the northern part of Alicante in

general. In the southern sites which are suffering water deficit under the current climate conditions, the changes are not important even if they present negative trends.

Table 6.10: Mean projected trends in the HydrobalPCR outputs over the period 2010-2099 under the two RCP scenarios, and the nine CMIP5 models in the forested and not forested areas in the four sites. Pr: Precipitation, netPr: Net rainfall, Eto: reference evapotranspiration, Eta: actual evapotranspiration DP: deep percolation, SWC: soil water content. All trends are expressed as mm/decade except SWC (%)/decade. * significant at 5%.

		Forested					Not forested				
		Pr	Eto	netPr	Eta	DP	SWC	netPr	Eta	DP	SWC
RCP 4.5	Ventós	-0.3	10.1*	-0.2	0.1	-0.4	-0.1	-0.3	0.1	-0.5	-0.1
	Águilas	-2.3	10.5*	-1.7	-1.8	-0.2	-0.1	-2.1	-1.8	-0.4	-0.1
	Cabeço	-2.3	10.3*	-1.8	-1.2	-0.7	-0.1	-1.8	-1.4	-0.5	-0.1
	Mela	-7.8	11.2*	-5.4	-2.8	-2.7	-0.2	-6.8	-1.7	-5.1	-0.1
RCP 8.5	Ventós	0.4	24.2*	0.3	0.5	-0.3	-0.1	0.4	0.6	-0.3	-0.1
	Águilas	-4.4	25.9*	-3.3	-3.3	-0.2	-0.2*	-3.9	-3.7	-0.4	-0.2*
	Cabeço	-3.4	24.8*	-2.8	-2.2	-0.7	-0.1*	-2.9	-2.5	-0.4	-0.2*
	Mela	-12	28.2*	-8.2	-5.3	-2.9	-0.3*	-10.3	-4.1	-6.2	-0.2*

To highlight the expected changes in the water balance in the study area by the end of 21st century we made a comparison between the first and the last projected 30-year periods (2010-2039 and 2070-2099 respectively). Tables in Annex 6.6 and 6.7 show the average water balance of the nine CMIP5 models under the two RCP scenarios in the four sites and the change between the two periods 2010-2039 and 2070-2099. Figure 6.5 shows the percentage of change in the model outputs in the 30-year period 2070-2099 with respect to the period 2010-2039. The major change in the last projected period with respect to the first period is expected in aquifer recharge (DP). A reduction of above 30% is expected for the two vegetation types in the four sites and under the two RCP scenarios except in the case of Ventós site. In this site, aquifer recharge is expected to suffer a reduction of above 20% under the RCP4.5 and less than 10% under the RCP8.5 scenario. In absolute values, aquifer recharge is expected to suffer an important reduction in Mela site for both vegetation types and above all in the not forested area (-31.2 and -40.3 mm under the RCP4.5 and RCP 8.5 scenarios respectively). In the forested area, the reduction expected will be of -15.6 and -18.6 mm under the RCP4.5 and RCP8.5 scenarios respectively. Aquifer recharge in not forested area will suffer higher reduction than in the forested one because of the high reduction of the netPr.

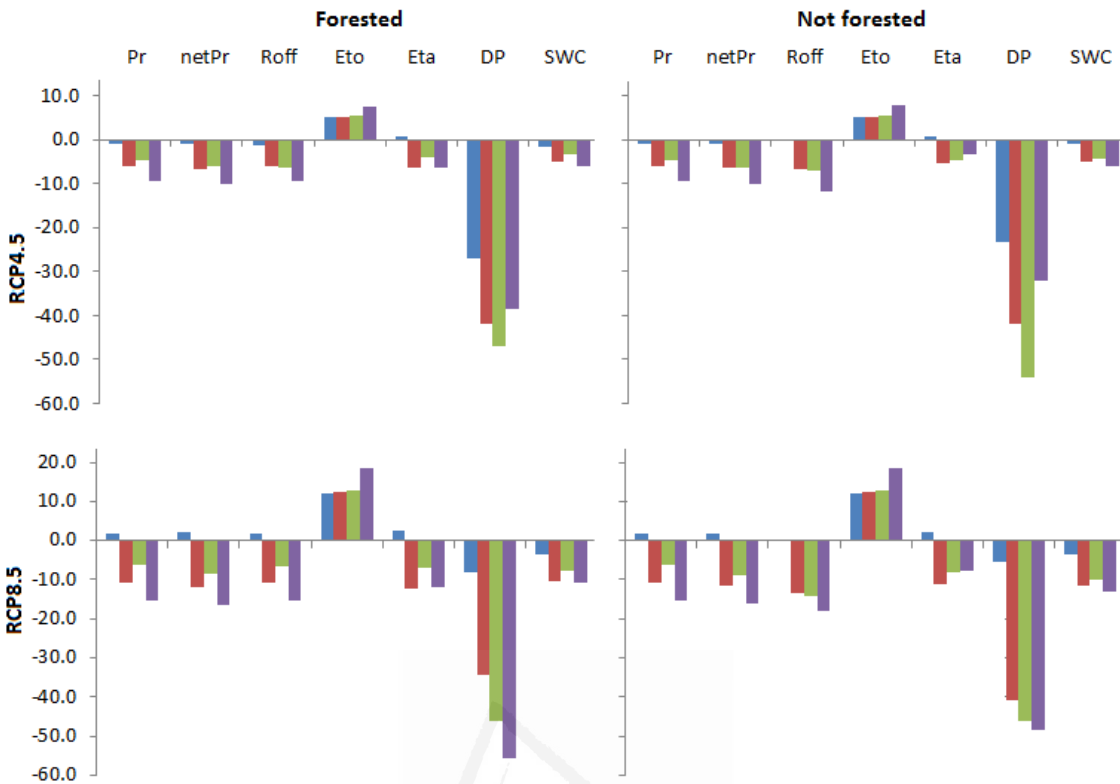


Figure 6.5: Percent of change in the model outputs in the 30-year period 2070-2099 with respect to the period 2010-2039 in the four sites and two vegetation types under the two RCP scenarios and nine CMIP5 models. Pr: Precipitation, netPr: Net rainfall, Eto: reference evapotranspiration, Eta: actual evapotranspiration DP: deep percolation, SWC: soil water content.

7. Discussion

In this work, we built a model based on HYDROBAL (Bellot and Chirino, 2013) using PCRaster-Python framework (van Deursen, 1995, Karssenberg and de Jong, 2005; PCRaster, 2016). The model calculates the water balance by simulating the main water flows at the plant-soil level and at a daily basis. This model is based on HYDROBAL which was used successfully in different studies (Bellot et al., 1998, Bellot et al., 2001, Bellot et al., 2005, Bellot and Chirino, 2013, Manrique-Alba et al., 2015a; 2015b; Ruiz-Yanetti et al., 2015; Touhami et al., 2013; 2014, 2015). However, when used to assess the effect of climate change on the water balance, Touhami et al., (2015) were forced to choose data from only one global climate model and a small number of years because HYDROBAL cannot handle large sets of data. The HydrobalPCR model overcomes this problem thanks to the possibilities that offers the Python programming language.

The use of environmental modelling frameworks based on higher level programming languages for model construction presents the advantage of not requiring expert knowledge in programming. Moreover, the use of a programming language allows a flexibility of adapting the model to use different sets of data and to communicate with other frameworks. In this work, we used the AMORI (2009) framework to calibrate our model which saved us the time of programming our own calibration tool. We used a random run to calibrate our model but the AMORI framework offers other techniques like the Genetic Algorithm Optimization or the Markov Simulations. The modeler can take advantage of the PCRaster-Python framework itself which was extended by data assimilation and optimization frameworks (Karssenberg et al., 2007; 2010) and tools allowing access to external model components (Schmitz et al., 2009).

HYDROBAL model was specifically developed to semiarid areas (Bellot and chirino, 2013). It has some similarities with other models used in semiarid regions like the semi-distributed hydrological model DREAM (Gigante et al., 2009 and Milella et al., 2012) and VisualBALAN model (Samper et al., 1999). HYDROBAL presents some advantages. It can be applied on several vegetation cover types with different structure and species composition. It uses few variables from soil and vegetation to determine the soil-water balance. Finally and more important, the vegetation factor is highly considered. HydrobalPCR inherits all these characteristics from HYDROBAL and benefits of the strengths of using PCRaster-Python framework to be extended by other software frameworks like the use of AMORI (2009) framework for calibration.

HydrobalPCR was successfully applied to the study area showing acceptable performances. The application of HydrobalPCR to four sites along a climate gradient allowed the appreciation of the differences in the effect of climate change on the water balance between the northern and southern sites. These differences are due to the differences in the changes in climate variables. This match with other studies in the province of Alicante which showed similar differences in climate variables trends between the northern half part of Alicante and its southern half part (Moutahir et al., 2014, Moutahir et al., under review). Differences in the effect of climate change on the water balance are also expected between different vegattion covers. Manrique-Alba et al., (2015b) also highlithed such differences and in ECOBAL Project (CGL2011-30531-

C02-01) final report authors suggested that pine forest and shrub can be a viable solution depending on the density and structure.

8. Conclusions

The evaluation of HydrobalPCR for two vegetation types in the study area showed acceptable results. HydrobalPCR was successfully used to assess the likely effects of climate change on water balance for two types of vegetation in four sites along a climate gradient in Alicante province. The model allowed the iteration over large set of daily climate data from nine CMIP5 models under two RCP scenarios over the period 2010-2099. This shows the advantage of using environmental modelling frameworks based on higher level programming languages for model construction with no expert knowledge in programming.

References

- Abdelli F., (1999). Análisis comparativo de distintas comunidades vegetales a la distribución del agua de lluvia, a la conservación del agua en el suelo y a la recarga de acuíferos en medios semiáridos. M.Sc. thesis dissertation, Instituto Agronómico Mediterráneo de Zaragoza (IAMZ). p. 160.
- Ajami, N. K., Duan, Q., & Sorooshian, S. (2007). An integrated hydrologic Bayesian multimodel combination framework: Confronting input, parameter, and model structural uncertainty in hydrologic prediction. *Water Resources Research*, 43(1).
- AMORI, Februari 2009. Automatic Model Optimization Reference Implementation. Available from: <http://sourceforge.net/projects/amori>
- Beeson, P. C., Martens, S. N., & Breshears, D. D. (2001). Simulating overland flow following wildfire: mapping vulnerability to landscape disturbance. *Hydrological Processes*, 15(15), 2917-2930.
- Bellot, J., & Escarre, A. (1998). Stemflow and throughfall determination in a resprouted Mediterranean holm-oak forest. In *Annales des sciences forestières* (Vol. 55, No. 7, pp. 847-865). EDP Sciences.
- Bellot, J., Sanchez, J. R., Chirino, E., Hernandez, N., Abdelli, F., & Martinez, J. M. (1999). Effect of different vegetation type cover on the soil water balance in semi-arid

areas of south eastern Spain. Physics and Chemistry of the Earth, Part B: Hydrology, Oceans and Atmosphere, 24(4), 353-357.

Bellot, J., Bonet, A., Sánchez, J.R., Chirino, E. (2001). Likely effects of land use changes on the runoff aquifer recharge in a semiarid landscape using a hydrological model. *Landscape Urban Plan.* 778, 1–13.

Bellot, J., Chirino, E., (2013). Hydrobal: An eco-hydrological modelling approach for assessing water balances in different vegetation types in semi-arid areas. *Ecological Modelling.* 266.

Blöschl, G., Reszler, C., & Komma, J. (2008). A spatially distributed flash flood forecasting model. *Environmental Modelling & Software,* 23(4), 464-478.

Chirino, E., (2003). Influencia de las precipitaciones y de la vegetación en el balance hídrico superficial y la recarga de acuíferos en clima semiárido. PhD Dissertation, Universidad de Alicante, Spain. <http://rua.ua.es/dspace/handle/10045/3386>.

Delgado, J., Llorens, P., Nord, G., Calder, I. R., & Gallart, F. (2010). Modelling the hydrological response of a Mediterranean medium-sized headwater basin subject to land cover change: the Cardener River basin (NE Spain). *Journal of Hydrology,* 383(1), 125-134.

Derouiche, A., (1996). Estimation et modelisation des composantes du bilan hidrique chez différentes firmatios arborees, arbustives et herbacees mediterraneennes. M.Sc. Thesis Dissertation, Instituto Agronómico Mediterráneo de Zaragoza (IAMZ), Departamento de Ecología. Universidad de Alicante. 158 pp.

Fuentes Yagüe, J., Cruz Roche, J., (1990). Curso elemental de riego. In: Ministerio de Agricultura, Pesca y Alimentación (eds), *Manuales de Capacitación.* Madrid, pp. 3- 21.

Gigante, V., Iacobellis, V., Manfreda, S., Milella, P., & Portoghesi, I. (2009). Influences of Leaf Area Index estimations on water balance modeling in a Mediterranean semi-arid basin. *Natural Hazards and Earth System Sciences,* 9(3), 979-991.

- Gracia, C. A., Tello, E., Sabaté, S., & Bellot, J. (1999). GOTILWA: An integrated model of water dynamics and forest growth. In *Ecology of Mediterranean evergreen oak forests* (pp. 163-179). Springer Berlin Heidelberg.
- Hargreaves, G.H. and Samani, Z.A., (1982). Estimating reference evapotranspiration. Tech. Note. *Journal of Irrigation and Drainage Engineering*, ASCE, 108 (3), 225–230.
- Huang, M., Gallichand, J., Wang, Z., & Goulet, M. (2006). A modification to the Soil Conservation Service curve number method for steep slopes in the Loess Plateau of China. *Hydrological processes*, 20(3), 579-589.
- Karssenberg, D. (2002). The value of environmental modelling languages for building distributed hydrological models. *Hydrological Processes*, 16(14), 2751-2766.
- Karssenberg, D., De Jong, K. (2005). Dynamic environmental modelling in GIS: 1. Modelling in three spatial dimensions. *International Journal of Geographical Information Science*, 19(5), 559-579.
- Karssenberg, D., de Jong, K., & Van Der Kwast, J. (2007). Modelling landscape dynamics with Python. *International Journal of Geographical Information Science*, 21(5), 483-495.
- Karssenberg, D., Schmitz, O., Salamon, P., de Jong, K., & Bierkens, M. F. (2010). A software framework for construction of process-based stochastic spatio-temporal models and data assimilation. *Environmental Modelling & Software*, 25(4), 489-502.
- Kendall, M.G., 1975. Rank Correlation Methods. Griffin, London, UK.
- Kraft, P., Vaché, K. B., Frede, H. G., & Breuer, L. (2011). CMF: a hydrological programming language extension for integrated catchment models. *Environmental modelling & software*, 26(6), 828-830.
- Kremer, R. G., & Running, S. W. (1996). Simulating seasonal soil water balance in contrasting semi-arid vegetation communities. *Ecological Modelling*, 84(1), 151-162.
- Mann, H.B., 1945. Nonparametric tests against trend. *Econometrica* 13 (3), 245–259.

Manrique-Alba, A., Ruiz-Yanetti, S., Moutahir, H., Novak, N., De Luis, M., Bellot, J., (under review). Soil moisture and its role in growth-climate relationships across an aridity gradient in semiarid *Pinus halepensis* forests. *Science of the Total Environment*.

Manrique-Alba, A., Ruiz-Yanetti, S., Chirino, E., Moutahir, H., González, C., & Bellot, J. (2015a). El balance hídrico en el suelo de 4 pinares (*Pinus halepensis*) de repoblación de la provincia de Alicante. *Cuadernos de la Sociedad Española de Ciencias Forestales*, (41), 183–194.

Manrique-Alba, A., Ruiz-Yanetti, S., Moutahir, H., Chirino, E., Lledó, MJ. and Bellot, J., (2015b). Role of afforestation on soil water balance in Mediterranean areas. In Breil, P., (Ed). *Measuring, Modeling and Managing of the natural processes related to water flows - Social values of the linked ecosystem services*. Book of abstracts of the international conference Ecohydrology, Lyon, France.

Martí, V. P., & Soto, M. D. S. (1994). Valores de torrecialidad R: su cálculo y distribución en la provincia de Alicante. *Cuadernos de geografía*, (56), 163-174.

MATLAB (2016). MATLAB product website, accessed 6/8/2016. Available from: URL: <http://www.mathworks.com/> (2005)

Milella, P., Bisantino, T., Gentile, F., Iacobellis, V., & Liuzzi, G. T. (2012). Diagnostic analysis of distributed input and parameter datasets in Mediterranean basin streamflow modeling. *Journal of hydrology*, 472, 262-276.

Monjo, R., Gaitán, E., Pórtoles, J., Ribalaygua, J., Torres, L., (2015). Changes in extreme precipitation over Spain using statistical downscaling of CMIP5 projections. *International Journal of Climatology*.

Moradkhani, H., Sorooshian, S., Gupta, H. V., & Houser, P. R. (2005). Dual state-parameter estimation of hydrological models using ensemble Kalman filter. *Advances in Water Resources*, 28(2), 135-147.

Moriasi, D. N., Arnold, J. G., Van Liew, M. W., Bingner, R. L., Harmel, R. D., & Veith, T. L. (2007). Model evaluation guidelines for systematic quantification of accuracy in watershed simulations. *Transactions of the ASABE*, 50(3), 885-900.

Moutahir, H., De Luis, M., Serrano-Notivoli, R., Touhami, I., Bellot, J., (2014). Análisis de los eventos climáticos extremos en la provincia de Alicante, Sureste de España. En: Fernández-Montes, S. y Rodrigo, F.S. (Eds). Cambio climático y cambio global. Publicaciones de la Asociación Española de Climatología (AEC). Serie A, nº9. Almería. ISBN: 978-84-16027-69-9. pp. 457-466.

Moutahir, H., Bellot, J., Monjo, R., Bellot, P., Garcia, M., Touhami, I., (under review). Likely effects of climate change on groundwater availability in a Mediterranean region of Southeastern Spain. *Hydrological Processes*.

Nash, J. E., & Sutcliffe, J. V. (1970). River flow forecasting through conceptual models part I—A discussion of principles. *Journal of hydrology*, 10(3), 282-290.

Nizinski, J., & Saugier, B. (1989). A model of transpiration and soil-water balance for a mature oak forest. *Agricultural and forest meteorology*, 47(1), 1-17.

PCRaster (2016). PCRaster Environmental Modelling Language, accessed 5/24/2016. Available from: <http://pcraster.geo.uu.nl/>

Pullar, D. (2004). SimuMap: a computational system for spatial modelling. *Environmental Modelling & Software*, 19(3), 235-243.

Python (2016). Python Programming Language, accessed 5/24/2016. Available from: <http://www.python.org>.

Ruiz-Yanetti, S., Manrique-Alba, A., Moutahir, H., Chirino, E., Lledó, MJ., Maturano, A. and Bellot, J. (2015). Soil water conservation and deep percolation in Mediterranean shrublands in a climatic gradient of southeast Spain. In Breil, P., (Ed). Measuring, Modeling and Managing of the natural processes related to water flows - Social values of the linked ecosystem services. Book of abstracts of the international conference Ecohydrology, Lyon. France.

Reed, M., Cuddy, S. M., & Rizzoli, A. E. (1999). A framework for modelling multiple resource management issues—an open modelling approach. *Environmental Modelling & Software*, 14(6), 503-509.

Samper, J. (1997). Métodos de evaluación de la recarga por la lluvia por balance de agua: utilización, calibración y errores. *La Evaluación de la Recarga a los Acuíferos en*

la Planificación Hidrológica. Seminario de la AIH-GE-Instituto Tecnológico Geominero de España. Madrid, 41-79.

Samper, J., Huguet, L., Ares, J., García-Vera, M.A., (1999). Manual del usuario del programa VISUAL BALAN v.1.0: Código interactivo para la realización de balances hidrológicos y la estimación de la recarga (VISUAL BALAN v1.0 user manual: an Interactive code for water balance and recharge estimation). Technical Publication ENRESA, Madrid (in Spanish). 1999.

Schmitz, O., Karssenberg, D., van Deursen, W. P., & Wesseling, C. G. (2009). Linking external components to a spatio-temporal modelling framework: coupling MODFLOW and PCRaster. Environmental Modelling & Software, 24(9), 1088-1099.

SCS. (1972). Soil Conservation Service National Engineering Handbook , Section 4. Hydrology, Soil Conservation Service, US Department of Agriculture:Washington, DC.

Sood, A., & Smakhtin, V. (2015). Global hydrological models: a review. Hydrological Sciences Journal, 60(4), 549-565.

Specht, R. L. (1972). Water use by perennial evergreen plant communities in Australia and Papua New Guinea. Australian Journal of Botany, 20(3), 273-299.

Taylor, K.E., Stouffer, R.J., Meehl, G.A., (2009). A summary of the CMIP5 experiment design. PCMDI Rep. http://cmip-pcmdi.llnl.gov/cmip5/docs/Taylor_CMIP5_design.pdf (accessed 10th April 2015).

Touhami, I., Andreu, J.M., Chirino, E., Sánchez, J.R., Moutahir, H., Pulido-Bosch, A., Martínez-Santos, P., Bellot, J. (2013). Recharge estimation of a small karstic aquifer in a semiarid Mediterranean region (southeastern Spain) using a hydrological model. Hydrological Processes. 27(2), 165-174.

Touhami, I., Andreu, J. M., Chirino, E., Sánchez, J. R., Pulido-Bosch, A., Martínez-Santos, P., Moutahir, H., & Bellot, J. (2014). Comparative performance of soil water balance models in computing semi-arid aquifer recharge. Hydrological Sciences Journal, 59(1), 193-203.

Touhami, I., Chirino, E., Andreu, J.M., Sánchez, J.R., Moutahir, H., Bellot, J. (2015). Assessment of climate change impacts on soil water balance and aquifer recharge in a semiarid region in south east Spain. *Journal of Hydrology*. 527, 619-629.

USDA (1986). Urban hydrology for small watersheds. Technical release, 55, 2-6.

Van Deursen W.P.A. 1995. Geographical Information Systems and Dynamic Models. Ph.D. thesis, Utrecht University, NGS Publication 190, 198 pp. Electronically available through www.carthago.nl



Annex 6.1: HydrobalPCR - Quick start

Moutahir H. and Bellot J., 2016

Requirements

HydrobalPCR for the moment only can be used on Windows but with little modifications can be used on Linux

PCRaster-Python framework can be downloaded from <http://pcraster.geo.uu.nl/>

To run PCRaster Python models you need Python 2.7 (for Windows 32 or 64-bit) and the corresponding NumPy 1.8 package.

HydrobalPCR needs other Python packages. You need to install them or to install a Python environment that comes with the needed packages (we suggest to install [winPython](#)).

A quick installation guide for PCRaster and Python can be found in
<http://pcraster.geo.uu.nl/getting-started/pcraster-on-windows/>

An important step to finish the PCRaster installation is the update of the *PATH* and the *PYTHONPATH environment variable* with the path of the *bin* and *python* directories of the extracted PCRaster package to the Variable value field.

HydrobalPCR in Action

- Unzip HydrobalPCR.zip into your home directory
- Open the python environment by double click on Spyder (in your winPython directory)
- Open the *SimpleRunScript.py* script and execute it to run HydrobalPCR with the example data.
- To run the HydrobalPCR for several times you need to modify the *MultipleRunScript.py* with your own data.

Directory Structure

The HydrobalPCR zip contains:

- 1-The main HydrobalPCR script (*HydrobalPCRmain.py*) which calls different functions and organizes the water balance calculation.
- 2-The *HydrobalPCRfunctions.py* script which contains the functions calculating the different water balance components.
- 3-The *simpleRunScript.py* script which runs HydrobalPCR one time and organizes the outputs in a csv file.

- 4-The *MultipleRunScript.py* script which runs HydrobalPCR multiple times and organizes the outputs in a csv file.
- 5-The *InputData* folder that contains the input files to HydrobalPCR. Users should not make any change in this folder.
- 6- The *InputData_User* folder where users should put their input data consisting in Precipitation, Eto, Vegetation Params, Vegetation cover and Soil Params.
- 7-The *Resultss* folder where are saved the output time series of: Pr.tss : Precipitation, netPr.tss: Net rainfall, Eto.tss: reference evapotranspiration , Eta.tss: actual evapotranspiration, DP.tss: deep percolation, SWC.tss: soil water content, kk.tss: k factor and RunOff.tss: Run off.

Running HydrobalPCR one time

-Open the *SimpleRunScript.py* script with Spyder or with any Python environment.

-Modify the next lines if necessary:

1) Change the word 'Pine' to your vegetation type

`VegType='Pine'`

2) Change the word 'Con' to the name of your site

`Zone='Con'`

3) Put the name of the Precipitation file without the ".tss" format

`PrecFile='Precip_2012_2014_Con'`

4) Put the name of the Eto file without the ".tss" format

`EToFile='Eto_2012_2014_Con'`

5) Put the number of time steps (in this case in days)

`NTS=730`

6) Change the name of the output file (in this case it will be

"Outputs_VegType_Zone_date.csv") but if you want you can change it to a given name by modifying the next line to `OutputFilee='Output_your_name.csv'`
`OutputFilee=".join(['Outputs_',VegType,'_',Zone,'_',datee,'.csv'])"`

-Execute the script and visualize the results (a csv file will be saved to your working directory)

Annex 6.2: Vegetation structure in the study area.

Abbreviations represent different plant species: Em: *Erica multiflora*, Pl: *Pistacia lentiscus*, Ro: *Rosmarinus officinalis*, St (Alpha_grass): *Stipa tenacissima*, Ph (Pine): *Pinus halepensis*, Jo: *Juniperus oxycedrus*, Qc: *Quercus coccifera*, Tv: *Thymus vulgaris*.

Table 1: Vegetation structure and cover (%) in Pine (forested) areas in the four sites. Nine classes + bare soil were differentiated (Grey cells). In some classes, different sub-classes were differentiated.

Ventós		Águilas		Cabeço		Mela	
Class	Cover (%)						
Grass	6.67	Grass	17.14	Grass	0.95	Grass	4.76
Alpha_Grass	3.81	Alpha_Grass	0.48	Alpha_Grass	12.38	Shrub	5.24
Shrub	21.90	Shrub	5.71	Shrub	14.29	Jo	2.86
Ro	10.95	Pl	3.81	Ro	7.14	Ro	1.90
Pl	5.71	Jo	0.95	Pl	7.14	Pl	0.48
Em	5.24	Ro	0.48	Shrub+Grass	3.33	Shrub+Grass	2.38
Shrub+Grass	11.43	Em	0.48	Ro+Grass	2.38	Ro+Grass	2.38
Em+Grass	5.71	Shrub+Grass	5.24	Pl+Grass	0.95	Pine	36.19
Ro+Grass	4.76	Pl+Grass	3.81	Pine	17.14	Pine+Grass	20.95
Pl+Grass	0.95	Ro+Grass	0.48	Pine+Grass	10.00	Pine+Shrub	20.48
Pine	7.14	Em+Grass	0.48	Pine+Alpha_Grass	11.43	Ph+Jo	9.52
Pine+Grass	14.29	Jo+Grass	0.48	Pine+Shrub	10.48	Ph+Ro	4.76
Pine+Alpha_Grass	0.48	Pine	11.90	Ph+Ro	5.24	Ph+Em	2.38
Pine+Shrub	10.95	Pine+Grass	35.71	Ph+Pl	4.29	Ph+Pl	2.38
Ph+Pl	6.19	Pine+Alpha_Grass	2.86	Ph+Qc	0.95	Ph+Qc	0.95
Ph+Ro	3.33	Pine+Shrub	3.33	Pine+Shrub+Grass	6.67	Ph+Tv	0.48
Ph+Em	1.43	Ph+Pl	2.38	Ph+Pl+Grass	5.24	Pine+Shrub+Grass	7.62
Pine+Shrub+Grass	16.67	Ph+Em	0.48	Ph+Ro+Grass	0.95	Ph+Pl+Grass	2.86
Ph+Pl+Grass	11.90	Ph+Jo	0.48	Ph+Qc+Grass	0.48	Ph+Ro+Grass	1.90
Ph+Ro+Grass	7.86	Pine+Shrub+Grass	6.67	Total (vegetated)	86.67	Ph+Jo+Grass	1.90
Ph+Em+Grass	1.43	Ph+Pl+Grass	5.24	Bare Soil	13.33	Ph+Tv+Grass	0.48
Ph+Jo+Grass	0.48	Ph+Em+Grass	0.95			Ph+Em+Grass	0.48
Total (vegetated)	93.33	Ph+Ro+Grass	0.48			Total (vegetated)	97.62
Bare Soil	6.67	Total (vegetated)	89.05			Bare Soil	2.38
		Bare Soil	10.95				

Table 2: Vegetation structure and cover (%) in shrub (not forested) areas in the four sites. Four classes + bare soil were differentiated (Grey cells). In some classes, different sub-classes were differentiated

Ventós		Águilas		Cabeço		Mela	
Class	Cover (%)						
Grass	6.19	Grass	22.38	Grass	22.38	Grass	18.57
Alpha_Grass	23.81	Shrub	23.33	Alpha_Grass	7.14	Shrub	17.14
Shrub	15.24	Em	15.71	Shrub	12.38	Ro	6.19
Qc	5.71	Pl	7.14	Pl	10.00	Jo	3.33
Em	5.24	Jo	0.48	Em	1.43	Pl	2.86
Pl	7.38	Shrub+Grass	23.33	Qc	0.95	Qc	1.90
Tv	1.43	Em+Grass	12.86	Shrub+Grass	49.52	Em	1.90
Ro	0.48	Pl+Grass	8.57	Qc+Grass	20.95	Tv	0.95
Shrub+Grass	12.38	Tv+Grass	0.48	Pl+Grass	10.95	Shrub+Grass	48.57
Qc+Grass	8.10	Jo+Grass	0.48	Ro+Grass	10.00	Pl+Grass	18.57
Em+Grass	2.86	Ro+Grass	0.95	Em+Grass	6.19	Ro+Grass	11.90
Tv+Grass	0.95	Total (vegetated)	69.05	Tv+Grass	0.95	Jo+Grass	8.57
Pl+Grass	0.48	Bare Soil	30.95	Jo+Grass	0.48	Tv+Grass	3.81
Ro+Grass	0.00			Total (vegetated)	91.43	Em+Grass	2.86
Total (vegetated)	57.62			Bare Soil	8.57	Qc+Grass	2.86
Bare Soil	42.38					Total (vegetated)	84.29
						Bare Soil	15.71

Annex 6.3: Projected trends in mean air temperature (Tm), reference evapotranspiration (Eto) and rainfall (Pr) over the period 2006-2099 in the four sites.

Table 1: Mean Tm increment °C/decade over the period 2006-2099 in the four sites. Nine CMIP5 models and two RCP scenarios.

CMIP5 models	RCP4.5				RCP8.5			
	Ventós	Aguilas	Cabeço	Mela	Ventós	Aguilas	Cabeço	Mela
BCC-CSM1-1	0.17	0.2	0.18	0.19	0.46	0.51	0.46	0.53
CanESM2	0.25	0.27	0.25	0.3	0.68	0.75	0.67	0.79
CNRM-CM5	0.18	0.19	0.18	0.2	0.49	0.53	0.48	0.53
GFDL-ESM2M	0.19	0.2	0.18	0.2	0.47	0.51	0.46	0.52
HADGEM2-CC	0.38	0.4	0.38	0.42	0.85	0.88	0.83	0.92
MIROC-ESM-CHEM	0.37	0.41	0.35	0.39	0.79	0.91	0.79	0.9
MPI-ESM-MR	0.19	0.21	0.2	0.23	0.54	0.6	0.54	0.63
MRI-CGCM3	0.25	0.27	0.25	0.27	0.49	0.52	0.5	0.54
NorESM1	0.26	0.28	0.27	0.29	0.49	0.55	0.5	0.56
Average	0.25	0.27	0.25	0.28	0.58	0.64	0.58	0.66

Table 2: Mean Eto increment mm/decade over the period 2006-2099 in the four sites. Nine CMIP5 models and two RCP scenarios.

CMIP5 models	RCP4.5				RCP8.5			
	Ventós	Aguilas	Cabeço	Mela	Ventós	Aguilas	Cabeço	Mela
BCC-CSM1-1	6.7	7.4	7.2	7.3	18.6	20.5	19.4	21.9
CanESM2	10	10.8	10.9	12.4	28.1	31.9	29.8	35.7
CNRM-CM5	7.2	7.3	7.8	7.8	20.7	20.6	20.8	22.1
GFDL-ESM2M	8.7	8.4	7.7	8.8	21.2	21.5	20.2	23.9
HADGEM2-CC	15.6	15.7	15.4	17	35.2	34.7	32.8	38
MIROC-ESM-CHEM	14.4	13.9	14.3	15.6	31.2	33	33.4	38.1
MPI-ESM-MR	8.5	9.7	8.9	10.6	21.3	24.3	23.6	26
MRI-CGCM3	9.8	10	10.1	10.8	18.8	19.5	20.4	20.9
NorESM1	9.8	10.6	10.2	10.6	20.2	22.4	20	22.9
Average	10.1	10.4	10.3	11.2	23.9	25.4	24.5	27.7

Table 3: Mean Pr change mm/decade over the period 2006-2099 in the four sites. Nine CMIP5 models and two RCP scenarios.

CMIP5 models	RCP4.5				RCP8.5			
	Ventós	Aguilas	Cabeço	Mela	Ventós	Aguilas	Cabeço	Mela
BCC-CSM1-1	-2.1	-4.5	-2.3	-7.2	-1.6	-7.6	-7.9	-16
CanESM2	-0.01	-1.1	+0.2	-8.1	-6.1	-7.6	-6.8	-16.3
CNRM-CM5	+3.4	-1.5	-1.1	-7.6	+0.7	-5.8	-5.6	-15.9
GFDL-ESM2M	+3.6	+2.8	+0.7	-0.3	+5.3	-2.7	-0.3	-5.7
HADGEM2-CC	-2.7	-6.1	-6.2	-14.1	-4.6	-9.5	-4.8	-17.8
MIROC-ESM-CHEM	+0.1	-2.8	-3.7	-10.5	+2.9	-1.7	-1.5	-9.9
MPI-ESM-MR	-1.7	-1.8	-3.6	-4.0	+1.7	-1.0	-1.1	-4.5
MRI-CGCM3	-4.4	-4.9	-5.0	-14.6	+4.7	-0.6	+1.0	-5.3
NorESM1	+0.6	-0.7	+0.6	-4.0	+0.6	-2.8	-3.5	-16.2
Average	-0.3	-2.3	-2.3	-7.8	+0.4	-4.4	-3.4	-12

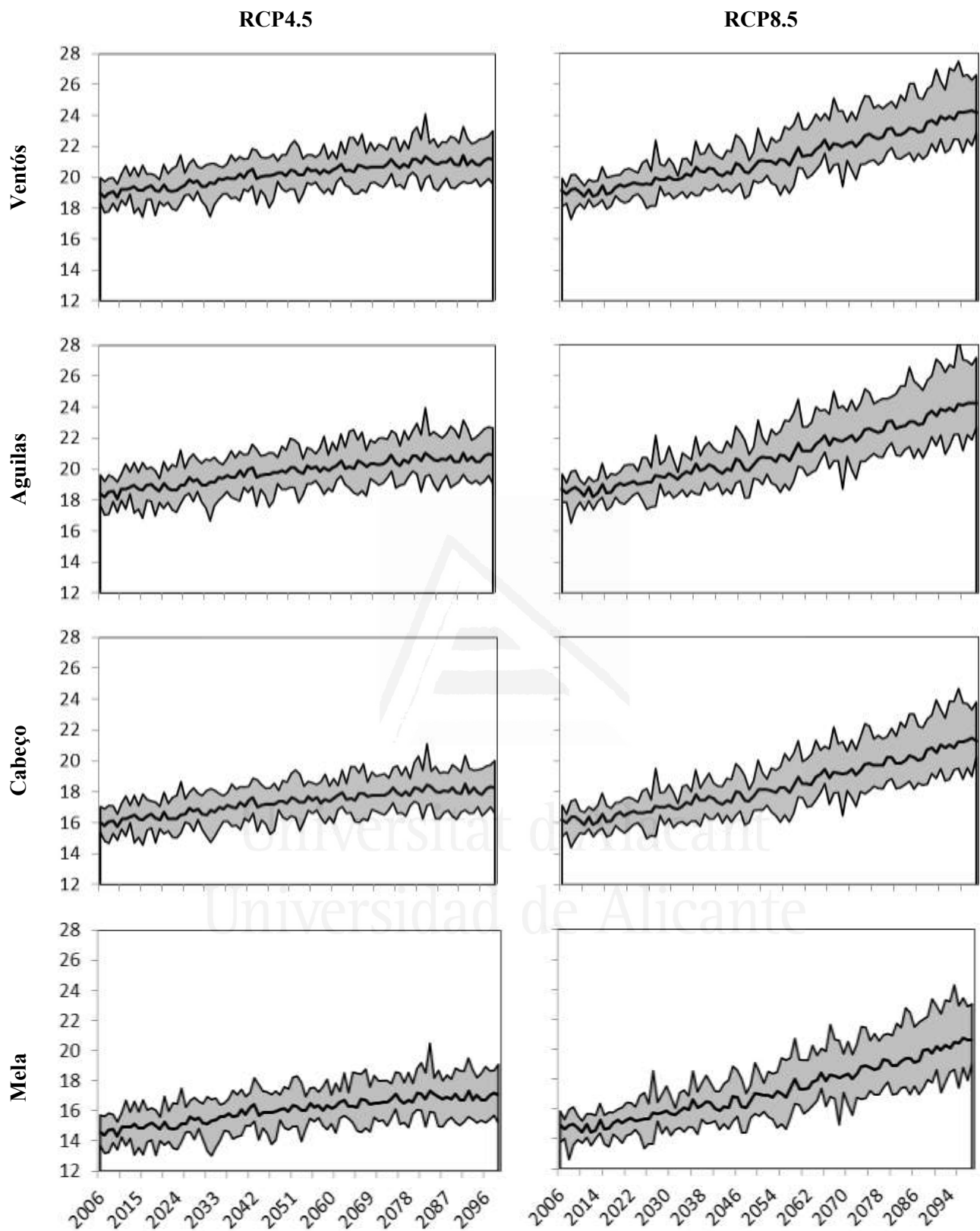


Fig.1: Projected evolution of mean air temperatures ($^{\circ}\text{C}$) under the two RCP scenarios in the four sites in the period 2006-2099. Temperature time series (Thick lines) are averages of the nine projections from nine CMIP5 models. Thin lines represent the maximum and minimum of the nine CMIP5 models. X axis represents T_m ($^{\circ}\text{C}$) and Y axis represents time (years).

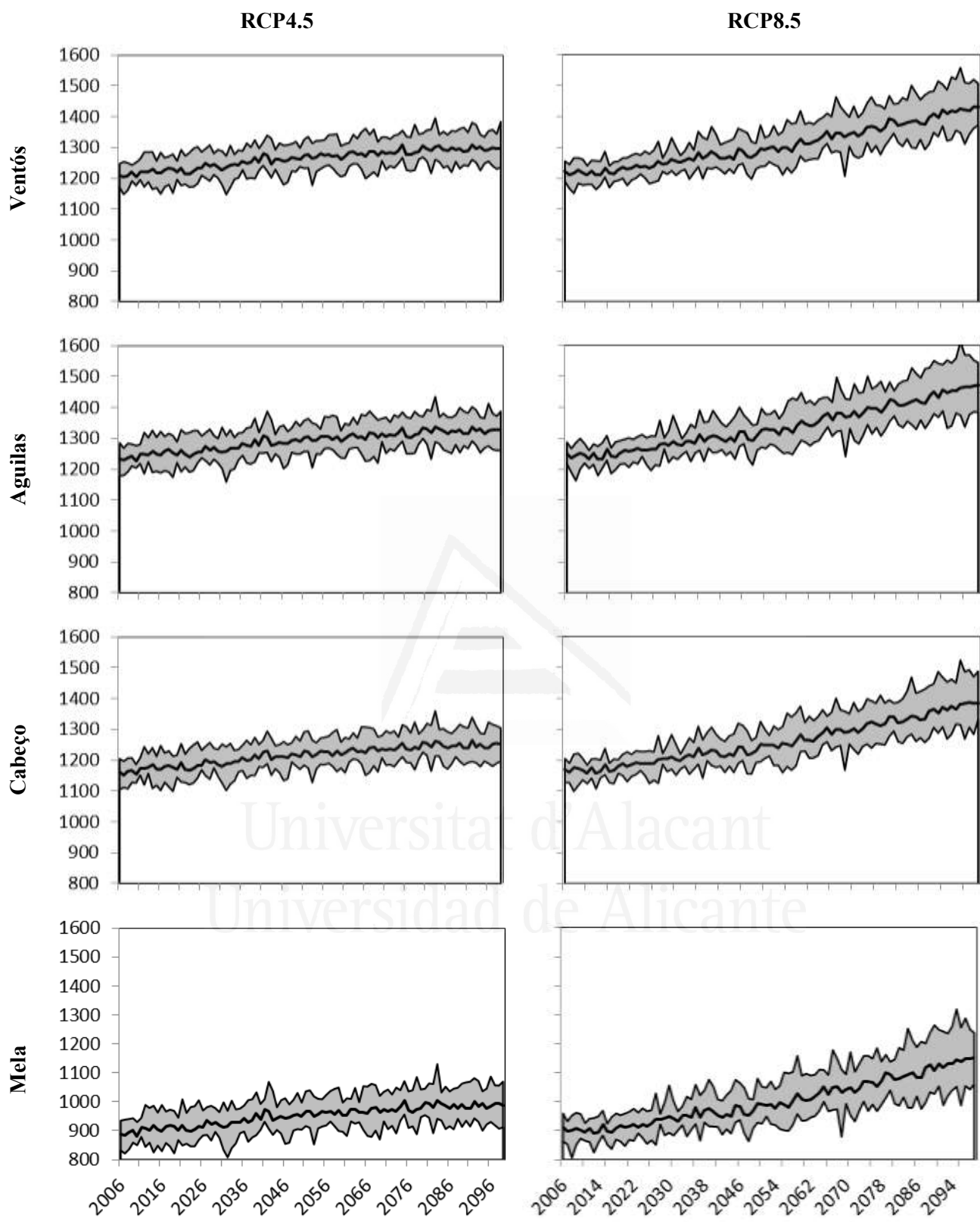


Fig.2: Projected evolution of Eto (mm) under the two RCP scenarios in the four sites in the period 2006-2099. Eto time series (Thick lines) are averages of the nine projections from nine CMIP5 models. Thin lines represent the maximum and minimum of the nine CMIP5 models. X axis represents Eto (mm) and Y axis represents time (years).

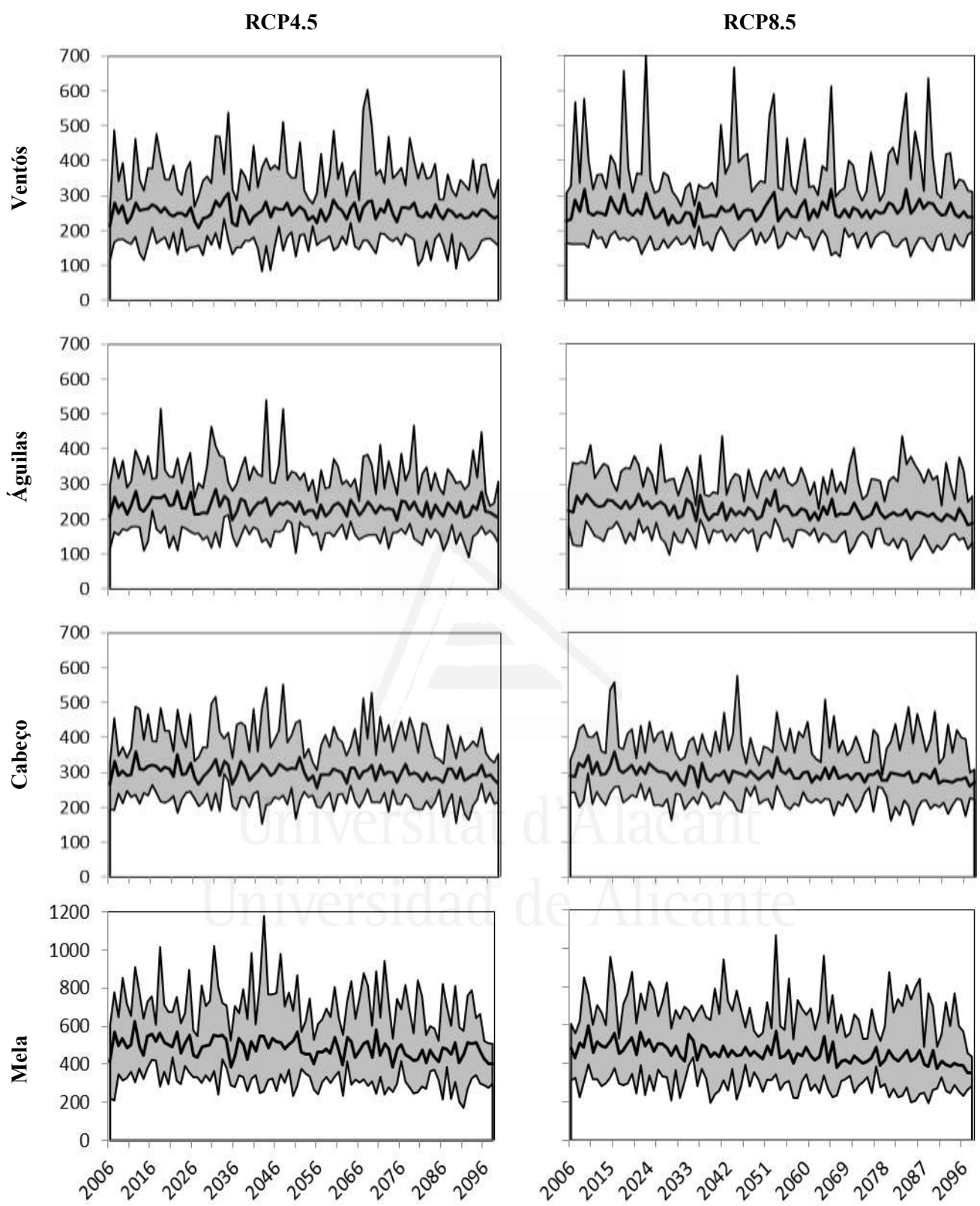


Fig.3: Projected evolution of Pr (mm) under the two RCP scenarios in the four sites in the period 2006-2099. Pr time series (Thick lines) are averages of the nine projections from nine CMIP5 models. Thin lines represent the maximum and minimum of the nine CMIP5 models. X axis represents Pr (mm) and Y axis represents time (years).

Annex 6.4: Projected trends in the HydrobalPCR outputs over the period 2010-2099 under the two RCP scenarios, and the nine CMIP5 models in the forested areas in the four sites. Pr: Precipitation, netPr: Net rainfall, Eto: reference evapotranspiration, Eta: actual evapotranspiration DP: deep percolation, SWC: soil water content. All trends are expressed as mm/decade except SWC (%)/decade. * significant at 5%.

Ventós		RCP4.5						RCP8.5					
		Pr	netPr	Eto	Eta	DP	SWC	Pr	netPr	Eto	Eta	DP	SWC
BCC-CSM1-1		-2.1	-1.6	6.5*	-0.8	-0.8	-0.1	-1.6	-1	19*	-1.4	0.4	-0.1*
CanESM2		-	-	10.1*	-0.4	0.3	-	-6.1*	-4.7*	28.5*	-2.9*	-2	-0.1*
CNRM-CM5		3.4	2.6	7.4*	1.8	0.6	-	0.7	0.9	21*	0.4	0.4	-0.1*
GFDL-ESM2M		3.6	3	8.7*	1.6	1.4	-	5.3*	4.2*	21.3*	2.6*	1.4	-
HADGEM2-CC		-2.7	-1.9	15.5*	-1.9	-0.2	-0.1*	-4.6	-3.7*	35.7*	-2	-1.9	-0.1*
MIROC-ESM		0.1	0.2	14.3*	1	-0.8	-0.1	2.9	2.1	31.5*	3.2*	-1.2*	-
MPI-ESM-MR		-1.7	-1.1	8.3*	-0.3	-0.9	-	1.7	1.5	21.6*	1.1	0.2	-0.1
MRI-CGCM3		-4.4	-3.3	10.1*	-1.4	-2	-0.1*	4.7	3.4	19*	1.4	1.8	-
NorESM1		0.6	0.2	10*	1.5	-1.4	-	0.6	0.4	20.6*	1.8	-1.5	-0.1*
Average		-0.3	-0.2	10.1*	0.1	-0.4	-	0.4	0.3	24.2*	0.5	-0.3	-0.1
Águilas		RCP4.5						RCP8.5					
		Pr	netPr	Eto	Eta	DP	SWC	Pr	netPr	Eto	Eta	DP	SWC
BCC-CSM1-1		-4.5	-3.5	7.3*	-3	-0.7	-0.1	-7.6*	-5.8*	21.1*	-5.7*	-0.3	-0.2*
CanESM2		-1.1	-0.9	10.9*	-0.6	-0.5	-	-7.6*	-5.7*	32.4*	-5.4*	-0.5*	-0.2*
CNRM-CM5		-1.5	-1.2	7.6*	-1.2	-0.3	-0.1	-5.8*	-4.2*	21*	-3.8*	-0.6	-0.2*
GFDL-ESM2M		2.8	2.3	8.5*	1.1	0.9	-	-2.7	-1.9	21.7*	-2.2	0.1	-0.1*
HADGEM2-CC		-6.1*	-4.6*	15.6*	-4.8*	-0.2	-0.2*	-9.5*	-7.1*	35.5*	-6.5*	-0.8*	-0.2*
MIROC-ESM		-2.8	-2.4	13.9*	-2.3	-0.4	-0.1*	-1.7	-1.2	33.8*	-1.7	0.1	-0.1*
MPI-ESM-MR		-1.8	-1.1	9.5*	-1.3	-0.1	-	-1	-0.5	24.8*	-1.2	0.3	-0.1*
MRI-CGCM3		-4.9*	-3.7*	10.3*	-3*	-0.8	-0.1*	-0.7	-0.5	19.8*	-1.1	0.4	-0.1*
NorESM1		-0.7	-0.7	10.8*	-1	0.1	-0.1	-2.8	-2.4	23*	-2.1	-0.6	-0.1*
Average		-2.3	-1.7	10.5*	-1.8	-0.2	-0.1	-4.4	-3.3	25.9*	-3.3	-0.2	-0.2*
Cabeço		RCP4.5						RCP8.5					
		Pr	netPr	Eto	Eta	DP	SWC	Pr	netPr	Eto	Eta	DP	SWC
BCC-CSM1-1		-2.3	-1.9	7.1*	-1.2	-0.8	-	-7.9*	-6*	19.9*	-4.8*	-1.2	-0.1*
CanESM2		0.2	-0.3	10.9*	-0.5	-	-	-6.8*	-5.3*	30.1*	-3.8*	-1.7*	-0.1*
CNRM-CM5		-1.1	-1	8*	-0.6	-0.6	-0.1*	-5.6*	-4*	21*	-2.9*	-1.2*	-0.1*
GFDL-ESM2M		0.8	0.7	7.8*	0.2	0.3	-	-0.3	-0.3	20.3*	-0.7	0.3	-0.1*
HADGEM2-CC		-6.2*	-4.6*	15.3*	-3.7*	-1	-0.1*	-4.8*	-3.8*	33.5*	-3.2*	-0.7	-0.1*
MIROC-ESM		-3.7*	-3.1*	14.3*	-1.5	-1.8*	-0.1*	-1.5	-1.8	33.6*	-0.8	-1.1*	-0.1*
MPI-ESM-MR		-3.6	-2.5	8.7*	-1.1	-1.5*	-	-1.1	-0.9	24*	-1.4	0.3	-0.1*
MRI-CGCM3		-5*	-3.6*	10.3*	-3*	-0.9	-0.1*	1	0.2	20.5*	-0.3	0.4	-0.1*
NorESM1		0.6	0.3	10.4*	0.2	-	-	-3.5	-3.1*	20.4*	-1.9	-1.3*	-0.1*
Average		-2.3	-1.8	10.3*	-1.2	-0.7	-0.1	-3.4	-2.8	24.8*	-2.2	-0.7	-0.1*
Mela		RCP4.5						RCP8.5					
		Pr	netPr	Eto	Eta	DP	SWC	Pr	netPr	Eto	Eta	DP	SWC
BCC-CSM1-1		-7.2	-5	7.2*	-2.9	-2.1	-0.1	-16*	-10.9*	22.5*	-6.9*	-4*	-0.3*
CanESM2		-8.1	-5.8	12.5*	-1.8	-4*	-0.2*	-16.3*	-11.1*	36.1*	-7.9*	-3.3*	-0.4*
CNRM-CM5		-7.6	-5.2	8*	-1.5	-3.8	-0.2*	-15.9*	-10.8*	22.4*	-6*	-4.9*	-0.3*
GFDL-ESM2M		-0.3	-0.2	8.7*	-0.3	-	-	-5.7	-3.8	24*	-3	-0.9	-0.1*
HADGEM2-CC		-14.1*	-9.6*	16.8*	-6.7*	-3	-0.2*	-17.8*	-12.2*	38.8*	-7.5*	-4.7*	-0.4*
MIROC-ESM		-10.5*	-7.5*	15.5*	-1.3	-6.2*	-0.2*	-9.9	-6.9	38.5*	-4	-2.9*	-0.2*
MPI-ESM-MR		-4	-2.3	10.3*	-2.9	0.6	-0.1	-4.5	-2.8	26.6*	-3.4	0.4	-0.2*
MRI-CGCM3		-14.6*	-10.2*	11.1*	-5.1*	-5.2*	-0.2*	-5.3	-3.7	21.2*	-2.7	-1.1	-0.2*
NorESM1		-4	-2.8	10.9*	-2.4	-0.6	-0.1*	-16.2*	-11.5*	23.6*	-6.6*	-5*	-0.3*
Average		-7.8	-5.4	11.2*	-2.8	-2.7	-0.2	-12	-8.2	28.2*	-5.3	-2.9	-0.3*

Annex 6.5: Projected trends in the HydrobalPCR outputs over the period 2010-2099 under the two RCP scenarios, and the nine CMIP5 models in the not forested areas in the four sites. Pr: Precipitation, netPr: Net rainfall, Eto: reference evapotranspiration, Eta: actual evapotranspiration DP: deep percolation, SWC: soil water content. All trends are expressed as mm/decade except SWC (%)/decade. * significant at 5%.

Ventós	RCP4.5						RCP8.5					
	Pr	netPr	Eto	Eta	DP	SWC	Pr	netPr	Eto	Eta	DP	SWC
BCC-CSM1-1	-2.1	-1.9	6.5*	-1	-1	-	-1.6	-1.4	19*	-1.8	0.3	-0.1*
CanESM2	-	-	10.1*	-0.4	0.4	-	-6.1*	-5.7*	28.5*	-3.2*	-2.6	-0.1*
CNRM-CM5	3.4	3.2	7.4*	2.2	0.9	-	0.7	0.9	21*	0.1	0.7	-0.1*
GFDL-ESM2M	3.6	3.5	8.7*	1.8	1.6	-	5.3*	5.1*	21.3*	3*	1.9	-
HADGEM2-CC	-2.7	-2.5	15.5*	-2.4	-0.3	-0.1*	-4.6	-4.4	35.7*	-2	-2.5	-0.1*
MIROC-ESM	0.1	0.2	14.3*	1	-0.9	-0.1*	2.9	2.7	31.5*	4.1*	-1.5	-
MPI-ESM-MR	-1.7	-1.5	8.3*	-0.2	-1.3	-	1.7	1.7	21.6*	1.1	0.4	-0.1*
MRI-CGCM3	-4.4	-4.1	10.1*	-1.7	-2.4	-0.1*	4.7	4.3	19*	1.5	2.5	-
NorESM1	0.6	0.5	10*	2	-1.5	-	0.6	0.6	20.6*	2.3	-1.9	-0.1*
Average	-0.3	-0.3	10.1*	0.1	-0.5	-	0.4	0.4	24.2*	0.6	-0.3	-0.1
Águilas	RCP4.5						RCP8.5					
	Pr	netPr	Eto	Eta	DP	SWC	Pr	netPr	Eto	Eta	DP	SWC
BCC-CSM1-1	-4.5	-4.1	7.3*	-3.1	-1	-0.1	-7.6*	-6.9*	21.1*	-6.3*	-0.6	-0.2*
CanESM2	-1.1	-1	10.9*	-0.4	-0.8	-	-7.6*	-6.9*	32.4*	-6.1*	-0.8*	-0.3*
CNRM-CM5	-1.5	-1.4	7.6*	-0.9	-0.6	-0.1	-5.8*	-5.1*	21*	-4.2*	-0.9	-0.2*
GFDL-ESM2M	2.8	2.7	8.5*	1.3	1.2	-	-2.7	-2.3	21.7*	-2.5	0.1	-0.1*
HADGEM2-CC	-6.1*	-5.5*	15.6*	-5.2*	-0.5	-0.2*	-9.5*	-8.6*	35.5*	-7.4*	-1.1*	-0.3*
MIROC-ESM	-2.8	-2.7	13.9*	-2.3	-0.6	-0.2*	-1.7	-1.5	33.8*	-1.6	-0.1	-0.2*
MPI-ESM-MR	-1.8	-1.5	9.5*	-1.5	-	-0.1	-1	-0.7	24.8*	-1.3	0.3	-0.1*
MRI-CGCM3	-4.9*	-4.4*	10.3*	-3.3	-1.1	-0.1*	-0.7	-0.6	19.8*	-1.2	0.5	-0.1*
NorESM1	-0.7	-0.7	10.8*	-0.8	-	-0.1	-2.8	-2.7	23*	-2.2	-0.7	-0.2*
Average	-2.3	-2.1	10.5*	-1.8	-0.4	-0.1	-4.4	-3.9	25.9*	-3.7	-0.4	-0.2*
Cabeço	RCP4.5						RCP8.5					
	Pr	netPr	Eto	Eta	DP	SWC	Pr	netPr	Eto	Eta	DP	SWC
BCC-CSM1-1	-2.3	-1.9	7.1*	-1.1	-0.8	-0.1	-7.9*	-6.1*	19.9*	-5.2*	-0.9	-0.2*
CanESM2	0.2	-0.4	10.9*	-0.6	0.1	-0.1	-6.8*	-5.5*	30.1*	-4.5*	-1.1*	-0.2*
CNRM-CM5	-1.1	-1.1	8*	-0.7	-0.4	-0.1	-5.6*	-4*	21*	-3.2*	-0.9*	-0.2*
GFDL-ESM2M	0.8	0.8	7.8*	0.4	0.3	-	-0.3	-0.3	20.3*	-0.8	0.4	-0.1*
HADGEM2-CC	-6.2*	-4.7*	15.3*	-4*	-0.8	-0.1*	-4.8*	-3.9*	33.5*	-3.4*	-0.5	-0.2*
MIROC-ESM	-3.7*	-3.2*	14.3*	-2.2	-1.1*	-0.1*	-1.5	-1.9	33.6*	-1.2	-0.8*	-0.1*
MPI-ESM-MR	-3.6	-2.5	8.7*	-1.4	-1.1*	-0.1	-1.1	-0.9	24*	-1.6	0.5	-0.1*
MRI-CGCM3	-5*	-3.7*	10.3*	-2.9*	-0.9	-0.1*	1	0.2	20.5*	-0.3	0.4	-0.1*
NorESM1	0.6	0.2	10.4*	0.1	-	-0.1	-3.5	-3.3*	20.4*	-2.7	-0.7	-0.2*
Average	-2.3	-1.8	10.3*	-1.4	-0.5	-0.1	-3.4	-2.9	24.8*	-2.5	-0.4	-0.2*
Mela	RCP4.5						RCP8.5					
	Pr	netPr	Eto	Eta	DP	SWC	Pr	netPr	Eto	Eta	DP	SWC
BCC-CSM1-1	-7.2	-6.2	7.2*	-2.7	-3.5	-0.1	-16*	-13.7*	22.5*	-6.4*	-7.2*	-0.2*
CanESM2	-8.1	-7.2	12.5*	-0.1	-7.1*	-0.1*	-16.3*	-13.9*	36.1*	-6.2*	-7.7*	-0.3*
CNRM-CM5	-7.6	-6.5	8*	0.3	-6.9*	-0.1*	-15.9*	-13.6*	22.4*	-4.7*	-8.8*	-0.2*
GFDL-ESM2M	-0.3	-0.3	8.7*	0.2	-0.6	-	-5.7	-4.8	24*	-3.5	-1.4	-0.1*
HADGEM2-CC	-14.1*	-12.1*	16.8*	-5.3*	-6.9*	-0.2*	-17.8*	-15.2*	38.8*	-5.3*	-9.9*	-0.3*
MIROC-ESM	-10.5*	-9.3*	15.5*	1.5	-10.8*	-0.1*	-9.9	-8.7	38.5*	-3	-5.7*	-0.2*
MPI-ESM-MR	-4	-3.1	10.3*	-2.2	-0.9	-0.1	-4.5	-3.6	26.6*	-2.4	-1.3	-0.2*
MRI-CGCM3	-14.6*	-12.7*	11.1*	-4.8*	-7.9*	-0.2*	-5.3	-4.6	21.2*	-1.6	-3	-0.2*
NorESM1	-4	-3.6	10.9*	-1.9	-1.7	-0.1*	-16.2*	-14.3*	23.6*	-3.7	-10.5*	-0.2*
Average	-7.8	-6.8	11.2*	-1.7	-5.1	-0.1	-12	-10.3	28.2*	-4.1	-6.2	-0.2*

Annex 6.6: Water balance under the two RCP scenarios, average of the nine CMIP5 models in the forested areas in the four sites. Pr: Precipitation, netPr: Net rainfall, Eto: reference evapotranspiration, Eta: actual evapotranspiration DP: deep percolation, SWC: soil water content. All the variables are expressed as mm except SWC (%). Change is between the two 30-year periods 2010-2039 and 2070-2099.

Ventós		Pr	netPr	Roff	Eto	Eta	DP	SWC
2006-2099	RCP4.5	252.9	166.3	2.5	1259.4	154.0	10.0	9.8
	RCP8.5	256.7	168.6	2.6	1303.3	155.1	11.2	9.7
2010-2039	RCP4.5	253.3	166.4	2.5	1226.0	153.6	10.8	9.9
	RCP8.5	254.1	166.6	2.5	1235.3	153.4	11.3	9.9
2040-2069	RCP4.5	254.9	168.1	2.5	1266.6	154.1	11.3	9.8
	RCP8.5	257.5	169.3	2.6	1297.6	154.7	11.9	9.7
2070-2099	RCP4.5	250.4	164.5	2.5	1288.9	154.5	7.9	9.7
	RCP8.5	258.8	170.2	2.6	1383.7	157.2	10.4	9.5
Change	RCP4.5	-2.9	-1.9	0.0	62.8	1.0	-2.9	-0.2
	RCP8.5	4.8	3.5	0.0	148.5	3.8	-0.9	-0.4
Águilas		Pr	netPr	Roff	Eto	Eta	DP	SWC
2006-2099	RCP4.5	234.2	159.9	2.3	1285.0	155.0	3.1	8.5
	RCP8.5	225.2	153.0	2.2	1332.4	148.8	2.5	8.2
2010-2039	RCP4.5	242.5	166.2	2.4	1250.4	160.9	4.2	8.7
	RCP8.5	238.4	162.8	2.4	1259.8	158.7	3.3	8.6
2040-2069	RCP4.5	231.7	158.0	2.3	1292.2	153.1	2.5	8.4
	RCP8.5	223.6	151.9	2.2	1326.1	147.5	2.0	8.2
2070-2099	RCP4.5	227.6	154.9	2.3	1315.9	150.4	2.4	8.3
	RCP8.5	212.4	143.4	2.1	1418.4	139.2	2.2	7.7
Change	RCP4.5	-14.9	-11.3	-0.1	65.5	-10.5	-1.8	-0.4
	RCP8.5	-26.0	-19.4	-0.3	158.6	-19.5	-1.1	-0.9
Cabeço		Pr	netPr	Roff	Eto	Eta	DP	SWC
2006-2099	RCP4.5	300.4	187.2	3.0	1207.7	177.3	7.4	9.0
	RCP8.5	295.1	182.8	2.9	1252.0	174.2	6.1	8.9
2010-2039	RCP4.5	307.2	192.5	3.1	1173.8	180.8	9.6	9.2
	RCP8.5	304.2	190.1	3.0	1182.8	179.9	8.2	9.2
2040-2069	RCP4.5	301.1	187.8	3.0	1214.4	177.7	7.4	9.0
	RCP8.5	295.2	183.1	2.9	1245.7	174.8	5.5	8.9
2070-2099	RCP4.5	292.4	180.9	2.9	1238.2	173.2	5.1	8.9
	RCP8.5	285.1	174.3	2.8	1334.3	167.3	4.4	8.5
Change	RCP4.5	-14.8	-11.6	-0.1	64.3	-7.6	-4.5	-0.3
	RCP8.5	-19.1	-15.8	-0.2	151.5	-12.6	-3.9	-0.6
Mela		Pr	netPr	Roff	Eto	Eta	DP	SWC
2006-2099	RCP4.5	486.6	311.3	4.9	956.4	273.7	33.1	15.7
	RCP8.5	453.4	287.9	4.5	1007.5	259.4	24.3	15.0
2010-2039	RCP4.5	508.1	325.9	5.1	919.2	281.2	40.5	16.1
	RCP8.5	488.9	312.3	4.9	929.4	274.9	33.4	15.8
2040-2069	RCP4.5	489.8	314.0	4.9	964.3	275.6	33.2	15.7
	RCP8.5	453.0	287.8	4.5	999.3	259.2	23.9	15.0
2070-2099	RCP4.5	459.6	292.4	4.6	989.5	263.5	24.8	15.2
	RCP8.5	414.6	261.1	4.1	1101.6	242.4	14.8	14.1
Change	RCP4.5	-48.6	-33.5	-0.5	70.3	-17.7	-15.6	-1.0
	RCP8.5	-74.4	-51.2	-0.7	172.1	-32.5	-18.6	-1.7

Annex 6.7: Water balance under the two RCP scenarios, average of the nine CMIP5 models in the not forested areas in the four sites. Pr: Precipitation, netPr: Net rainfall, Eto: reference evapotranspiration, Eta: actual evapotranspiration DP: deep percolation, SWC: soil water content. All the variables are expressed as mm except SWC (%). Change is between the two 30-year periods 2010-2039 and 2070-2099.

Ventós		Pr	netPr	Roff	Eto	Eta	DP	SWC
2006-2099	RCP4.5	252.9	226.3	1.5	1259.4	209.4	15.7	8.5
	RCP8.5	256.7	229.8	1.5	1303.3	211.7	16.7	8.5
2010-2039	RCP4.5	253.3	226.6	1.5	1226.0	208.9	16.7	8.6
	RCP8.5	254.1	227.3	1.5	1235.3	209.5	16.8	8.6
2040-2069	RCP4.5	254.9	228.3	1.5	1266.6	209.3	17.3	8.5
	RCP8.5	257.5	230.5	1.5	1297.6	211.5	17.4	8.4
2070-2099	RCP4.5	250.4	224.0	1.5	1288.9	210.1	12.8	8.5
	RCP8.5	258.8	231.7	1.5	1383.7	214.2	15.9	8.3
Change	RCP4.5	-2.9	-2.6	0.0	62.9	1.2	-3.9	-0.1
	RCP8.5	4.7	4.4	0.0	148.4	4.7	-0.9	-0.3
Águilas		Pr	netPr	Roff	Eto	Eta	DP	SWC
2006-2099	RCP4.5	234.2	201.1	1.5	1285.0	194.9	5.1	9.4
	RCP8.5	225.2	192.8	1.4	1332.4	187.8	4.0	9.1
2010-2039	RCP4.5	242.5	208.6	1.5	1250.4	200.9	6.9	9.7
	RCP8.5	238.4	204.6	1.5	1259.8	198.7	5.4	9.6
2040-2069	RCP4.5	231.7	198.9	1.5	1292.2	193.2	4.2	9.4
	RCP8.5	223.6	191.4	1.4	1326.1	186.8	3.1	9.0
2070-2099	RCP4.5	227.6	195.2	1.4	1315.9	190.1	4.0	9.2
	RCP8.5	212.4	181.3	1.3	1418.4	176.9	3.2	8.5
Change	RCP4.5	-14.9	-13.4	-0.1	65.5	-10.8	-2.9	-0.5
	RCP8.5	-26.0	-23.3	-0.2	158.6	-21.8	-2.2	-1.1
Cabeço		Pr	netPr	Roff	Eto	Eta	DP	SWC
2006-2099	RCP4.5	300.4	183.2	1.3	1207.7	177.7	4.7	8.7
	RCP8.5	295.1	178.5	1.3	1252.0	173.8	3.9	8.5
2010-2039	RCP4.5	307.2	188.7	1.4	1173.8	181.8	6.3	8.9
	RCP8.5	304.2	186.2	1.4	1182.8	180.7	5.2	8.9
2040-2069	RCP4.5	301.1	183.9	1.3	1214.4	178.0	4.8	8.7
	RCP8.5	295.2	178.9	1.3	1245.7	174.2	3.7	8.5
2070-2099	RCP4.5	292.4	176.6	1.3	1238.2	173.0	2.9	8.5
	RCP8.5	285.1	169.7	1.2	1334.3	166.0	2.8	8.0
Change	RCP4.5	-14.8	-12.1	-0.1	64.4	-8.8	-3.4	-0.4
	RCP8.5	-19.1	-16.5	-0.2	151.5	-14.7	-2.4	-0.9
Mela		Pr	netPr	Roff	Eto	Eta	DP	SWC
2006-2099	RCP4.5	486.6	397.1	3.3	956.4	311.1	83.1	9.8
	RCP8.5	453.4	368.0	3.0	1007.5	301.9	63.5	9.4
2010-2039	RCP4.5	508.1	415.5	3.4	919.2	315.2	97.5	10.1
	RCP8.5	488.9	398.6	3.3	929.4	313.0	83.2	10.0
2040-2069	RCP4.5	489.8	400.3	3.3	964.3	312.8	83.9	9.8
	RCP8.5	453.0	367.8	3.0	999.3	302.3	62.4	9.4
2070-2099	RCP4.5	459.6	373.5	3.0	989.5	304.7	66.3	9.5
	RCP8.5	414.6	334.5	2.7	1101.6	289.2	42.9	8.7
Change	RCP4.5	-48.5	-42.0	-0.4	70.3	-10.5	-31.2	-0.6
	RCP8.5	-74.3	-64.1	-0.6	172.2	-23.8	-40.3	-1.3



Universitat d'Alacant
Universidad de Alicante

CAPÍTULO 7

Resumen de los resultados

Universitat d'Alacant
Universidad de Alicante



Universitat d'Alacant
Universidad de Alicante

Resumen de los principales resultados

En esta sección se presentan los principales resultados obtenidos en el marco de esta tesis doctoral. Estos resultados se organicen en cinco puntos refiriéndose a los cinco capítulos 2 a 6 de la tesis. Para evitar repeticiones no se hace la discusión de estos resultados en esta sección que se hizo en sus correspondientes capítulos.

1. Análisis de los eventos climáticos extremos en la provincia de alicante

El análisis de los eventos extremos de precipitación en la provincia de Alicante mostró una gran variabilidad temporal y espacial de los índices calculados.

1.1. La variabilidad temporal

Los índices de extremos climáticos en la provincia de Alicante se analizaron a dos escalas temporales; por un lado a escala de un periodo de 60 años desde 1953 hasta 2012 , y por otro a escala de dos sub-periodos de 30 años cada uno, de 1953 a 1982 y de 1983 a 2012. Los resultados mostraron una gran variabilidad en los valores medios de los índices y sus tendencias en los tres periodos estudiados.

El índice PRCPTOT que representa la precipitación total anual es del orden de 477.1 mm en el periodo largo pero esta media se ha visto reducida en más de 30 mm entre el primer sub-periodo y el segundo, pasando de 492.4 a 461.8 mm. Esa misma tendencia negativa se observa en el caso del índice SDII que representa el índice simple de intensidad diaria. Al contrario del descenso observado en los dos índices citados anteriormente, se observa un aumento en los índices R95ptot y R99ptot de los días muy húmedos y extremadamente húmedos al igual que el índice Rx1day que representa la cantidad máxima de precipitación en un día. El test de comparación de medias indicó que solo 3 índices (SDII, R10mm y R20mmm) mostraron diferencias significativas entre el periodo 1953-1982 y el periodo 1983-2012. Los mayores porcentajes de cambio se observaron en los mismos índices con diferencias significativas superando el 20% con signo negativo y en el índice R99ptot superando el 33% con un signo positivo.

Una de las tendencias más destacadas es la inversión en la tendencia del índice de precipitación total (PRCPTOT). Mientras que se obtiene una tendencia negativa a escala del periodo 1953-2012 y del sub-periodo 1953-1982, la misma es positiva en el último (1983-2012) lo que señala que el descenso en el valor medio de la PRCPTOT entre el

primer sub-periodo y el segundo es debido a años más secos al inicio del segundo sub-periodo (1983-2012), y que el final de este periodo es más húmedo. Otro aspecto destacado es la tendencia negativa en los índices Rx1day, Rx5day, R95ptot y R99ptot a pesar de la tendencia positiva en la precipitación total anual. Finalmente cabe destacar una tendencia negativa en el número de días secos consecutivos CDD en los tres periodos estudiados.

1.2. La variabilidad espacial

El análisis de la variabilidad espacial se hizo mediante creación de mapas de valores medios de los índices calculados y de sus tendencias. Las precipitaciones medias anuales siguen un gradiente latitudinal y van de menos de 300mm en el centro y el sur hasta más de 800mm en el norte y superando el umbral de 900mm en zonas puntuales. A pesar de que el valor medio de la tendencia del índice PRCPTOT es negativo para toda la zona, esa tendencia no es la misma en todo el territorio alicantino. En efecto, las tendencias negativas solo se concentran en la zona central y sobre todo en la zona sur de la mitad norte de la provincia en las mismas comarcas donde se registraron bajadas significativas en la precipitación total anual entre los dos sub-periodos estudiados en este trabajo. En la parte sur y suroeste se registra una ligera tendencia positiva mientras que una tendencia positiva significativa se observa en la parte norte entre la comarca de la Marina Alta y el Comtat.

La distribución espacial de la mayoría de los índices y sus tendencias siguen los mismos patrones que el índice PRCPTOT con algunas diferencias. En efecto, las tendencias del índice SDII son negativas y significativas en el todo el territorio. Las tendencias del índice R1mm son positivas y significativas en la mayor parte de la provincia y las zonas de mayor aumento se concentran en el norte y en el oeste en la frontera con la provincia de Albacete y Murcia. Los días con precipitaciones mayores a 10mm y 20mm (R10mm y R20mm) también mostraron tendencias diferentes en el espacio con valores negativos y significativos en la parte sur de la mitad norte de la provincia.

El índice del número máximo de días secos consecutivos (CDD) que puede ser un indicador de la longitud de la estación seca puede ir de una media de 54.5 días consecutivos sin lluvia en el norte hasta 90 días en la parte sur en el límite con Murcia. La media de este índice es de 70 días y se registra en una gran parte del territorio. La

tendencia de este índice es negativa y significativa en una gran parte del territorio y es positiva en las comarcas de Alacantí, del Bajo Vinalopó y del Bajo Segura.

2. Posibles efectos del cambio climático en la disponibilidad de los recursos subterráneos.

En trabajos anteriores se puso de manifiesto que solo los eventos grandes de lluvia (HREs de las siglas en inglés Heavy Rainfall Events) son susceptibles de producir apreciables recargas de los acuíferos. En este capítulo se intentó buscar un umbral para definir los HREs a escala de toda la provincia de Alicante. Al mismo tiempo se definió el concepto de periodos de no recarga (NARP de las siglas en inglés No Aquifer Recharge Period) que representa los períodos máximos (en días) entre dos HREs consecutivos dentro del mismo año. Luego se analizaron los cambios observados (periodo 1953-2012) y proyectados (2040-2099) en estas dos variables.

2.1. Selección del umbral para definir los HREs

Se utilizaron datos diarios de lluvia de 111 estaciones meteorológicas y datos mensuales del nivel piezométrico de 21 puntos en el periodo 2006-2012 bien repartidos en toda la provincia de Alicante. Por la falta de datos diarios de piezometría para relacionar los incrementos en el nivel piezométrico con sus eventos de lluvia causantes, se hizo una correlación entre el número de incrementos en todo el periodo 2006-2012 y el número de HREs (tomando en cuenta solo un HREs por mes en caso que hayan sido más de uno). Un análisis de sensibilidad variando el umbral en el intervalo 5 a 60 mm/día a un paso de 5mm ayudó a determinar el umbral buscado. El mayor R^2 se obtuvo con el umbral 20mm/día ($R^2=0.76$) aunque el umbral 15mm/día también presentó un R^2 muy alto ($R^2=0.74$); sin embargo, el 94% de estos eventos mayores a 15 son mayores a 20mm/día. Por lo que se ha elegido el umbral 20mm/día para definir los HREs.

2.2. Los cambios observados en las métricas de los HREs

Las 111 estaciones meteorológicas se agruparon en 10 clústeres usando como criterio la correlación entre las series temporales. Las métricas de los HREs se refieren al número, tamaño y el total de agua aportado por los HREs.

2.2.1. El análisis wavelet

El análisis wavelet se aplicó a las series mensuales del número de HREs en cada clúster. Una concentración de potencia se observó en las bandas mensuales 4-8 (or 6 ± 2) y 8-16 (or 12 ± 4). Eso se confirma analizando el espectro global del wavelet (GWS de las siglas en inglés Global Wavelet Spectrum) donde se observaron picos significativos alrededor de las bandas mensuales arriba mencionadas. El resultado más importante del análisis wavelet ha sido el cambio en la significación de los picos de GWS in las bandas 6 ± 2 y 12 ± 4 entre los dos periodos 1953-1982 y 1983-2012. En efecto, excepto en el caso de los clústeres 3, 4 y 9, los otros siete clústeres mostraron picos significativos en la banda 6 ± 2 en el primer periodo y que no lo son en el segundo. Los picos anuales (12 ± 4) dejaron de ser significativos en 3 clústeres.

2.2.2. Cambios en los valores medios de las métricas de HREs y sus tendencias

El número medio de HREs por año varía entre 3 eventos en los clústeres del sur y 11 en el clúster 10 situado en el extremo noreste de Alicante en el periodo 1953-2012. El número de HREs ha disminuido entre los dos sub-periodos 1953-1982 y 1983-2012 en nueve clústeres y el cambio es significativo en 4 de ellos donde el cambio es más de -30%. Esta reducción en el número de HREs provoca un descenso en el total de agua aportado por estos eventos al total anual de lluvia. Esta reducción del agua total aportado por los HREs se ve compensada parcialmente por un aumento en el tamaño medio de estos eventos. En efecto, en siete de los nueve clústeres donde se ha visto una reducción en el número de los HREs, el tamaño medio de estos eventos aumentó un 8%.

Igual que los cambios observados en los valores medios entre los dos sub-periodos, las tendencias tienen un signo negativo en los nueve clústeres donde se observó una reducción en el número de los eventos. Sin embargo, solo tres clústeres mostraron tendencias significativas. En el mismo sentido, tendencias negativas se observaron en el total de agua aportado por los HREs mientras que el tamaño medio de estos eventos mostró una tendencia positiva en seis clústeres.

2.2.3. Cambios en la media de longitud de NARP

La longitud media de los periodos de no recarga NARP ha aumentado en promedio unos 21 día en el segundo sub-periodo con respecto al primer sub-periodo (1953-1982) en ocho clústeres. Sin embargo, este aumento es significativo en solo dos clústeres.

2.3. Los cambios proyectados en las métricas de los HREs

Según los nueve modelos CMIP5, la misma tendencia de cambio, en las métricas de los HREs, observada en el periodo 1953-2012 es probable bajo los dos escenarios RCP en los últimos sesenta años del siglo 21. Una reducción del número de los HREs y en el total de agua aportado por estos eventos es esperada bajo los dos escenarios con mayor descenso bajo el escenario extremo RCP8.5. Un aumento en el tamaño medio de los HREs es esperado bajo los escenarios de cambio climático lo que compensa parcialmente la reducción en el número de los HREs.

3. Los cambios en la fenología de superficie del terreno (LSP) en relación con las variables climáticas en áreas naturales de la provincia de Alicante: cambios observados y proyectados.

Para analizar la fenología de superficie del terreno (LSP) y sus cambios en relación a las variables del clima, se utilizaron más de 300 imágenes MODIS-NDVI compuestas (una imagen cada 16 días) en el periodo 2000-2012. El uso del programa TIMESAT permitió la determinación de tres métricas de LSP: inicio de la estación de crecimiento (SOS), final de la estación (EOS) y la longitud de la estación (LOS). El SOS y el EOS son fechas cada 16 días que en este trabajo llamamos M-dates que llevan códigos de 0 a 22 y donde el 1 es el 28 de Agosto y que coincide con el inicio de la época de lluvia en Alicante (año hidrológico). La determinación de estas métricas se hizo para seis clases de la cartografía CORINE de coberturas vegetales en áreas naturales de Alicante que en este trabajo llamamos “vegetación natural”. Estas seis coberturas son subclases de las dos clases: bosque y matorral. Dos de las tres subclases del bosque han sido excluidas del análisis por el bajo número de pixeles en cada clase y por el efecto de borde.

Los datos del clima han sido organizados de forma que coincidan con las fechas de las imágenes MODIS y en este trabajo los llamamos métricas del clima.

3.1. Valores medios de las métricas LSP

El valor medio de SOS para la vegetación natural en la Provincia de Alicante en el periodo 2000-2012 es alrededor de M-date 4 que corresponde al 15 de octubre. Este valor es similar entre las dos clases de bosque y matorral, y entre las cuatro subclases.

Al contrario del SOS, el valor medio de EOS es alrededor de M-date 16 (22 de abril) y es significativamente ($p<0.05$) diferente entre bosque y matorral (M-date 15.2 y M-date 16.1 respectivamente). Dentro de la clase matorral no hay diferencias significativas entre las tres subclases.

La LOS depende del SOS y el EOS. El valor medio es del orden de 191.5 días y es significativamente diferente entre bosque y matorral (181.4 y 193.9 días respectivamente). Dentro de la clase matorral no hay diferencias significativas entre las tres subclases.

3.2. La variabilidad espacial de las métricas LSP

Se observaron diferencias en las métricas LSP entre el norte y el sur de la provincia de Alicante. La mayoría de los píxeles donde el SOS ocurre antes de la fecha M-date 4 se localizan en el norte mientras que los píxeles donde el SOS ocurre después se localizan en la parte sur. Si analizamos las clases bosque y matorral por separado se observa que los píxeles con un SOS después de M-date 4 se ubican en la clase matorral. De manera similar los píxeles con EOS antes de M-date 16 pertenecen a la clase bosque mientras que los píxeles con EOS después de esa fecha pertenecen a la clase matorral. Se ha observado un EOS temprano en la parte sur e interior de la provincia.

La altitud y orientación son dos variables topográficas que tienen efecto en las métricas LSP. En efecto, una fuerte correlación negativa ($R^2=0.89$) se observó entre la altitud y el SOS mientras que no se observó ninguna correlación con EOS. Las áreas orientadas hacia el norte y el noroeste mostraron un SOS y EOS temprano en comparación con el sur y el sureste.

3.3. Las métricas LSP vs clima

La ocurrencia del SOS y el EOS dependen de las condiciones climáticas previas. El SOS y el EOS dependen de las precipitaciones y temperaturas de agosto-septiembre y

de enero a abril respectivamente. Las métricas del clima que mejor se correlacionan con las métricas del LSP son la precipitación (Pr8+9) y la temperatura máxima (Tx8+9) de agosto-septiembre y el ratio entre las dos (Tx8+9/Pr8+9) en el caso del SOS y la precipitación de enero a abril (Pr1-4) y la temperatura de abril (Tx4) y el ratio entre las dos (Tx/Pr1-4) en el caso del EOS.

Correlaciones positiva con la precipitación y negativa con la temperatura indica que las condiciones climáticas en septiembre estimulan un SOS temprano. Lo contrario pasa con el EOS, lo que muestra que buenas condiciones en el periodo enero a abril alarga la estación de crecimiento. Estas variables climáticas que controlan los cambios en SOS y EOS afectan a la longitud de la estación. En efecto, una buena correlación se observó entre LOS y la suma de las variables Pr8+9 y Pr1-4 ($0.5 < R^2 < 0.7$).

3.4. Los cambios proyectados en las métricas LSP

La exploración de los posibles efectos del cambio climático en las métricas LSP se hizo mediante las seis métricas del clima que mejor se correlacionan con estas últimas. Una reducción en la precipitación y un aumento en las temperaturas se esperan en general bajo los escenarios del cambio climático. Una reducción importante en la Pr1-4 y un aumento en la Tx8+9 son los cambios más destacados a un ritmo mayor bajo el escenario extremo RCP8.5 en comparación con el escenario moderado RCP4.5. Para proyectar las métricas LSP bajo las condiciones futuras del clima, se utilizaron las ecuaciones de regresión entre las métricas LSP y las del clima.

La mayoría de las tendencias de cambio esperada en las métricas LSP son significativas ($p < 0.05$). Un retraso en el SOS, un adelanto en el EOS y un LOS más corta son esperados mientras nos adentramos en el siglo 21.

4. Evaluación del período de crecimiento de los cultivos de acuerdo con las previsiones del cambio climático para la Marina Baixa

Datos climáticos del modelo HadCM3 (the atmosphere-ocean-coupled model of the Hadley Centre (UK), version 3) bajo el escenario A2 se usaron en este capítulo para evaluar el posible efecto del cambio climático en el periodo de crecimiento de los cultivos (LGP de las siglas en inglés Length of Growing Season) en la Marina Baixa,

Alicante. El LGP se calcula como el periodo de tiempo cuando la precipitación (P) supera la mitad de la evapotranspiración (Eto) con una probabilidad de 75%.

Un análisis exploratorio del balance entre P y Eto a una escala diaria mostró que el número de días cuando la P supera la mitad de la Eto con una probabilidad de 75% varía entre 0 y 10. Aunque en algunos años la P superó a la mitad de la Eto pero no cumplió el criterio del 75% debido al carácter torrencial de las lluvias en la zona de estudio.

El LGP se calculó como el periodo de décadas (10 días) consecutivos cuando la P supera la mitad de la Eto. Sin embargo, al igual que en el caso de la escala diaria pocas décadas cumplían con el requisito del 75% de probabilidad. Después de una exploración de varios umbrales se eligió el umbral 30% de probabilidad porque coincide con el inicio y el final de la época de lluvias en la zona.

El LGP varía entre el suroeste (SO) y el noreste (NE) de la zona. El LGP es más corto (150-180 días) in las estaciones del SO y de la costa y más largo (220-230 días) en las estaciones de NE. El LGP es probable que se reduzca al final del siglo 21. En efecto, la reducción esperada en el LGP es entre 60 a 70 días en las estaciones del SO y entre 40 a 50 días en las estaciones del NE en el periodo 2071-2099.

5. HydrobalPCR: un modelo basado en una plataforma de modelización ambiental para evaluar los posibles efectos del cambio climático en el balance hídrico en diferentes tipos de vegetación.

En este capítulo se construyó una versión modificada del modelo eco-hidrológico HYDROBAL usando una plataforma de modelización ambiental con el objetivo de manejar grandes bases de datos simulando el balance hídrico en varios tipos de vegetación, en varias zonas y bajo varios escenarios del cambio climático de diferentes fuentes. Otro objetivo de este trabajo era hacer de la nueva versión HydrobalPCR una herramienta flexible que se puede conectar a otras herramientas para la optimización de modelos (en este caso la calibración).

La plataforma PCRaster-Python permite la construcción de modelos dinámicos para diferentes fines. El uso del lenguaje Python de alto nivel permite sacar provecho de un lenguaje de programación para programar bucle para iterar sobre grandes bases de datos.

El HydrobalPCR se calibró con datos de humedad del suelo de dos años (2012-2014) medidos en cuatro zonas ubicadas en la ventana de recarga de cuatro acuíferos localizados a lo largo de un gradiente climático en la provincia de Alicante. La validación del modelo con datos del año hidrológico 2014-2015 dio resultados satisfactorios ($0.34 < \text{NSE} < 0.70$ y $0.56 < \text{RSR} < 0.95$).

El HydrobalPCR se utilizó luego para evaluar los posibles efectos del cambio climático en el balance hídrico en dos tipos de vegetación en cuatro zonas de Alicante y bajo 18 escenarios de cambio climático (9 modelos CMIP5 y dos escenarios RCP).



Universitat d'Alacant
Universidad de Alicante



Universitat d'Alacant
Universidad de Alicante

CAPÍTULO 8

CONCLUSIONES

Universitat d'Alacant
Universidad de Alicante



Universitat d'Alacant
Universidad de Alicante

Conclusiones

1-Los resultados obtenidos en esta Tesis indican que durante las últimas décadas y a escala de toda la provincia de Alicante, ha habido tendencias de cambio positivas y negativas en las precipitaciones, según zonas. Sin embargo las tendencias negativas son las más significativas.

2-El estudio del cambio según la escala temporal y espacial afecta a los resultados obtenidos. Las tendencias observadas a lo largo del periodo 1953-2012 no siempre coinciden con las tendencias observadas en los sub-periodos de 1953 a 1982 y de 1983 a 2012. En el espacio las tendencias varían en general de norte a sur, aunque las tendencias significativas se han visto concentradas en zonas limitadas del territorio coincidiendo con la mayoría de los índices de extremos analizados en este trabajo.

3- Los resultados obtenidos muestran que el número de eventos de lluvia grandes (HREs) susceptibles de producir recargas apreciables han sufrido una reducción importante en los últimos 60 años hasta el 2012, por lo que deducimos que la recarga de acuíferos en Alicante ha sufrido una reducción importante.

4-La reducción en el número de los HREs es probable que se reduzca de manera significativa en la provincia de Alicante bajo el cambio climático, según se deduce del estudio de los nueve modelos climáticos CMIP5 usados y sobre todo bajo el escenario extremo RCP8.5.

5-Aunque el mayor porcentaje de reducción de los HREs se espera en las zonas del norte de la provincia de Alicante, la reducción puede tener mayores repercusiones en las zonas del sur. En efecto, las zonas del sur sufren actualmente un déficit importante de agua y cualquier reducción en el futuro puede suponer mayores riesgos para los ecosistemas.

6-La reducción en el número de HREs puede verse compensada en parte por el aumento en el tamaño medio de los HREs. Aunque esto significaría que el volumen de agua recibido no varía, sin embargo, puede tener efectos negativos a nivel ambiental y socio-económico, al cambiar el régimen de precipitaciones.

7-La reducción en el número de HREs hace que los períodos de no recarga sean más largo acentuando la llamada sequía de las aguas subterráneas (groundwater droughts) en la región.

8-Los resultados de esta tesis ponen en evidencia la importancia de la ventana temporal de estudio. Las tendencias significativas observadas en análisis de los HREs sobre todo el periodo de 60 años cambian al utilizar la ventana temporal de 30 años. Además, las tendencias observadas sobre una ventana temporal móvil de 30 años muestran cambios de dirección, magnitud y significación en función de los años considerados en la ventana elegida.

9-El uso de las métricas de fenología de superficie (LSP) para describir la respuesta de la vegetación al clima actual e histórico permite la exploración de los posibles cambios en el futuro bajo los escenarios de cambio climático. Aunque es sensible a la variabilidad espacial de la vegetación

10-El análisis del LSP aplicado a las áreas naturales de la provincia de Alicante indica que una reducción en la precipitación y un aumento en las temperaturas máximas es probable que produzca un acortamiento en la longitud de la estación de crecimiento (LOS) de la vegetación, debido principalmente a un final temprano de la estación de crecimiento (EOS).

11-Con el cambio climático el periodo de crecimiento de los cultivos también parece que tiene tendencia al acortamiento. Los resultados de la Marina Baixa indican que la probabilidad de que el total anual de precipitaciones supere el umbral de 400 mm es probable que baje del 29% bajo las condiciones climáticas históricas al 9% bajo los escenarios a finales del siglo 21. Al mismo tiempo se espera que la evapotranspiración potencial (Eto) suba un 18% en la comarca de la Marina Baja (Alicante).

12-El anterior resultado indica que la zona de la Marina Baja va a enfrentarse a un importante desafío en términos de suficiencia de agua en el futuro. Una de las posibles soluciones a este problema es el uso de variedades de cultivos que se adapten mejor a las esperadas condiciones climáticas futuras. Este resultado se puede extrapolar a toda la provincia de Alicante, aunque las necesidades y demandas de agua sean diferentes.

13-La evaluación del modelo HydrobalPCR, desarrollado usando una plataforma para la modelización ambiental basada en un lenguaje de programación de alto nivel, dio resultados aceptables en facilidad de manejo y tiempo de operación, al aplicarlo a dos tipos de vegetación.

14-HydrobalPCR ha sido aplicado de manera satisfactoria para evaluar el efecto del cambio climático en el balance hídrico en dos tipos de vegetación en cuatro zonas y bajo 18 escenarios de cambio climático (nueve modelos climáticos CMIP5 y dos escenarios de emisión) para el siglo 21. HydrobalPCR ha permitido el manejo de grandes bases de datos climáticos.





Universitat d'Alacant
Universidad de Alicante

APENDICES



Universitat d'Alacant
Universidad de Alicante



Universitat d'Alacant
Universidad de Alicante

APÉNDICE 1

Download and process of MODIS Data from the Data Pool using MODIS R-package

Hassane MOUTAHIR (hassane_moutahir@yahoo.fr)

-----June, 2013-----

MODIS download and processing package (named as MODIS R package in this short tutorial) can be used to download, re-project, resample, mosaic, format conversion, SDS-extraction, bit-encoding and filtering/smoothing capabilities. It allows downloading data from FTP/http (local processing) or usingSSOAP (online processing) via the MODIS web-service. It allows preprocessing data with GDAL, MRT, SSOAP (see MODIS R manual <http://ivfl-arc.boku.ac.at/owncloud/public.php?service=files&t=c4481aebe031c26fb62722ace11da4>).

Part 1: Installation of MODIS R package and the software required for its run

1-Download and install the last version of R (for windows: <http://cran.r-project.org/bin/windows/base/>).

2- Get and install Rstudio, a free and open source integrated development environment for R (<http://www.rstudio.com/ide/download/desktop>) (it's not obligatory but it's the best IDE to work with R)(in this short tutorial we will use RStudio because it makes the use of R more easier but you can use the Rgui which is installed with R)

3-Download and install the MODIS REPROJECTION TOOL (MRT) (<https://lpdaac.usgs.gov/tools/>)

3-1-Update Java from www.java.com and **add Java to the environment variables**(see <http://stevemosher.wordpress.com/step-two-get-to-know-your-windows-system/>)

3-2-For a rapid and automatic installation see the user manual, page 15 https://lpdaac.usgs.gov/sites/default/files/public/mrt41_usermanual_032811.pdf

4-Install OSGeo4w which is the preferred source for gdal on Windows. Gdal utilities can be used to transform and reproject data prior to importing it into R. Those functionalities can be performed by MRT but it's important to install gdal to run some MODIS R commands like runGdal(). OSGeo4W is basically an installer that installs a variety of open source GIS tools like GRASS, QGIS and also gdal. You can get the installer at this location: <http://download.osgeo.org/osgeo4w/osgeo4w-setup.exe>

5-Install MODIS R package:

5-1-You can install MODIS R using two ways:

5-1-1- Typing in **Rstudio Console** the following command line:
`install.packages("MODIS", repos="http://R-Forge.R-project.org")`(to locate the Rstudio Console see figure 1,Part 2)

5-1-2- Or downloading the MODIS R zip (https://r-forge.r-project.org/R/?group_id=1252) to your Computer and using **Rstudio install packages tool** and choosing, in Install from, the option: **Package Archive File (.zip:.tar.gz)**(to locate the **install packages button** see the figure 1,Part 2)

5-2- Type `help(package="MODIS")` in Rstudio Console to see the documentation for this package in the bottom-right window. Click on **DESCRIPTION file** which gives a short description of the package but the most important is the point *Suggests: RCurl, rgeos, rgdal, bitops, mapdata, maptools, SSOAP, XML, XMLSchema, snow, ptw.* In this point you can see the R packages needed when working with MODIS R.

5-3- To install all the packages above cited, Except for SSOAP see point 5-4, use **Rstudio install packages** button (or in the main menu Tools/install packages) and choose to install from a CRAN repository and type de name of the package.

5-4- To install the SOAP package, which is a package that provides a client interface to SOAP (Simple Object Access Protocol) servers from within R, use the Rstudio Console and type: `install.packages("SSOAP", repos = "http://www.omegahat.org/R", dependencies = TRUE, type = "source")`

NB: You can just copy and paste all the command lines to the RStudio Console but you need to change the quotes “” to " " or ''

Part 2: DownloadingData using MODIS R package

1-Using Rstudio: (more documentation in <http://www.rstudio.com>)

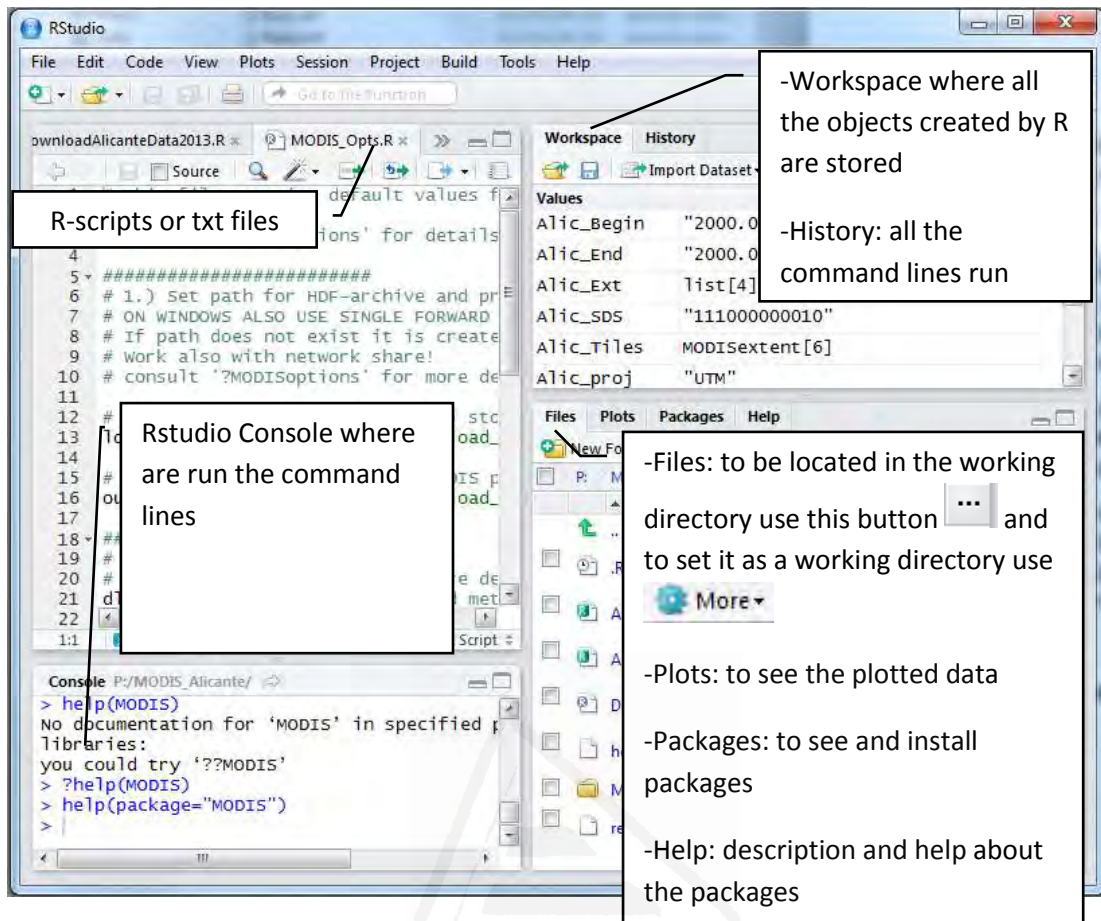


Figure 1: RStudio interface

2-Modifying the MODIS_Opts.R file located in C:\Program Files\R\R-3.0.1\library\MODIS\external or in the R directory in your computer:

Open the MODIS_Opts.R with any text editor or use RStudio and change:

- localArcPath<- '~/MODIS_ARC' to the directory where you want to save the hdf files (for example: D:/MODIS_MyStudyArea_HDF)
- outDirPath<- '~/MODIS_ARC/PROCESSED' to the directory where you want to save the processed files by MRT or Gdal.(for example: D:/MODIS_MyStudyArea_HDF/PROCESSED)
- gdalPath<- 'C:/OSGeo4W/bin' to the directory where the OSGeo4W is installed and **to use Gdal delete the # because all command lines after an # are considered as comments.**

NB:

-You can change those options using the MODISoptions()function and typing in the RStudio Console, for example, the following command lines:

```
MODISoptions(localArcPath='D:/MODIS_ARC',
outDirPath='D:/MODIS_ARC/PROCESSED')
```

-When typing a directory use slash '/' and not backslash '\'

3-R-scripts:

When using R commands you can just type your commands in the RStudio Console or you can save your commands in R file (which can be a simple txt file) and run each command line by selecting it and making click on the button  **In this tutorial we will save all commands in a file.**

4- Downloading MODIS DATA:

To show you how to use the MODIS R package I will use a simple example of an R script that illustrate how to download MODIS vegetation index for the region of Spokane (US). Below you can see the example with some comments on each step:

```
#####
#Script created to download and process MODIS vegetation index data of Spokane #
# Region (US) from MODIS DATA POOL. #
# Author: Hassane Moutahir #
# Date: 11-june-2013 #
# This Script uses "MODIS download and processing package" #
#####

setwd("P:/MODIS_Spokane")# to set your directory as a working directory

library("MODIS")# to load the MODIS R package

#Setting the Path where to store downloaded MODIS files.Default is "~/MODIS_ARC".
localArcPath1 <- 'P:/MODIS_Spokane/MODISSpok_ARC'

#Setting the output path where to store results of runGdal() or runMrt() functions.
#Default is "#~/MODIS_ARC/PROCESSED"
outDirPath1 <- 'P:/MODIS_Spokane/MODISSpok_ARC/PROCESSED'

#Setting the format. The Default format is 'Geotiff'
Format2<-"raw binary"

#If you don't want to edit and change the 'MODIS_Opts.R' file you can change the
#default #options using MODISoptions() function.

MODISoptions(localArcPath=localArcPath1, outDirPath=outDirPath1,
dataFormat=Format2)

#Setting the extent and tiles (if you don't know the MODIS tiles of your region you can
#use the #geographic coordinates to define which tiles you need (using coordinates from
#Google Earth #works good))
# to delimit the geographic extent of your study area you need the x min, x max, y min
#and y #max
Spok_Ext<- list(xmin=-118,xmax=-100,ymin=47,ymax=48)
```

```

Spok_Tiles<-getTile(extent=Spok_Ext) # you can type Spok_tiles in the RStudio
Console to see #your tiles in the screen

#Choosing the SDS (the two vegetation index: NDVI and EVI)
Spok_SDS<-"110000000000"

#the projection system
Spok_proj<-"UTM"

#Dates: begin and end
Spok_Begin<-"2000.02.01"
Spok_End<-"2000.02.20"

#Downloading, mosaicking, re-projecting and format conversion of Spokane files using
MRT (to #know more about the runMrt() options see the MODIS R manual)
runMrt( product="MOD13Q1", begin=Spok_Begin, end=Spok_End,
tileH=c(Spok_Tiles$tileH[1],Spok_Tiles$tileH[2]), tileV=Spok_Tiles$tileV,
extent=Spok_Ext, collection=005, quiet=FALSE, wait=0.5, checkIntegrity=FALSE,
SDSstring=Spok_SDS, outProj=Spok_proj)

```

NB:

1-It's not obligatory to use R objects (like Spok_Ext, Spok_Tiles...) to define the options of runMrt(). You can just fill those options directly with their values as it's illustrated in the next example:

```

runMrt( product="MOD13Q1", begin="2000.02.01", end="2000.02.20",
tileH=c(10,11), tileV=4, extent=list(xmin=-118,xmax=-100,ymin=47,ymax=48),
collection=005, quiet=FALSE, wait=0.5, checkIntegrity=FALSE,
SDSstring="110000000000", outProj="UTM")

```

2-If you want just to download the HDF files without any type of processing you can use the getHdf() function (see the manual).

3-You can run this example just by copying this short script to a text editor (or to new script in RStudio) and saving it as R file than you can run it.

**4- For more details see:“Beginners Guide Using MODIS in R” by Steven Mosher:
<http://stevemosher.wordpress.com/modis-tutorial/>**

APÉNDICE 2

Preparación de la base de datos de temperaturas

Para la realización de este trabajo se han usado registros diarios de temperaturas máximas (T_{\max}) y mínimas (T_{\min}) de 100 observatorios dentro de la provincia de Alicante y en una franja de 20km alrededor de la misma. El criterio para la elección de los observatorios usados ha sido la disponibilidad de al menos 15 años de datos en la serie temporal en el periodo de estudio de 1953 a 2012. Entre esos 102 observatorios solo 45 tienen más del 50% de los datos disponibles y 12 con más del 90%. Los observatorios elegidos están muy bien repartidos en el espacio. Sin embargo, la mayoría de los observatorios con más del 90% de datos disponibles se concentran en la parte sur de la zona de estudio (Figura 1). Un control de calidad de las series usadas se hizo graficando los datos diarios, mensuales y anuales con el fin de detectar valores imposibles como el caso de las temperaturas mínimas que superan a las máximas.



Figura1: Distribución espacial de los 102 observatorios meteorológicos con datos de temperaturas usados en este trabajo.

Para la reconstrucción y homogeneización de las series de temperaturas se usó la versión 2.1 del software “CLIMATOL” (Guijarro, 2011). CLIMATOL es un paquete para R que contiene funciones para la homogeneización de series climatológicas además de otras funciones para el relleno de las lagunas en las series. La principal función de CLIMATOL es la función *homogen()* que requiere un conjunto de parámetros que deben ajustarse en relación a las particularidades de la serie climáticaa analizar. Según los parámetros elegidos se puede limitarse a un relleno de lagunas en o realizar el proceso de homogeneización completo. El estudio de la homogeneidad de una serie implica la comparación de la misma con una serie de referencia. Dentro de CLIMATOL la serie de referencia se obtiene como promedio de los valores de las series de los observatorios escogidos utilizando un método de ponderación basado en el método del inverso de distancia para dar mayor peso a los más próximos y mejor correlacionados. Como primer paso CLIMATOL permite eliminar los valores anómalos superando determinado umbral de desviaciones estándares (***dz.max***) fijado por el usuario. A continuación, se procede a detectar las inhomogeneidades presentes en las series, haciendo uso, para ello, del test SNHT (Alexandersson, 1986) que sirve para detectar saltos en los valores medios. El proceso se finaliza con el relleno de las lagunas y de los outliers eliminados y reconstruyendo las sub-series divididas por el proceso de homogeneización. El test de homogeneidad se aplicó a las series mensuales y anuales y en este trabajo se trabajó con las series reconstruidas a partir las sub-series más recientes.

La elección final de los parámetros de la función *homogen()* se hizo después de una exploración de varios valores de esos, consultas directas al señor Guijarro y con el apoyo de los resultados del trabajo de Hernández García *et al.*, (2012) realizado en una zona cercana a la nuestra.

1-Los argumentos para la función *homogen()* para la reconstrucción de las series de Temperaturas máximas usados en este trabajo:

```
homogen('Tmax100', anyi=1953, anyf=2012, nref=10, dz.max=25, wd=c(0,0,20),
tVt=60, tVf=0.02, swa=60, snhtt=120, snht1=60, snht2=120, mxdif=0.05,
force=FALSE, a=0, b=1, wz=0.001, deg=FALSE, rtrans=0, std=3, ndec=1, mndat=0,
leer=TRUE, gp=3, na.strings=NA, nclust=100, maxite=50, vmin=NA, vmax=NA,
verb=TRUE)
```

2-Los argumentos para la función *homogen()* para la reconstrucción de las series de Temperaturas mínimas usados en este trabajo:

```
homogen('Tmin100', anyi=1953, anyf=2012, nref=10, dz.max=25, wd=c(0,0,20),  
tVt=120, tVf=0.02, swa=60, snhtt=240, snht1=120, snht2=240, mxdif=0.05,  
force=FALSE, a=0, b=1, wz=0.001, deg=FALSE, rtrans=0, std=3, ndec=1, mndat=0,  
leer=TRUE, gp=3, na.strings=NA, nclust=100, maxite=50, vmin=NA, vmax=NA,  
verb=TRUE)
```

Para saber el significado de cada argumento hay que consultar el manual de usuario del Climatol (Guijarro, 2011).

Referencias

Guijarro, J.A. (2011). User'sguide to Climatol. Instituto Nacional de Meteorología, Centro Meteorológico en Illes Balears.

Hernández García, E. M., García Valero, J. A., Palenzuela Cruz, J. E., Belda Esplugues, F., (2012). Ejercicio de homogeneización y relleno de series diarias de temperatura máxima, mediante el uso de Climatol. En Cambio climático. Extremos e impactos. Rodríguez Puebla, C., Ceballos Barbancho, A., González Reviriego, N., Morán Tejeda, E., Hernández Encinas H., (Eds.)Publicaciones de la Asociación Española de Climatología (AEC), 2012, Serie A, nº 8.Salamanca, 998 pp. ISBN: 978-84-695-4331-3

Universitat d'Alacant
Universidad de Alicante